EVALUATION AND VALIDATION OF CHATTER DETECTION BY PERIODIC SAMPLING OF TIME DOMAIN MILLING SIGNALS AND SPINDLE SPEED SELECTION FOR STABLE CUTTING CONDITIONS

A Dissertation Presented for the

Doctor of Philosophy

Degree

The University of Tennessee, Knoxville

Tobechukwu D. Nwabueze

December 2025

Copyright © 2025 by Tobechukwu D. Nwabueze

All rights reserved.

ACKNOWLEDGEMENTS

Thank you to Dr. Siamak Farhad, Dr. Sekhar Rakurty, Dr Bradley Jared, Dr Tony Shi, Dr. Michael Gomez, and Dr. Tony Schmitz.

ABSTRACT

This study evaluates and validates a novel chatter detection method in milling operations by periodic sampling of time domain milling signals. The periodic sampling frequency is scanned over a preselected range, and the sampled values of the time domain milling signals are used to calculate a stability metric for each sampling frequency. For stable cutting conditions, the sampled point repeats for each tooth passage, and a local minimum in the stability metric occurs at the tooth passing frequency. For unstable cutting conditions, the sampled point does not repeat and a local minimum in the stability metric occurs at or near the chatter frequency instead of at the tooth passing frequency. It is also observed that at stable cutting conditions, the stability metric values are less than those from unstable cutting conditions, for the same experimental setup.

The location of the local minima in the stability metric with respect to the tooth passing frequency and the chatter frequency, is used to confirm whether the cut is stable or unstable, which validates the novel approach. The stability of the cut is further confirmed by plotting and comparing the locations and values of the stability metric with the frequency content of the milling signals using FFT (fast Fourier transform), by visually inspecting the cut surface of the workpiece for regular or irregular tooth or chatter marks, and by measuring the roughness of the cut surface of the workpiece. Studies are completed using in situ milling signals including displacement, acceleration, and sound.

To evaluate spindle speed selection, unstable cuts are performed, and a new spindle speed is calculated based on the chatter frequency and the number of teeth of the

used cutting tool. The new spindle speed and a new feed rate are then applied to achieve a stable cut while maintaining all other cutting parameters and conditions.

This study also introduces a fundamental feasibility study for closed loop chatter detection and spindle speed selection using an algorithm that could be integrated into open-source machine controls to enable automatic identification of both the tooth passing and chatter frequencies using in-built once-per-revolution machine data.

TABLE OF CONTENTS

Chapter One: Introduction and General Information 1

Chatter 1

Periodic Sampling 2

Milling Signals 3

Chapter Two: Literature Review 5

Background Studies 5

Sensors for Signal Acquisition 10

Chatter Detection Methods 12

Chapter Three: Materials and Methods 43

Experimental Setup 43

Experimental Plan and Procedure 48

Chapter Four: Results and Discussion 58

Stable, Marginal, and Unstable Cuts 58

Spindle Speed Selection 155

Closed loop feasibility study 178

Chapter Five: Conclusions and Recommendations for Future Works 216

Appendix 228

Vita 249

LIST OF TABLES

Table 2.1. Sensors for signal acquisition..... 36

Table 2.2. Chatter detection methods..... 37

Table 4.1. Tool tip modal parameters for the two-flute endmill..... 60

Table 4.2. Workpiece modal parameters of the 6061-T6 aluminum workpiece before the unstable cut. 60

Table 4.3. Profilometer results from six measured locations on the unstable cut surface of the 6061-T6 aluminum..... 68

Table 4.4. Workpiece modal parameters of the 6061-T6 aluminum before the marginal cut..... 70

Table 4.5. Profilometer results from six measured locations on the marginally unstable cut surface of the 6061-T6 aluminum..... 78

Table 4.6. Workpiece modal parameters of the 6061-T6 aluminum before the stable cut. 80

Table 4.7. Profilometer results from six measured locations on the stable cut surface of the 6061-T6 aluminum..... 88

Table 4.8. Cutting parameters and peak spindle power for the experimental cuts using the two-flute endmill on 6061-T6 aluminum..... 89

Table 4.9. Tool tip modal parameters of the four-flute endmill..... 92

Table 4.10. Workpiece modal parameters of the AISI 4140 steel before the unstable cut. 93

Table 4.11. Profilometer results from six measured locations on the unstable cut surface of the AISI 4140 steel workpiece. 101

Table 4.12. Workpiece modal parameters of the AISI 4140 steel before the marginal cut. 103

Table 4.13. Profilometer results from six measured locations on the marginal cut surface of the AISI 4140 steel workpiece. 111

Table 4.14. Workpiece modal parameters of the AISI 4140 steel before the stable cut. 113

Table 4.15. Profilometer results from six measured locations on the stable cut surface of the AISI 4140 steel workpiece. 121

Table 4.16. Cutting parameters and peak spindle power for the experimental cuts using the four-flute endmill on the AISI 4140 steel workpiece. 122

Table 4.17. Tool tip modal parameters of the five-flute endmill. 126

Table 4.18. Workpiece modal parameters of the AISI 4140 steel before the unstable cut. 126

Table 4.19. Profilometer results from six measured locations on the unstable cut surface of the AISI 4140 steel workpiece. 134

Table 4.20. Workpiece modal parameters of the AISI 4140 steel before the marginal cut. 136

Table 4.21. Profilometer results from six measured locations on the marginal cut surface of the AISI 4140 steel workpiece. 144

Table 4.22. Workpiece modal parameters of the AISI 4140 steel before the stable cut. 146

Table 4.23. Profilometer results from six measured locations on the stable cut surface of the AISI 4140 steel workpiece. 154

Table 4.24. Cutting parameters and peak spindle power for the experimental cuts using the five-flute endmill on the AISI 4140 steel workpiece. 156

Table 4.25. Tool tip modal parameters of the four-flute endmill. 159

Table 4.26. Workpiece modal parameters of the AISI 4140 steel before the unstable cut. 160

Table 4.27. Profilometer results from six measured locations on the unstable cut surface of the AISI 4140 steel workpiece. 168

Table 4.28. Workpiece modal parameters of the AISI 4140 steel before the stable cut. 170

Table 4.29. Profilometer results from six measured locations on the stable cut surface of the AISI 4140 steel workpiece. 178

Table 4.30. Tool tip modal parameters of the five-flute endmill. 180

Table 4.31. Workpiece modal parameters of the AISI 1018 steel before the marginal cut. 181

Table 4.32. Profilometer results from six measured locations on the marginal cut surface of the AISI 1018 steel workpiece. 185

Table 4.33. Workpiece modal parameters of the AISI 4140 steel before the stable cut. 186

Table 4.34. Profilometer results from six measured locations on the stable cut surface of the AISI 1018 steel workpiece. 190

Table 4.35. Workpiece modal parameters of the AISI 1018 steel before the unstable cut. 192

Table 4.36. Profilometer results from six measured locations on the unstable cut surface of the AISI 1018 steel workpiece. 196

Table 4.37. Workpiece modal parameters of the AISI 1018 steel before the stable cut. 198

Table 4.38. Profilometer results from six measured locations on the stable cut surface of the AISI 1018 steel. 202

Table 4.39. Workpiece modal parameters of the AISI 1018 steel before the unstable cut. 203

Table 4.40. Profilometer results from six measured locations on the unstable cut surface of the AISI 1018 steel. 208

Table 4.41. Workpiece modal parameters of the AISI 1018 steel before the stable cut. 209

Table 4.42. Profilometer results from six measured locations on the stable cut surface of the AISI 1018 steel workpiece. 214

LIST OF FIGURES

Figure 2.1. Magnified time interval of a time domain simulation (blue lines) and periodic sampling (red circles) result for a stable operating parameter. 11

Figure 2.2. Magnified time interval of a time domain simulation (blue lines) and non-periodic sampling (red circles) result for an unstable operating parameter. 11

Figure 3.2. The standard experimental setup showing the tool, microphone position, workpiece, accelerometer, and the CMD. 53

Figure 3.3. The standard experimental setup with the Dino-lite Edge digital microscope positioned in front of the workpiece. 54

Figure 3.4. The standard experimental setup with the Mitutoyo SJ-210 profilometer positioned on the cut surface of the workpiece. 54

Figure 3.5. The power sensor connected to the spindle motor's three-phase input cables. 55

Figure 3.6. The MetalMax data acquisition device. 55

Figure 3.7. The National Instruments data acquisition device. 56

Figure 3.8. The algorithm for the in situ, low-latency chatter detection and spindle speed selection MATLAB code for closed loop application. 56

Figure 3.9. A typical tap testing scenario to measure the tool tip modal parameters in the x direction. 57

Figure 4.1. Tool tip and workpiece, *x* (blue lines) and *y* (red lines) directions, frequency response function. 61

Figure 4.2. Stability lobe diagram with the selected point (black dot) at an unstable region corresponding to a spindle speed of 5550 rpm and an axial depth of cut of 8 mm. 61

Figure 4.3: The total time interval of the signal from the CMD (displacement signal) showing when the tool interacts with the workpiece. 62

Figure 4.4: The magnified time interval of the signal from the CMD (displacement signal)..... 62

Figure 4.5: Magnitude plot of *x* frequency content for 150 rotations, with f_c (red dot) identified at 776 Hz and f_{tooth} (black circle) at 185 Hz. 63

Figure 4.6: Variation in *M* value with periodic f_s. Local minima occur at f_c of 776 Hz (red dot) where M = 1.6 µm, and at f_c subharmonics (red dots), not at f_{tooth} (black circle). 63

Figure 4.7: The total time interval of the signal from the accelerometer (acceleration signal) showing when the tool interacts with the workpiece. 64

Figure 4.8: The magnified time interval of the signal from the accelerometer (acceleration)..... 64

Figure 4.9: Magnitude plot of *a* frequency content for 150 rotations, with f_c (red dot) identified at 776 Hz and f_{tooth} (black circle) at 185 Hz. 65

Figure 4.10: Variation in *M* value with periodic f_s. Local minima occur at f_c of 776 Hz (red dot) where M = 32 m/s^2, and at f_c subharmonics (red dots), not at f_{tooth} (black circle). 65

Figure 4.11: The total time interval of the signal from the microphone (sound pressure signal) showing when the tool interacts with the workpiece. 66

Figure 4.12: The magnified time interval of the signal from the microphone (sound pressure). 66

Figure 4.13: Magnitude plot of p frequency content for 150 rotations, with f_c (red dot) identified at 776 Hz and f_{tooth} (black circle) at 185 Hz. 67

Figure 4.14: Variation in M value with periodic f_s. Local minima occur at f_c of 776 Hz (red dot) where M = 0.99 Pa, and at f_c subharmonics (red dots), not at f_{tooth} (black circle). 67

Figure 4.15: Surface of the aluminum 6061-T6 workpiece with visible chatter marks after the unstable cut. 68

Figure 4.16: Tool tip and workpiece, x (blue lines) and y (red lines) directions, frequency response function. 71

Figure 4.17. Stability lobe diagram with the selected marginally unstable point (black dot) corresponding to a spindle speed of 5450 rpm and axial depth of cut of 6.28 mm. 71

Figure 4.18: The total time interval of the signal from the CMD (displacement signal) showing when the tool interacts with the workpiece. 72

Figure 4.19: The magnified time interval of the signal from the CMD (displacement signal). 72

Figure 4.20: Magnitude plot of x frequency content for 150 rotations, with f_c (red dot) identified at 776 Hz and f_{tooth} (black circle) at 182 Hz. 73

Figure 4.21: Variation in M value with periodic f_s. Local minima occur at f_c of 776 Hz (red dot) where M = 1.5 µm, and at f_c subharmonics (red dots), not at f_{tooth} (black circle). 73

Figure 4.22: The total time interval of the signal from the accelerometer (acceleration signal) showing when the tool interacts with the workpiece. 74

Figure 4.23: The magnified time interval of the signal from the accelerometer (acceleration)..... 74

Figure 4.24: Magnitude plot of a frequency content for 150 rotations, with f_c (red dot) identified at 776 Hz and f_{tooth} (black circle) at 182 Hz. 75

Figure 4.25: Variation in M value with periodic f_s. Local minima occur at f_c of 776 Hz (red dot) where M = 23 m/s^2, and at f_c subharmonics (red dots), not at f_{tooth} (black circle). 75

Figure 4.26: The total time interval of the signal from the microphone (sound pressure signal) showing when the tool interacts with the workpiece. 76

Figure 4.27: The magnified time interval of the signal from the microphone (sound pressure). 76

Figure 4.28: Magnitude plot of p frequency content for 150 rotations, with f_c (red dot) identified at 776 Hz and f_{tooth} (black circle) at 182 Hz. 77

Figure 4.29: Variation in M value with periodic f_s. Local minima occur at f_c of 776 Hz (red dot) where M = 0.94 Pa, and at f_c subharmonics (red dots), not at f_{tooth} (black circle). 77

Figure 4.30: Surface of the aluminum 6061-T6 workpiece with visible chatter marks after the marginally unstable cut. 78

Figure 4.31: Tool tip and workpiece, *x* (blue lines) and *y* (red lines) directions, frequency response function. 81

Figure 4.32: Stability lobe diagram with the selected stable point (black dot) corresponding to a spindle speed of 6200 rpm and axial depth of cut of 8 mm. 81

Figure 4.33: The total time interval of the signal from the CMD (displacement signal) showing when the tool interacts with the workpiece. 82

Figure 4.34: The magnified time interval of the signal from the CMD (displacement signal). 82

Figure 4.35: Magnitude plot of *x* frequency content for 150 rotations, with f_{tooth} at 207 Hz and its harmonics identified (black circles). 83

Figure 4.36: Variation in *M* value with periodic f_s. A local minimum is observed at f_{tooth} of 207 Hz (black circle) where M = 0.93 µm. 83

Figure 4.37: The total time interval of the signal from the accelerometer (acceleration signal) showing when the tool interacts with the workpiece. 84

Figure 4.38: The magnified time interval of the signal from the accelerometer (acceleration). 84

Figure 4.39: Magnitude plot of *a* frequency content for 150 rotations, with f_{tooth} at 207 Hz and its 1st harmonic identified (black circles). 85

Figure 4.40: *M* value variation with periodic f_s. Local minima at f_{tooth} at M = 8.5 m/s^2, its 1st harmonic (black circles), and near a runout frequency (magenta dot). 85

Figure 4.41: The total time interval of the signal from the microphone (sound pressure signal) showing when the tool interacts with the workpiece. 86

Figure 4.42: The magnified time interval of the signal from the microphone (sound pressure signal). 86

Figure 4.43: Magnitude plot of p frequency content for 150 rotations, with f_{tooth} at 207 Hz and its 1st harmonic identified (black circles). 87

Figure 4.44: Variation in M value with periodic f_s. A local minimum is observed at f_{tooth} of 207 Hz (black circle) where M = 0.38 Pa. 87

Figure 4.45: Surface of the aluminum 6061-T6 workpiece, with no chatter marks, after the stable cut. 88

Figure 4.46: Spindle power consumption peaked at 1.21 kW during the unstable cut at a spindle speed of 5550 rpm, axial and radial depths of cut of 8 mm and 3 mm respectively. 89

Figure 4.47: Spindle power consumption peaked at 1.14 kW during the marginally unstable cut at 5450 rpm, 6.28 mm and 3 mm axial and radial depths of cut respectively. 90

Figure 4.48: Spindle power consumption peaked at 1.86 kW during the stable cut at a spindle speed of 6200 rpm, 8 mm and 3 mm axial and radial depths of cut respectively. 90

CHAPTER ONE

INTRODUCTION AND GENERAL INFORMATION

Chatter

Chatter is a self-excited vibration in milling that occurs when the steady forced excitation from the teeth impacting the workpiece matches and amplifies vibrations near the machine's natural frequency. Thus, chatter is characterized by regenerative vibrations between the cutting tool and the workpiece. Unlike forced vibrations, which are driven by periodic tooth impacts and repeat predictably with each spindle rotation, chatter arises from a feedback loop where the surface waviness created by a previous tooth pass interacts destructively with the subsequent tooth pass. This phenomenon becomes particularly problematic when the frequency of the regenerative effect aligns with one or more of the system's natural frequencies, resulting in a resonance condition.

The consequences of chatter are both detrimental and multifaceted. Mechanically, it produces excessive cutting forces that can compromise tool life, accelerate spindle wear, and deform the workpiece. From a manufacturing standpoint, chatter leads to unacceptable surface finish, dimensional inaccuracies, and increased scrap rates. In high-precision machining applications, even brief instances of chatter can invalidate an entire operation.

Milling signals can be used to detect chatter and the information from the signals can provide recommendations for new stable operating parameters. In situ periodic sampling of time domain milling signals including displacement, acceleration, and sound are used to detect chatter in this study.

Periodic Sampling

Periodic sampling of time domain milling signals introduces a novel approach for detecting chatter by analyzing discrete signal behavior at controlled sampling intervals. This method is used in this study to strategically sample displacement, acceleration, and sound signals at a range of user-defined frequencies. The primary objective is to isolate and identify whether the dominant vibration present in the milling process is periodic (forced) or non-periodic (self-excited) through a stability metric calculated using the sampled values of the milling signals.

Under stable cutting conditions, the periodic sampling reveals a repeating pattern in the signal values due to the consistency of tooth impacts on the workpiece particularly at the tooth passing frequency. Thus, in stable cutting conditions, the tooth passing frequency dominates and periodic sampling at this frequency yields consistent, repeated measurements resulting in a local minimum at the tooth passing frequency in the stability metric. This repeating nature results in a low variability metric for the corresponding sampling frequency. Alternatively, when chatter occurs, the presence of self-excited vibrations disrupts this pattern, and the sampled values no longer exhibit repetition. Instead, a local minimum in the stability metric emerges at or near the dominant chatter frequency, displacing the expected minimum at the tooth passing frequency.

By scanning across a frequency range and identifying the location of the local minima in the stability metric, this method provides a reliable and interpretable means to distinguish between stable and unstable cutting. This information can then be used not only to detect chatter but also to recommend corrective actions such as changing spindle speed.

Milling Signals

Milling signals are dynamic responses generated during the material removal process and contain critical information about the interaction between the cutting tool and the workpiece. These signals, which can include displacement, acceleration, force, and sound, reflect the mechanical and vibrational behavior of the system during machining. In particular, variations in these signals can indicate changes in cutting conditions, tool engagement, material properties, or the presence of process instabilities such as chatter. These signals are inherently linked to the dynamics of the milling operation, therefore they serve as effective inputs for process monitoring and stability evaluations.

Among the various types of milling signals, displacement and acceleration are commonly obtained using sensors such as optical sensors, Hall effect sensors, and accelerometers which can be pointed towards or mounted on the tool holder or the workpiece depending on the operator and the desired result. These signals capture relative motion between the cutting tool and the workpiece and are especially useful for detecting vibrations that may indicate the onset of chatter. Acceleration signals, in particular, offer a high signal-to-noise ratio and a broad frequency response, making them well-suited for capturing both low-frequency tool motions and high-frequency chatter vibrations. Displacement signals, while more sensitive to machine structural dynamics, offer direct insight into tool deflection and surface waviness.

Acoustic signals also provide valuable information about milling dynamics. Microphones and acoustic emission sensors capture high-frequency stress waves generated by tool-workpiece interaction, chip formation, and tool wear. These signals are non-contact and

easy to implement, making them attractive for real-time monitoring. However, they can be susceptible to ambient noise, requiring careful signal processing or filtering to isolate chatter-related features.

In this study, displacement, acceleration, and sound time domain milling signals are collected in situ. By correlating the characteristics of the milling signals with observed surface finish, frequency content, cutting conditions, and a stability metric, the study establishes a fundamental feasibility study for closed loop chatter detection and spindle speed selection for subsequent process optimization.

CHAPTER TWO

LITERATURE REVIEW

Background Studies

Honeycutt and Schmitz [1] presented an automated approach for identifying the stability of time domain simulation signals using the stability metric employed in this study. The metric *M* is achieved by calculating the normalized sum of the absolute values of the differences between sequentially sampled points as shown in **Equation 1** where x_s is the vector of sampled points and *N* is the number of sampled points. Thus, the stability metric is based on once-per-tooth sampled data. In another study [2], they introduced a subharmonic sampling approach to differentiate various instability types in milling processes. By sampling time-domain milling signals at integer multiples of the tooth period, the method automatically identifies secondary Hopf and period-n bifurcations. Using the stability metric *M*, a stability map that delineates stable regions and distinct bifurcation zones derived from time domain simulations was developed.

$$M = \frac{1}{N}\sum_{i=2}^{N}|x_s(i) - x_s(i-1)| \quad (1)$$

Schmitz et al [3, 4] introduced a chatter detection technique based on the statistical variance in once-per-revolution sampled audio signals in milling operations. The method distinguishes between stable and unstable cutting by leveraging their synchronous (stable) and asynchronous (unstable) characteristics. In stable cutting the signal exhibits low variance, while in unstable cutting the signal exhibits higher variance.

Rubeo and Schmitz [5] used peak-to-peak (PTP) force diagrams derived from time domain simulation and experiments in flexible workpiece milling as a stability metric,

where higher PTP indicates instability. In another study [6] they proposed a metric (amplitude ratio) which quantifies chatter severity by comparing the amplitude of the expected tooth passing frequency and harmonics to the amplitude of the chatter frequency using time domain simulation.

Landge [7] compared traditional analytic milling stability methods (average tooth-angle and Fourier series approaches) with time domain simulation across a range of milling conditions (radial immersion, up vs down milling). To achieve a direct comparison of the time domain simulation to the analytical stability limits without user interpretation, the stability metric *M* was defined in the simulation to automatically identify the stability at a specific spindle speed and axial depth of cut.

Shepard [8] developed a chatter detection algorithm for milling that samples cutting forces once per spindle revolution and computes the variance of differences between successive samples, thereby taking variance over a threshold as an indicator for chatter. It modified an existing milling simulation to generate stability lobe diagrams mapping stable, marginally stable, and unstable cuts, and integrates the detection algorithm into the simulation.

Schmitz et al [9] integrated physics-based Receptance Coupling Substructure Analysis (RCSA) with machine learning to predict milling stability. The hybrid stability metric is a binary stable/unstable label combined with the identified chatter frequency if unstable. These metrics feed the ML/Bayesian framework to improve stability prediction accuracy.

The approach combines test outcomes with dynamic modelling for hybrid stability assessment

Miao Xie et al [10] proposed a milling chatter recognition method combining dynamic characteristics and wavelet packet decomposition (WPD). Cutting forces are decomposed into sub-bands, and sub-bands around the system's natural frequencies are reconstructed. The stability metric is the energy of the reconstructed sub-band; high energy indicates chatter. Experiments on aluminum milling validate the method's effectiveness in detecting chatter.

Zhan et al [11] introduced a chatter-detection method for thin-wall milling that fuses acceleration and cutting-force signals, converts them to the frequency domain via FFT, and feeds spectra into a dual-stream residual-attention convolution neural network (CNN) to classify stable vs chatter states. The metric used for stability is essentially the CNN's classification accuracy in distinguishing machining states rather than a hand-derived threshold in signal features; accuracy reached up to 98.68%. Thus, rather than a classic stability metric (e.g., variance or energy), the stability indicator is the supervised model's predicted machining state from fused multi-sensor features.

Schmitz [12] described a modeling approach for milling stability that uses sample partitioning of stability map results combined with selected experimental test points flagged by observed chatter frequency. It builds the broader context of how stability metrics and test strategy integrate into modern stability map generation and uncertainty

reduction. It shows the evolution of stability metric usage from pure signal-based features to hybrid modeling/testing frameworks.

Schmitz et al [13] introduced an approach for detecting chatter using periodic sampling of time domain milling signals, where the periodic sampling frequency is scanned over a preselected range, and the sampled values of the milling signal are used to calculate the stability metric *M* from **Equation 1**. Time domain simulation was used to generate the feed direction tool tip displacement signals that were applied to the study. The variation in the *M* value together with the sampling frequency is then used to determine stable or unstable operating parameters. In the *M* variation plots, the local minima occurs at the tooth passing frequency for stable operating parameters while the local minima occurs at or near the chatter frequency for unstable operating parameters. Figure 2.1 and 2.2 show time domain simulations with periodic and non-periodic sampling results for stable and unstable operating parameters from the study. The study also implements spindle speed updating using **Equation 2** [14], where Ω is the spindle speed in rpm (revolutions per minute), N_t is the number of teeth of the tool, and f_c is the chatter frequency in Hz.

$$\Omega = \frac{60 f_c}{j N_t} \text{ , } j = 1, 2, 3, \ldots \quad (2)$$

The stability metric utilized in this study provides a simple and quantitative means of characterizing the dynamic behavior of milling processes directly from time domain signals without requiring frequency domain transformations or model-based simulations. Building on the foundation established by Honeycutt and Schmitz [1, 2, 13], the metric *M* (the normalized sum of absolute differences between sequential samples) captures both the amplitude and temporal irregularities in periodically sampled signals. Unlike purely

frequency domain or machine learning based metrics, this metric operates directly in the time domain, enabling in situ implementation with low computational overhead.

This study advances the previous work by applying the *M* metric experimentally rather than solely in simulation, extending it across multiple sensing modalities (displacement, acceleration, and sound pressure) and validating it under practical machining conditions. Furthermore, this study introduces a fundamental feasibility study for a closed loop algorithm which could be integrated into open-source machine controls to enable automatic identification of both the tooth passing and chatter frequencies using machine once-per-revolution in-built data. This transforms *M* from a static stability indicator into a dynamic chatter detection and suppression tool, capable not only of identifying chatter onset but also quantifying its severity. This represents a meaningful advancement in linking signal-based stability metrics to actionable process control.

Earlier stability metrics, such as peak-to-peak force amplitude [5], variance-based chatter detection [3, 8], or energy-based frequency decomposition [10], each possess notable limitations. Peak-to-peak and variance methods are sensitive to baseline drift and noise, often requiring manual thresholding or user interpretation, which limits their automation and robustness. Frequency domain energy metrics, while effective in distinguishing chatter frequencies, depend on FFT or wavelet decomposition and therefore lose responsiveness due to their computational intensity. In contrast, the *M* metric used here is self-normalizing, threshold-free, and directly interpretable from raw sensor data, allowing automatic chatter detection and stability mapping without complex preprocessing. Thus, it unifies simplicity, speed, and interpretability, addressing key shortcomings of prior

methods while enabling practical in situ chatter monitoring and spindle speed control in modern machining environments.

Sensors for Signal Acquisition

Commonly used milling signals include force, displacement, velocity, acceleration, and sound. Dynamometers [15, 16] for cutting measurements have been used in pioneer studies and are still commonly used today for chatter detection in milling. In [15], accelerometers were recommended for recording tool vibration geared towards chatter detection.

Ryabov et al. [17] used a laser displacement sensing system projected unto the cutting tool for chatter detection. The system was made up of two laser sensors with 40 μm spot size and 0.5 μm displacement resolution. The displacement signal for tool chatter was extracted and analyzed.

In a study on regenerative chatter, displacement of a milling tool was measured using eddy current sensors [18], while a Kistler dynamometer was used for cutting force measurements and a rotary encoder for measuring the tool rotation angle. The once per revolution displacement signals measured using an eddy current sensor by Mann et al [19] were used to construct a Poincaré map for chatter detection in up and down milling.

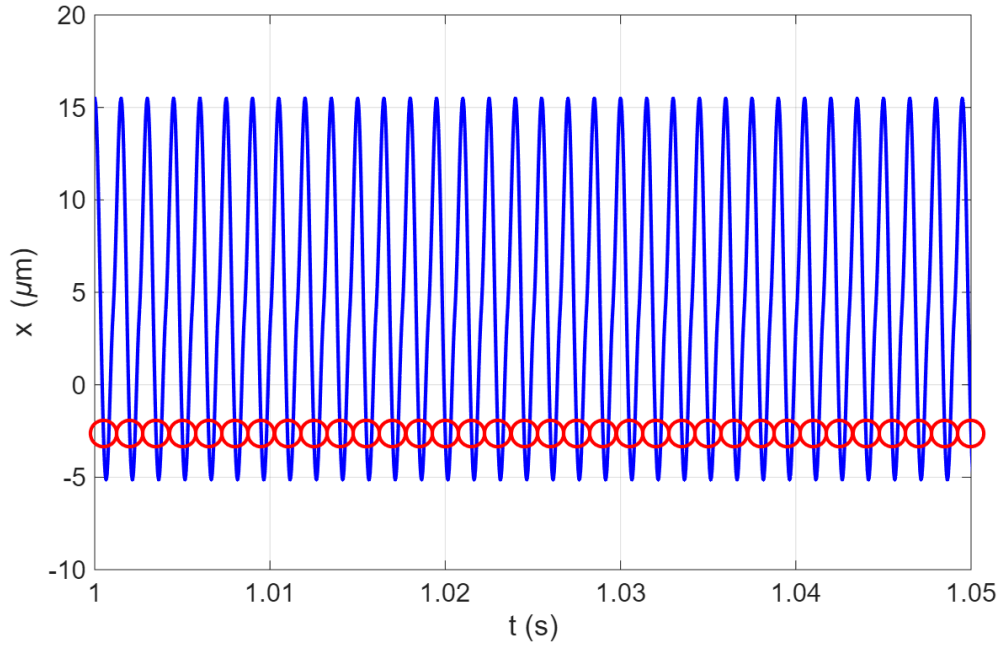


Figure 2.1. Magnified time interval of a time domain simulation (blue lines) and periodic sampling (red circles) result for a stable operating parameter.

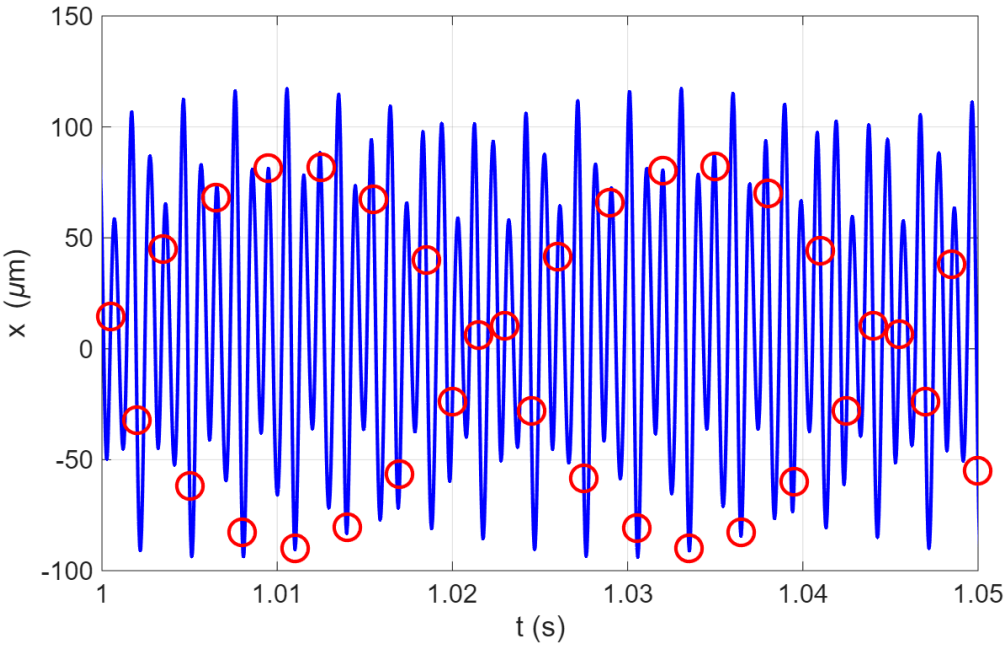


Figure 2.2. Magnified time interval of a time domain simulation (blue lines) and non-periodic sampling (red circles) result for an unstable operating parameter.

Displacement sensors such as laser [17, 20], eddy current/inductive [18, 19], and capacitive [21] sensors, measure the deflection between the tool and workpiece caused by cutting forces. They are widely used for vibration measurements.

Microphone audio signal measurements were also used in early chatter detection studies [22]. In recent studies, there is a growing trend of multi-sensor [23] approaches for chatter detection. A multi-sensory tool holder made up of a temperature sensor, a triaxial accelerometer, and strain gauges was developed to measure axial force and bending moment signals for chatter detection [24]. In another multi-sensory study, signals from a free field microphone, a single axis piezoelectric accelerometer, and a multi-axis piezoelectric accelerometer were combined for chatter detection [25].

Chatter Detection Methods

After data acquisition of the signals, they are processed using chatter detection methods [26] such as frequency domain analysis, time domain analysis, time-frequency domain analysis, statistical methods, and machine learning. Some methods like time domain and frequency domain methods are advantageous for faster processing, while others like machine learning and time-frequency domain methods are the most effective. For real-time applications, time domain and statistical methods are lightweight and therefore suitable for embedded systems, while machine learning methods can generalize better and are more suitable for adaptability but require significant training effort.

Frequency domain

Delio et al. [22] compared signals from various sensors (dynamometers, displacement probes, and accelerometers) and showed that a microphone is an excellent sensor to be

used for chatter detection and control, especially in cases involving flexible tooling and workpieces. When using time domain milling simulations of low-radial-immersion, low feed finishing operations, it was shown that chatter was not adequately detected from the force signals because of the short contact time, but it was clearly seen in the displacement signal. However, using frequency domain processing and the deterministic frequency domain chatter theory, a microphone was shown to provide a proper and consistent signal for reliable chatter detection and control. The study discussed important areas for the practical implementation of a microphone for chatter detection in an industrial setting and limitations of the microphone. Examples of chatter identification in the frequency domain using microphones were shown. The study improved upon previous similar research [27] where a bare microphone mounted 2 meters to 3 meters from the cutting process was used for most testing and the system recognized chatter in approximately 250 milliseconds to 500 milliseconds. Delio et al. [22] reiterated that the chatter identification time could be reduced when sound intensity measurements (a vector quantity denoting direction) as a method of isolating sound signal and better recognition techniques are utilized. The study also pointed out that in the frequency domain, sound intensity measurements can be determined by a single convolution and provides a discrete representation of sound intensity over the measured bandwidth using two matched microphones separated by a known distance, because the imaginary portion of the cross-spectrum of the two microphones indicates the intensity spectrum. Thus, using an efficient fast Fourier transform (FFT) algorithm, intensity as a function of direction can be obtained in a short time. Compared to previous sound isolation methods, sound

intensity measurements using matched microphones and a rapid FFT algorithm was superior in frequency response and bandwidth. It was also better suited for practical and noisy environments. Tests showed that even if the effects of speed and feed on material removal rate (MRR) are neglected, the sensitivity of the microphone permitted increases in stable depths-of-cut from 20% to 500%, so MRR can be increased substantially. A sufficient chatter signal is available even in low-immersion cuts.

Hashimoto et al. [18] studied the property of regenerative chatter vibration in a plain milling operation from the viewpoint of cutting force and variation. A cantilever milling arbor was mounted rigidly on the main spindle of a lathe via a Morse taper connection. Displacement of the milling cutter used in the study was measured using eddy current type gap sensors located perpendicularly to each other. While the cutting force was measured by a Kistler model 9257A dynamometer. A rotary encoder attached to the opposite end of the main spindle was used to measure the cutter rotation angle. Data is recorded on magnetic tapes and analyzed by an FFT analyzer and a PC. The displacement of the cutter and the cutting force components in tangential and normal directions were calculated based on the multi-sensor measured dataset. In recognizing primary chatter vibrations, a significant difference between the up and down milling processes was not observed. However, through the regenerative chatter effect, an acute chatter vibration occurred, especially in the down milling process. Thus, their experiments showed that the regenerative chatter vibration in down milling occurs more easily than in up milling. The cutting operation was characterized by a transient and intermittent cutting process, in which the undeformed chip thickness varied gradually.

Toh [28] presented an approach using FFT for the vibration analysis of the cutting path orientations used in rough and finish milling. FFT analysis was used on the cutting force signals obtained from new and worn cutting tools. The results showed that high axial depths of cut for both up and down milling resulted in minimal vibrational effects and the FFT analysis suggested that using a vertical upward orientation during finish cuts resulted in minimal vibrations regardless of the cutter condition. Hardened AISI H13 hot work tool steel was used for all the experiments. Workpieces were mounted on a dynamometer and cutting tests were performed on a vertical prismatic high speed machining center, using ultra-fine grain tungsten carbide 6-flute corner radius end mills for rough milling and 6-flute ball nose end mills for finish milling. Both cutting tools were coated with a monolayer aluminum titanium nitride ((Al, Ti)N) film with film thickness of about 2.5 μm. Tool wear measurements were based on tool deterioration phenomena observation set out on ISO 8688-2 and measured using a Toolmaker's microscope with a magnification of 30X equipped with digital micrometer actuators. All cutting force measurements were performed dry and carried out using a tri-axial piezoelectric platform dynamometer with a resonant frequency of 2.3 kHz in the *x* and *y* axes and 3.5 kHz in the *z*-axis. A FFT program was written to carry out the vibration analysis of the cutting force signals. Cutting force measurements were triggered and recorded as the cutter reached the midpoint of the workpiece to achieve complete stabilization and avoid the transient state. According to the study, the dynamic F_Y force was more sensitive to changes in the cutting conditions and thus, it was appropriate to transform the dynamic data from the time to frequency domain through the FFT algorithm to identify frequency components classified

as chatter. Frequency spectrums of the FFT analysis transformed from the F_Y force signals during up an down milling were compared. The FFT analysis suggested that chatter vibrations were predominant when utilizing a single direction vertical downward cutting tool path using a worn cutting tool at a down milling orientation. The analysis also showed that utilizing a single direction vertical upward tool path, regardless of up or down milling, indicated that chatter vibration was not evident despite the use of a worn cutting tool, because the increase in cutting forces were minimal.

Aslan et al. [29]. presented an on-line chatter detection method in milling using spindle drive motor current commands supplied by a CNC machine in real time. The transfer function of the spindle velocity controller was constructed by reading the control law parameters and measuring the frequency response function (FRF) of the system automatically using an external computer communicating with the CNC machine in real time. The FRF of the rigid body was subtracted from the measured FRF to derive the structural modes of the spindle drive. The proposed chatter detection method was experimentally validated on a Quaser UX-600 CNC machining center. The algorithms were run on the external computer which communicated with a Heidenhein iTNC 530 controller of the machining center via ethernet connection. The spindle drive motor current command data was collected at 10 kHz sampling frequency via the Heidenhein iTNC 530 controller. An aluminum 7050 workpiece material was milled at full immersion with regular pitch tools of different diameters and number of flutes. Tool tip FRF in the feed and normal directions were measured and plotted, as well as their corresponding stability maps. A feed rate of 0.1 mm/tooth was selected for all the

experiments. Sound signals were collected using a cardioid SHURE PG81 microphone and compared with the machine supplied current commands. It is shown that the bandwidth of the spindle drive's torque disturbance transfer function can be significantly increased by compensating the effects of structural dynamic modes which distort the transmitted cutting torque from tool tip to spindle drive servo. The proposed methodology does not require an experience based or case dependent frequency region selection for seeking the chatter frequency since it considers the true dynamics of the drive for the entire frequency range without any need to install external sensors on the machine.

Chang et al. [30] proposed a novel frequency-domain search (FDS) algorithm for chatter identification during milling using cutting force signals and vibration signals. The proposed algorithm had three main characteristics:

1. The FDS algorithm does not need complicated signal processing algorithms before feature extraction, ensuring the simplicity of the method.
2. An inherent feature of chatter named vibration base frequency is directly extracted to identify chatter and stable conditions.
3. Only a small amount of signal data is needed for the algorithm which ensures timely chatter identification.

Results show that the proposed algorithm can identify milling chatter accurately, whether using force signal or vibration signal, including slight chatter in the initial machining stage. The research further reveals that dominant chatter frequencies appear around the natural frequency of the spindle-tool system, but is not exactly equal to its natural

frequency. The chatter frequencies are determined by the combination of natural characteristics of the system and cutting conditions.

Time domain

Schmitz et al. [31] described three advances toward the rapid identification of the tool point frequency response and corresponding stable cutting parameters for high speed machining: 1) determination of stable speeds using non-contact periodic impulsive excitation of the tool point (produced by spindle rotation and a stationary magnet) in conjunction with once-per-revolution sampling. Experimental results showed that synchronous sampling of the tool point displacement at peak force during spindle speed ramping allowed calculation of qualitative representations of the real part of the system frequency response and corresponding stability lobes. Thus, this information allowed intelligent selection of optimum spindle speed(s). The predicted best speeds were verified by impact testing. It was also suggested that if the magnet force were also recorded, quantitative descriptions of the real part of the system FRF and resulting stability lobes would be possible; 2) receptance coupling substructure analysis (RCSA) for the analytical prediction of the tool tip FRF. It was shown that the RCSA model provides the ability to select the overhang length (within the allowable range for a particular tool) to achieve optimum material removal rate. Machining tests were done to verify the method; and 3) once-per-revolution sampling of the audio signal during cutting to determine stability behavior was also applied. Experimental results demonstrated a large increase in the statistical variance of the once-per-revolution audio data from stable to unstable cutting conditions. A milling simulation code was also developed to calculate the

variance in the synchronously sampled tool point displacement over a range of spindle speeds and chip widths. The study showed that this information could be used to construct plots that indicate stable/unstable behavior, similar to the common stability lobe and peak-to-peak diagrams. The study explained three stability identification methods: 1) pre-process experimental methods (pre-process measurement), for measuring tool tip FRF and calculating stability behavior using analytic or time-domain algorithms, or for directly determining stable spindle speeds by cutting tests; 2) pre-process analytic techniques (pre-process prediction) to predict the tool tip FRF and use the predicted FRF as input to analytic or time-domain simulations; and 3) in-process procedures (in-process identification) to monitor the cutting performance and suggest/implement changes to the cutting parameters (e.g., spindle speed).

Schmitz et al. [32] also carried out an evaluation of the statistical variance in the once-per-revolution sampled audio signal during milling as an in-process chatter indicator. The study provides a comparison of stability maps with good agreement developed using: 1) analytic techniques, and 2) the variance from once-per-revolution sampled time-domain simulations. Also, experimental agreement was demonstrated between the new variance-based technique and the commonly used FFT chatter detection method that analyzes the content of the FFT spectrum for chatter frequencies. This in-process chatter detection method is derived from Poincaré sectioning techniques traditionally applied to problems in nonlinear dynamics. Periodic motions in continuous time history are seen as fixed points for stable cuts or as elliptical point distributions for unstable cuts in a Poincaré map. In the study, Poincaré sectioning techniques were extended to include once-per-

revolution sampling of the milling audio signal and a statistical evaluation of the results. Stable cuts generate content synchronous with spindle rotation and, therefore, the periodically sampled audio signal will be characterized by a tightly spaced cluster of values with a low statistical variance. While an unstable cut (due to regenerative chatter) demonstrates asynchronous motion and gives a more distributed set of audio samples with a corresponding larger variance. This method senses chatter using a much less computationally intensive procedure, i.e., the variance of the time-based signal compared to the frequency-domain FFT and subsequent filtering. It also requires much less data set, such that only one sample per spindle revolution is required compared to tens of kilohertz sampling rates required to avoid aliasing in the FFT analysis. Experiments were carried out using a unidirectional microphone (Optimus 33-3023) mounted inside the machine enclosure, a microphone amplifier (PCB 482A17), once-per-revolution signal generator comprised of an infrared emitter/detector pair and reflective tool mark, and a digital oscilloscope for collection of the time-based audio and once-per-revolution signals. The study deduced that a preferred setup for industrial applications would include use of the microphone and access to the spindle encoder's once-per-revolution signal to sample the audio data, employing available data acquisition channels in the machine tool controller or a data acquisition card in a computer. This sampled data could then be represented in either: 1) a real-time display showing a continuously updated histogram indicating the process stability; or 2) a trend line showing the calculated variance during a machining operation. The identification of chatter using data represented in either of these manners would require no knowledge of the machine dynamics, process specific cutting energy

coefficients, process parameters, or vibrations theory and could potentially reduce the difficulties associated with the practical implementation of high speed machining on the shop floor.

Zhao et al. [33] proposed a maximum entropy (MaxEnt) feature-based reliability model (MFRM) method for real-time detection of early chatter in high-speed milling based on multiple sampling per revolution (MSPR) technique and second-order reliability method (SORM). The MSPR is used to acquire multiple sets of once-per-revolution sampled data to overcome the shortcomings of the once-per-revolution sampling, thereby enhancing the detection reliability. The method proposed by this study consists of five steps; 1) prior parameters are set; 2) data is collected using the MSPR technique; 3) a set of the standard deviation of the data collected as a chatter feature is calculated; 4) the failure hazard function (FHF) as a chatter indicator is estimated by applying the SORM with the MaxEnt feature; and 5) implementation of the real-time detection of early chatter based on the estimated chatter indicator FHF and the threshold FHF_0. In the time domain, chatter features can be extracted by calculating the statistical characteristics of the collected signal, such as mean, variance, and standard deviation. According to the study, this proposed MFRM method is independent of machining parameters and has a less computational cost. The method can also be used to monitor the degradation in rotor-bearing systems and the instability in pulse energy conversion systems. However, during milling, the transient behavior caused by the entry and exit of the cutting tool affects the chatter feature of the MSPR data, which reduces the detection accuracy of the proposed MFRM method.

Time-Frequency domain

Yang et al. [34] developed a novel method of on-line chatter identification for milling processes where optimized variational mode decomposition (OVMD) is used to decompose cutting force measurements, and the sub-components containing chatter information are extracted using a simulated annealing (SA) algorithm. The approximate entropy and the sample entropy are used to detect the onset of chatter. Five milling operating conditions were tested and their force measurements collected to evaluate the effectiveness of the proposed method. Their results showed that the proposed method is suitable for detecting both continuous and intermittent chatter and the method is shown to have greater sensitivity and stability than empirical mode decomposition (EMD). Early chatter is identified from relative changes in the entropy with time that occur under various cutting conditions. VMD is an advanced signal processing method that analyses signals based on sequential iterative sifting and offers satisfactory noise removing performance. The approximate entropy and the sample entropy, which are effective for analyzing nonlinear signals, are used to detect chatter from the onset. The approximate entropy was proposed to measure the complexity of the time series, while the sample entropy is used to evaluate the complexity of a signal that reflects the probability of generating a new pattern when the time series dimension changes. To test the effectiveness of their proposed method, milling operations were performed using a five-axis DMU80T machining station. 7075-T6 aluminum alloy workpieces with a length of 80 mm were machined using a 10 mm in diameter two-flute end mill. A dynamometer (Kistler 9257A) and a charge amplifier (DLF-3) were used to transmit the milling forces

at a sampling rate of 10 kHz. A macro-scale image of the machined surfaces was obtained for each group using a three-dimensional microscope (model VHX-1000). The time domain cutting force signals with and without chatter were analyzed. To identify chatter in the frequency domain, OVMD was performed on the segmented cutting force signals to extract the approximate entropy and the sample entropy from the filtered signal. A simulated annealing (SA) algorithm was used for parameter optimization of the VMD to obtain sub-components containing significant chatter information. According to their results, the OVMD algorithm performed better than EMD in extracting chatter information.

Xie et al. [35] proposed a milling chatter identification method based on dynamic wavelet packet decomposition (WPD) from the perspective of signal processing. Since the chatter frequency will reach a peak value near the natural frequency of the system, the original milling force signal is decomposed by WPD, and the sub-signals containing adequate chatter information are selected for signal reconstruction. Thus, the cutting force signals are reconstructed based on the inherent frequency of the system. The WPD was based on the demy wavelet basis function used to denoise the milling force signal, with three decomposition layers. According to the study, after numerical analysis and spectrum comparison, the reconstruction scheme proved to be robust. The time–frequency domain image of the reconstructed signal and the Hilbert spectrum feature are then compared and analyzed to identify the chatter.

Cao et al. [36] proposed a new chatter detection method based on synchro squeezing transform (SST) of sound signals. SST is a time-frequency (TF) domain analysis tool

with high resolution. In this work, the SST is based on short-time Fourier transform (STFT). High speed milling experiments were conducted to validate the proposed method. The flowchart of the proposed method is summarized below:

1. Signal acquisition: The sound signal is recorded using a MPA201 microphone in real time.
2. Perform SST on measured signals: SST is used to analyze the sound signal and a TF representation is calculated with STFT. Thus, a TF matrix is obtained.
3. Filtering in TF domain: The spindle rotating frequency, tooth passing frequency, and their harmonics are filtered in the TF matrix to remove noise.
4. Singular value decomposition (SVD) of filtered TF matrix: SVD is applied to condense the TF matrix into a one-dimensional time series.
5. Set threshold: The chatter detection threshold is set based on 3σ criterion. Lilliefors test is used to examine whether the chatter indicator in stable cutting meets the norm distribution assumption.

Fu et al. [37] proposed an energy aggregation characteristic-based Hilbert-Huang transform method for on-line chatter detection where a measured vibration signal is first broken down into a series of intrinsic mode functions (IMFs) using ensemble empirical mode decomposition (EMD). Feature IMFs are then selected according to the majority energy rule and Hilbert spectral analysis is applied on these feature IMFs to calculate the Hilbert time/frequency spectrum. The aim of this method was to effectively protect the workpiece from severe chatter damage within acceptable time complexity. A series of dry end milling operations were conducted using uncoated M2Al tools with three teeth on a

TC500 Drilling and Tapping Center able to operate at a high spindle speed of 15000 rpm. Accelerometers (PCB 356A15 3D 2-5 kHz ±5%) were mounted on the spindle housing and LM SCADAS Lab was used to collect the vibration signals and transmit them to a personal computer. Impact testing was conducted to ascertain the natural frequencies of the cutting system. To generate chatter, the spindle speed was varied from 3000 rpm to 10000 rpm and the axial depth of cut was varied from 1 mm to 10 mm. The radial depth of cut was also varied for different experiments.

Statistical

Schmitz [4] described a chatter detection technique for condition-based monitoring of milling process stability, based on statistical variance in the once-per-revolution milling audio signal. To identify regenerative chatter, this technique uses the synchronous and asynchronous nature of stable and unstable cuts, respectively. This is because stable cuts generate content synchronous with spindle rotation, and thus, the once-per-revolution milling signal is characterized by a tightly spaced cluster of values with a corresponding low variance. Meanwhile, unstable cuts caused by regenerative chatter demonstrate asynchronous motion and give a more distributed set of once-per-revolution values with a subsequent larger variance. Variance values for a number of stable and unstable cuts were compared for various strategies in obtaining the once-per-revolution trigger. In all three strategies, the calculated variance values detected the transition from stable to unstable, which included:

1. Obtaining the once-per-revolution signal using a locally derived trigger.

2. Generating a synthetic once-per-revolution sampling trigger using the actual spindle speed.
3. Producing the once-per-revolution signal from the nominal (commanded) spindle speed.

The experimental setup included a unidirectional microphone (Optimus 33-3023) mounted inside the machine enclosure of a high-speed, horizontal spindle (20000 rpm/20 kW) machining center, a microphone amplifier (PCB 482A17), once-per-revolution signal generator made up of an infrared emitter/detector pair and reflective tool mark, and a digital oscilloscope for collecting the time-based audio and once-per-revolution signals. The study pointed out that a preferred set-up for industrial applications would include use of the microphone and access to the spindle encoder's once-per-revolution signal to trigger audio data collection, employing available data acquisition channels in the machine tool controller or a data acquisition card in a local computer with network connections.

Wang et al. [38] presented a statistical chatter detection method based on the study of discrete wavelet transform (DWT) scheme and statistical analysis of wavelet transform modulus maxima (WTMM). WTMM describes a point where the local maximum of the wavelet transform is at a corresponding time location. Thus, a non-dimensional chatter index (CI) was developed based on the WTMM and statistical analysis. According to the study, the advantages of the chatter index include:

1. It reflects the random and statistical nature of the metal cutting process.

2. It is sensitive to chatter as it is based on WTMM, which is well known to be effective in detecting singularities.
3. It should be less susceptible to process changes because the WTMM ratio instead of the absolute WTMM is used in developing the chatter index.
4. It varies between 0 and 1 independent of cutting processes and can therefore be used in different machining processes.

Experiments to test the effectiveness of the proposed method were carried out on a CNC SERVO 2000 milling machine. The spindle of the milling machine was driven by a 3-HP AC motor with a three-phase G3 drive. A Wilcoxon 993B-6 piezoelectric accelerometer was mounted near the tool holder to collect vibration signal which was transmitted through an amplifier and sampled by an NI DAQ AT-MIO16DE-10 data acquisition card with up to 100 kS/s reading capacity and 12-bit resolution. The tests indicate that chatter is directly related to the depth of cut, furthermore, the tests indicate that even for identical depths of cut, the cutting processes could be either stable or unstable depending on spindle speed and feed rate. The CI value is a probability measure of the occurrence that the WTMM are above a certain level and has a variation range always between 0 and 1 regardless of the changes in machining parameter, tool, workpiece, and machine. The test results suggest that chatter severity could be estimated by the CI value. For example, CI above 0.75 indicates severe chatter, CI in the range of 0.6 to 0.75 indicates moderate chatter, and CI below 0.6 indicates a stable state.

Jo et al. [39] proposed a framework to monitor chatter and to diagnose the variables that cause it during hot strip milling process (HSMP). A chatter index (CI) that quantifies

chatter by confirming that it occurred was developed for monitoring chatter. Based on the data classified as normal by the CI, a multivariate statistical process monitoring model for detecting chatter is constructed using the modified independent component analysis (MICA) method. The monitoring results showed that the model based on the MICA outperformed other models based on principal component analysis and independent component analysis. First, the study developed the frequency-based CI that quantifies chatter using measured tension signals. The statistical monitoring model was then constructed using MICA. According to the study, the monitoring model based on the MICA overcame limitations of commonly used statistical monitoring methods like principal component analysis (PCA) and independent component analysis (ICA). Using MICA, statistically independent features were extracted from the process variables of chatter-free samples. The chatter detection rate of the model was 86.7%.

Machine Learning

The effectiveness of deep learning for chatter detection, with its automatic feature extraction and feature learning capabilities relies on well-labeled training data, which is a challenge. Jauhari et al. [40] introduced a novel hybrid deep CNN architecture that combines a stem block and inception modules with a channel-spatial attention mechanism (SIRCS-CNN: stem inception channel-spatial CNN) embedded in a residual network block (RCS-block). It bridges a raw input image with deeper layers of a CNN by extracting meaningful features and preparing the data for further processing by the deeper layers. The RCS-block consists of a ResNet block, a channel-attention block, and a spatial-attention block. Multi-scale features of cutting vibration signals are automatically

extracted by two inception sequential blocks to enhance the depth of the feature maps. The data collected for analysis include three-dimensional acceleration signals, which are segmented into individual data frames using a windowing technique. Each window contains 5000 data samples with a 0.1 s sampling time. 2500 data samples move from one window to the next in 0.05 s. A frame shift is applied to convert the one-dimensional signal (2500 data length) into a two-dimensional representation using continuous wavelet transform (CWT), which results in a collection of datasets representing the cutting process conditions. The two-dimensional image dataset is then fed into the SIRCS-CNN network model for a sequential learning process that finally classifies the output into three machining states: stable cutting, slight chatter, and severe chatter. Machining tests were carried out on a 3-axis CNC vertical milling center with a 12 mm diameter end-mill and an AISI420 stainless steel workpiece. A triaxial accelerometer (DYTRAN 3413A2) was mounted on the workpiece while a uniaxial accelerometer (PCB 352C33) was attached to the spindle housing. The vibration signals were amplified, thereby converting the original acceleration signals into low-impedance voltage outputs which were acquired at a sampling rate of 50 kHz. In creating a dataset to indicate stable to unstable cutting processes, color distributions of varying concentrations represent multiple frequencies related to the tooth passing frequency, spindle speed, natural frequency, or chatter frequency. Confusion matrices were generated for validating and testing the proposed SIRCS-CNN and ResNet-CNN models. According to the study, the confusion matrices for the validation set indicated that the SIRCS-CNN and ResNet-CNN models achieved 100% classification accuracy across all categories compared to a hybrid CNN integrated

with squeeze and excitation attention mechanism (ISR-CNN) which achieved 100% accuracy for most categories except a slight chatter state classification that was less than 100%.

Kounta et al. [41] presented an approach based on vibration analysis and deep learning. Images from the Fast Fourier Transform (FFT) analysis of vibration signals were analyzed using pre-trained deep neural networks for chatter detection in an industrial machining process, with non-ideal sensor placement. The images are cropped to normalize the signal scale thereby eliminating the common bias of signal amplitude. In this study, time signal was recorded using a Kistler accelerometer type 8776A50M6, magnetized to the workpiece holder, connected to a Roga Plug-n-Daq signal conditioner, and recorded at 22 kHz. The study showed that by depleting the signal (renormalized amplitude and absence of information on the rotation speed), the proposed model achieved an high accuracy of 99% in the training and validation phases, and an accuracy of 98.82% in the testing phase. Additional test dataset containing noisy and more or less ambiguous images are classified by the model which detected these cases from its training of unambiguous dataset, showing that the obtained generalization was efficient with an accuracy of 73.71%.

Alberts et al. [42] explored the application of machine learning techniques, specifically the Random Forest (RF) classification model to accurately categorize simulated vibration data for the prediction and classification of chatter in machining. The research investigated the efficacy of a novel approach to an RF model. The study utilizes less than 10,000 datasets thereby bypassing resource-intensive real-world data collection. The

feature extraction process combined time-series features and Fast Fourier Transform (FFT) data features. The model achieved a classification accuracy of 87% on data that extends beyond the initial training scope, with a modest decline in performance to affirm its robustness and adaptability across diverse operational conditions.

Combined (Frequency domain, Time domain, Machine Learning)

Lamraoui et al. [43] proposed a chatter detection technique that classifies sensitive features extracted from accelerometer signals. The technique was sequentially grouped into data acquisition, signal processing, features generation, features selection, and classification. Accelerometers are used to collect multi-axial data which are filtered in the frequency domain using a multiband resonance filter, after which statistical features in the time domain are extracted and ranked based on their entropy factor. Neural networks where used for the classification of the extracted features into stable or unstable conditions. A vertical machine center Huron K2X10, able to attain 28,000 rpm spindle speed, was used for their experiments. The workpiece was 7075-T6 Aluminum samples, cut with two flute micro grain solid carbide end mills. Three uniaxial piezoelectric accelerometers were used to capture the vibrations from 1 to 10 kHz. Two of the accelerometers were attached to the free end of the non-rotating part of the spindle and aligned along the *x* and *y* directions parallel to the machine axis. The third accelerometer oriented along the cutting direction was attached to the workpiece parallel to the *y* axis of the machine's center. A tap test is done on the tool tip in *x* and *y* directions to measure the modal parameters of the spindle (tool and tool holder). Two nonlinear classifiers, radial

basis function (RBF) and multi-layer perceptron (MLP) were used for feature classification.

Combined (Frequency domain, Machine Learning)

Kuljanic et al. [44] developed a multi-sensor chatter detection system made up of two sets of multi-sensor combinations and four experimental configurations for applications in industrial conditions and tested using 2 machine tools, 9 cutting tools, and 2 workpieces. In the study, one multi-sensor set was made up of a Kistler 9123C rotating dynamometer clamped between the spindle adaptor and the cutting tool, and two Kistler accelerometers mounted in the *x* and *y* direction on the spindle housing, while the second set was made up of a Kistler 9255B plate dynamometer clamped between the workpiece and the table, and a Kistler triaxial accelerometer type 8792A50 mounted on the spindle housing. Dynamic receptance at the tool tip was measured (modal testing) which yielded amplitude vs frequency transfer functions for each experimental configuration. The acceleration and force signals were sampled at 20 kHz using a National Instruments data acquisition board, while the data analysis was done on MATLAB. A reference chatter indicator (*RCI*) term based on the thrust force and normal force was defined as a numerical value proportional to the degree of instability of the system, which is the maximum ratio between the periodic energy and aperiodic energy of the thrust and normal forces. The periodic and aperiodic energies are calculated based on summations of the spindle speed and the power spectral densities (frequency domain analysis) of the signal. The *RCI* ranges from 0 (stable system) to 1 (extremely unstable system), and when equal to or greater than 0.2 the system is considered unstable. The multi-sensor

system was developed such that first, the sensor signals were pre-processed and filtered to remove noise and to compensate the transfer function of the sensors, then statistical parameters were calculated from each signal using wavelet decomposition. A neural network classification system was then applied to obtain a sensor chatter indicator (*SCI*) which aggregates the *RCI* values for each sensor, after which a multi-sensor classification system was applied to determine a multi-sensor chatter indicator (*MCI*) which combines the *SCI* from all sensors into a unified chatter index.

Combined (Time domain, Machine Learning)

Wang et al. [45] proposed chatter-related signal identification and diagnosis of thin-walled parts from mirror milling based on signal Q-factor and support vector machine (SVM). The introduction of a supporting head in mirror milling influences the dynamic characteristics of the tool-workpiece system. Thus, because the measured raw signal contains more coupled components and exhibits more oscillatory and aperiodic behaviors, it is difficult to identify mirror milling chatter using the monitoring signals. Q-factor was precisely calculated with linear predictive analysis and the frequency band with maximal variation of Q-factors is taken as the chatter-related signal. Using the feature vector constructed by Q-factors and power spectrum values of the determined frequency band, the SVM is used for milling state diagnosis with a prediction accuracy of up to 88.02%. The experimental setup was made up of a mirror milling system able to operate at a spindle speed of 18,000 rpm, a thin-walled aluminum plate of 1100 mm × 750 mm × 6 mm vertically mounted on a fixture with two sides fixed. A multi-component Kistler dynamometer 9317C, coupled with charge amplifiers, was used to

measure the supporting forces in three orthogonal directions (f_x, f_y, f_z). Three Keyence eddy current displacement sensors EX-V10 were mounted around the Kistler dynamometer to measure the vibration displacement signal. An acquisition card (PCI1716L) with a sampling rate of 250 kHz for each channel was used to collect the supporting forces and vibration displacement signal. The study introduced SVM as a new type of machine learning method based on statistical learning theory that adopts structural risk minimization criteria and solves the problems of nonlinearity, high dimensionality, and local minimum.

Combined (Time-Frequency domain, Markov Transition Field, Machine Learning)

Gao et al [46] proposed a multi-modal denoised data-driven milling chatter detection method using an optimized hybrid neural network architecture to address the low accuracy in chatter detection caused by limitations of both one-dimensional temporal and two-dimensional image modal information. A data denoising model combining complementary ensemble empirical mode decomposition (CEEMD) and singular value decomposition (SVD) was established for comparison with the proposed method. Multi-modal data features of different machining states were obtained using time-frequency domain methods and Markov transition field method which transforms time-series data into spatial image data. Sensitivity analysis of time-frequency domain features was conducted using Pearson correlation coefficient analysis. A hybrid neural network model (DBMA) for chatter detection was constructed by integrating dual-scale parallel convolutional neural networks, bidirectional gated recurrent units, and multi-head attention mechanisms. Their results reiterated that effective denoising of machining

signals and the use of multi-modal data can significantly improve the accuracy of stable to unstable state detection with improved stability and robustness. The experimental setup was made up of a VDL-1000E three-axis CNC machine, a 10 mm diameter flat-end mill cutting tool with 4 teeth, a TC4 titanium alloy workpiece, a force hammer with 3.41 Pc/n sensitivity for modal testing, a PCB accelerometer with a sensitivity of 10.42 mV/g and a Donghua DH5922 acquisition system. Simulations were conducted using MATLAB. Compared to SVD and CEEMD, the proposed denoising method achieved up to 23.9% improvement in signal-to-noise ratio, 14.3% reduction in Kurtosis ratio, and 16.67% improvement in correlation coefficient, with a prediction time of 83.23 ms for 40 samples. The accuracy of the proposed method in detecting machining status under variable working conditions was 94.94%.

Fuzzy Logic

Xu [47] developed a system for chatter detection and suppression where the coherence function values of the frequency spectra from two accelerometers in orthogonal directions were used as a chatter indicator. A fuzzy logic control approach was used for chatter suppression based on both the coherence function value and vibration energy level. To improve the adaptability of the fuzzy controller, a self-learning algorithm was also developed for on-line updating of the fuzzy rule base. A direct output tuning method was also proposed to improve the responsiveness of the system. Tests were conducted using both steel and aluminum workpieces with and without thin walls. The system featured simultaneous adjustment of spindle speed and feed rate to enhance the chatter suppression process.

Liang et al. [48] reported a fuzzy logic approach for chatter suppression in end milling. Vibration energy and the peak value of a vibration frequency spectrum were jointly used as chatter indicators and inputs to the proposed fuzzy controller. The outputs of the fuzzy controller were the adjusted machining parameters for chatter suppression. According to the study, this approach does not require a pre-selected nominal spindle speed and has avoided the difficulties in selecting spindle speed modulation parameters present in several other spindle speed variation methods. Their results showed that chatter could be effectively suppressed by altering spindle speed alone or by simultaneously adjusting feed rate and spindle speed. However, chatter could not be suppressed by only adjusting feed rate.

The reviewed literatures from sensors for signal acquisition and chatter detection methods have been summarized and categorized in **Table 2.1** and **2.2**.

Table 2.1. Sensors for signal acquisition.

Sensor	**Topic**	**Reference**
Dynamometer	A critical review of sensors for unmanned machining.	Tlusty, J. and Andrews, G.C., 1983 [15]
Dynamometer	Special aspects of chatter in milling.	Tlusty, J. and Ismail, F., 1983 [16]
Laser displacement sensor	Laser displacement meter application for milling diagnostics.	Ryabov, O., Mori, K. and Kasashima, N., 1998 [17]
Laser displacement sensor	On stability prediction for milling.	Gradišek, J., Kalveram, M., Insperger, T., Weinert, K., Stépán, G., Govekar, E. and Grabec, I., 2005 [20]
Eddy current sensor	Experimental research on cutting force variation during regenerative chatter vibration in a plain milling operation.	Hashimoto, M., Marui, E. and Kato, S., 1996 [18]

Table 2.2. continued: Sensors for signal acquisition.

Sensor	Topic	Reference
Eddy current sensor	Stability of up-milling and down-milling, part 2: experimental verification.	Mann, B.P., Insperger, T., Bayly, P.V. and Stépán, G., 2003 [19]
Capacitance displacement sensor	High frequency bandwidth cutting force measurement in milling using capacitance displacement sensors.	Albrecht, A., Park, S.S., Altintas, Y. and Pritschow, G., 2005 [21]
Microphone	Use of audio signals for chatter detection and control.	Delio, T., Tlusty, J. and Smith, S., 1992 [22]
Multisensory (microphone and accelerometer)	Effective multi-sensor data fusion for chatter detection in milling process.	Tran, M.Q., Liu, M.K. and Elsisi, M., 2022 [23]
Multisensory (temperature sensor, accelerometer, strain gauge)	Multi-Sensory Tool Holder for Process Force Monitoring and Chatter Detection in Milling.	Schuster, A., Otto, A., Rentzsch, H. and Ihlenfeldt, S., 2024 [24]
Multisensory (microphone and accelerometer)	Chatter identification using multiple sensors and multi-layer neural networks.	Arriaza, O.V., Tumurkhuyagc, Z. and Kim, D.W., 2018 [25]

Table 2.2. Chatter detection methods.

Method	Summary	Reference
Frequency domain	Compared signals from various sensors (dynamometers, displacement probes, and accelerometers) and showed that a microphone is an excellent sensor to be used for chatter detection and control.	Delio, T., Tlusty, J. and Smith, S., 1992 [22]
Frequency domain	Studied the property of regenerative chatter vibration in a plain milling operation from the viewpoint of cutting force variation.	Hashimoto, M., Marui, E. and Kato, S., 1996 [18]

Table 2.2. continued: Chatter detection methods.

Method	Summary	Reference
Frequency domain	Presented an approach using fast Fourier transform (FFT) for the vibration analysis of the cutting path orientations used in rough and finish milling.	Toh, C.K., 2004 [28]
Frequency domain	On-line chatter detection method in milling using spindle drive motor current commands supplied by a CNC machine in real time.	Aslan, D. and Altintas, Y., 2018 [29]
Frequency domain	Proposed a novel frequency-domain search (FDS) algorithm for chatter identification during milling, using cutting force signals and vibration signals.	Chang, L., Weiwei, X. and Lei, G., 2020 [30]
Time domain	Improving high-speed machining material removal rates by rapid dynamic analysis where three advances are described toward the rapid identification of the tool point frequency response and corresponding stable cutting parameter.	Schmitz, T.L., Davies, M.A., Medicus, K. and Snyder, J., 2001 [31]
Time domain	Exploring the variance from once-per-revolution sampled time-domain simulations from audio signal as a chatter indicator.	Schmitz, T.L., Medicus, K. and Dutterer, B., 2002 [32]
Time domain	A maximum entropy (MaxEnt) feature-based reliability model method for real-time detection of early chatter in high-speed milling.	Zhao, Y., Adjallah, K.H., Sava, A. and Wang, Z., 2021 [33]

Table 2.2. continued: Chatter detection methods.

Method	Summary	Reference
Time-Frequency domain	Developed a novel method of on-line chatter identification for milling processes where optimized variational mode decomposition (OVMD) is used to decompose cutting force measurements, and the sub-components containing chatter information are extracted using a simulated annealing (SA) algorithm.	Yang, K., Wang, G., Dong, Y., Zhang, Q. and Sang, L., 2019 [34]
Time-Frequency domain	Proposed a milling chatter identification method based on dynamic wavelet packet decomposition (WPD).	Xie, M., Yu, X., Ren, Z. and Li, Y., 2022 [35]
Time-Frequency domain	Proposed a new chatter detection method based on synchro squeezing transform (SST) of sound signals. SST is a time-frequency (TF) domain analysis tool with high resolution.	Cao, H., Yue, Y., Chen, X. and Zhang, X., 2017 [36]
Time-Frequency domain	Proposed an energy aggregation characteristic-based Hilbert-Huang transform method for on-line chatter detection where a measured vibration signal is first broken down into a series of intrinsic mode functions (IMFs) using ensemble empirical mode decomposition (EMD).	Fu, Y., Zhang, Y., Zhou, H., Li, D., Liu, H., Qiao, H. and Wang, X., 2016 [37]

Table 2.2. continued: Chatter detection methods.

Method	Summary	Reference
Statistical	Described a chatter detection technique for condition-based monitoring of milling process stability, based on statistical variance in the once-per-revolution milling audio signal.	Schmitz, T.L., 2003 [4]
Statistical	Presented a statistical chatter detection method based on the study of discrete wavelet transform (DWT) scheme and statistical analysis of wavelet transform modulus maxima (WTMM).	Wang, L. and Liang, M., 2009 [38]
Statistical	Proposed a framework to monitor chatter and to diagnose the variables that cause it during hot strip milling process (HSMP). A chatter index (CI) that quantifies chatter by confirming that it occurred was developed for monitoring chatter.	Jo, H.N., Park, B.E., Ji, Y., Kim, D.K., Yang, J.E. and Lee, I.B., 2020 [39]
Machine Learning	A hybrid deep learning-based approach for on-line chatter detection in milling using deep stem-inception networks and residual channel-spatial attention mechanisms.	Jauhari, K., Rahman, A.Z., Al Huda, M., Widodo, A. and Prahasto, T., 2025 [40]
Machine Learning	Images from the Fast Fourier Transform (FFT) analysis of vibration signals were analyzed using pre-trained deep neural networks for chatter detection in an industrial machining process.	Kounta, C.A.K.A., Arnaud, L., Kamsu-Foguem, B. and Tangara, F., 2023 [41]

Table 2.2. continued: Chatter detection methods.

Method	Summary	Reference
Machine Learning	Explored the application of machine learning techniques, specifically the Random Forest (RF) classification model to accurately categorize simulated vibration data for the prediction and classification of chatter in machining.	Alberts, M., St. John, S., Jared, B., Karandikar, J., Khojandi, A., Schmitz, T. and Coble, J., 2024 [42]
Frequency domain, Time domain, Machine Learning	A hybrid deep learning-based approach for on-line chatter detection in milling using deep stem-inception networks and residual channel-spatial attention mechanisms.	Lamraoui, M., Barakat, M., Thomas, M. and Badaoui, M.E., 2015 [43]
Frequency domain, Machine learning	Development of an intelligent multi-sensor chatter detection system in milling based on frequency domain analysis of the force and acceleration signals from dynamometers, accelerometers, and neural network classification.	Kuljanic, E., Totis, G. and Sortino, M., 2009 [44]
Time domain, Machine Learning	Mirror milling chatter identification using Q-factor and SVM.	Wang, Y., Bo, Q., Liu, H., Hu, L. and Zhang, H., 2018 [45]
Time-Frequency domain, Markov Transition Field, Machine Learning	Proposed a multi-modal denoised data-driven milling chatter detection method using an optimized hybrid neural network architecture to address the low accuracy in chatter detection.	Gao, H., Wang, H., Shen, H., Xing, S., Yang, Y., Wang, Y., Liu, W., Yu, L., Ali, M. and Khan, I.A., 2025 [46]

Table 2.2. continued: Chatter detection methods.

Method	Summary	Reference
Fuzzy Logic	A fuzzy logic control approach was used for chatter suppression based on both the coherence function value and vibration energy level.	Xu, D., 2003 [47]
Fuzzy Logic	Reported a fuzzy logic approach for chatter suppression in end milling. Vibration energy and the peak value of a vibration frequency spectrum were jointly used as chatter indicators and inputs to the proposed fuzzy controller.	Liang, M., Yeap, T. and Hermansyah, A., 2004 [48]

CHAPTER THREE

MATERIALS AND METHODS

Experimental Setup

Machining

To evaluate and validate the novel chatter detection method by periodic sampling of time domain milling signals in situ, and spindle speed selection to achieve stable cuts, experiments are conducted at the Tennessee Manufacturing and Design Enterprise facility, University of Tennessee, Knoxville.

All experimental cuts are conducted on a 3-axis Haas VF-4 CNC vertical milling machine using down milling and were all dry cuts (no coolant).

The cutting tools, all supplied by Accupro, used to conduct the experiments are:

1. Solid carbide endmill with two helical cutting flutes, 12.7 mm nominal cutting diameter, 15.9 mm cutting length, and a stub flute length. This tool is suitable for slotting, peripheral milling, and plunge operations, especially in softer materials such as aluminum and non-ferrous alloys.
2. Solid carbide end mill with four helical cutting flutes, 12.7 mm nominal cutting diameter, 15.9 mm cutting length, and a stub flute length. The tool has a titanium carbonitride (TiCN) coating, which improves wear resistance, surface hardness, and tool life compared to uncoated carbide. It is suitable for slotting, side milling, and finishing operations in a wide range of workpiece materials including steels, stainless steels, and non-ferrous alloys.

3. Solid carbide endmill with five helical cutting flutes, 12.7 mm nominal cutting diameter, 15.9 mm cutting length, a stub flute length, and high-performance 45° [degrees] helix angle. It is coated with aluminum titanium nitride (AlTiN), which provides high oxidation resistance, thermal stability, and wear resistance at elevated cutting speeds. This tool is particularly suitable for high-speed machining of steels, stainless steels, and heat-resistant alloys.

The two-flute carbide endmills are used to conduct experimental cuts on 6061-T6 aluminum workpieces with dimensions of 76.2 mm length, 50.8 mm width, and 25.4 mm height each. The four and five-flute carbide endmills are used to conduct experimental cuts on AISI 4140 steel workpieces with the same dimensions as the 6061-T6 aluminum workpieces. The five-flute carbide endmills are also used to conduct experimental cuts on a AISI 1018 steel workpiece with dimensions of 101.6 mm length, 50.8 mm width, and 25.4 mm height. Thus, three workpiece materials are used to conduct the experiments. A feed/tooth value of 0.1 mm/tooth is used for all the experimental cuts.

Sensors

The following sensors are used for time domain milling signal acquisition and surface finish inspections:

1. A constrained motion dynamometer (CMD) [49, 50, 51] equipped with a knife edge sensor with a sensitivity of 0.814 mm/V is used for measuring displacement. Measurements are recorded by mounting the workpieces on the CMD as experimental cuts are conducted.

2. Two PCB Piezotronics shear accelerometers with sensitivities of 5.79 and 5.24 mV/G respectively are used for measuring acceleration. Only one accelerometer could be used at a given time. Measurements are recorded by mounting the accelerometer on the workpiece as experimental cuts are conducted.
3. A Shure DM94 instrument microphone with a sensitivity of 825 Pa/V is used for measuring sound pressure. Measurements are recorded by mounting the microphone on the Haas VF-4 CNC machine table with the mouthpiece facing the cutting area.
4. A Dino-Lite Edge digital microscope is used to capture MJPG (Motion Joint Photographic Experts Group) images of the surfaces of each cut at a resolution of 2592 × 1944 pixels and 240 DPI (dots/inches). Images are captured by mounting the microscope on the machine table facing the cut surface.
5. A Mitutoyo SJ-210 surface roughness profilometer is used for measuring roughness average (Ra), root mean square (Rq), and the average maximum height of the profile (Rz). The following specifications are set for all measurements: ISO 4287:1997 standard, a cutoff wavelength (λc) of 0.8 mm, a short wavelength limit (λs) of 2.5 μm, a Gaussian filter, 4 sampling lengths, and a measurement speed of 0.5 mm/s. Six different points on the cut surface of a workpiece are measured per cut and the mean and standard deviation of each Ra, Rq, and Rz values are calculated.

The constrained motion dynamometer (CMD) [49, 50, 51] is a low-cost, monolithic device designed for in-process milling force measurement. Its structure is based on

constrained-motion/flexure-based kinematics, where a single degree of freedom (SDOF) moving platform is supported by four flexure elements arranged in an H-bar configuration. This design constrains motion in all directions except the compliant one, allowing precise, linear displacement under milling forces. The motion of the platform is sensed using an optical interrupter (a knife edge passing through an emitter–detector pair), converting beam interruption into voltage that represents displacement. The CMD is machined from 6061-T6 aluminum, designed to maintain elastic motion with a maximum displacement of about 50 μm, and offers a cost-effective, high-fidelity alternative to traditional piezoelectric dynamometers. Mathematically, the CMD operates using frequency domain analysis of the system's frequency response function (FRF). The relationship between force *F(w)* and displacement *X(w)* is given by **Equation 3**.

$$F(w) = \frac{1}{H(w)} X(w) \tag{3}$$

In **Equation 3**, *H(w)* is the measured FRF of the dynamometer. The process involves converting the measured time domain displacement into the frequency domain using a discrete Fourier transform (DFT), applying the inverted FRF to obtain the frequency domain force, and then transforming it back to the time domain. The maximum displacement is determined by the flexure design limit as expressed in **Equation 4**.

$$\delta_{max} = \frac{\sigma_{max} L^2}{3Et} \leq 50\mu m \tag{4}$$

In **Equation 4**, δ_{max} is the maximum allowable stress, *L* is the flexure length, *t* is the flexure thickness, and *E* the elastic modulus. These equations govern how displacement measurements are converted into accurate, time-resolved cutting forces, enabling real-

time milling force monitoring with minimal dynamic distortion. **Figure 3.1** shows the CMD design and optical interrupter placement.

The standard experimental setups with and without the surface finish inspection sensors are shown in **Figure 3.2**, **3.3**, and **3.4**.

A Load Controls Incorporated UPC-MB power sensor connected to the spindle motor of the Haas VF-4 CNC machine as shown in **Figure 3.5** is briefly used to visualize the changes in power consumption as the spindle speed increased or decreased for stable, marginal, and unstable cuts. It was determined that, for the experiments conducted, the changes in power consumption are negligible, even though visible, due to the minor changes in spindle speed.

Data Acquisition

A MetalMax sensor interface module, model DT9837B hardware with four channels, together with Spinscope the processing software sampling at a frequency of 25 kHz, are used for in situ sensor data acquisition of time domain milling signals. MATLAB is used to interpret the data from Spinscope, and to present the results.

An NI-9234 (National Instruments – 9234) vibration module connected to an NI CompactDAQ-9174 chassis is also used for in situ sensor data acquisition of time domain milling signals. MATLAB is used to collect and interpret the milling signal directly from the NI data acquisition device at a sampling frequency of 25 kHz, and to present the results with low-latency as experimental cuts are conducted. This is carried out to evaluate closed loop, in situ, low-latency chatter detection by periodic sampling of time

domain milling signals and spindle speed recommendation for achieving stable cutting conditions.

The two data acquisition hardware used to conduct the experiments (MetalMax and NI) are shown in **Figures 3.6** and **3.7** respectively.

Experimental Plan and Procedure

Experimental Plan

The experiments are conducted in three different phases. In the first phase, stable, marginal, and unstable experimental cuts are conducted. For each cut, the location of the local minima in the stability metric *M*, from **Equation 1**, with respect to the tooth passing frequency f_{tooth} and the chatter frequency f_c, is used to determine whether the cut is stable or unstable, which validates the novel chatter detection approach in situ. Thus, the variation in the *M* value with the sampling frequency f_s is used to determine whether a cut is stable or unstable. For the first phase, the two-flute carbide endmills are used to conduct experimental cuts on the 6061-T6 aluminum workpieces, while the four-flute and five-flute carbide endmills are used to conduct experimental cuts on the AISI 4140 steel workpieces. All available sensors are used in this phase.

In the second phase, unstable experimental cuts are conducted, after which the chatter frequencies are determined and used to calculate a new spindle speed based on **Equation 2**. The new spindle speeds are used to achieve stable experimental cuts. For the second phase, the four-flute endmill is used to conduct experimental cuts on the AISI 4140 steel workpiece. All available sensors are used in the phase as well.

The third phase is geared towards a closed loop feasibility study. A MATLAB code [Appendix A] for in situ, low-latency chatter detection and spindle speed selection is applied. The accelerometer and microphone sensors, as well as the surface finish inspection devices are used in this phase. The NI data acquisition device is used only for this phase, and the MATLAB code follows the algorithm shown in **Figure 3.8** [13]. For the third phase, the five-flute carbide endmill is used to conduct experimental cuts on the AISI 1018 steel workpiece.

Experimental Procedure

Tap testing, also known as impact testing, is performed before each experimental cut using a modal hammer and an accelerometer. This is carried out to determine the system dynamics of the tool and workpiece *x* and *y* directions before each cut. Tap testing is a common experimental technique used to characterize the dynamic behavior of the tool-workpiece system in milling. The modal hammer applies a transient impulse to the tool and workpiece in the *x* and *y* directions, while the accelerometer mounted on the tool and workpiece records the corresponding vibration response. The modal hammer provides the input force, and the accelerometer measures the output acceleration, allowing the frequency response function (FRF) to be measured as the ratio of output to input in the frequency domain. By repeating the test in both the *x* and *y* directions, the system's dynamic properties, also known as modal parameters, including natural frequencies, modal stiffness, and damping ratios, are identified, providing the essential parameters for stability predictions using stability lobe diagrams before each cut. **Figure 3.9** shows a typical tap testing scenario in the *x* direction.

The dynamic behavior of the tool-workpiece system is characterized through experimental modal analysis, performed independently in the principal x and y directions. Following the approach detailed by Schmitz and Smith [14], instrumented impact testing (tap testing) is conducted to obtain the FRFs of both the tool and the workpiece assemblies. These FRFs serve as the foundation for predicting regenerative chatter stability in milling through the construction of stability lobe diagrams.

As expressed in **Equation 5**, the measured FRF, *H(w)*, represents the complex ratio between the system's response (displacement, velocity, or acceleration) and the applied excitation force in the frequency domain.

$$H(w) = \frac{X(w)}{F(w)} = \frac{1}{-mw^2 + icw + k} \tag{5}$$

Where *k*, *m*, and *c* denote the system stiffness, mass, and damping coefficients, respectively, and *w* is the excitation frequency. In practice, a calibrated instrumented hammer provides the input force $F(t)$, while a tri-axial accelerometer mounted near the tool tip records the response $X(t)$. The discrete Fourier transforms of these signals yield $F(w)$ and $X(w)$, from which the complex FRF is computed.

For each direction, the measured FRFs are decomposed into modal components using curve fitting of the receptance function. The modal parameters including the natural frequency w_n, modal stiffness k_j, and damping ratio ζ_j are extracted through least-squares fitting of the measured data to the analytical single degree-of-freedom (SDOF) model as expressed in **Equation 6**.

$$H_j(w) = \frac{1}{k_j\left(1 - \left(\frac{w}{w_{n,j}}\right)^2 + 2i\zeta_j\frac{w}{w_{n,j}}\right)} \tag{6}$$

The total receptance at the tool tip in each direction is then obtained by summing over all identified modes as expressed in **Equation 7,** where *N* denotes the number of contributing modes.

$$H(w) = \sum_{j=1}^{N} H_j\,(w) \tag{7}$$

The measured FRFs for the tool and workpiece are subsequently combined according to the receptance coupling principle to obtain the dynamic response at the tool-workpiece interface as expressed in **Equation 8**, where H_t and H_w correspond to the tool and workpiece receptance, respectively.

$$H_{sys}(w) = H_t(w) + H_w(w) \tag{8}$$

The experimentally determined FRFs are then employed in the analytical prediction of regenerative chatter stability using the frequency domain approach described by Schmitz and Smith [14] to generate a stability lobe diagram. For a given spindle speed Ω and radial immersion ratio, the limiting axial depth of cut a_{lim} can be predicted from the real part of the FRF as expressed in **Equation 9**, where K_t is the tangential cutting force coefficient and $G(w_c)$ is the directional dynamic transfer function (receptance) evaluated at the chatter frequency w_c.

$$a_{lim} = \frac{1}{2K_t} \frac{-Re\{G(w_c)\}}{|Re\{G(w_c)\}|^2 + |Im\{G(w_c)\}|^2} \tag{9}$$

The chatter frequency corresponds to the intersection between the structural resonance and the tooth pass frequency harmonics as expressed in **Equation 10**, where *k* is an integer (lobes index) and N_t is the number of cutting teeth.

$$w_c = w_n + k\frac{N_t \Omega}{60} \tag{10}$$

The phase relationship between successive tooth passes determines the stability boundary, leading to the classical stability lobe diagram, which maps a_{lim} against spindle speed. The stability lobe diagram reveals regions of stable (chatter-free) and unstable (chatter-prone) operation, allowing the selection of optimal cutting parameters.

Despite their proven utility, stability lobe diagrams are inherently limited by uncertainties in system identification, cutting force coefficients, and boundary conditions, which can vary with tool wear, temperature, and clamping conditions. These uncertainties propagate through the analytical model, causing discrepancies between predicted and actual stability limits. Consequently, while stability lobe diagrams provide valuable guidance for parameter selection, they cannot guarantee chatter-free operations in practice. Therefore, complementary chatter detection methods are essential for validating and adapting stability predictions under actual machining conditions.

After each cut, the Dino-Lite digital microscope is used to take a picture of the cut surface, and the Mitutoyo profilometer is used to measure six different areas on the cut surface.

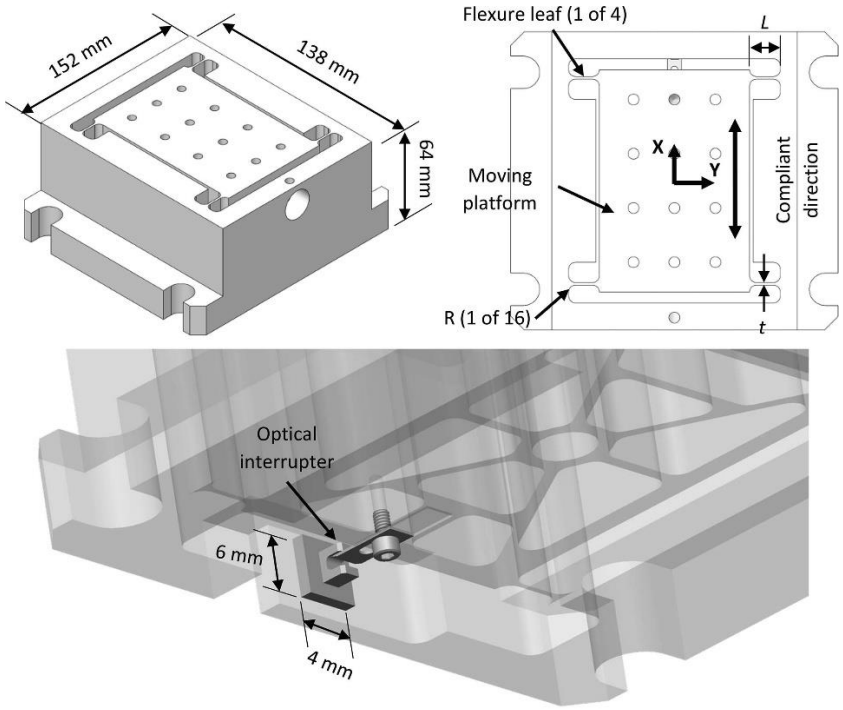


Figure 3.1. CMD design and optical interrupter placement [50].

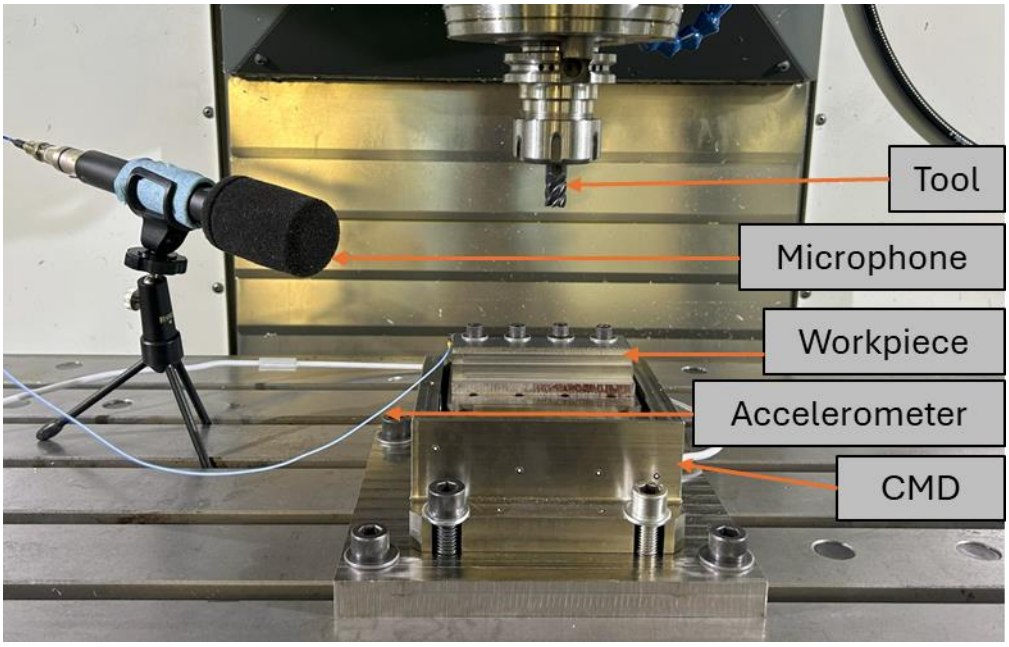


Figure 3.2. The standard experimental setup showing the tool, microphone position, workpiece, accelerometer, and the CMD.

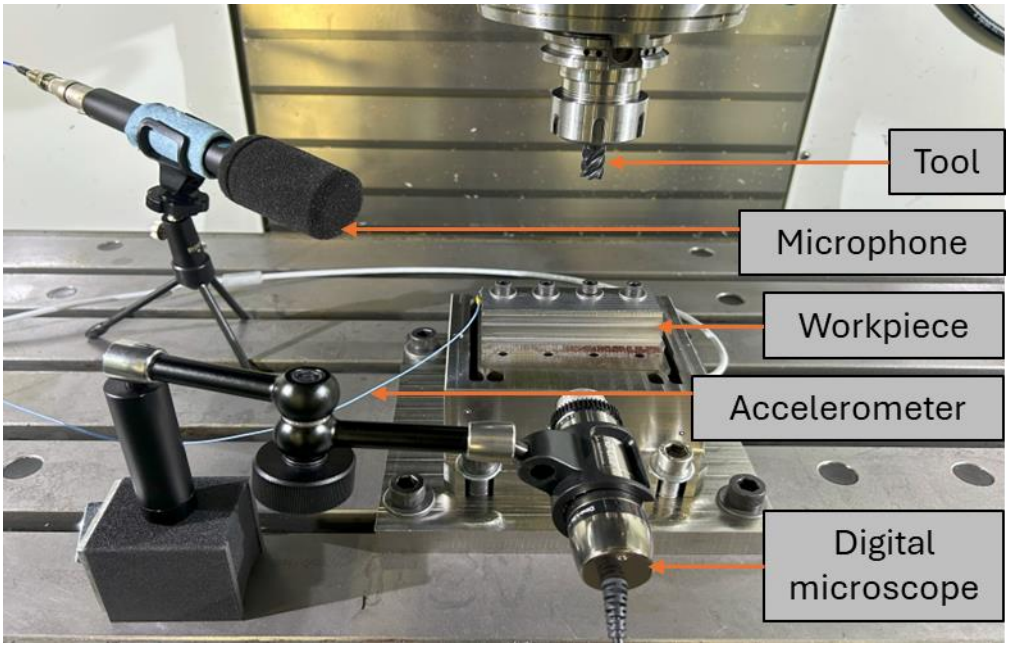


Figure 3.3. The standard experimental setup with the Dino-lite Edge digital microscope positioned in front of the workpiece.

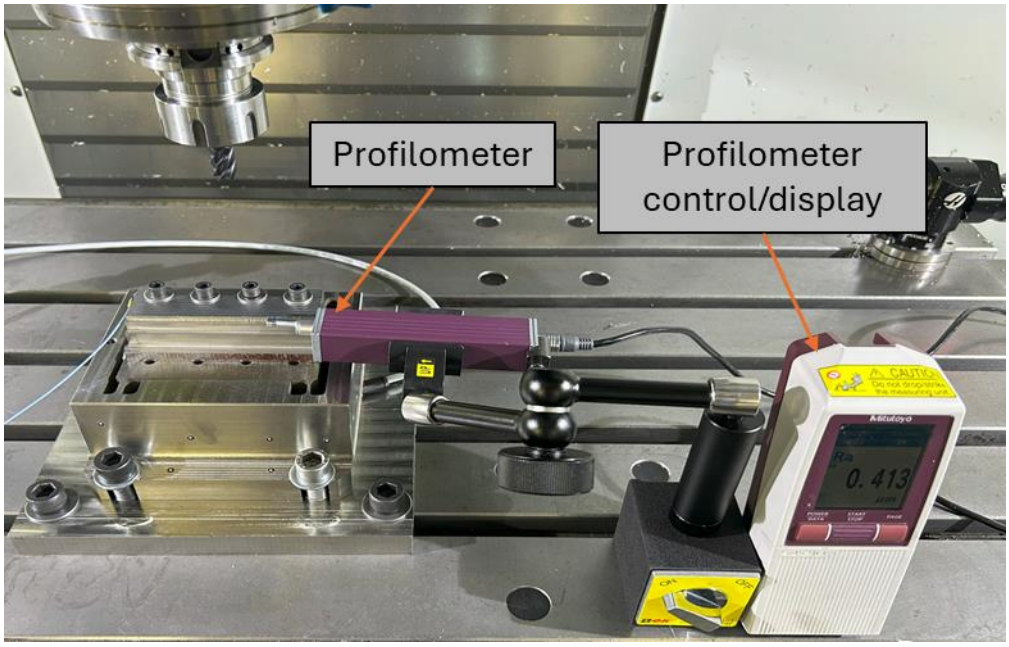


Figure 3.4. The standard experimental setup with the Mitutoyo SJ-210 profilometer positioned on the cut surface of the workpiece.

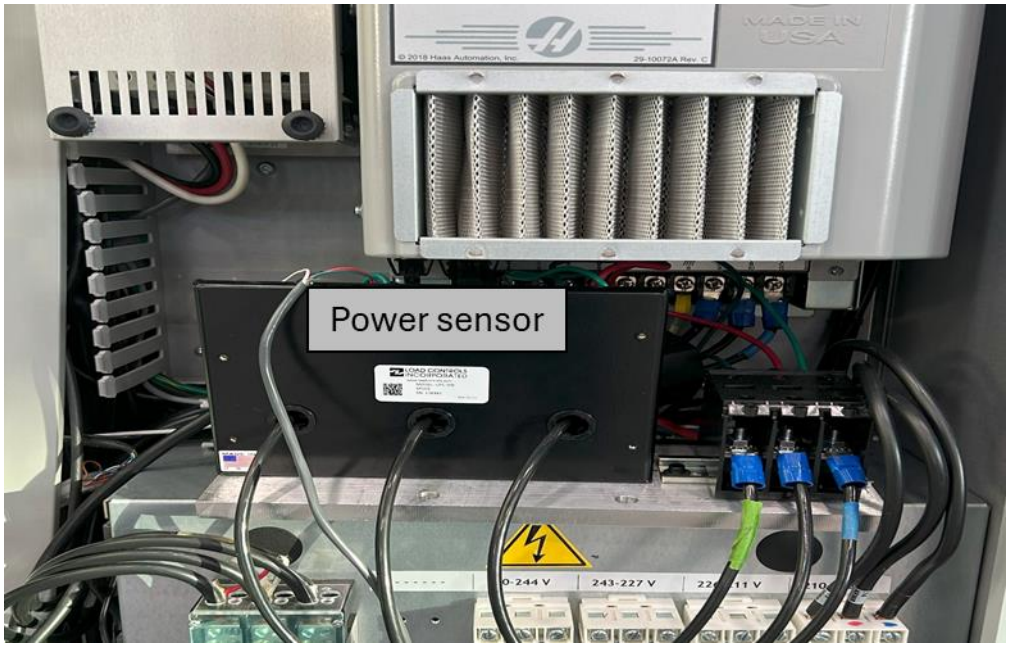


Figure 3.5. The power sensor connected to the spindle motor's three-phase input cables.



Figure 3.6. The MetalMax data acquisition device.



Figure 3.7. The National Instruments data acquisition device.

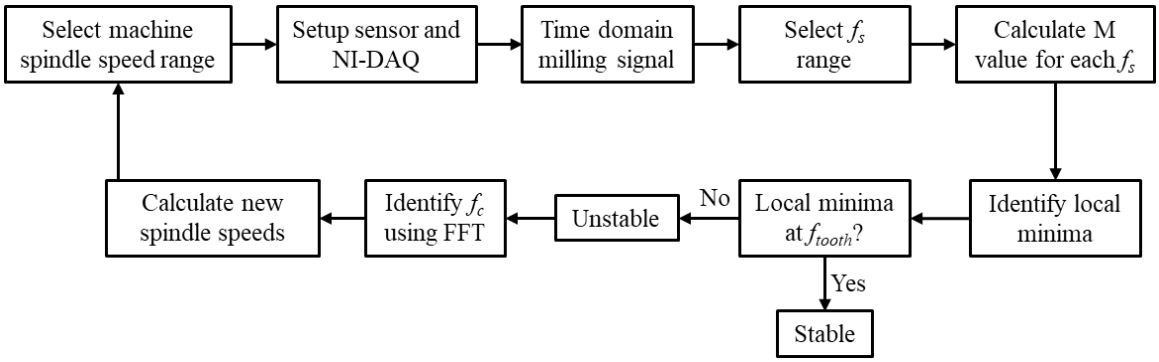


Figure 3.8. The algorithm for the in situ, low-latency chatter detection and spindle speed selection MATLAB code for closed loop application.

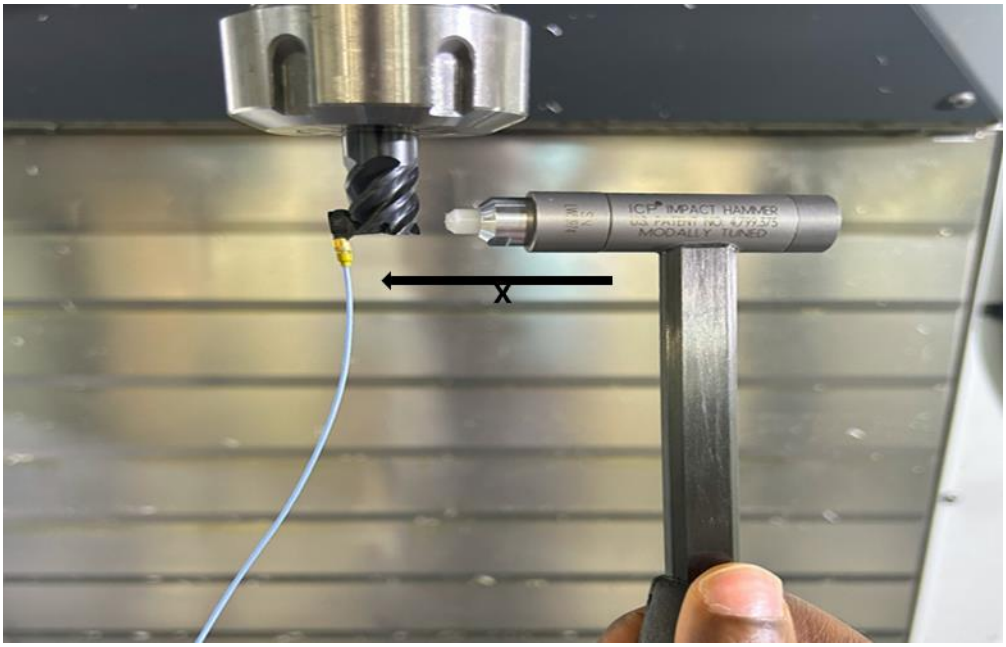


Figure 3.9. A typical tap testing scenario to measure the tool tip modal parameters in the x direction.

CHAPTER FOUR

RESULTS AND DISCUSSION

Stable, Marginal, and Unstable Cuts

Unstable cut: Two-flute endmill on 6061-T6 aluminum.

Results from tap testing and an unstable experimental cut using two-flute carbide endmill on 6061-T6 aluminum are presented below. **Tables 4.1** and **4.2** show the modal parameters of the tool tip and workpiece respectively, obtained after tap testing, while **Figures 4.1** and **4.2** show the frequency response function and the stability lobe diagram obtained using the modal parameters. A tangential force coefficient of 824.2 N/mm^2 and a normal force coefficient of 225.5 N/mm^2 for 6061-T6 aluminum [50] are selected. A radial depth of cut of 3 mm is selected, and an unstable point corresponding to a spindle speed of 5550 rpm and an axial depth of cut of 8 mm is selected on the stability lobe diagram, which achieves an unstable cut.

Results from the time domain milling signals of the displacement (x), the acceleration (a), and the sound pressure (p) are presented, including, the total time interval of each signal, the magnified time interval, magnitude plot of the frequency content, and the variation in the M value with the periodic sampling frequency, f_s. The variation in the M value with the periodic sampling frequency is the main plot which validates the hypothesis of the novel chatter detection method, thereby validating chatter detection by periodic sampling of time domain milling signals. The hypothesis is that for stable cutting conditions, a local minimum in the stability metric occurs at the tooth passing frequency, f_{tooth}, while for unstable cutting conditions, a local minimum in the stability metric occurs at or near

the chatter frequency, f_c. Also, the M value is less at stable cutting conditions than at unstable cutting conditions, for the same experimental setup (tool and workpiece combination).

Figures 4.3, **4.7**, and **4.11** show the total time interval of the cut from the CMD, the accelerometer, and the microphone milling signals respectively. **Figures 4.4**, **4.8**, and **4.12** show the magnified time interval of the cut from the CMD, the accelerometer, and the microphone milling signals respectively. **Figures 4.5**, **4.9**, and **4.13** show the magnitude plots of the frequency contents from the CMD, the accelerometer, and the microphone milling signals respectively. It is observed that the chatter frequency, f_c, has the highest peak in the magnitude plots, indicating an unstable cut. **Figures 4.6**, **4.10**, and **4.14** show the variations in the M values with the periodic sampling frequency of the time domain milling signals from the CMD, the accelerometer, and the microphone respectively. It is observed that local minima in the stability metric occur at the chatter frequency, f_c, and its subharmonics, not at the tooth passing frequency, f_{tooth}, thereby indicating an unstable cut.

Figure 4.15 shows the surface of the workpiece with visible chatter marks after the unstable cut, captured using the Dino-Lite digital microscope. Surface roughness measurements were conducted at six different locations on the cut surface using the Mitutoyo profilometer, yielding a mean Ra value of 1.32 µm with a standard deviation of 0.244 µm, a mean Rq value of 1.56 µm with a standard deviation of 0.295 µm, and a mean Rz value of 6.15 µm with a standard deviation of 1.254 µm. **Table 4.3** shows the Ra, Rq, and Rz values for the six measured locations.

Table 4.1. Tool tip modal parameters for the two-flute endmill.

***x*-direction**		
Frequency, f_n (Hz)	**Stiffness, k (N/m)**	**Damping ratio, ζ (-)**
173	1.83×10^8	0.0555
475	2.30×10^8	0.1035
937	1.57×10^8	0.1066
1409	1.30×10^8	0.1313
1509	1.23×10^8	0.0212
3528	2.41×10^8	0.0956
4478	1.18×10^9	0.0208
5385	2.31×10^8	0.0625
9453	6.66×10^7	0.0446
***y*-direction**		
Frequency, f_n (Hz)	**Stiffness, k (N/m)**	**Damping ratio, ζ (-)**
956	3.36×10^8	0.0328
1287	5.44×10^7	0.1478
1544	1.05×10^9	0.0188
1758	4.81×10^8	0.0225
3342	3.81×10^8	0.0669
5390	2.25×10^8	0.0656
9412	6.35×10^7	0.0460

Table 4.2. Workpiece modal parameters of the 6061-T6 aluminum workpiece before the unstable cut.

***x*-direction**		
Frequency, f_n (Hz)	**Stiffness, k (N/m)**	**Damping ratio, ζ (-)**
788	2.06×10^7	0.0080
***y*-direction**		
Frequency, f_n (Hz)	**Stiffness, k (N/m)**	**Damping ratio, ζ (-)**
2027	4.36×10^9	0.0111
2505	1.86×10^9	0.0181
3004	3.28×10^8	0.0158
3192	7.02×10^8	0.0087
3244	1.47×10^9	0.0048
3422	2.87×10^9	0.0072
3987	1.07×10^9	0.0328
4650	1.10×10^9	0.0178
5403	1.18×10^9	0.0217
8079	1.65×10^9	0.0249

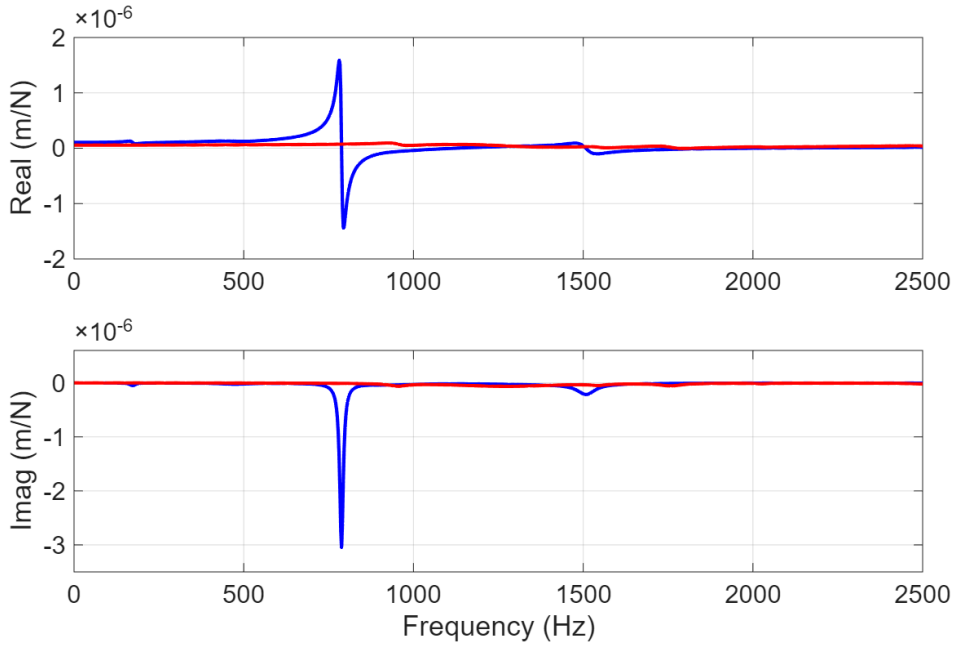


Figure 4.1. Tool tip and workpiece, *x* (blue lines) and *y* (red lines) directions, frequency response function.

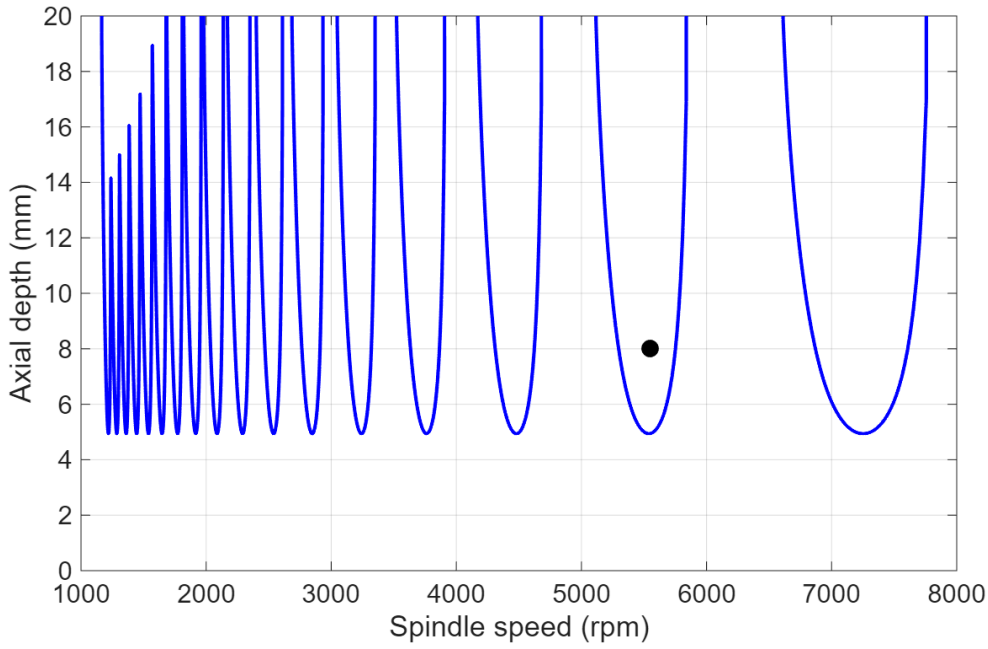


Figure 4.2. Stability lobe diagram with the selected point (black dot) at an unstable region corresponding to a spindle speed of 5550 rpm and an axial depth of cut of 8 mm.

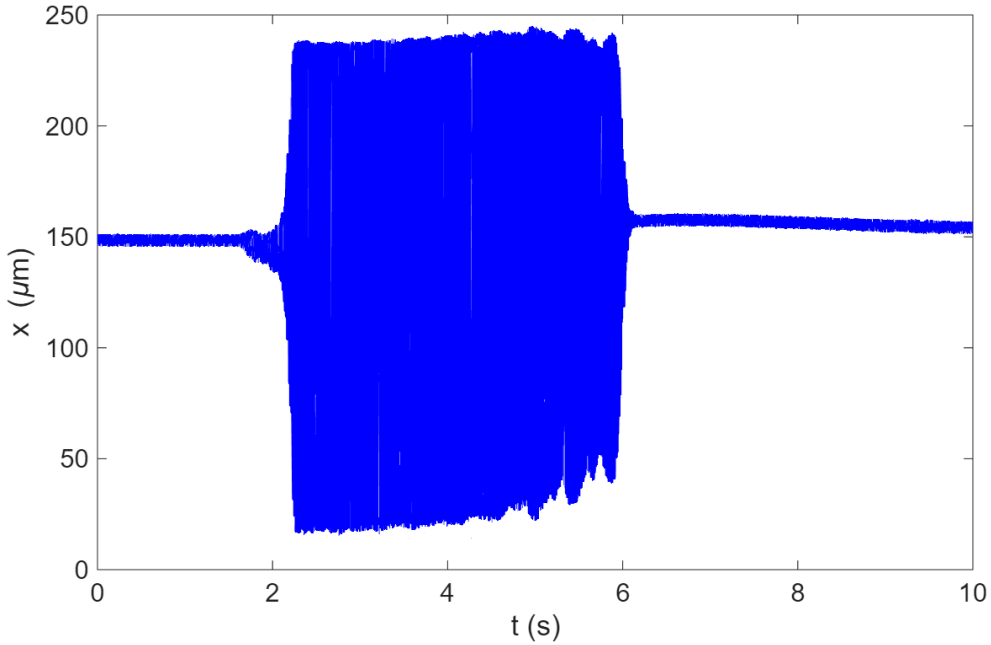


Figure 4.3: The total time interval of the signal from the CMD (displacement signal) showing when the tool interacts with the workpiece.

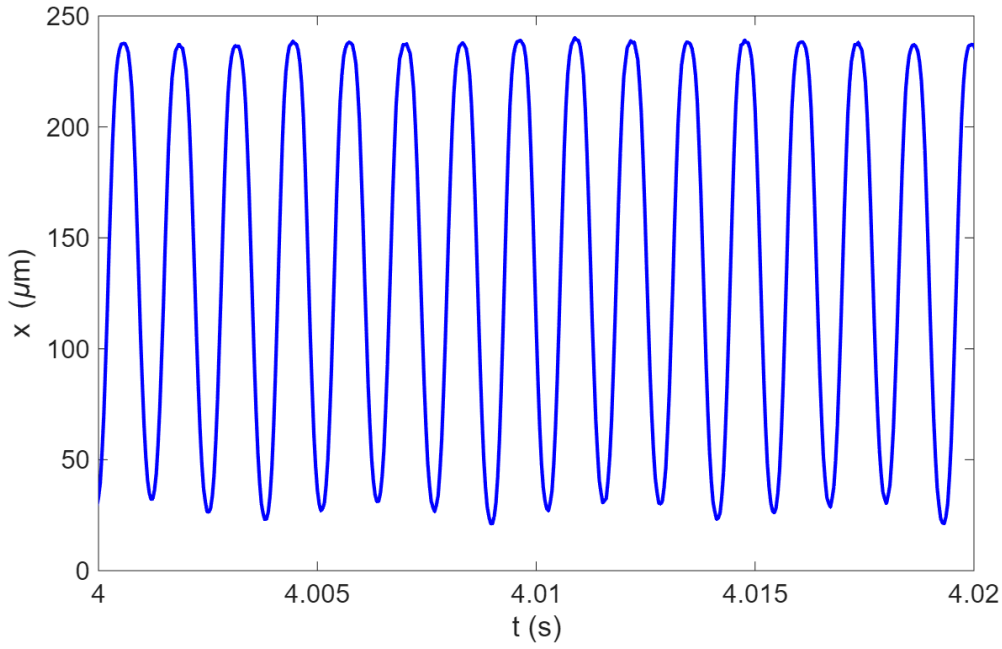


Figure 4.4: The magnified time interval of the signal from the CMD (displacement signal).

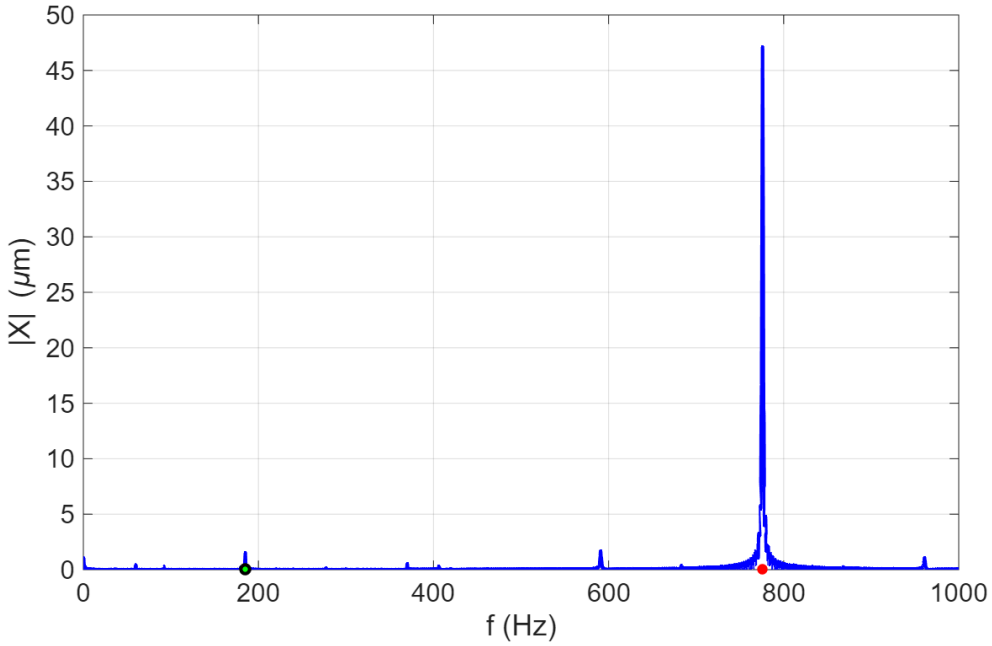


Figure 4.5: Magnitude plot of *x* frequency content for 150 rotations, with f_c (red dot) identified at 776 Hz and f_{tooth} (black circle) at 185 Hz.

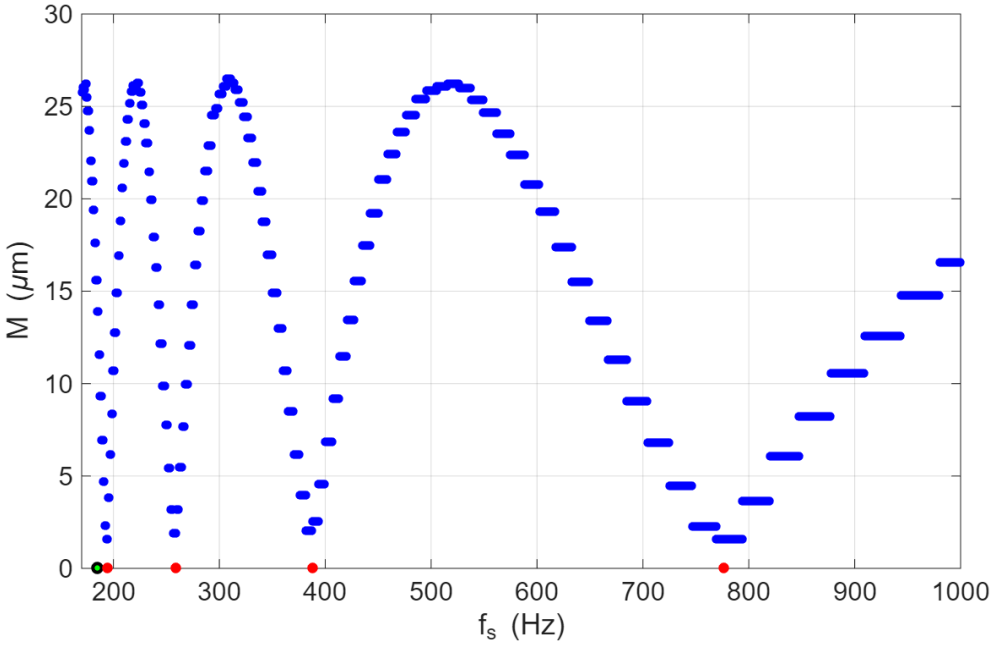


Figure 4.6: Variation in *M* value with periodic f_s. Local minima occur at f_c of 776 Hz (red dot) where M = 1.6 µm, and at f_c subharmonics (red dots), not at f_{tooth} (black circle).

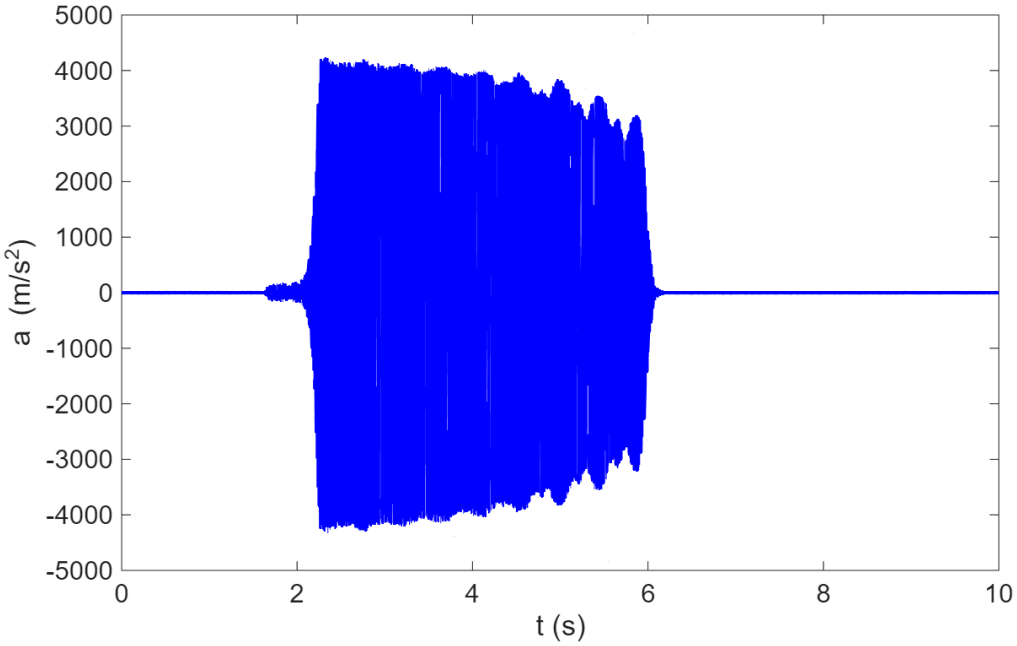


Figure 4.7: The total time interval of the signal from the accelerometer (acceleration signal) showing when the tool interacts with the workpiece.

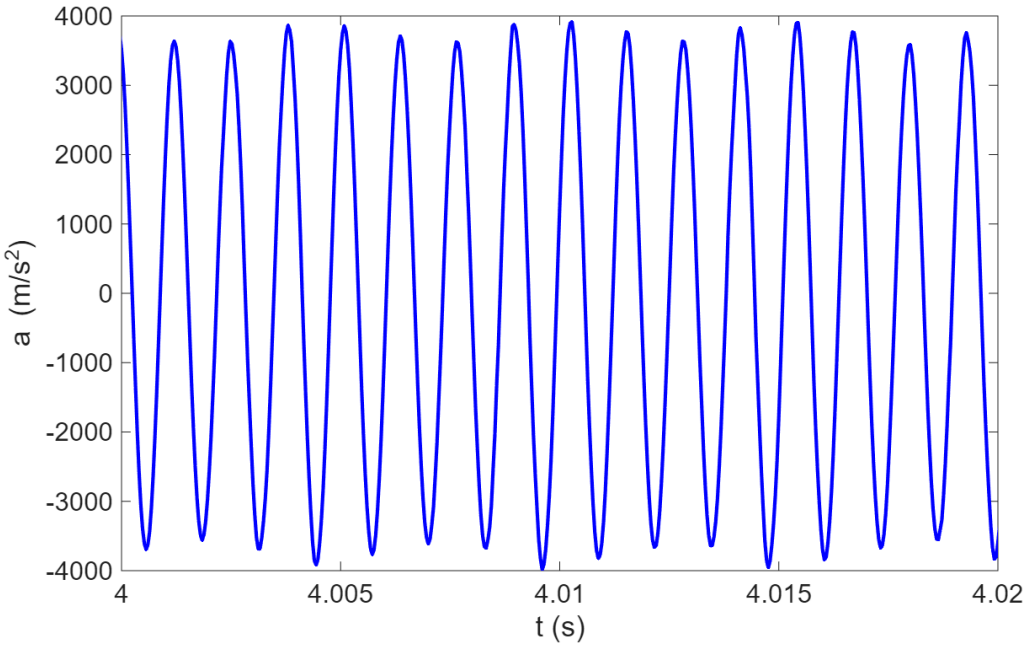


Figure 4.8: The magnified time interval of the signal from the accelerometer (acceleration).

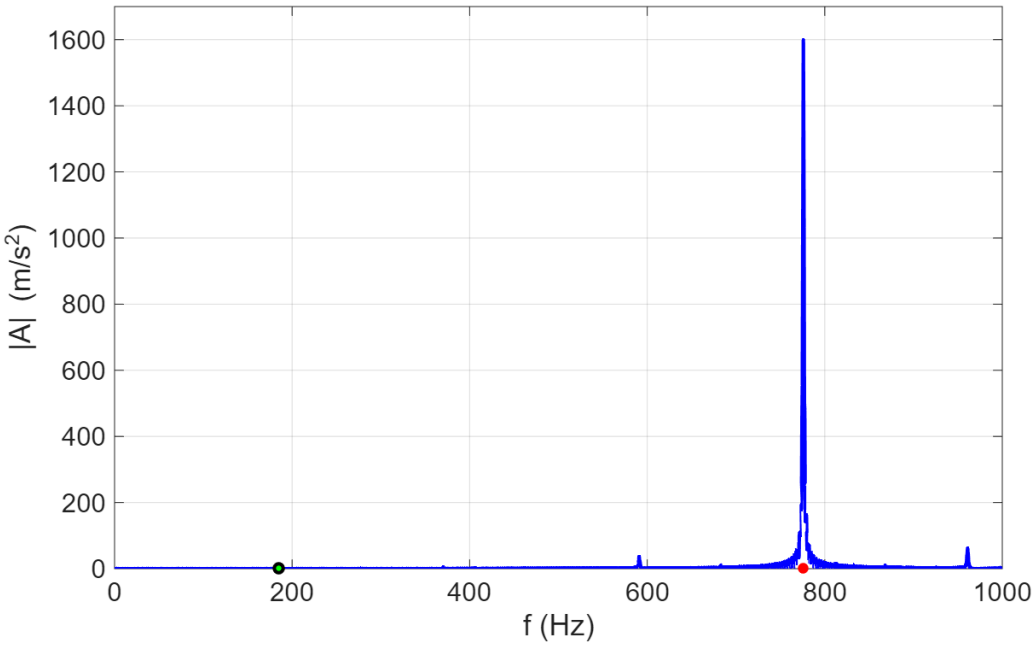


Figure 4.9: Magnitude plot of *a* frequency content for 150 rotations, with f_c (red dot) identified at 776 Hz and f_{tooth} (black circle) at 185 Hz.

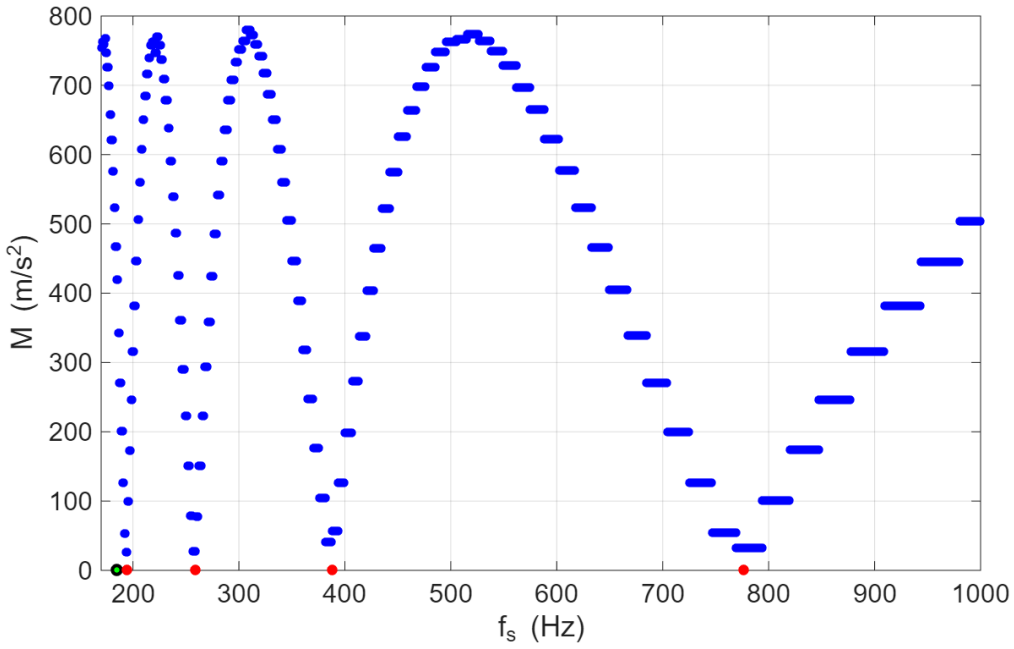


Figure 4.10: Variation in *M* value with periodic f_s. Local minima occur at f_c of 776 Hz (red dot) where M = 32 m/s^2, and at f_c subharmonics (red dots), not at f_{tooth} (black circle).

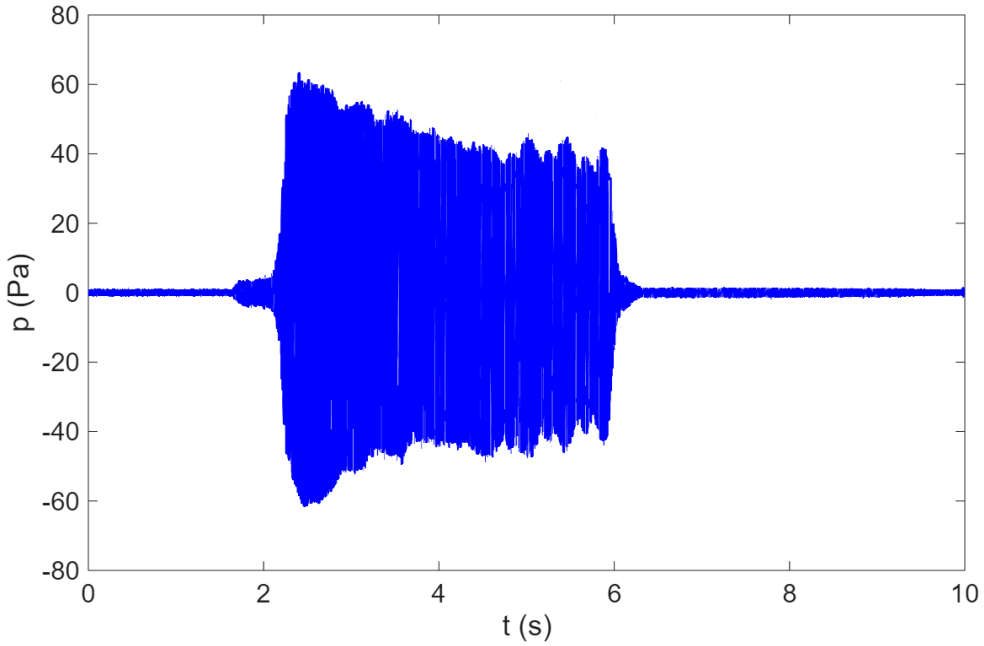


Figure 4.11: The total time interval of the signal from the microphone (sound pressure signal) showing when the tool interacts with the workpiece.

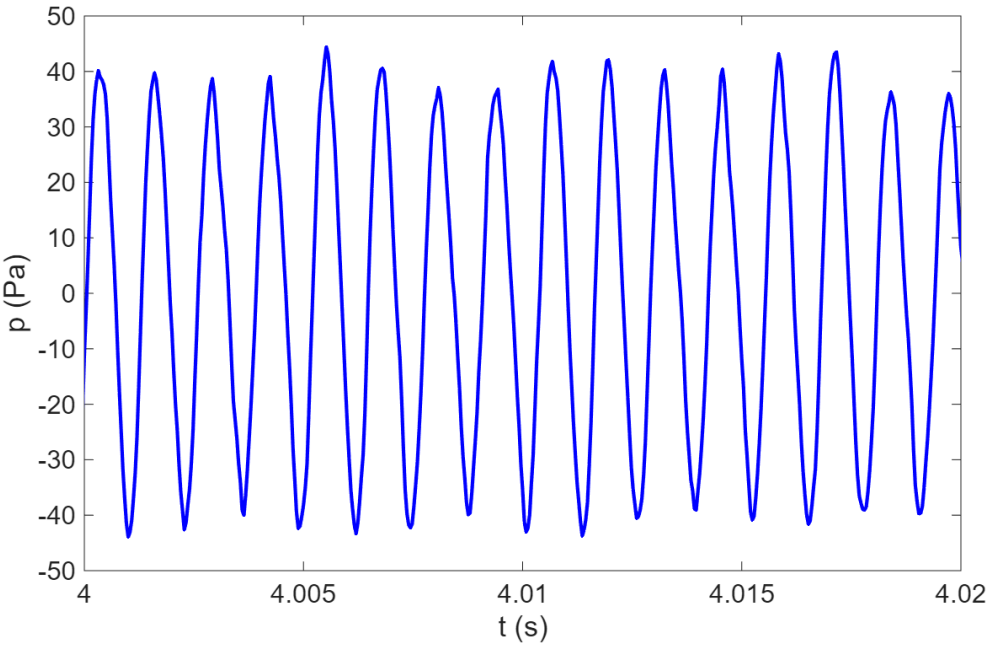


Figure 4.12: The magnified time interval of the signal from the microphone (sound pressure).

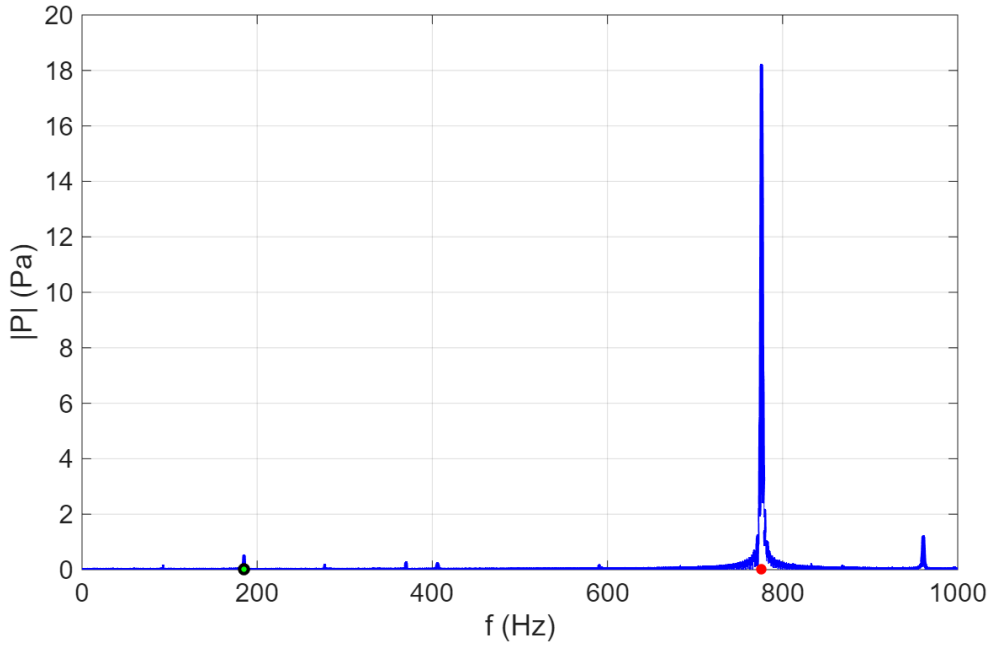


Figure 4.13: Magnitude plot of p frequency content for 150 rotations, with f_c (red dot) identified at 776 Hz and f_{tooth} (black circle) at 185 Hz.

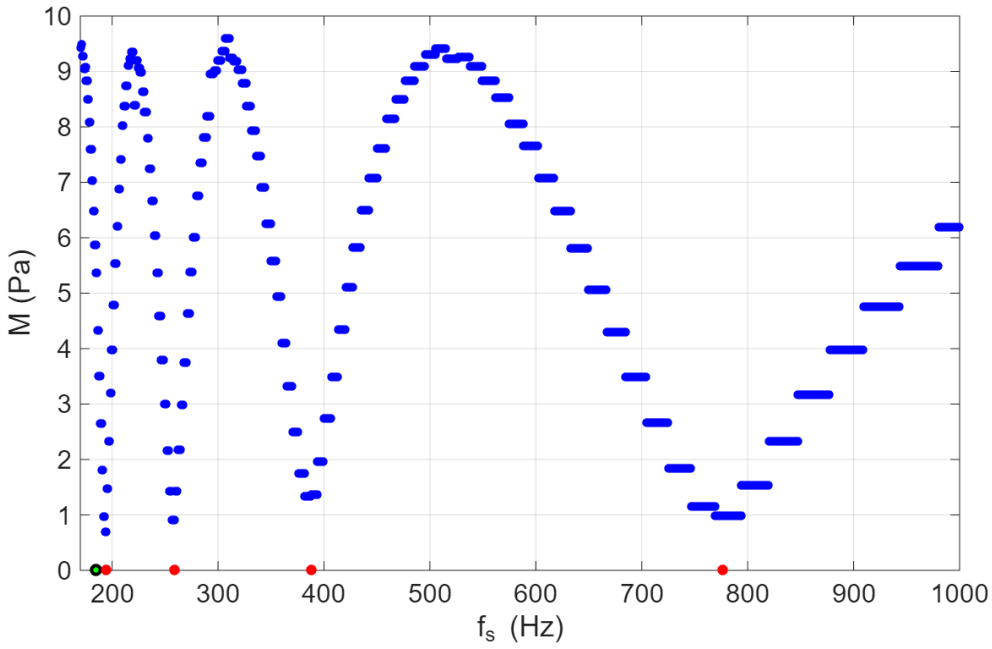


Figure 4.14: Variation in M value with periodic f_s. Local minima occur at f_c of 776 Hz (red dot) where M = 0.99 Pa, and at f_c subharmonics (red dots), not at f_{tooth} (black circle).

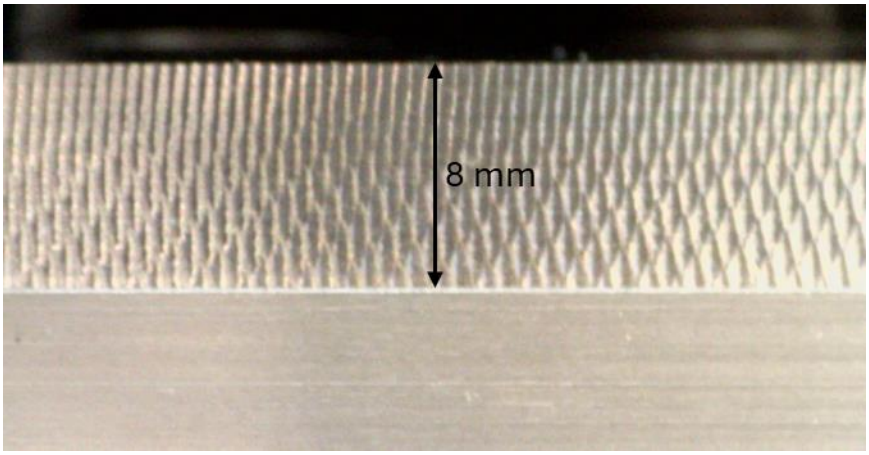


Figure 4.15: Surface of the aluminum 6061-T6 workpiece with visible chatter marks after the unstable cut.

Marginally unstable cut: Two-flute endmill on 6061-T6 aluminum.

Results from tap testing and a marginally unstable experimental cut using two-flute carbide endmill on 6061-T6 aluminum are presented below. **Table 4.4** shows the modal parameters of the workpiece obtained after tap testing. The tool tip modal parameters presented in **Table 4.1** are retained because, unlike the workpiece which experiences a reduction in mass after cutting, the tool remains unchanged from the previous experimental cut upon inspection.

Table 4.3. Profilometer results from six measured locations on the unstable cut surface of the 6061-T6 aluminum.

Location	Ra (μm)	Rq (μm)	Rz (μm)
1	0.95	1.158	4.722
2	1.491	1.710	6.337
3	1.276	1.460	5.617
4	1.365	1.592	6.183
5	1.651	2.029	8.434
6	1.184	1.419	5.620

Figures 4.16 and **4.17** show the frequency response function and the stability lobe diagram obtained using the modal parameters. A tangential force coefficient of 824.2 N/mm^2 and a normal force coefficient of 225.5 N/mm^2 for 6061-T6 aluminum are selected. A radial depth of cut of 3 mm is selected, and a marginally unstable point corresponding to a spindle speed of 5450 rpm and an axial depth of cut of 6.28 mm is selected on the stability lobe diagram, which achieves a marginally unstable cut. Results from the time domain milling signals of the displacement (x), the acceleration (a), and the sound pressure (p) are presented, including, the total time interval of each signal, the magnified time interval, magnitude plot of the frequency content, and the variation in the M value with the periodic sampling frequency, f_s, thereby validating chatter detection by periodic sampling of time domain milling signals.

Figures 4.18, **4.22**, and **4.26** show the total time interval of the cut from the CMD, the accelerometer, and the microphone milling signals respectively. **Figures 4.19**, **4.23**, and **4.27** show the magnified time interval of the cut from the CMD, the accelerometer, and the microphone milling signals respectively. **Figures 4.20**, **4.24**, and **4.28** show the magnitude plots of the frequency contents from the CMD, the accelerometer, and the microphone milling signals respectively. It is observed that the chatter frequency, f_c, has the highest peak in the magnitude plots, indicating an unstable cut. **Figures 4.21**, **4.25**, and **4.29** show the variations in the M values with the periodic sampling frequency of the time domain milling signals from the CMD, the accelerometer, and the microphone respectively. It is observed that local minima in the stability metric occur at the chatter frequency, f_c, and its subharmonics, not at the tooth passing frequency, f_{tooth}, thereby

indicating an unstable cut. It is also observed that the *M* values from the local minima occurring at f_c are less than those recorded in the previous cut.

Figure 4.30 shows the surface of the workpiece with visible chatter marks after the cut, although less extreme than the previous cut. Surface roughness measurements were conducted at six different locations on the cut surface, yielding a mean Ra value of 0.73 µm with a standard deviation of 0.160 µm, a mean Rq value of 0.87 µm with a standard deviation of 0.170 µm, and a mean Rz value of 3.83 µm with a standard deviation of 0.593 µm. **Table 4.5** shows the Ra, Rq, and Rz values for the six measured locations.

Table 4.4. Workpiece modal parameters of the 6061-T6 aluminum before the marginal cut.

***x*-direction**		
Frequency, f_n (Hz)	**Stiffness, *k* (N/m)**	**Damping ratio, ζ (-)**
781	1.13×10^7	0.0155
***y*-direction**		
Frequency, f_n (Hz)	**Stiffness, *k* (N/m)**	**Damping ratio, ζ (-)**
2512	1.30×10^9	0.0241
3021	3.60×10^8	0.0129
3252	2.51×10^8	0.0130
4717	1.11×10^9	0.0122
5416	1.95×10^9	0.0094
8231	3.57×10^9	0.0135
9237	1.66×10^9	0.0297
10202	4.47×10^9	0.0179

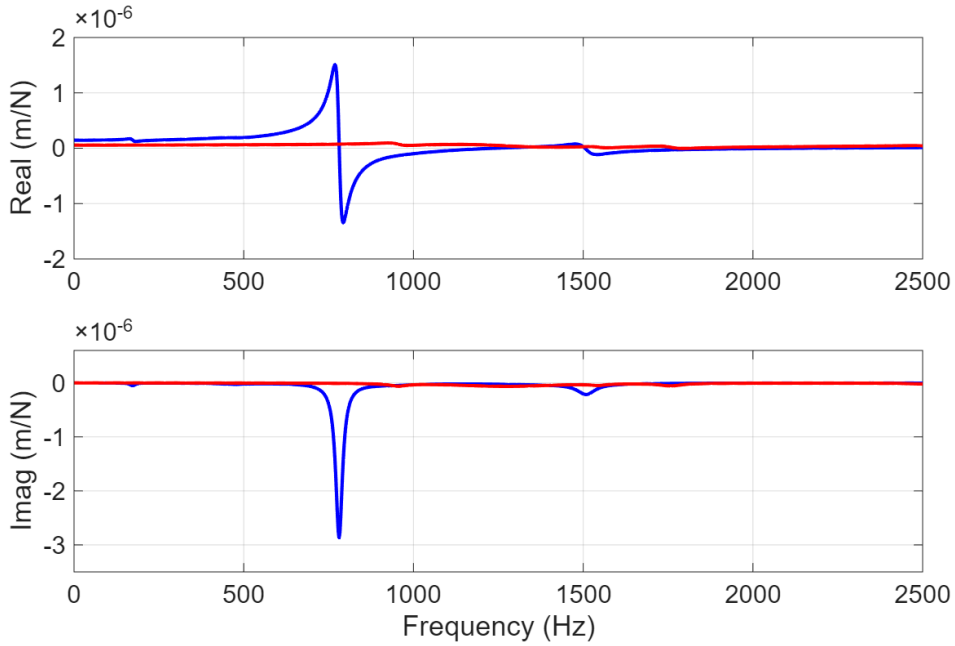


Figure 4.16: Tool tip and workpiece, *x* (blue lines) and *y* (red lines) directions, frequency response function.

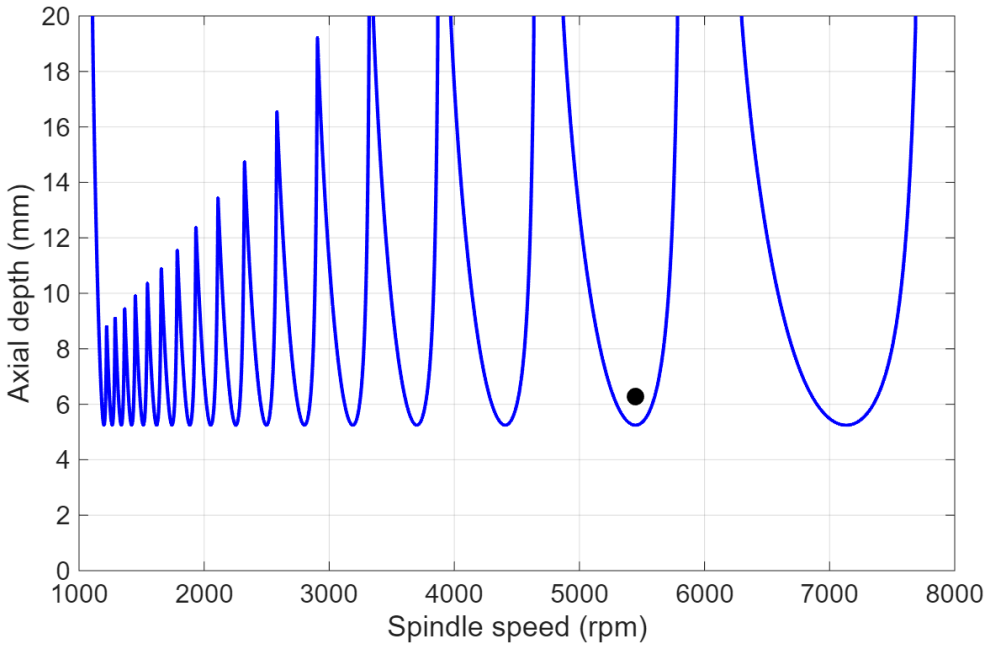


Figure 4.17. Stability lobe diagram with the selected marginally unstable point (black dot) corresponding to a spindle speed of 5450 rpm and axial depth of cut of 6.28 mm.

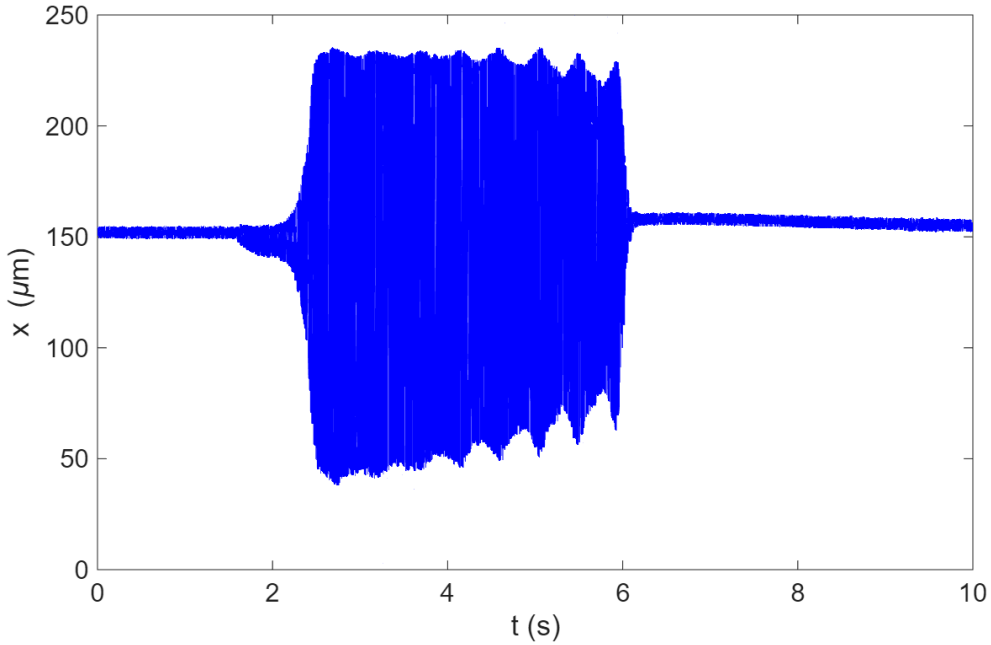


Figure 4.18: The total time interval of the signal from the CMD (displacement signal) showing when the tool interacts with the workpiece.

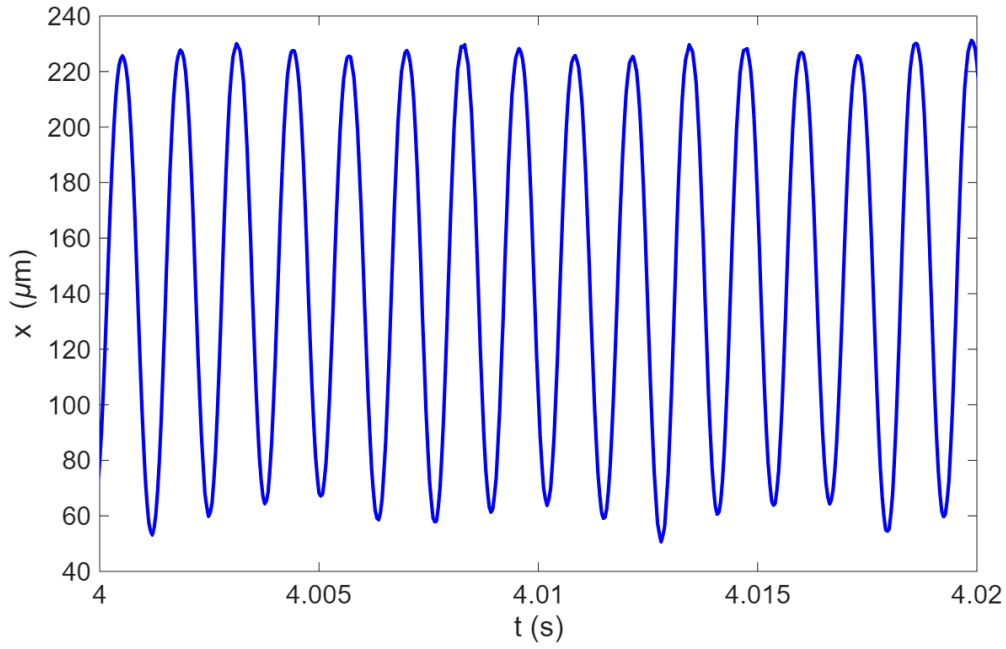


Figure 4.19: The magnified time interval of the signal from the CMD (displacement signal).

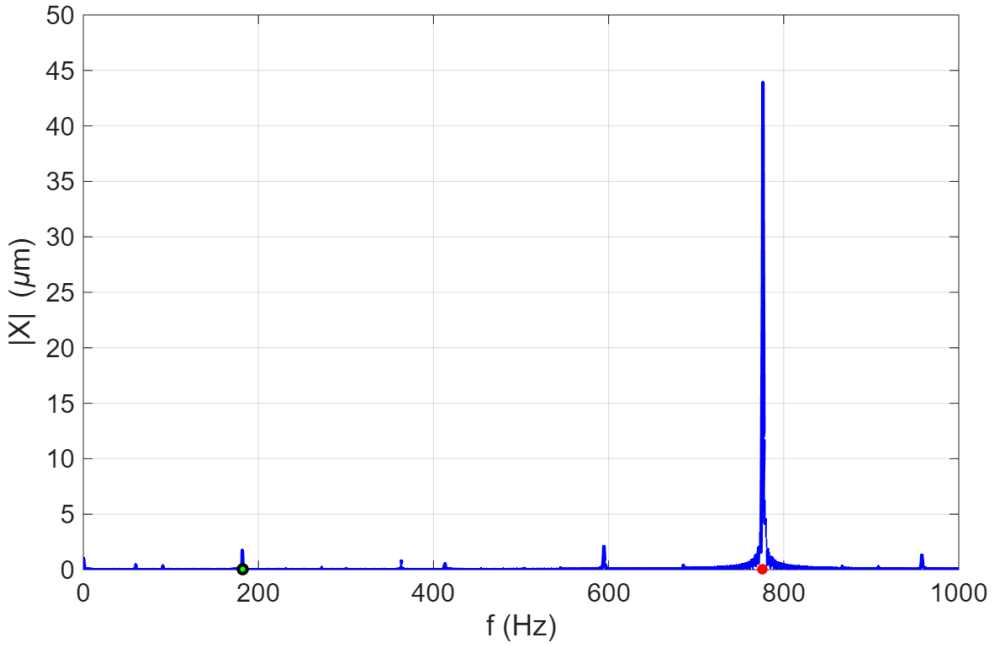


Figure 4.20: Magnitude plot of *x* frequency content for 150 rotations, with f_c (red dot) identified at 776 Hz and f_{tooth} (black circle) at 182 Hz.

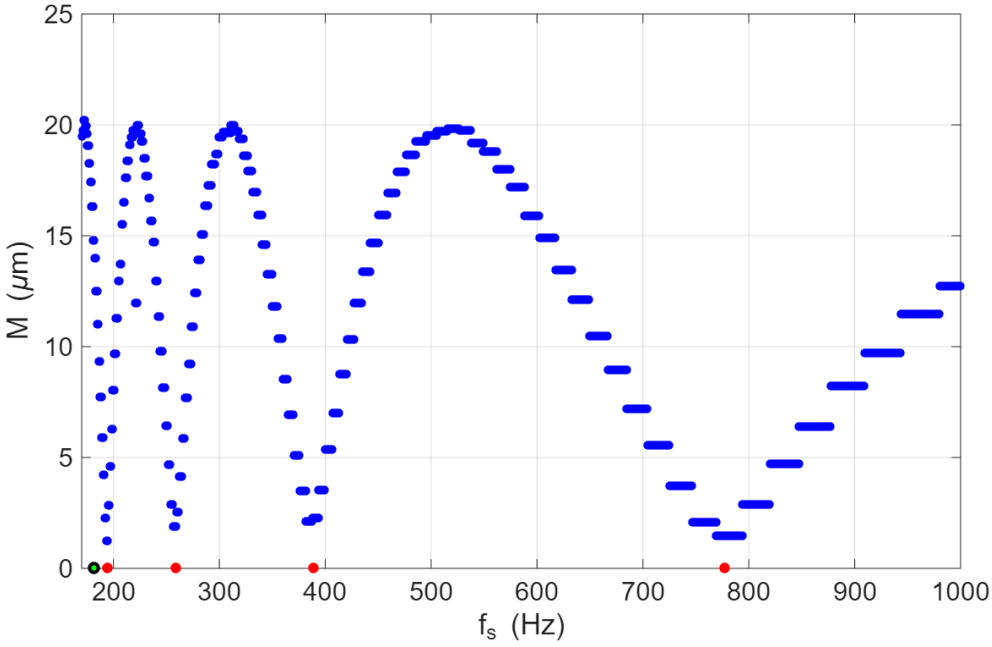


Figure 4.21: Variation in *M* value with periodic f_s. Local minima occur at f_c of 776 Hz (red dot) where M = 1.5 µm, and at f_c subharmonics (red dots), not at f_{tooth} (black circle).

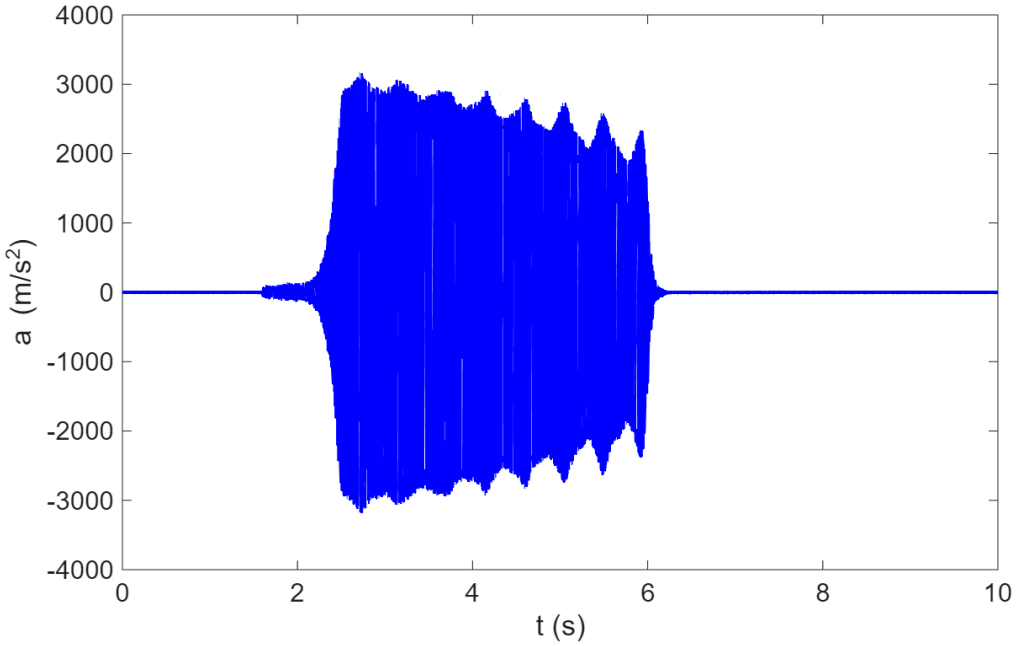


Figure 4.22: The total time interval of the signal from the accelerometer (acceleration signal) showing when the tool interacts with the workpiece.

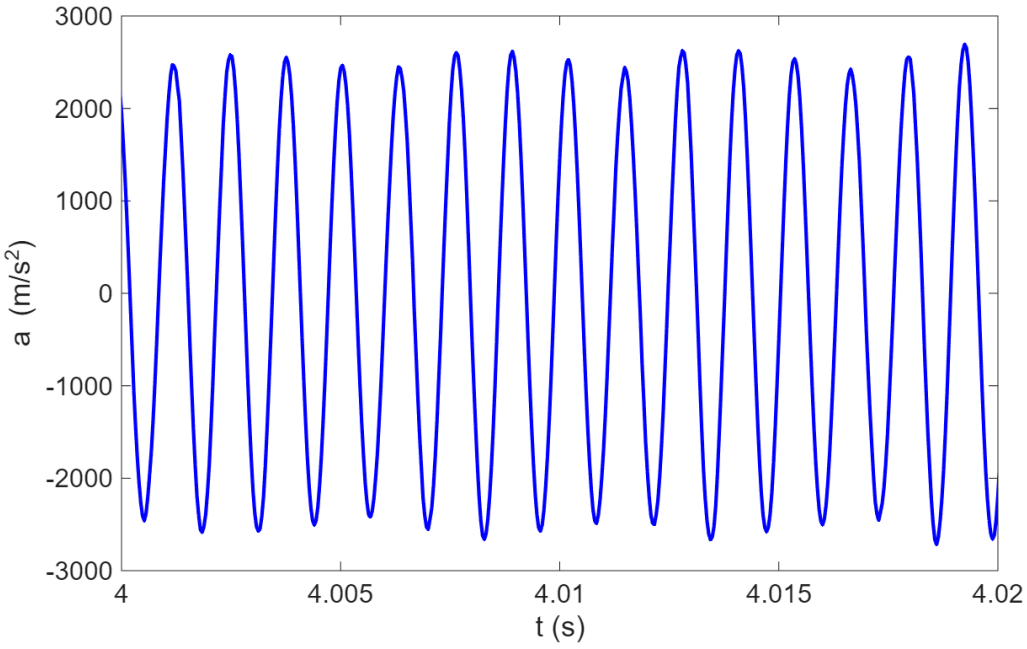


Figure 4.23: The magnified time interval of the signal from the accelerometer (acceleration).

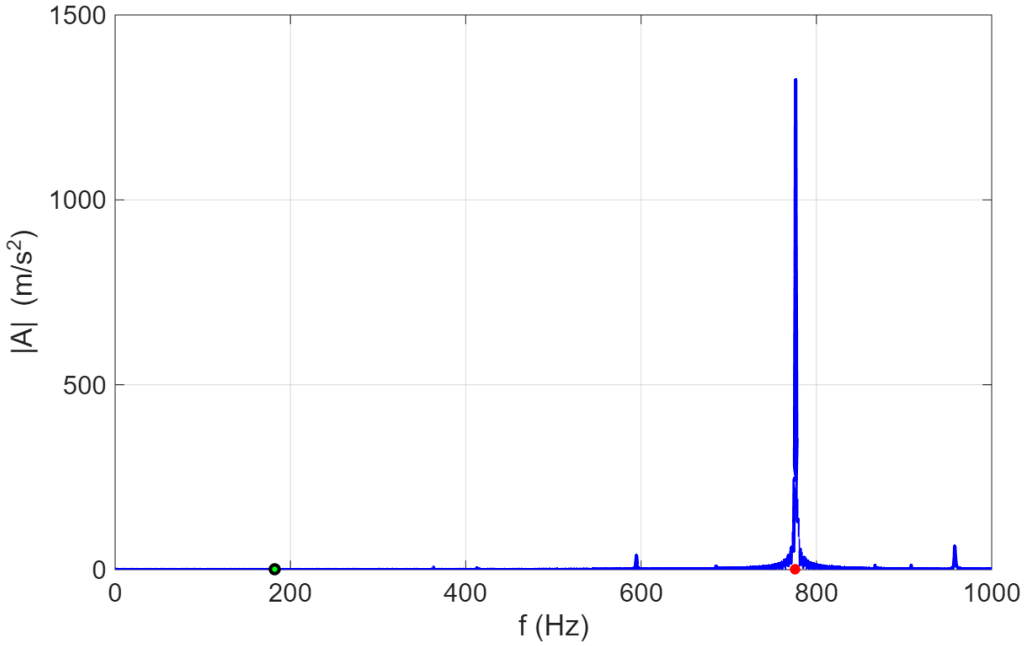


Figure 4.24: Magnitude plot of *a* frequency content for 150 rotations, with f_c (red dot) identified at 776 Hz and f_{tooth} (black circle) at 182 Hz.

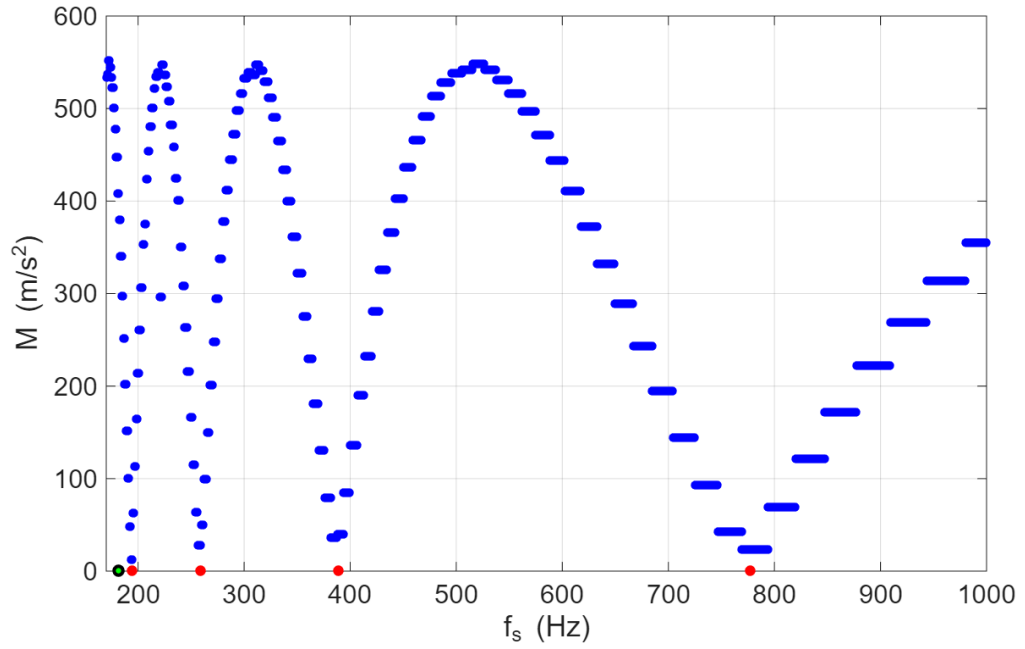


Figure 4.25: Variation in *M* value with periodic f_s. Local minima occur at f_c of 776 Hz (red dot) where M = 23 m/s^2, and at f_c subharmonics (red dots), not at f_{tooth} (black circle).

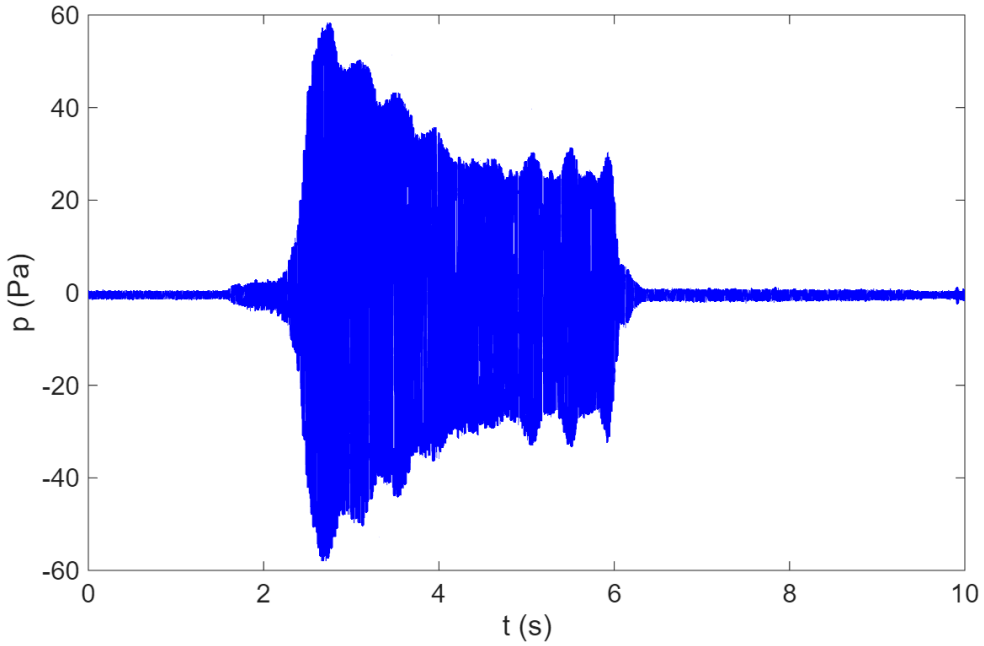


Figure 4.26: The total time interval of the signal from the microphone (sound pressure signal) showing when the tool interacts with the workpiece.

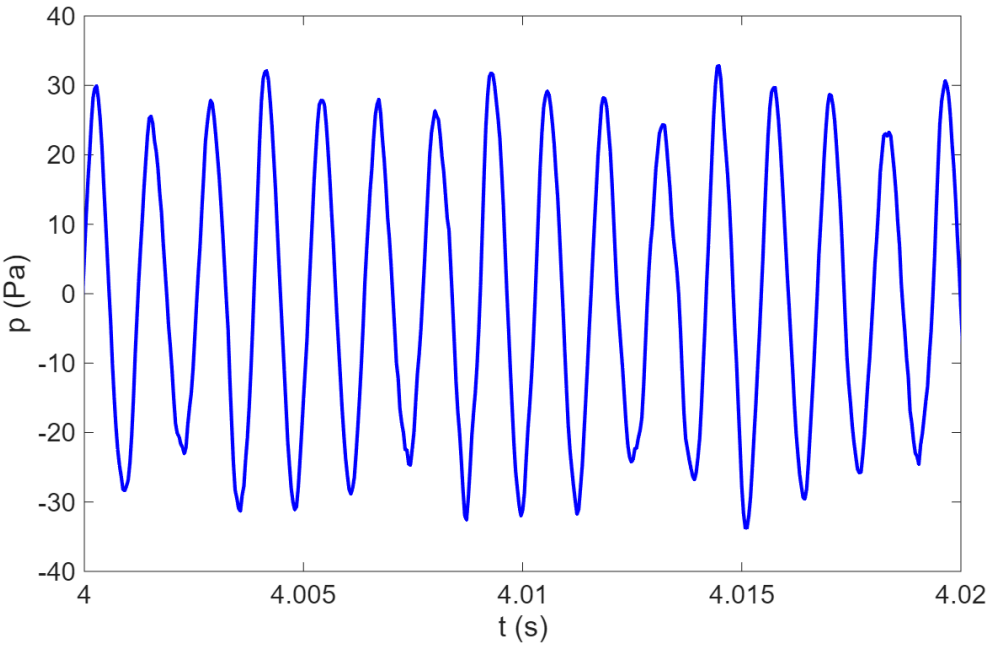


Figure 4.27: The magnified time interval of the signal from the microphone (sound pressure).

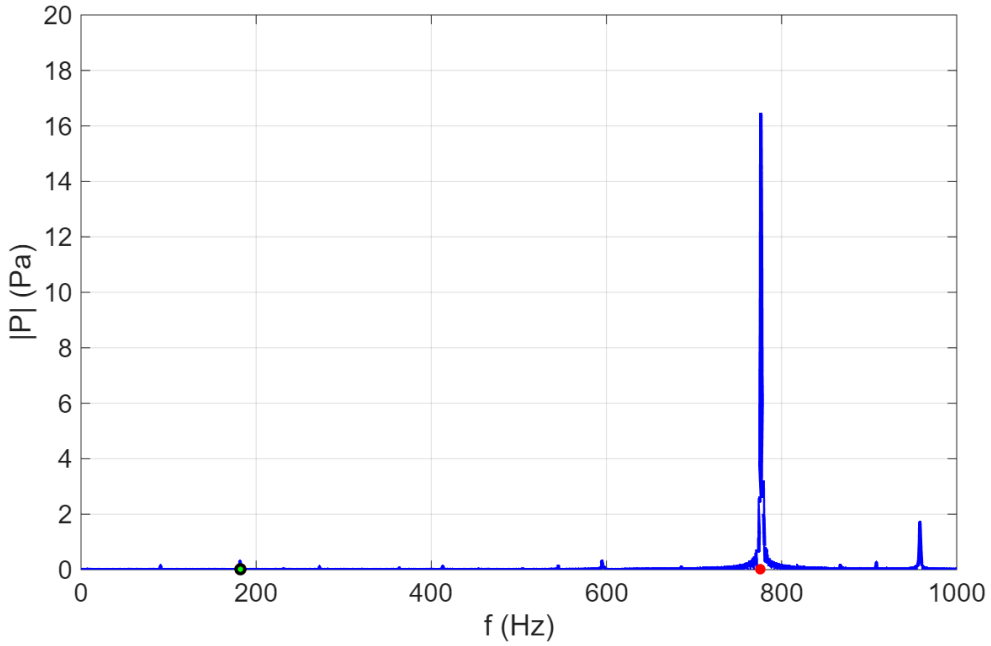


Figure 4.28: Magnitude plot of p frequency content for 150 rotations, with f_c (red dot) identified at 776 Hz and f_{tooth} (black circle) at 182 Hz.

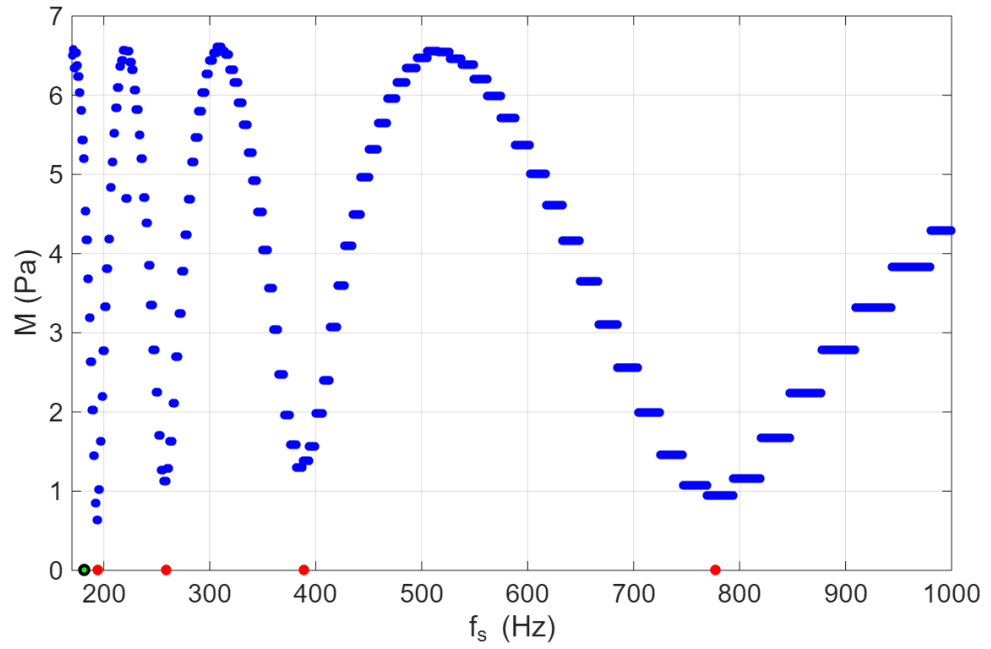


Figure 4.29: Variation in M value with periodic f_s. Local minima occur at f_c of 776 Hz (red dot) where M = 0.94 Pa, and at f_c subharmonics (red dots), not at f_{tooth} (black circle).

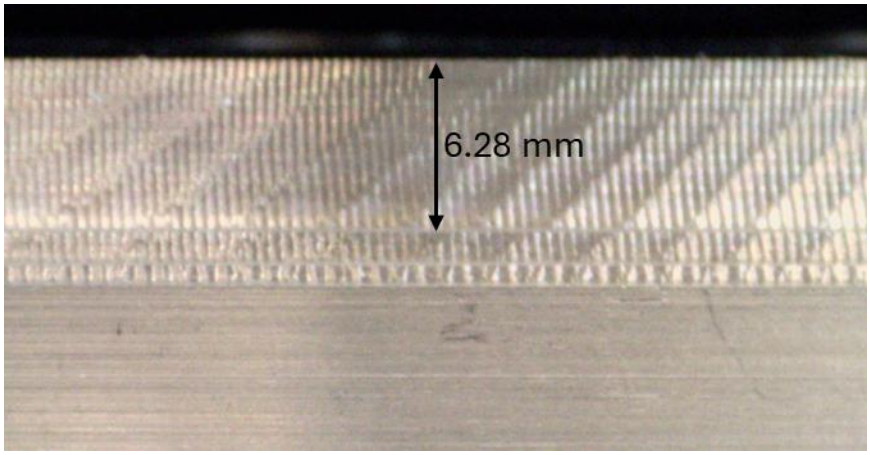


Figure 4.30: Surface of the aluminum 6061-T6 workpiece with visible chatter marks after the marginally unstable cut.

Stable cut: Two-flute endmill on 6061-T6 aluminum.

Results from tap testing and a stable experimental cut using two-flute carbide endmill on 6061-T6 aluminum are presented below. **Table 4.6** shows the modal parameters of the workpiece obtained after tap testing. The tool tip modal parameters presented in **Table 4.1** are retained because, unlike the workpiece which experiences a reduction in mass after cutting, the tool remains unchanged from the previous experimental cut upon inspection.

Table 4.5. Profilometer results from six measured locations on the marginally unstable cut surface of the 6061-T6 aluminum.

Location	Ra (μm)	Rq (μm)	Rz (μm)
1	0.764	0.915	3.961
2	0.703	0.865	4.077
3	0.730	0.891	4.401
4	0.592	0.710	2.818
5	1.007	1.156	4.278
6	0.555	0.684	3.468

Figures 4.31 and **4.32** show the frequency response function and the stability lobe diagram obtained using the modal parameters. A tangential force coefficient of 824.2 N/mm^2 and a normal force coefficient of 225.5 N/mm^2 for 6061-T6 aluminum are selected. A radial depth of cut of 3 mm is selected, and a stable point corresponding to a spindle speed of 6200 rpm and an axial depth of cut of 8 mm is selected on the stability lobe diagram, which achieves a stable cut.

Results from the time domain milling signals of the displacement (x), the acceleration (a), and the sound pressure (p) are presented, including, the total time interval of each signal, the magnified time interval, magnitude plot of the frequency content, and the variation in the M value with the periodic sampling frequency, f_s.

Figures 4.33, **4.37**, and **4.41** show the total time interval of the cut from the CMD, the accelerometer, and the microphone milling signals respectively. **Figures 4.34**, **4.38**, and **4.42** show the magnified time interval of the cut from the CMD, the accelerometer, and the microphone milling signals respectively. It is observed that the milling signal from the CMD is faint, however, the signal is able to accurately validate the stability of the cut.

Figures 4.35, **4.39**, and **4.43** show the magnitude plots of the frequency contents from the CMD, the accelerometer, and the microphone milling signals respectively. It is observed that the tooth passing frequency, f_{tooth}, or its harmonic in the case of the acceleration signal, has the highest peak in the magnitude plots, indicating a stable cut. **Figures 4.36**, **4.40**, and **4.44** show the variations in the M values with the periodic sampling frequency of the time domain milling signals from the CMD, the accelerometer, and the microphone respectively. It is observed that a local minimum in the stability metric occurs at the tooth

passing frequency, f_{tooth}, thereby indicating a stable cut. In the case of the acceleration milling signal, local minima occur at f_{tooth}, its harmonic, and near a runout frequency. The hypothesis that, for stable cutting conditions, a local minimum in the stability metric occurs at the tooth passing frequency, f_{tooth}, while for unstable cutting conditions, a local minimum in the stability metric occurs at or near the chatter frequency, f_c, remains valid. It is also observed that the M values from the local minima occurring at f_{tooth} are less than those recorded in the previous cut.

Figure 4.45 shows the surface of the workpiece after the cut, with no chatter marks. Surface roughness measurements were conducted at six different locations on the cut surface, yielding a mean Ra value of 0.28 µm with a standard deviation of 0.092 µm, a mean Rq value of 0.34 µm with a standard deviation of 0.105 µm, and a mean Rz value of 1.60 µm with a standard deviation of 0.471 µm. **Table 4.7** shows the Ra, Rq, and Rz values for the six measured locations.

Table 4.6. Workpiece modal parameters of the 6061-T6 aluminum before the stable cut.

***x*-direction**		
Frequency, f_n (Hz)	**Stiffness, k (N/m)**	**Damping ratio, ζ (-)**
783	1.29×10^7	0.0155
***y*-direction**		
Frequency, f_n (Hz)	**Stiffness, k (N/m)**	**Damping ratio, ζ (-)**
2511	1.50×10^9	0.0250
3025	4.85×10^8	0.0121
3257	2.70×10^8	0.0130
4720	1.09×10^9	0.0124
5422	2.60×10^9	0.0093
8234	3.81×10^9	0.0137
9471	1.15×10^9	0.0384
10234	4.83×10^9	0.0187

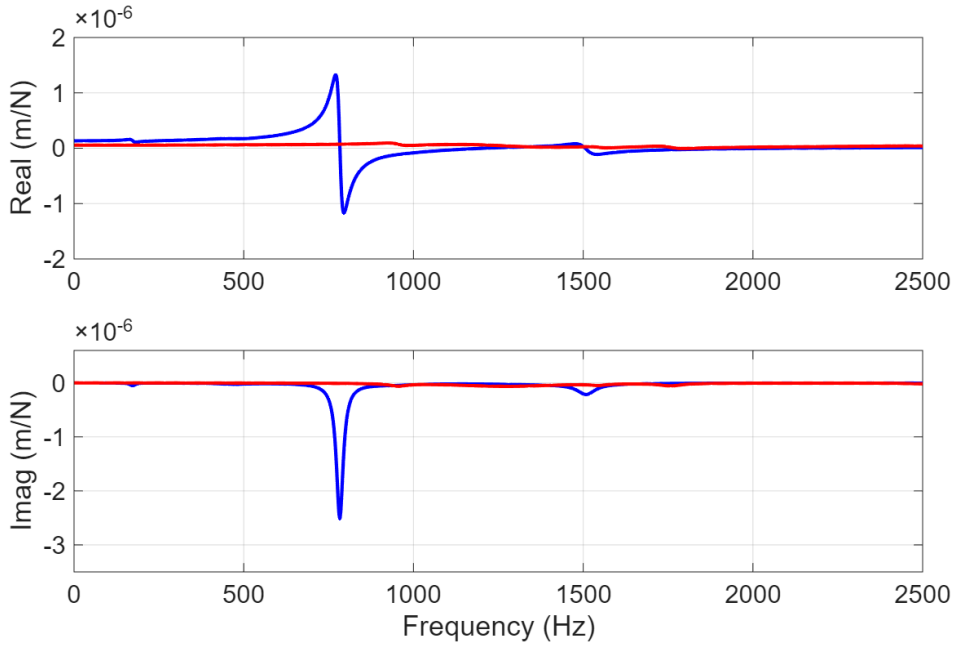


Figure 4.31: Tool tip and workpiece, *x* (blue lines) and *y* (red lines) directions, frequency response function.

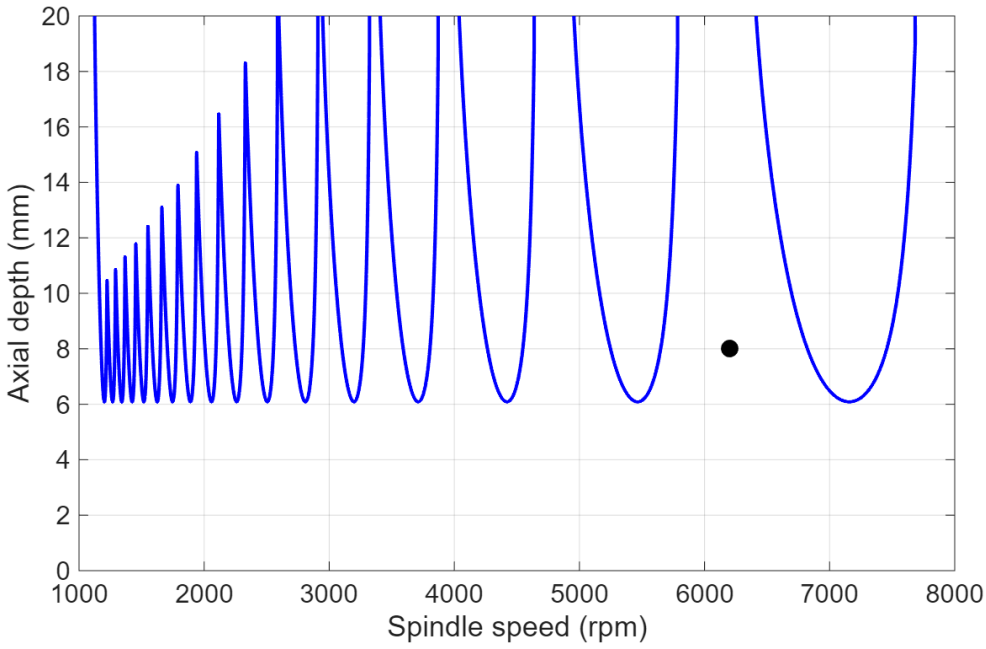


Figure 4.32: Stability lobe diagram with the selected stable point (black dot) corresponding to a spindle speed of 6200 rpm and axial depth of cut of 8 mm.

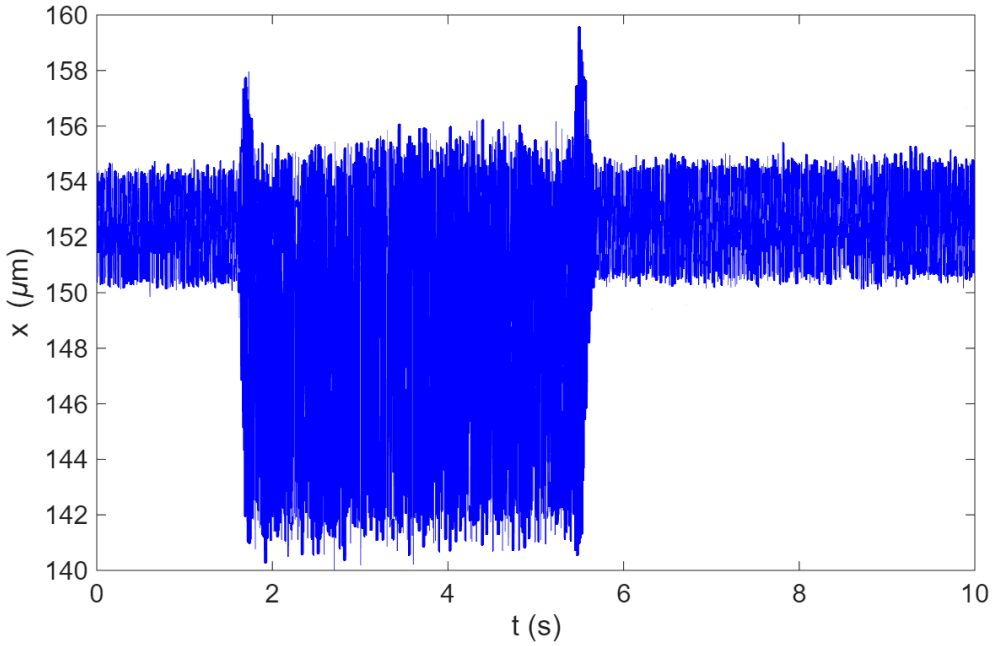


Figure 4.33: The total time interval of the signal from the CMD (displacement signal) showing when the tool interacts with the workpiece.

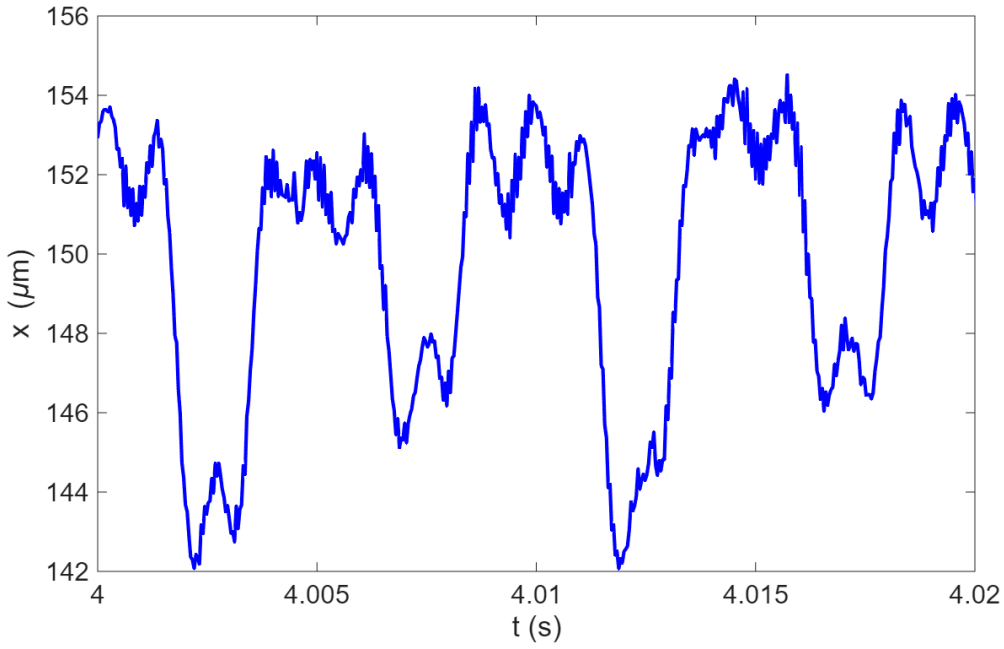


Figure 4.34: The magnified time interval of the signal from the CMD (displacement signal).

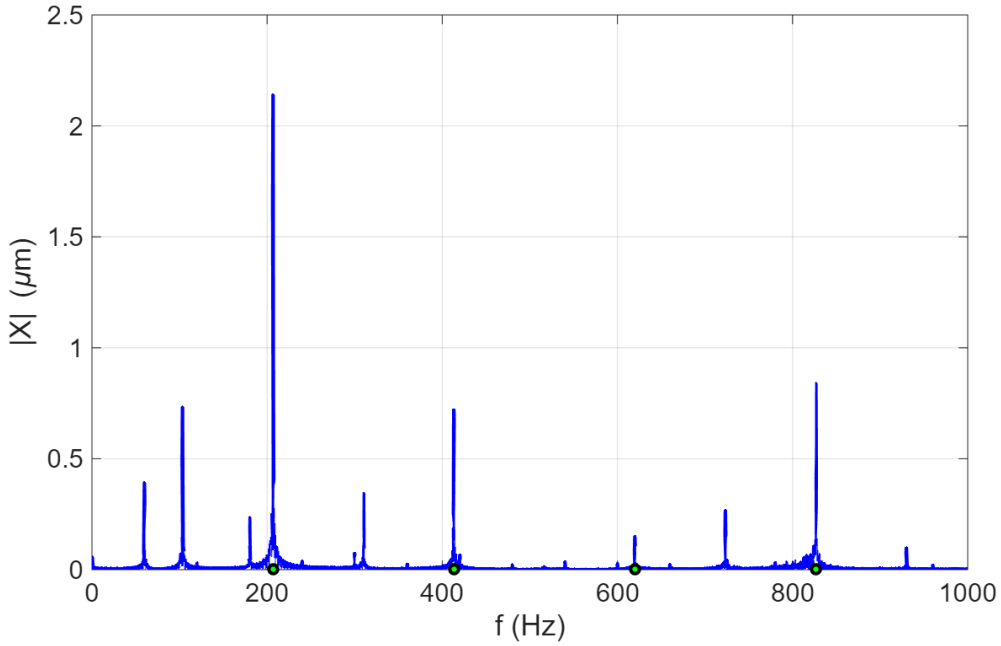


Figure 4.35: Magnitude plot of *x* frequency content for 150 rotations, with f_{tooth} at 207 Hz and its harmonics identified (black circles).

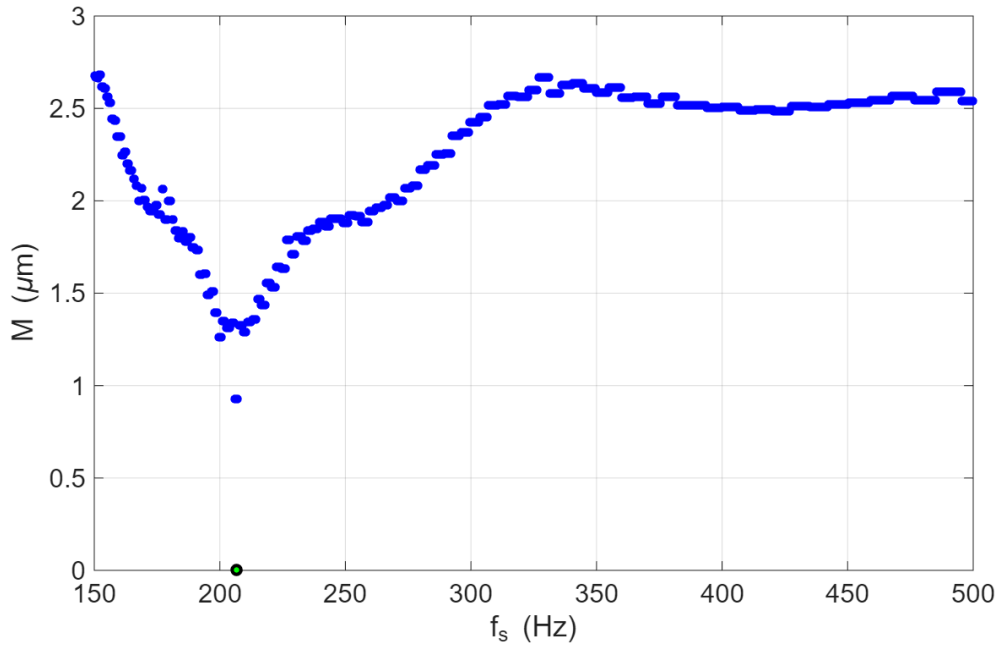


Figure 4.36: Variation in *M* value with periodic f_s. A local minimum is observed at f_{tooth} of 207 Hz (black circle) where *M* = 0.93 µm.

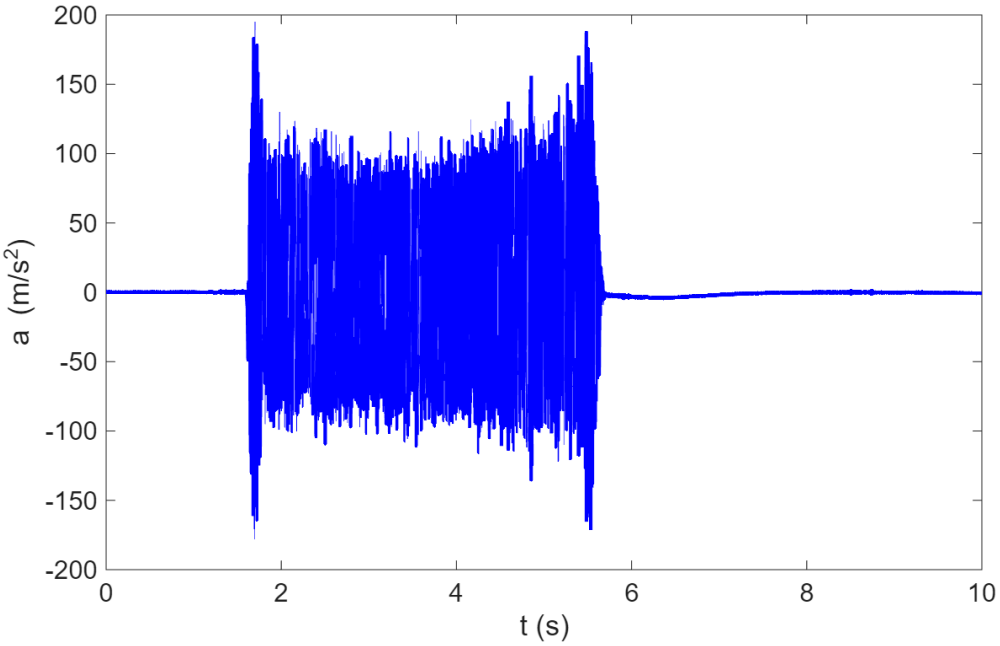


Figure 4.37: The total time interval of the signal from the accelerometer (acceleration signal) showing when the tool interacts with the workpiece.

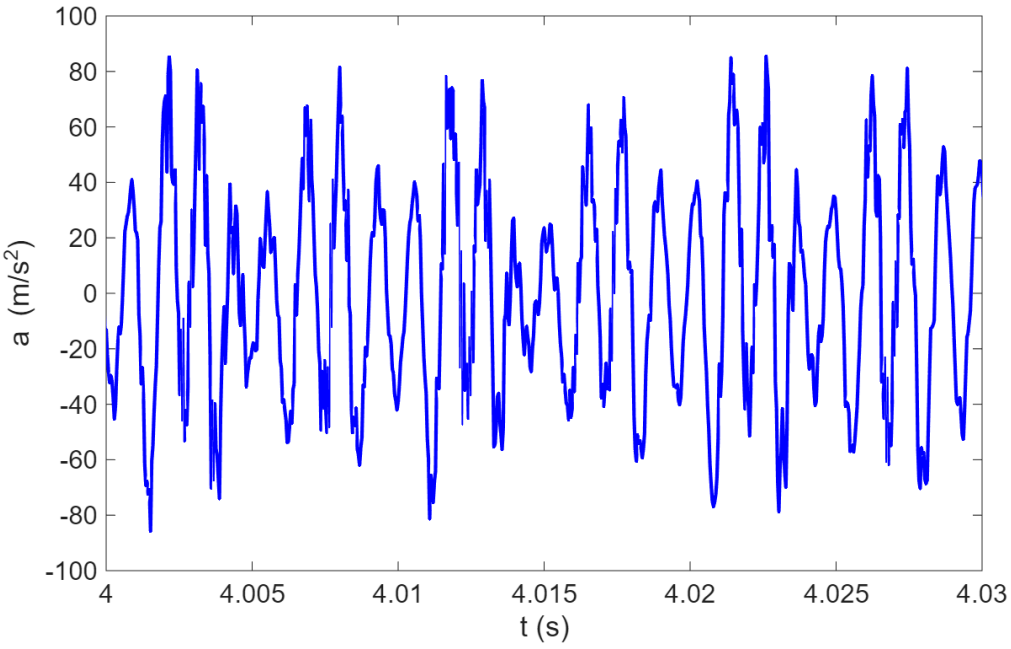


Figure 4.38: The magnified time interval of the signal from the accelerometer (acceleration).

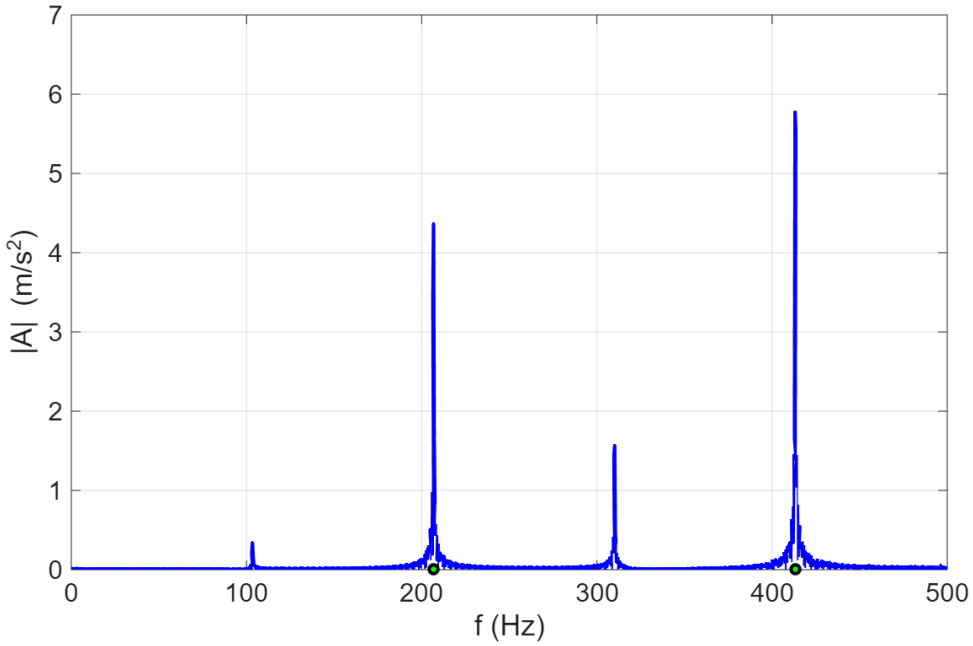


Figure 4.39: Magnitude plot of *a* frequency content for 150 rotations, with f_{tooth} at 207 Hz and its 1st harmonic identified (black circles).

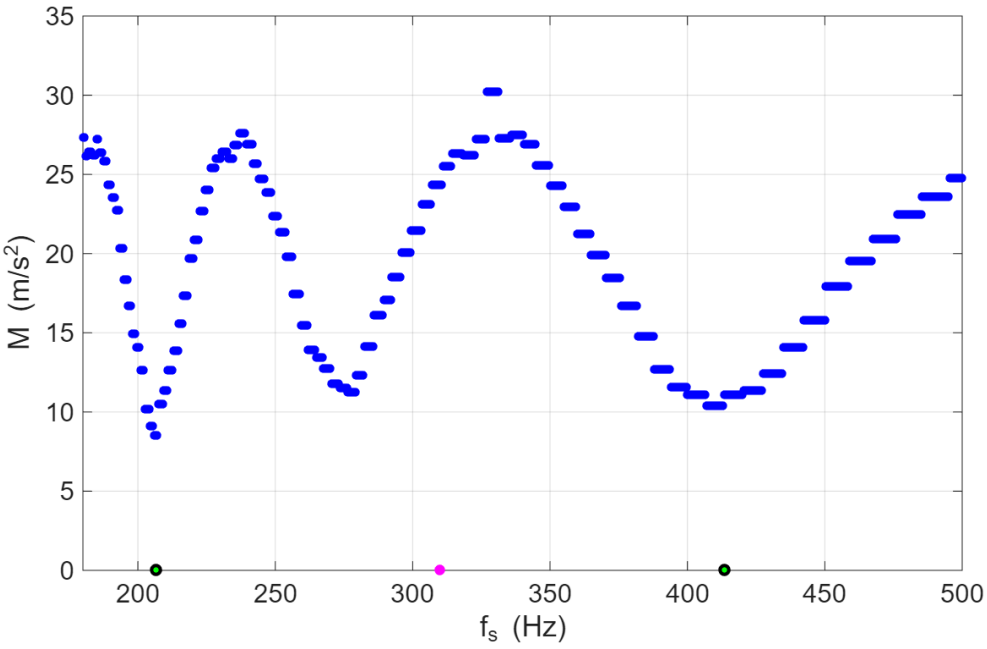


Figure 4.40: *M* value variation with periodic f_s. Local minima at f_{tooth} at M = 8.5 m/s^2, its 1st harmonic (black circles), and near a runout frequency (magenta dot).

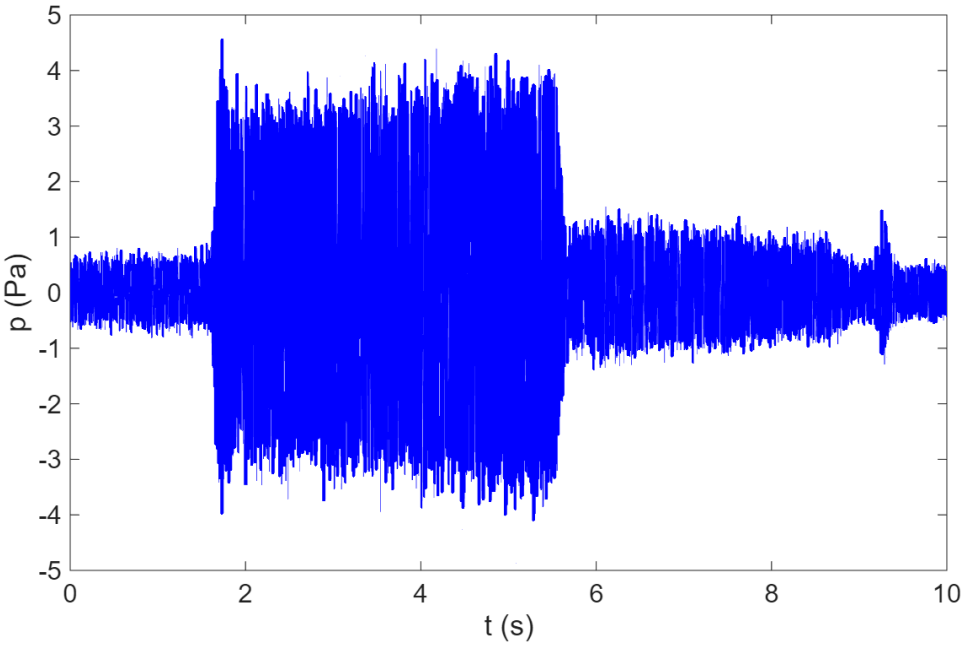


Figure 4.41: The total time interval of the signal from the microphone (sound pressure signal) showing when the tool interacts with the workpiece.

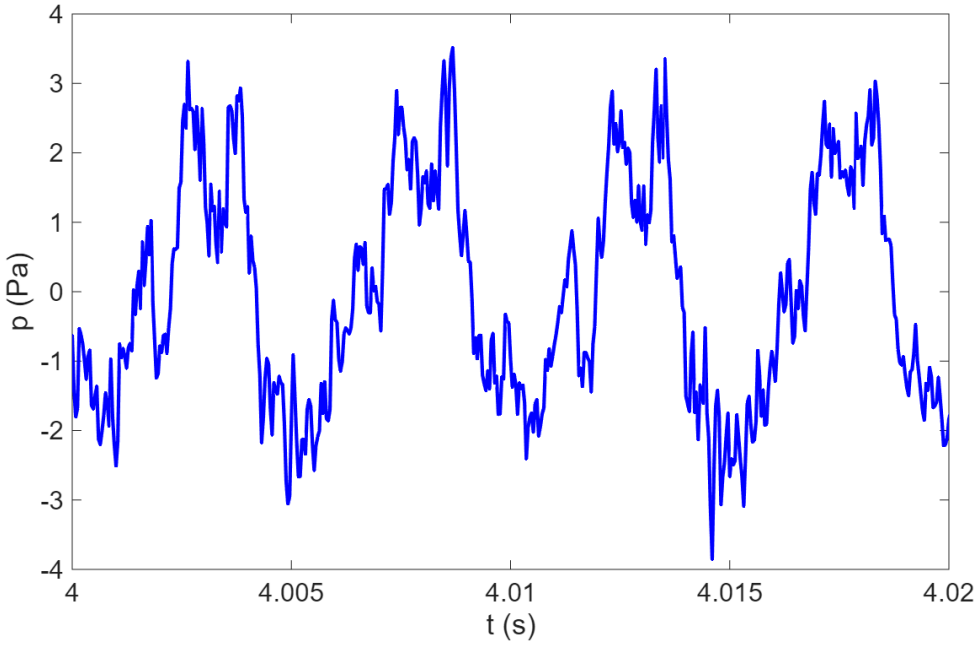


Figure 4.42: The magnified time interval of the signal from the microphone (sound pressure signal).

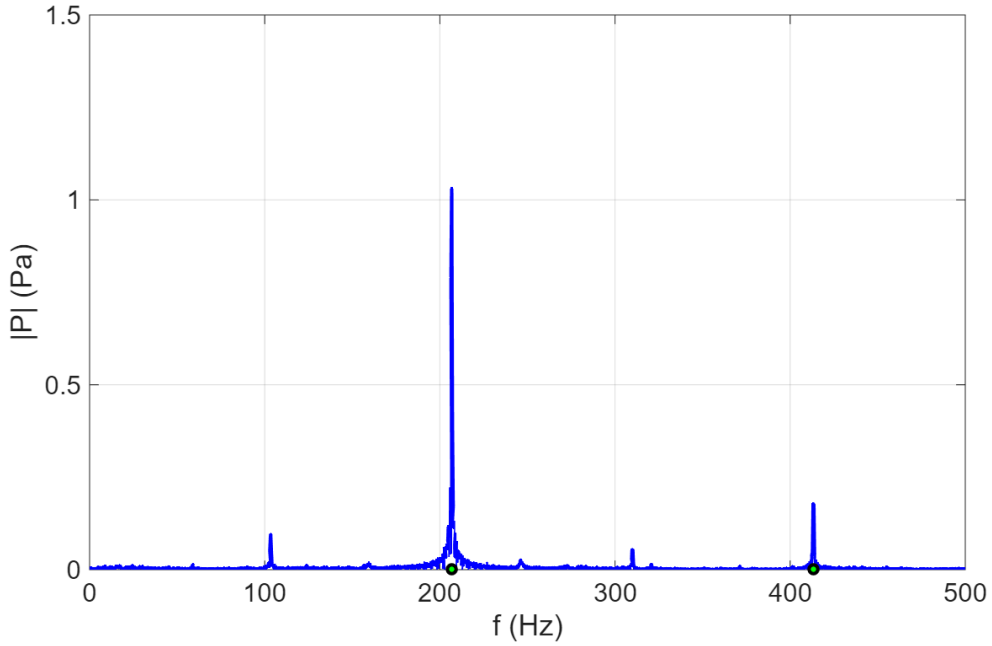


Figure 4.43: Magnitude plot of *p* frequency content for 150 rotations, with f_{tooth} at 207 Hz and its 1st harmonic identified (black circles).

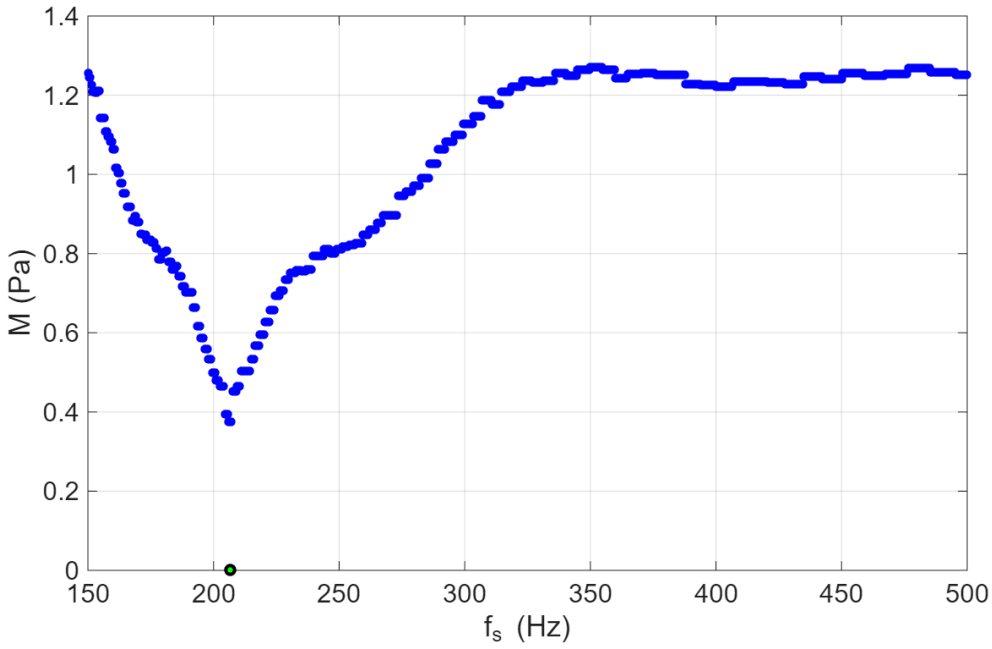


Figure 4.44: Variation in *M* value with periodic f_s. A local minimum is observed at f_{tooth} of 207 Hz (black circle) where *M* = 0.38 Pa.

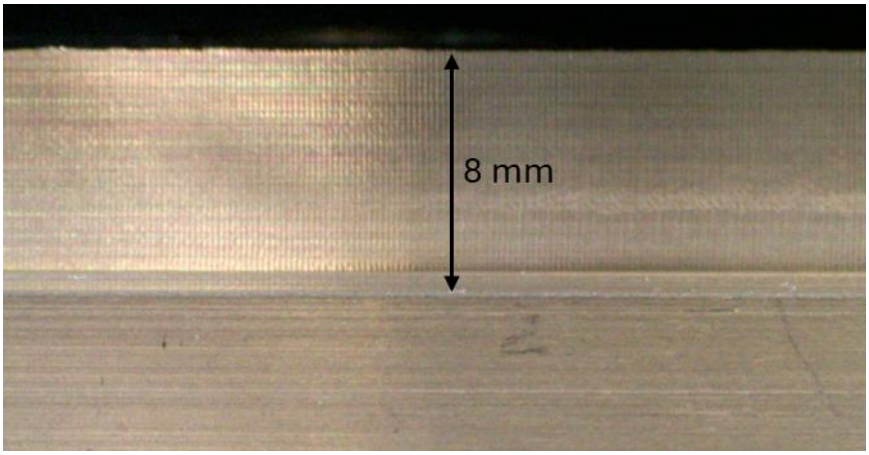


Figure 4.45: Surface of the aluminum 6061-T6 workpiece, with no chatter marks, after the stable cut.

Power sensor results.

Although the power sensor was not suitable for generating once-per-revolution signals, its measurements clearly indicate a monotonic rise in spindle power consumption with increasing spindle speed and depth of cut. This trend is consistent with the expected mechanical behavior of the spindle-tool system, where higher rotational speeds and depths of cut demand greater energy input to overcome inertia, friction, and cutting-related resistances.

Table 4.7. Profilometer results from six measured locations on the stable cut surface of the 6061-T6 aluminum.

Location	Ra (µm)	Rq (µm)	Rz (µm)
1	0.213	0.260	1.315
2	0.214	0.256	1.108
3	0.224	0.295	1.581
4	0.360	0.431	1.942
5	0.231	0.283	1.274
6	0.427	0.509	2.349

Figures 4.46, **4.47**, and **4.48** show the spindle power consumptions during the unstable, marginally unstable, and stable experimental cuts conducted using the two-flute endmill on the 6061-T6 aluminum workpieces. **Table 4.8** shows the spindle speeds, axial depths of cut, radial depths of cut, and the peak spindle power consumptions for the unstable, marginally unstable, and stable experimental cuts.

Table 4.8. Cutting parameters and peak spindle power for the experimental cuts using the two-flute endmill on 6061-T6 aluminum.

Experimental cut	Spindle speed (rpm)	Axial depth (mm)	Radial depth (mm)	Peak spindle power (kW)
Unstable	5550	8	3	1.21
Marginally unstable	5450	6.28	3	1.14
Stable	6200	8	3	1.86

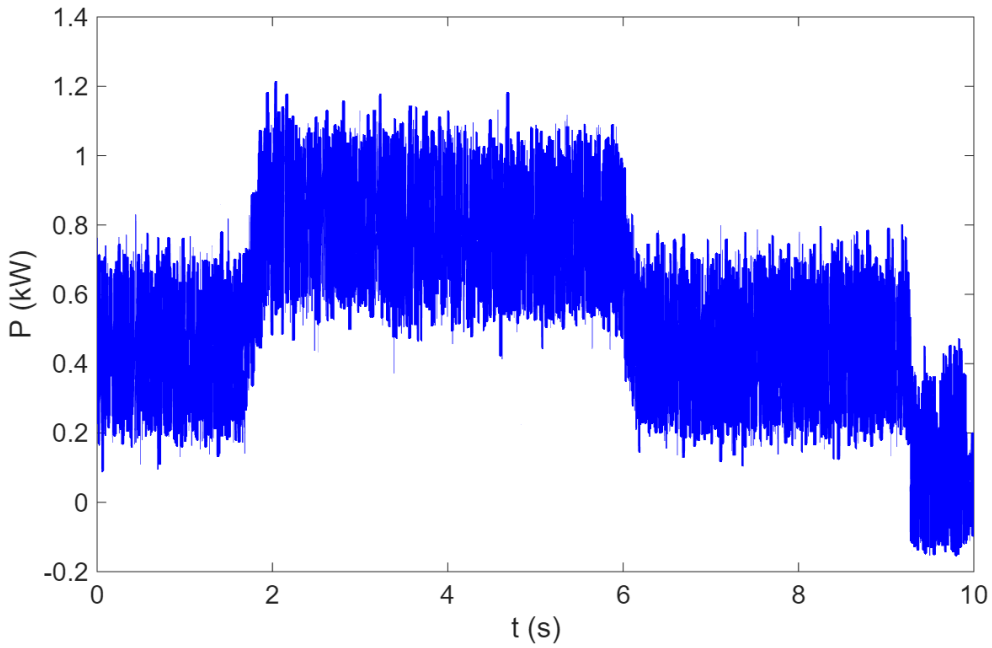


Figure 4.46: Spindle power consumption peaked at 1.21 kW during the unstable cut at a spindle speed of 5550 rpm, axial and radial depths of cut of 8 mm and 3 mm respectively.

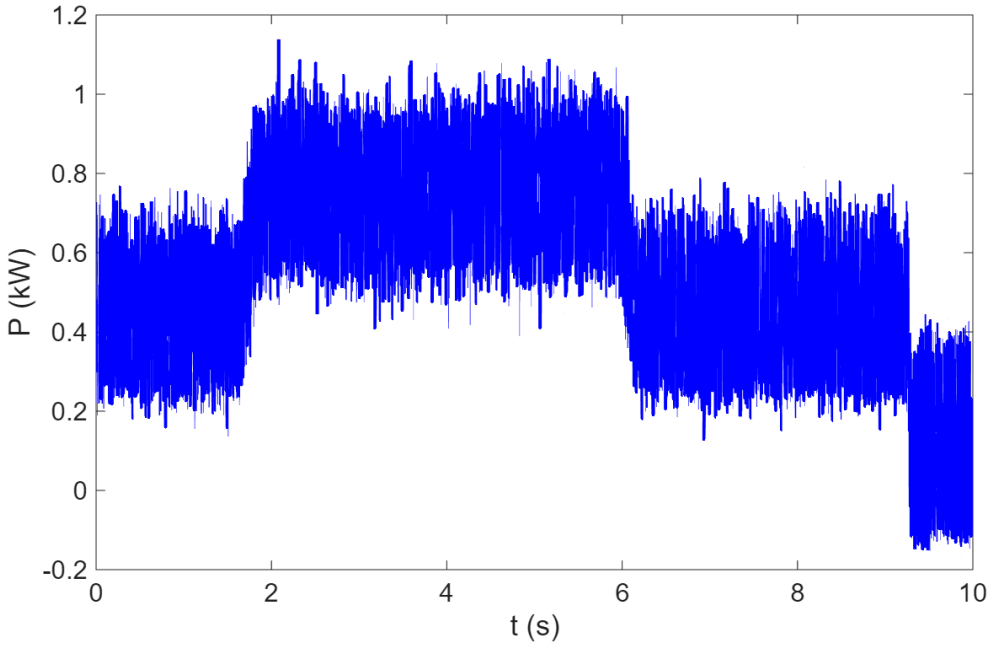


Figure 4.47: Spindle power consumption peaked at 1.14 kW during the marginally unstable cut at 5450 rpm, 6.28 mm and 3 mm axial and radial depths of cut respectively.

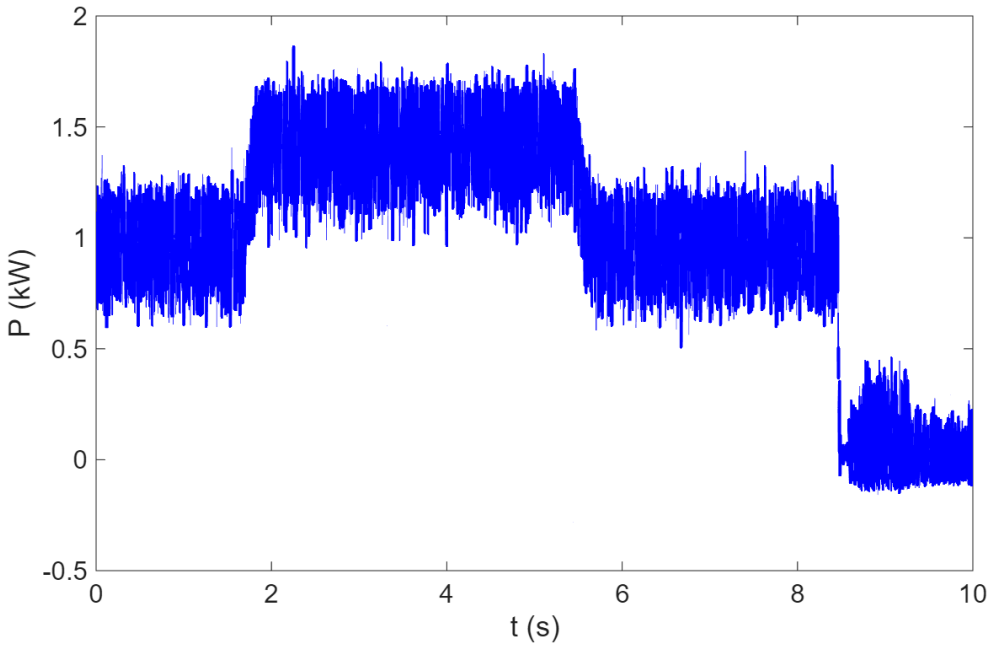


Figure 4.48: Spindle power consumption peaked at 1.86 kW during the stable cut at a spindle speed of 6200 rpm, 8 mm and 3 mm axial and radial depths of cut respectively.

Unstable cut: Four-flute endmill on AISI 4140 steel

Results from tap testing and an unstable experimental cut using four-flute carbide endmill on AISI 4140 steel are presented below. **Tables 4.9** and **4.10** show the modal parameters of the tool tip and workpiece respectively, obtained after tap testing, while **Figures 4.49** and **4.50** show the frequency response function and the stability lobe diagram obtained using the modal parameters. A tangential force coefficient of 2044.5 N/mm^2 and a normal force coefficient of 578.5 N/mm^2 for AISI 4140 steel [52] are selected. A radial depth of cut of 2 mm is selected, and an unstable point corresponding to a spindle speed of 7000 rpm and an axial depth of cut of 5 mm is selected on the stability lobe diagram, which achieves an unstable cut.

Results from the time domain milling signals of the displacement (x), the acceleration (a), and the sound pressure (p) are presented, including, the total time interval of each signal, the magnified time interval, magnitude plot of the frequency content, and the variation in the M value with the periodic sampling frequency, f_s. As stated earlier, the variation in the M value with the periodic sampling frequency, f_s, validates chatter detection by periodic sampling of time domain milling signals.

Figures 4.51, **4.55**, and **4.59** show the total time interval of the cut from the CMD, the accelerometer, and the microphone milling signals respectively. **Figures 4.52**, **4.56**, and **4.60** show the magnified time interval of the cut from the CMD, the accelerometer, and the microphone milling signals respectively. **Figures 4.53**, **4.57**, and **4.61** show the magnitude plots of the frequency contents from the CMD, the accelerometer, and the microphone milling signals respectively. It is observed that the chatter frequency, f_c, has

the highest peak in the magnitude plots, indicating an unstable cut. **Figures 4.54**, **4.58**, and **4.62** show the variations in the *M* values with the periodic sampling frequency of the time domain milling signals from the CMD, the accelerometer, and the microphone respectively. It is observed that a local minimum in the stability metric occurs at the chatter frequency, f_c, not at the tooth passing frequency, f_{tooth}, thereby indicating an unstable cut.

Figure 4.63 shows the surface of the workpiece with visible chatter marks after the unstable cut, captured using the Dino-Lite digital microscope. Surface roughness measurements were conducted at six different locations on the cut surface using the Mitutoyo profilometer, yielding a mean Ra value of 0.96 µm with a standard deviation of 0.066 µm, a mean Rq value of 1.16 µm with a standard deviation of 0.074 µm, and a mean Rz value of 4.94 µm with a standard deviation of 0.256 µm. **Table 4.11** shows the Ra, Rq, and Rz values for the six measured locations.

Table 4.9. Tool tip modal parameters of the four-flute endmill.

***x*-direction**		
Frequency, f_n (Hz)	**Stiffness, *k* (N/m)**	**Damping ratio, ζ (-)**
172	1.92×10^8	0.0560
458	2.08×10^8	0.1101
939	1.50×10^8	0.1142
1411	1.31×10^8	0.1249
1507	1.42×10^8	0.0179
2051	6.32×10^8	0.0523
3531	3.61×10^8	0.1005
9833	4.96×10^8	0.0560
***y*-direction**		
Frequency, f_n (Hz)	**Stiffness, *k* (N/m)**	**Damping ratio, ζ (-)**
480	3.30×10^8	0.1120
967	2.12×10^8	0.0533

Table 4.9. continued: Tool tip modal parameters of the four-flute endmill

Frequency, f_n (Hz)	**Stiffness, k (N/m)**	**Damping ratio, ζ (-)**
1271	9.10×10^7	0.1225
1538	1.17×10^9	0.0167
1593	1.74×10^9	0.0169
1750	6.59×10^8	0.0188
2041	1.56×10^9	0.0291
5418	6.32×10^8	0.0437

Table 4.10. Workpiece modal parameters of the AISI 4140 steel before the unstable cut.

***x*-direction**		
Frequency, f_n (Hz)	**Stiffness, k (N/m)**	**Damping ratio, ζ (-)**
613	1.82×10^7	0.0067
***y*-direction**		
Frequency, f_n (Hz)	**Stiffness, k (N/m)**	**Damping ratio, ζ (-)**
221	1.15×10^9	0.0606
1970	3.88×10^8	0.0105
2112	1.36×10^9	0.0114
2215	5.19×10^8	0.0194
2314	1.24×10^9	0.0107
2545	2.30×10^9	0.0127
3999	1.75×10^9	0.0055
4151	1.69×10^9	0.0109

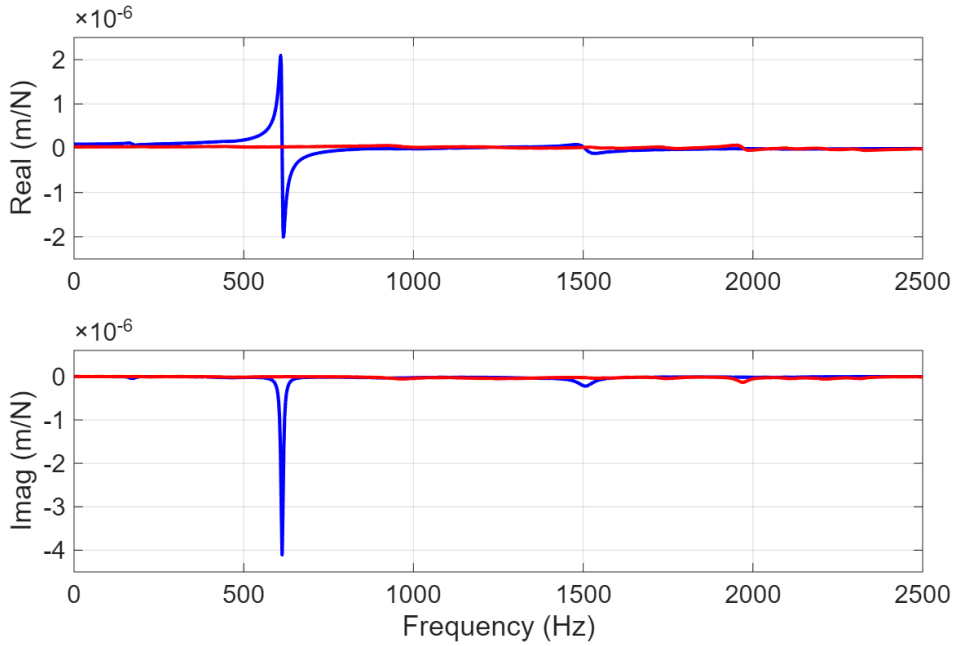


Figure 4.49: Tool tip and workpiece, *x* (blue lines) and *y* (red lines) directions, frequency response function.

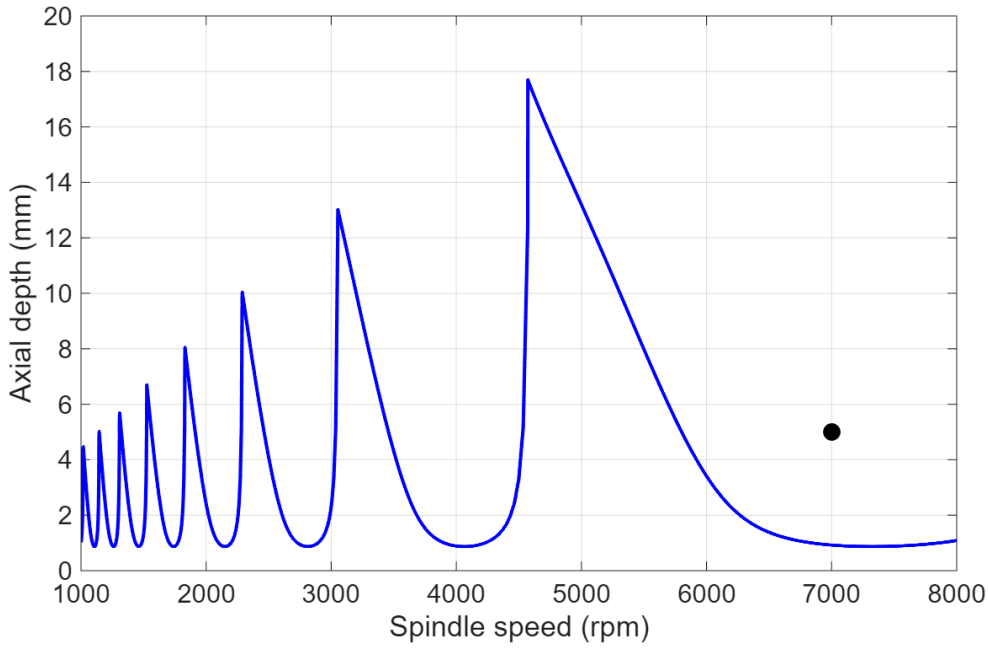


Figure 4.50: Stability lobe diagram with the selected unstable point (black dot) corresponding to a spindle speed of 7000 rpm and axial depth of cut of 5 mm.

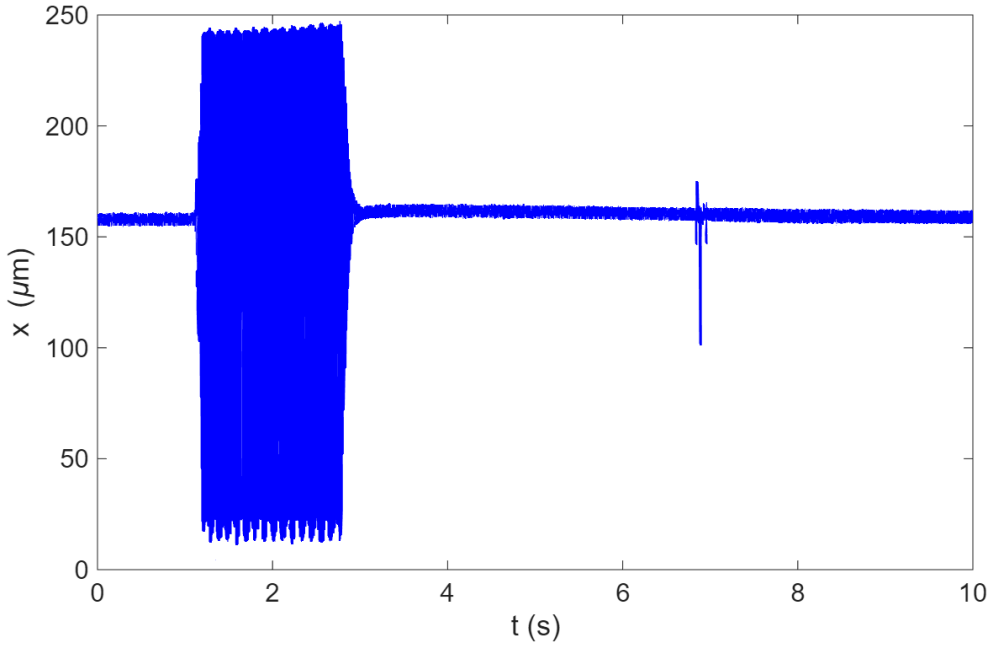


Figure 4.51: The total time interval of the signal from the CMD (displacement signal) showing when the tool interacts with the workpiece.

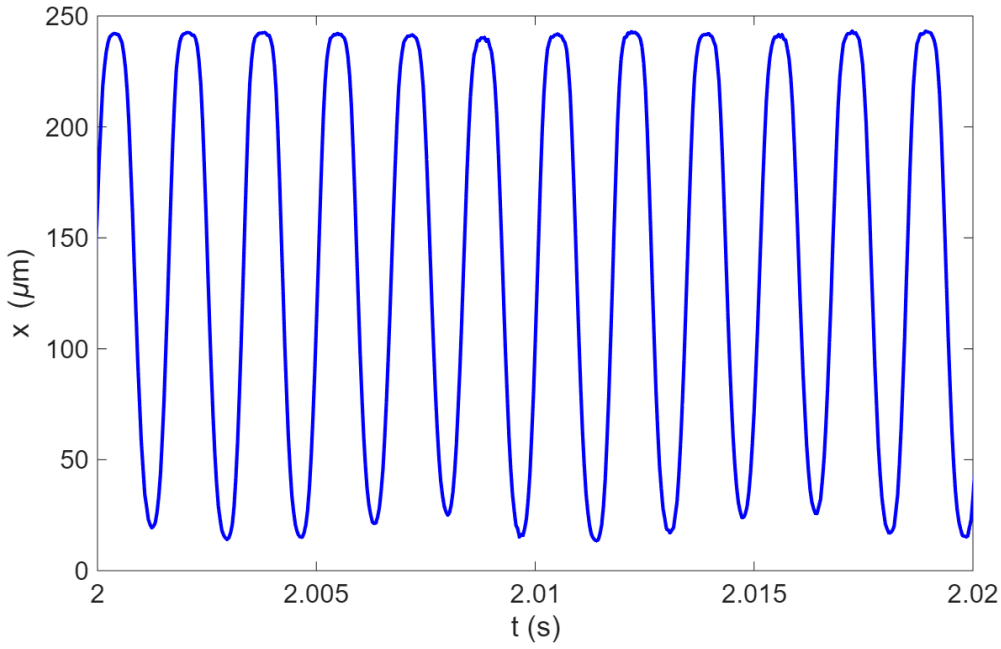


Figure 4.52: The magnified time interval of the signal from the CMD (displacement signal).

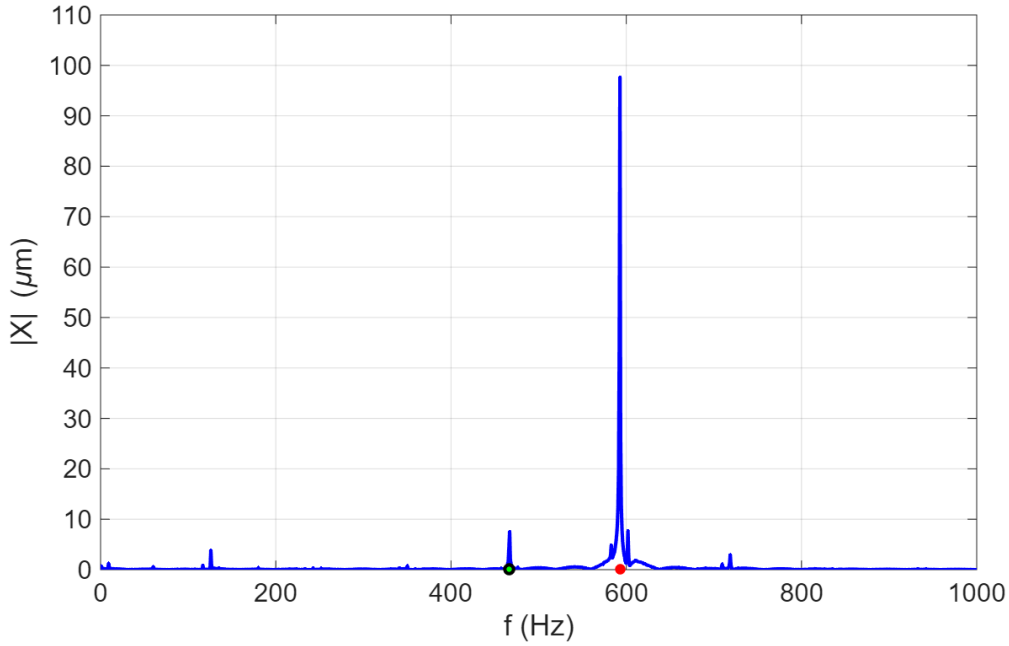


Figure 4.53: Magnitude plot of *x* frequency content for 150 rotations, with f_c (red dot) identified at 593 Hz and f_{tooth} (black circle) at 467 Hz.

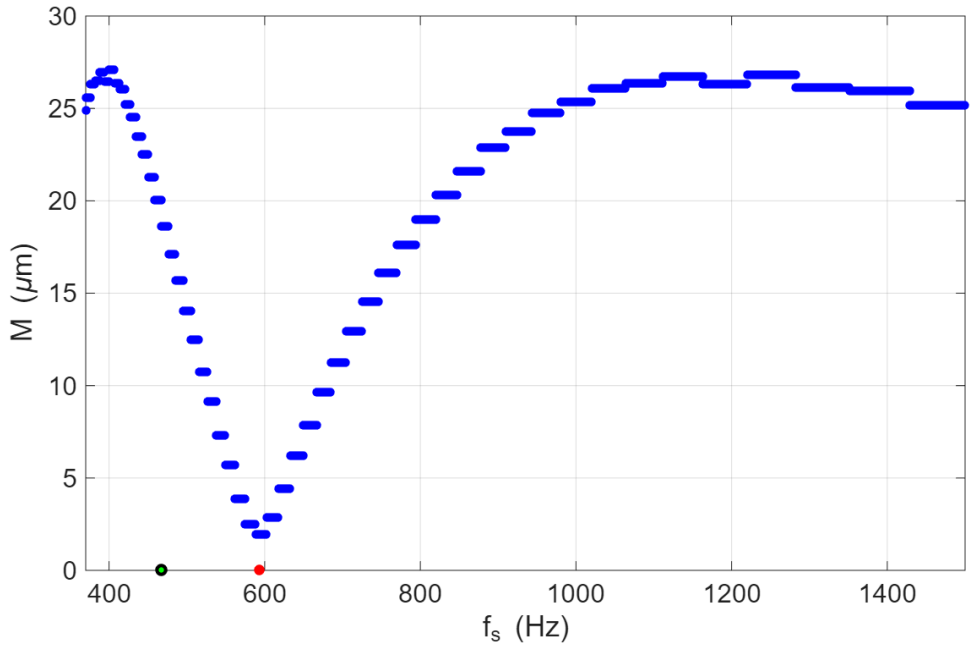


Figure 4.54: Variation in *M* value with periodic f_s. A local minimum occurs at f_c of 593 Hz (red dot) where M = 1.97 µm, not at f_{tooth} (black circle).

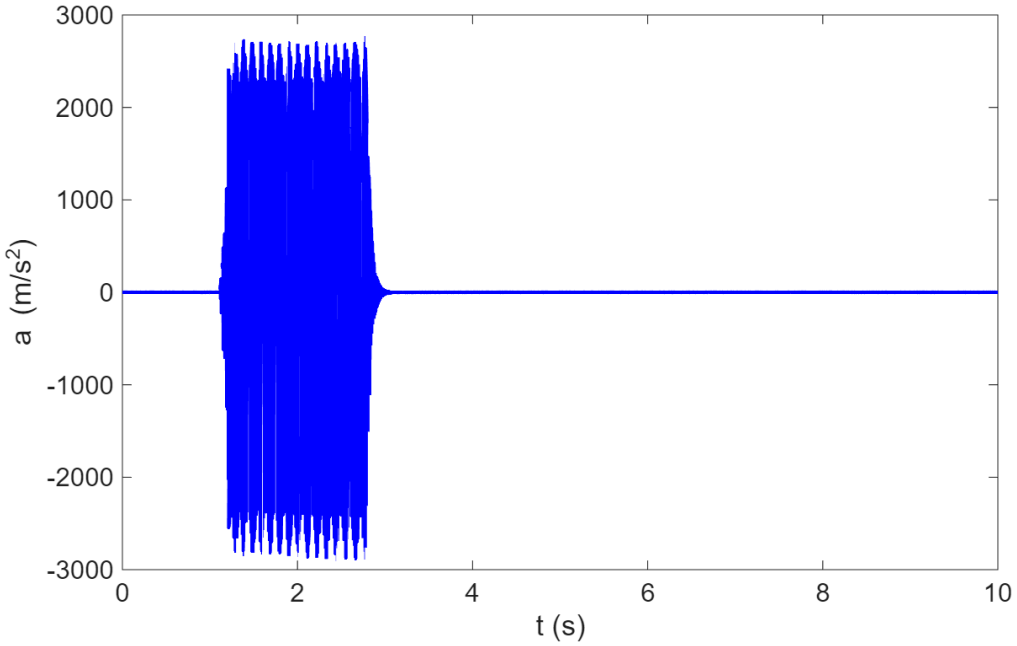


Figure 4.55: The total time interval of the signal from the accelerometer (acceleration signal) showing when the tool interacts with the workpiece.

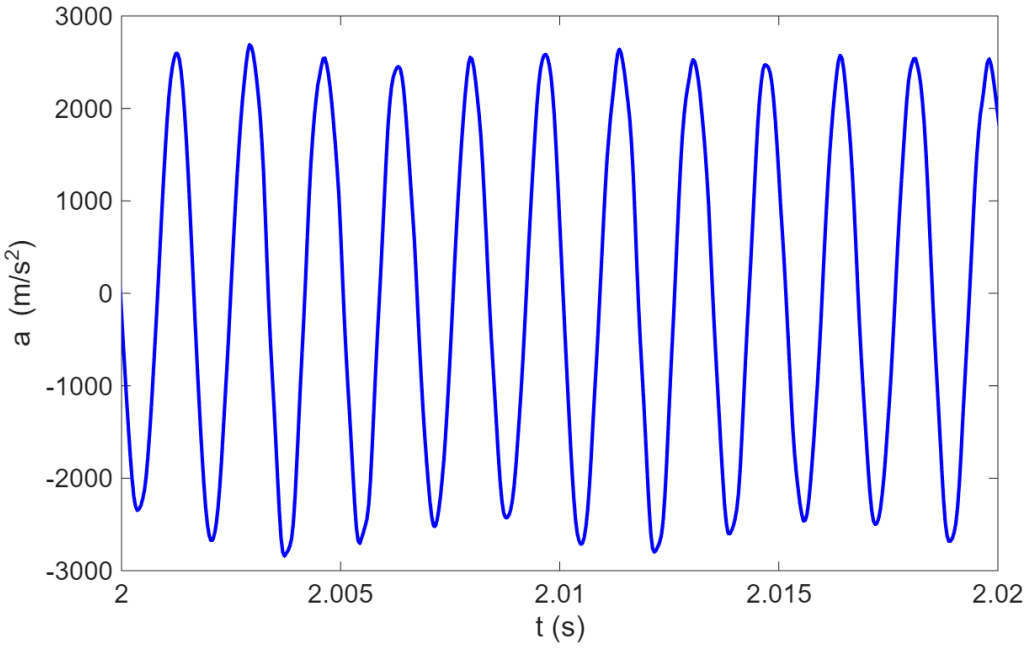


Figure 4.56: The magnified time interval of the signal from the accelerometer (acceleration signal).

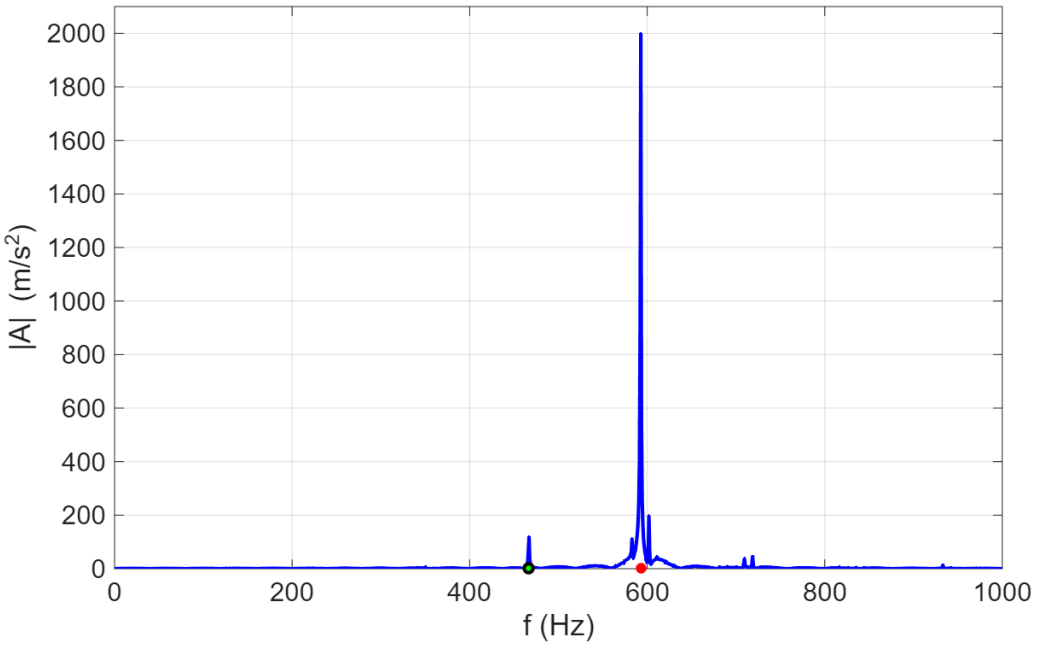


Figure 4.57: Magnitude plot of *a* frequency content for 150 rotations, with f_c (red dot) identified at 593 Hz and f_{tooth} (black circle) at 467 Hz.

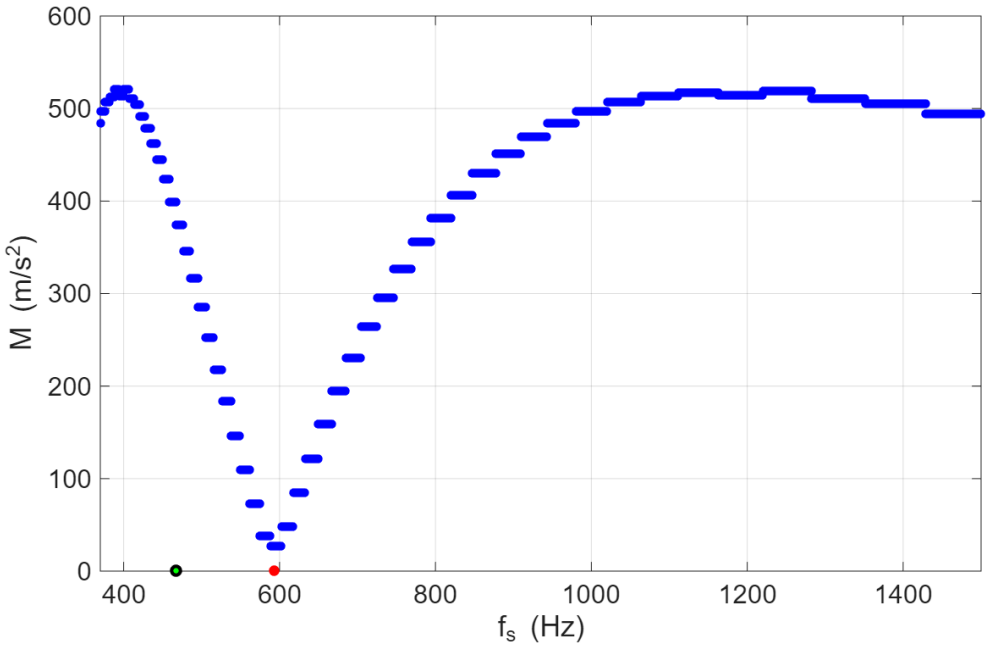


Figure 4.58: Variation in *M* value with periodic f_s. A local minimum occurs at f_c of 593 Hz (red dot) where M = 27 m/s^2, not at f_{tooth} (black circle).

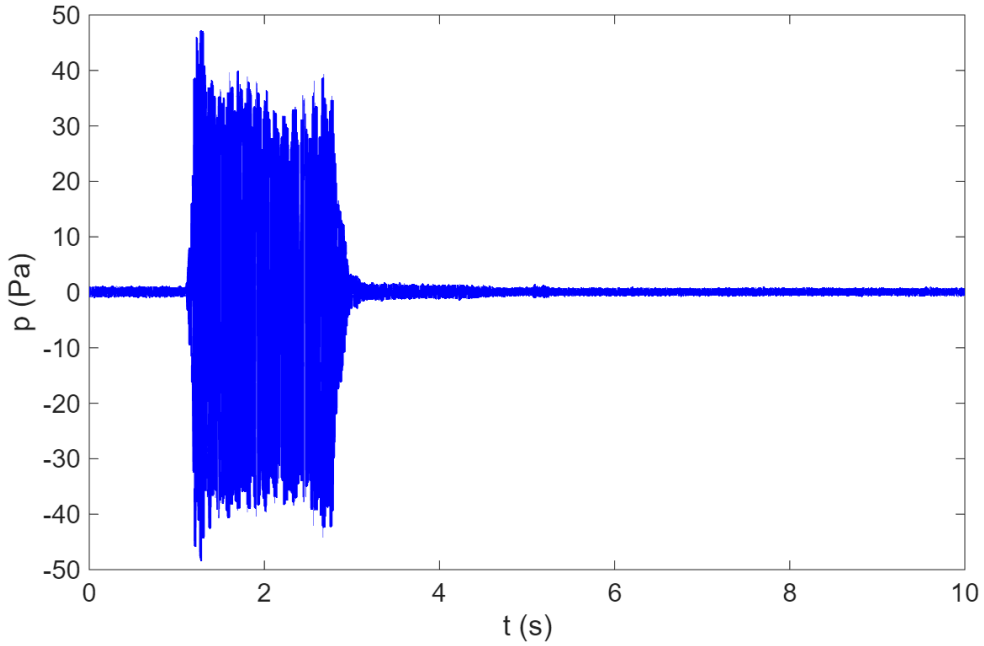


Figure 4.59: The total time interval of the signal from the microphone (sound pressure signal) showing when the tool interacts with the workpiece.

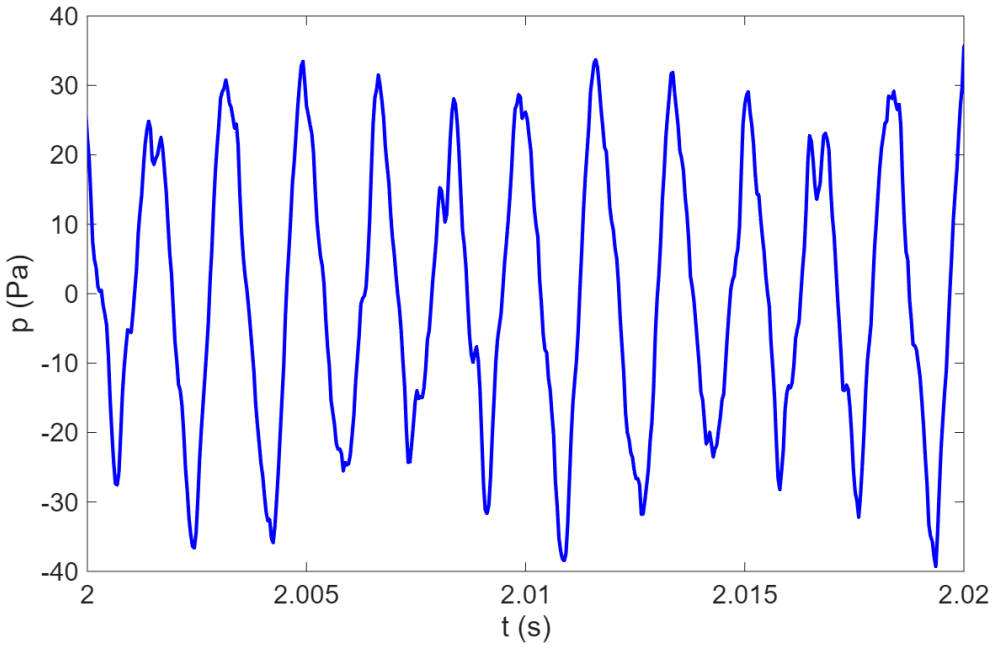


Figure 4.60: The magnified time interval of the signal from the microphone (sound pressure signal).

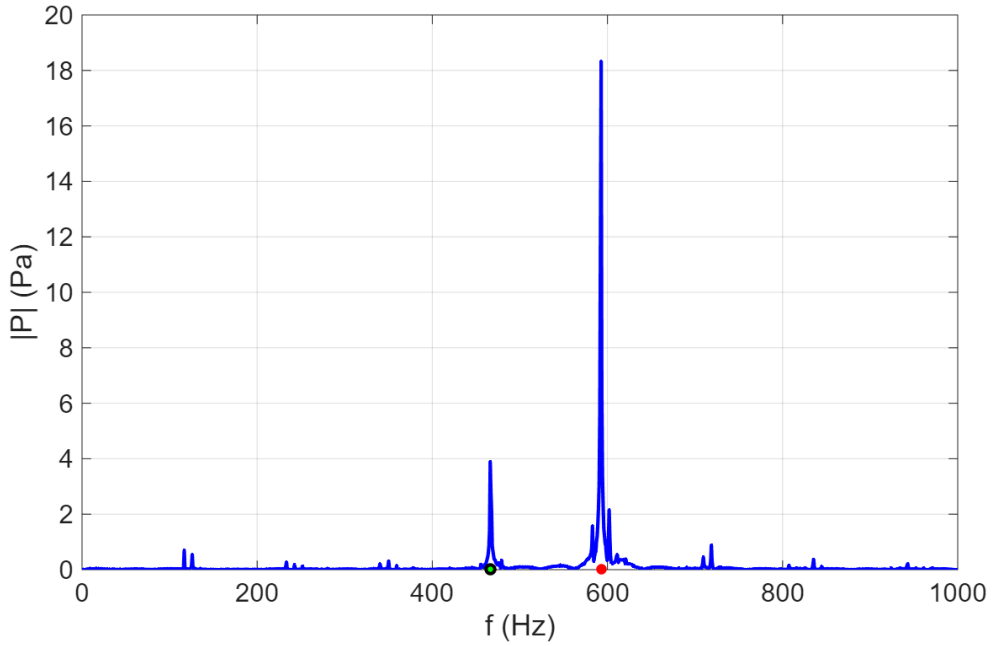


Figure 4.61: Magnitude plot of p frequency content for 150 rotations, with f_c (red dot) identified at 593 Hz and f_{tooth} (black circle) at 467 Hz.

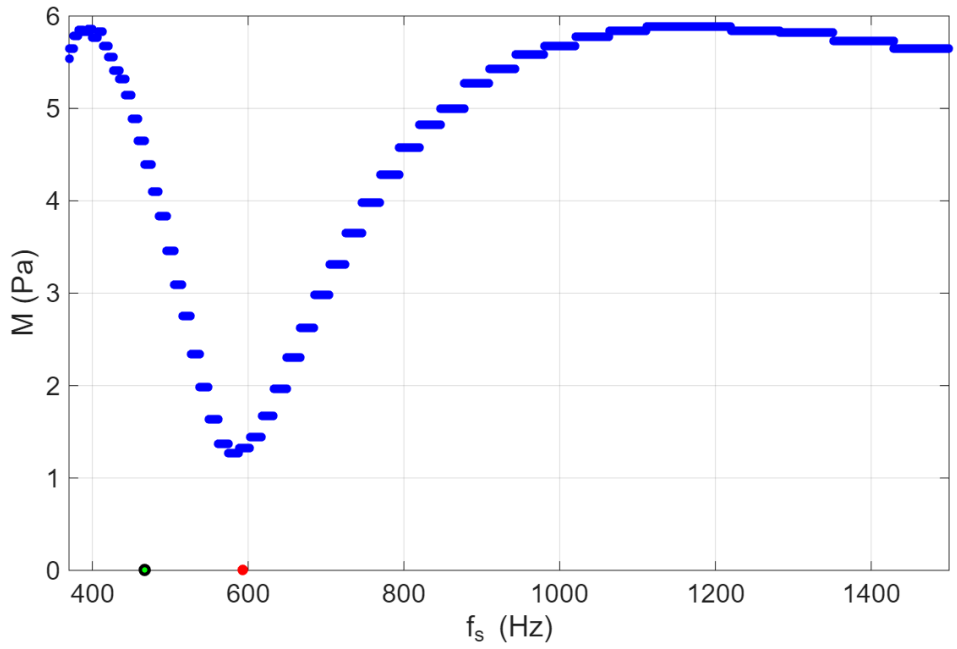


Figure 4.62: Variation in M value with periodic f_s. A local minimum occurs at f_c of 593 Hz (red dot) where M = 1.27 Pa, not at f_{tooth} (black circle).

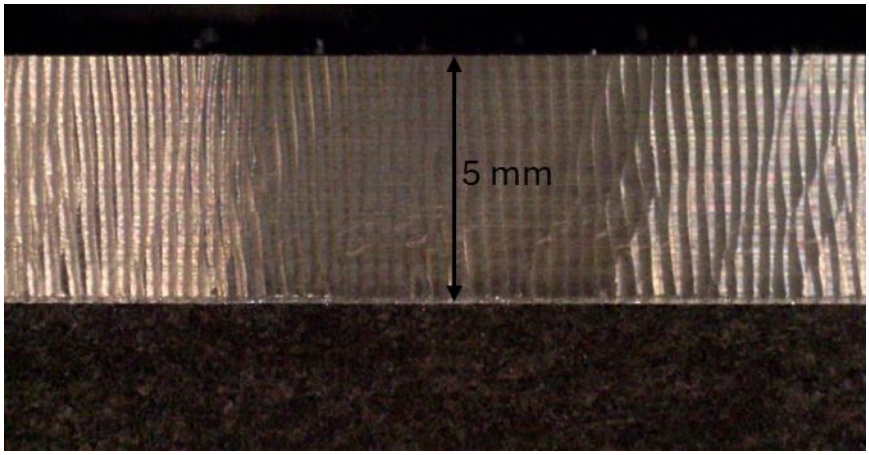


Figure 4.63: Surface of the AISI 4140 steel workpiece with visible chatter marks after the unstable cut.

Marginally stable cut: Four-flute endmill on AISI 4140 steel

Results from tap testing and a marginally stable experimental cut using a four-flute carbide endmill on AISI 4140 steel are presented below. **Table 4.12** shows the modal parameters of the workpiece obtained after tap testing. The tool tip modal parameters presented in **Table 4.9** are retained because, unlike the workpiece which experiences a reduction in mass after cutting, the tool remains unchanged from the previous experimental cut upon inspection.

Table 4.11. Profilometer results from six measured locations on the unstable cut surface of the AISI 4140 steel workpiece.

Location	Ra (µm)	Rq (µm)	Rz (µm)
1	1.065	1.282	5.084
2	0.870	1.079	4.613
3	0.955	1.137	5.235
4	0.997	1.198	4.953
5	0.961	1.169	5.106
6	0.925	1.099	4.650

Figures 4.64 and **4.65** show the frequency response function and the stability lobe diagram obtained using the modal parameters. A tangential force coefficient of 2044.5 N/mm^2 and a normal force coefficient of 578.5 N/mm^2 for AISI 4140 steel are selected. A radial depth of cut of 2 mm is selected, and a marginally stable point corresponding to a spindle speed of 5770 rpm and an axial depth of cut of 5 mm is selected on the stability lobe diagram, which achieves the marginally stable cut.

Results from the time domain milling signals of the displacement (x), the acceleration (a), and the sound pressure (p) are presented, including, the total time interval of each signal, the magnified time interval, magnitude plot of the frequency content, and the variation in the M value with the periodic sampling frequency, f_s, which validates chatter detection by periodic sampling of time domain milling signals. **Figures 4.66**, **4.70**, and **4.74** show the total time interval of the cut from the CMD, the accelerometer, and the microphone milling signals respectively. **Figures 4.67**, **4.71**, and **4.75** show the magnified time interval of the cut from the CMD, the accelerometer, and the microphone milling signals respectively. **Figures 4.68**, **4.72**, and **4.76** show the magnitude plots of the frequency contents from the CMD, the accelerometer, and the microphone milling signals respectively. In the case of the displacement and sound pressure signals, although it is observed that the tooth passing frequency, f_{tooth}, has the highest peak in the magnitude plots, an amplified runout frequency close to the systems natural frequency is also observed in both cases, indicating marginally stable behavior. In the case of the acceleration milling signal, the runout frequency is amplified to a slightly higher peak than the f_{tooth} peak, also indicating marginally stable behavior tending towards marginal

instability. **Figures 4.69**, **4.73**, and **4.77** show the variations in the *M* values with the periodic sampling frequency of the time domain milling signals from the CMD, the accelerometer, and the microphone respectively. It is observed that for the three milling signals, a local minimum in the stability metric occurs at the tooth passing frequency, f_{tooth}, thereby indicating a stable cut. However, the flattening and unusual nature of the local minima indicate marginally stable behavior. In the case of the acceleration milling signal, local minima occur at f_{tooth} and near the runout frequencies. It is also observed that the *M* values from the local minima occurring at f_{tooth} are less than those recorded in the previous unstable cut. **Figure 4.78** shows the surface of the workpiece with periodic feed marks after the cut, indicating the tool tooth trajectory. Surface roughness measurements were conducted at six different locations on the cut surface, yielding a mean Ra value of 0.88 µm with a standard deviation of 0.09 µm, a mean Rq value of 1.03 µm with a standard deviation of 0.089 µm, and a mean Rz value of 4.0 µm with a standard deviation of 0.248 µm. **Table 4.13** shows the Ra, Rq, and Rz values for the six measured locations.

Table 4.12. Workpiece modal parameters of the AISI 4140 steel before the marginal cut.

***x*-direction**		
Frequency, f_n (Hz)	**Stiffness, *k* (N/m)**	**Damping ratio, ζ (-)**
611	1.83×10^7	0.0062
***y*-direction**		
Frequency, f_n (Hz)	**Stiffness, *k* (N/m)**	**Damping ratio, ζ (-)**
204	8.60×10^8	0.0645
808	2.65×10^9	0.0454
1974	4.54×10^8	0.0112
2115	1.18×10^9	0.0103
2223	3.78×10^8	0.0256
2561	2.86×10^9	0.0082
4001	2.43×10^9	0.0075
4175	4.67×10^9	0.0047

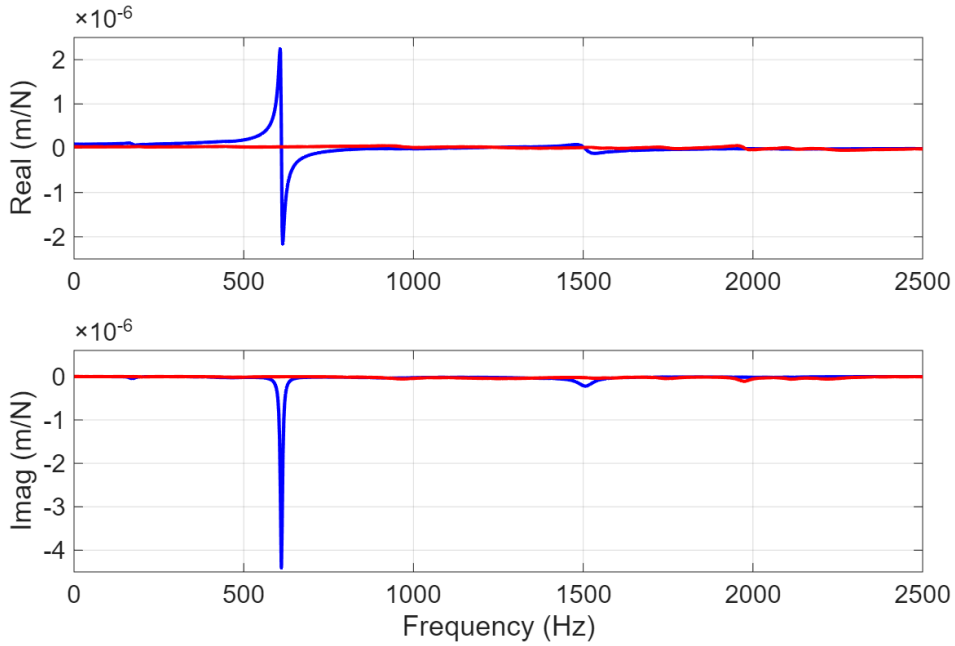


Figure 4.64: Tool tip and workpiece, *x* (blue lines) and *y* (red lines) directions, frequency response function.

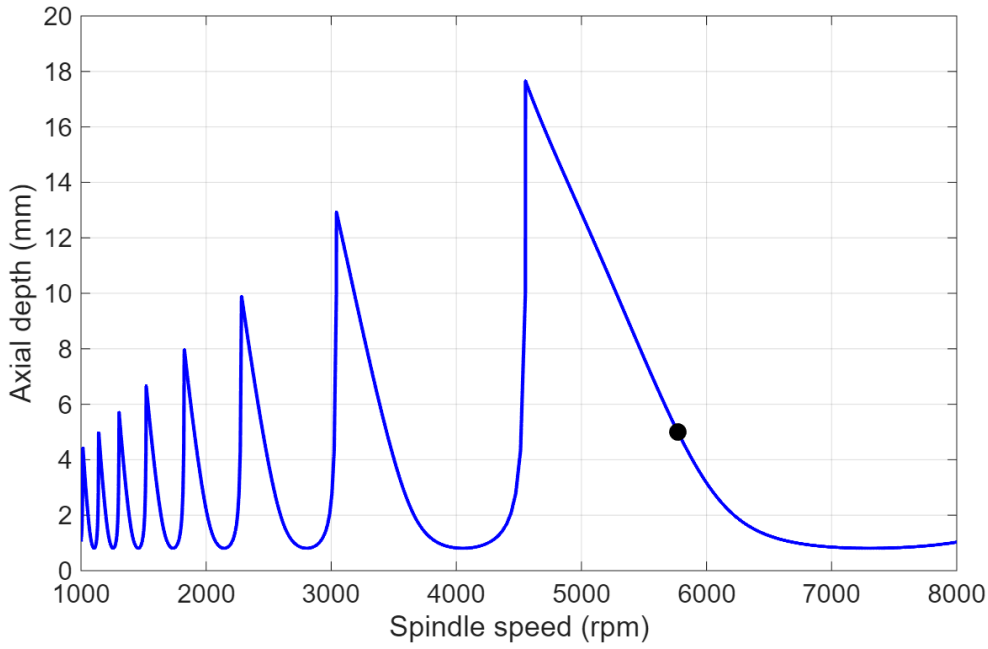


Figure 4.65: Stability lobe diagram with the selected marginally stable point (black dot) corresponding to a spindle speed of 5770 rpm and axial depth of cut of 5 mm.

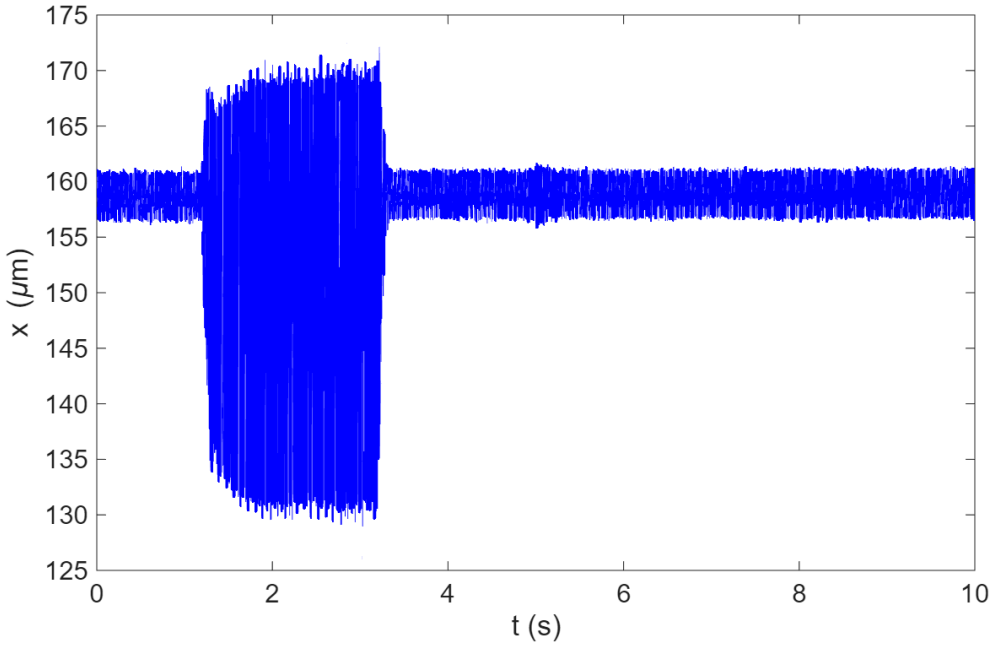


Figure 4.66: The total time interval of the signal from the CMD (displacement signal) showing when the tool interacts with the workpiece.

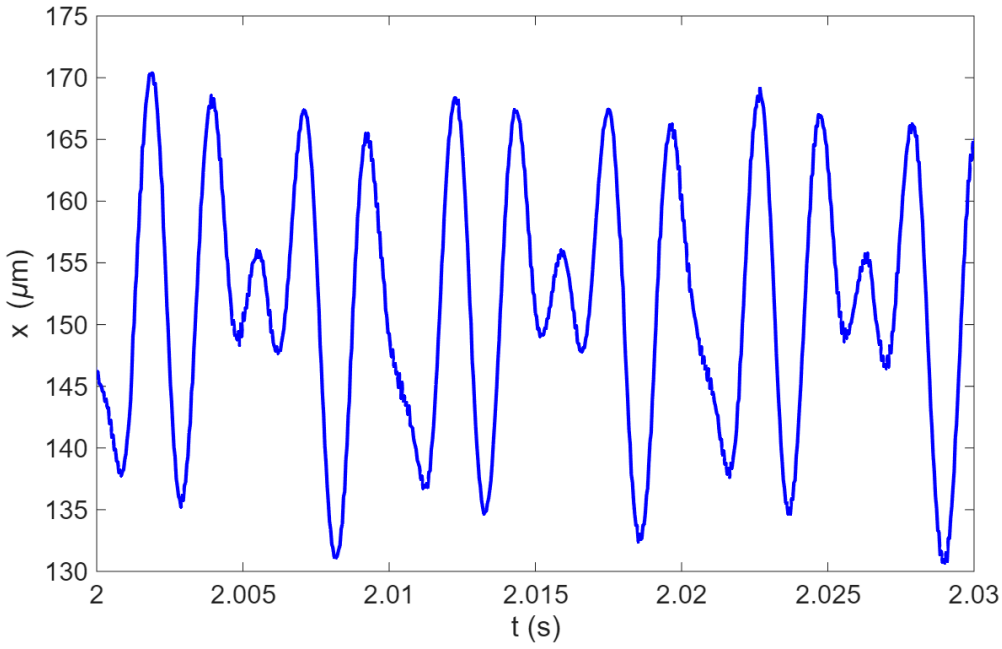


Figure 4.67: The magnified time interval of the signal from the CMD (displacement signal).

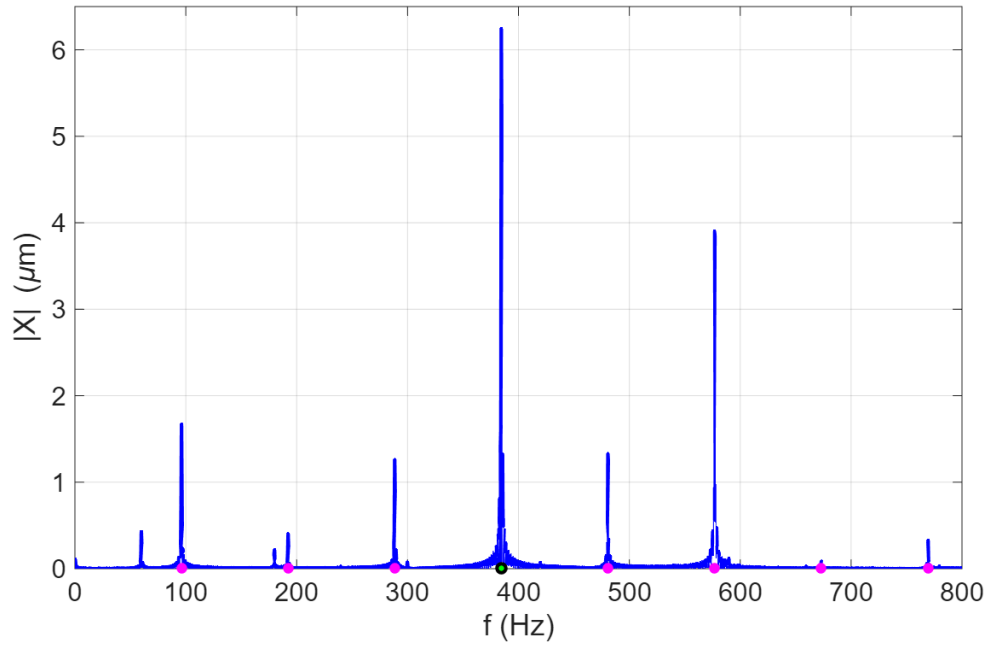


Figure 4.68: Magnitude plot of *x* frequency content for 150 rotations, with f_{tooth} (black circle) identified at 385 Hz and runout frequencies (magenta dots) also identified.

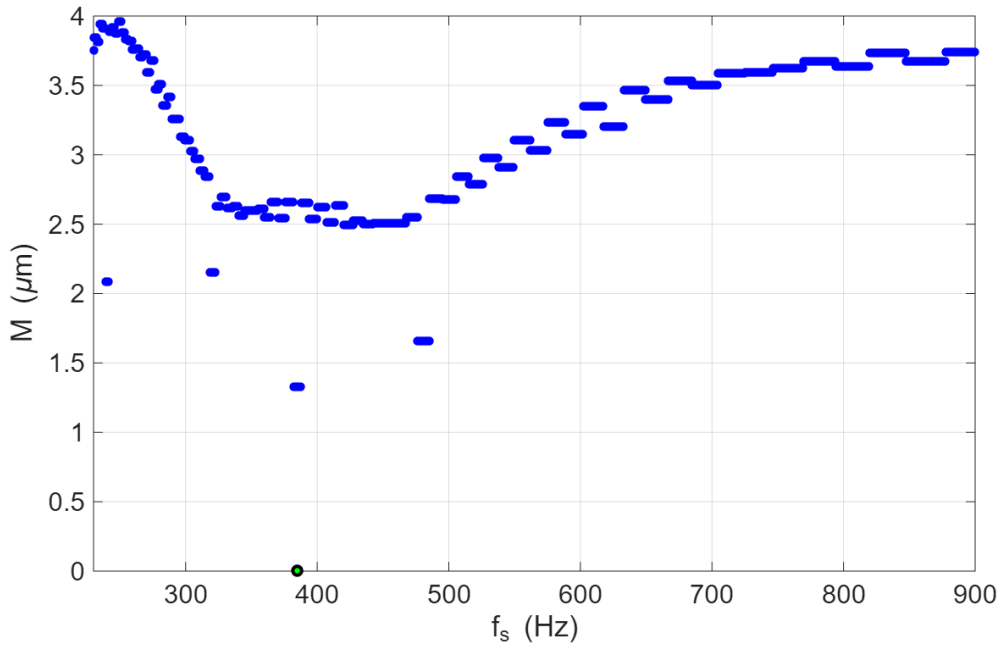


Figure 4.69: Variation in *M* value with periodic f_s. A local minimum occurs at f_{tooth} of 385 Hz (black circle) where M = 1.33 µm.

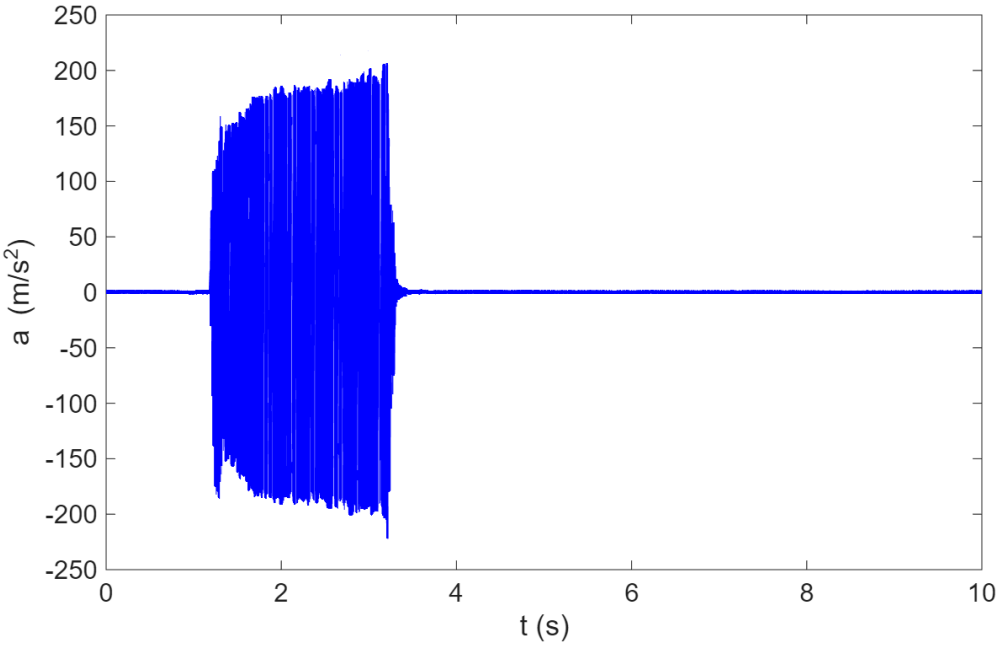


Figure 4.70: The total time interval of the signal from the accelerometer (acceleration signal) showing when the tool interacts with the workpiece.

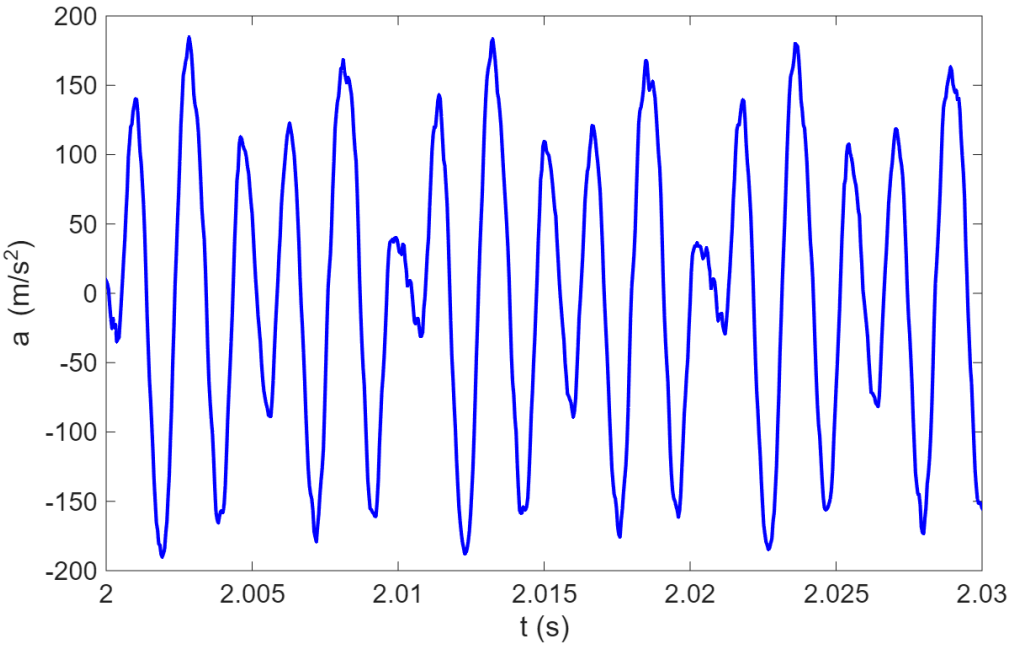


Figure 4.71: The magnified time interval of the signal from the accelerometer (acceleration signal).

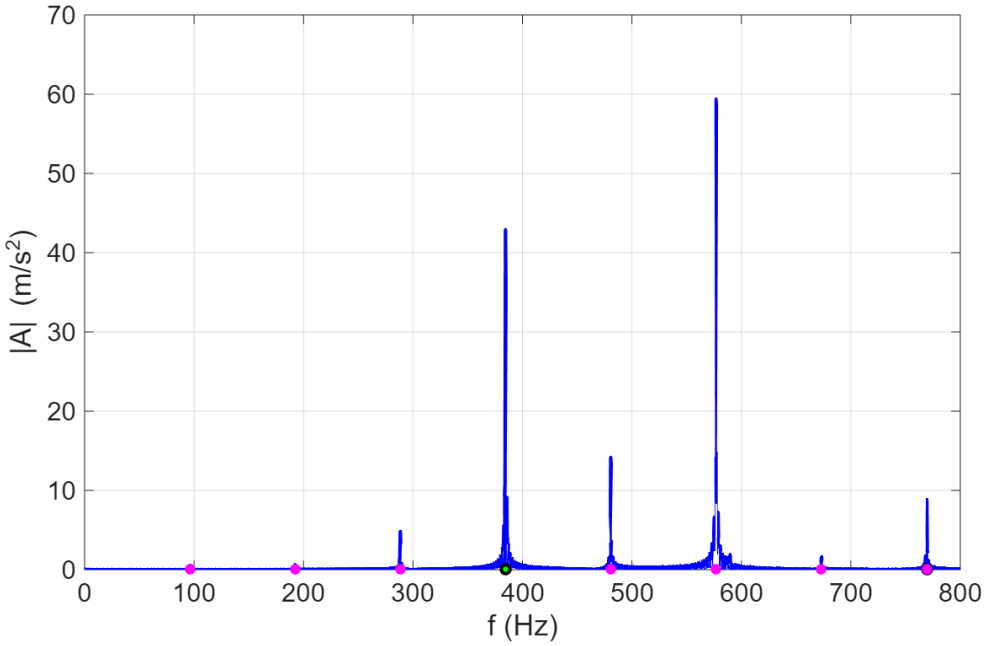


Figure 4.72: Magnitude plot of *a* frequency content for 150 rotations, with f_{tooth} (black circle) identified at 385 Hz and runout frequencies (magenta dots) also identified.

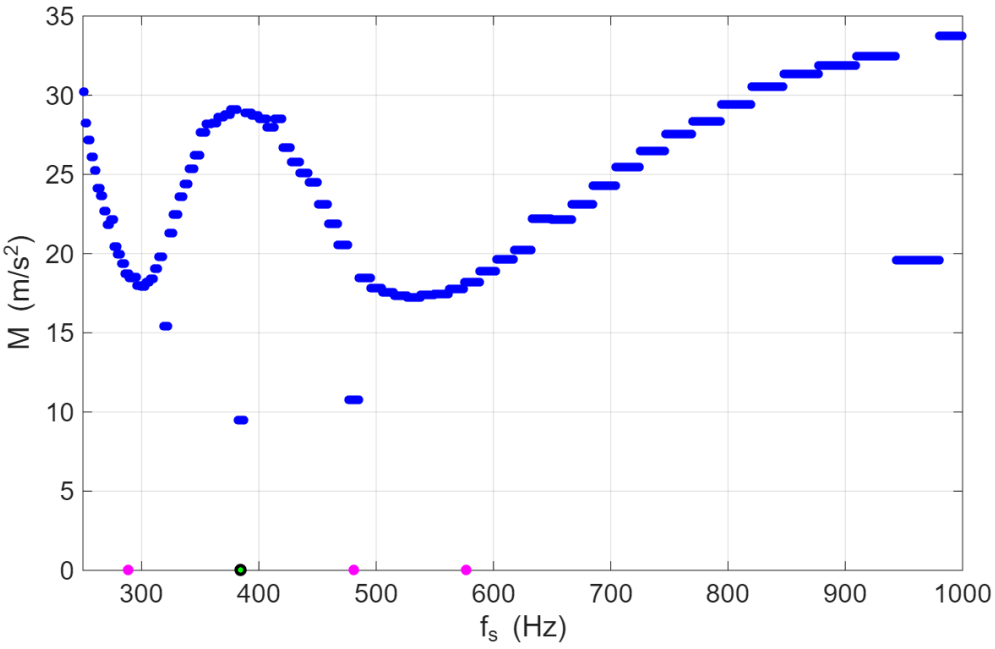


Figure 4.73: Variation in *M* value with periodic f_s. Local minima occur at f_{tooth} of 385 Hz (black circle) where M = 9.46 m/s^2 and near the runout frequencies (magenta dots).

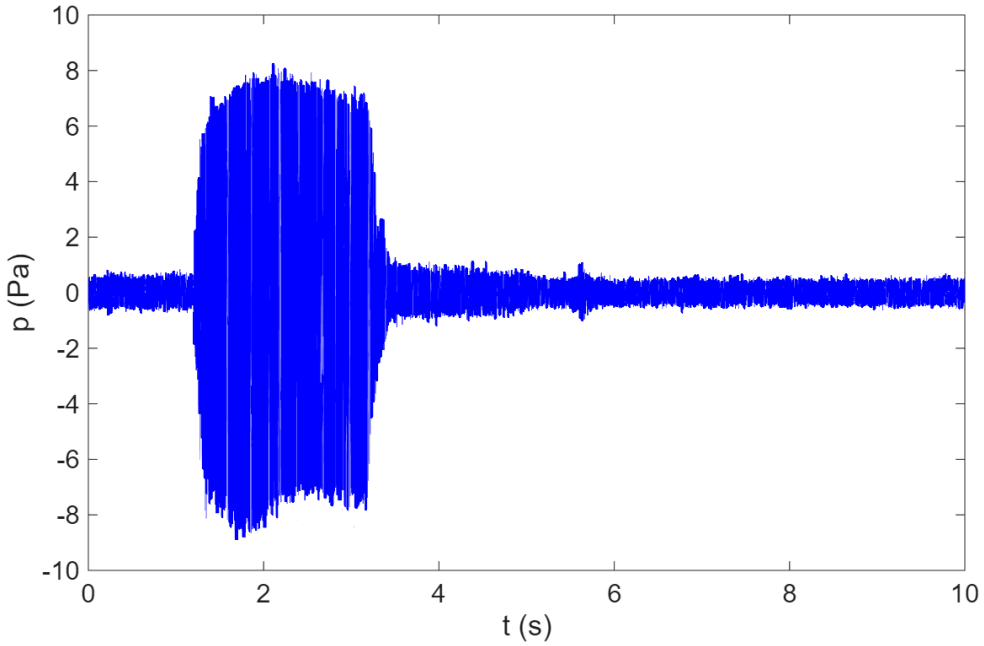


Figure 4.74: The total time interval of the signal from the microphone (sound pressure signal) showing when the tool interacts with the workpiece.

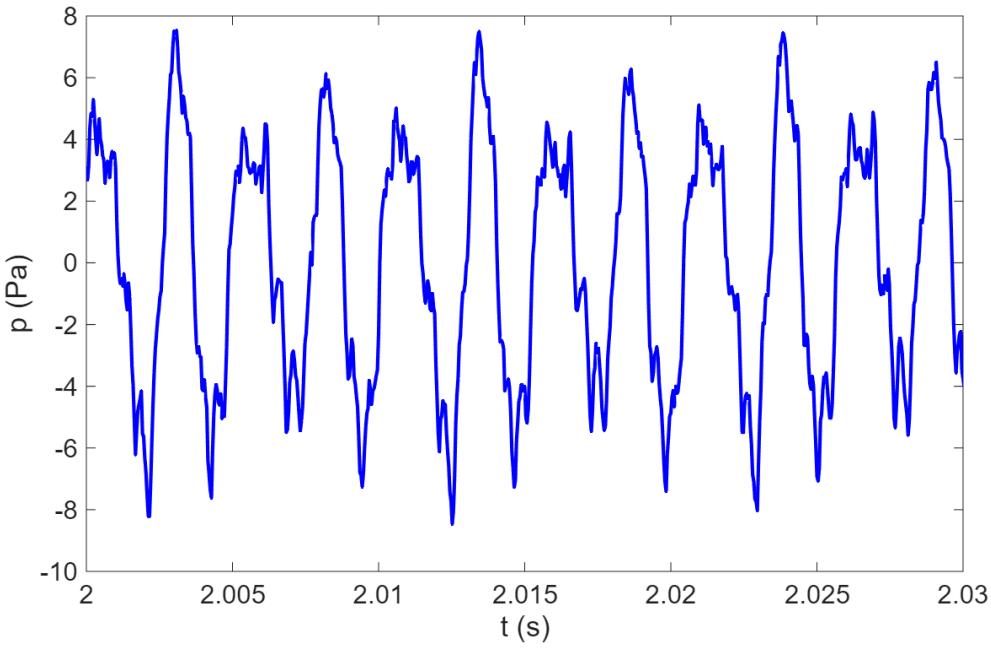


Figure 4.75: The magnified time interval of the signal from the microphone (sound pressure signal).

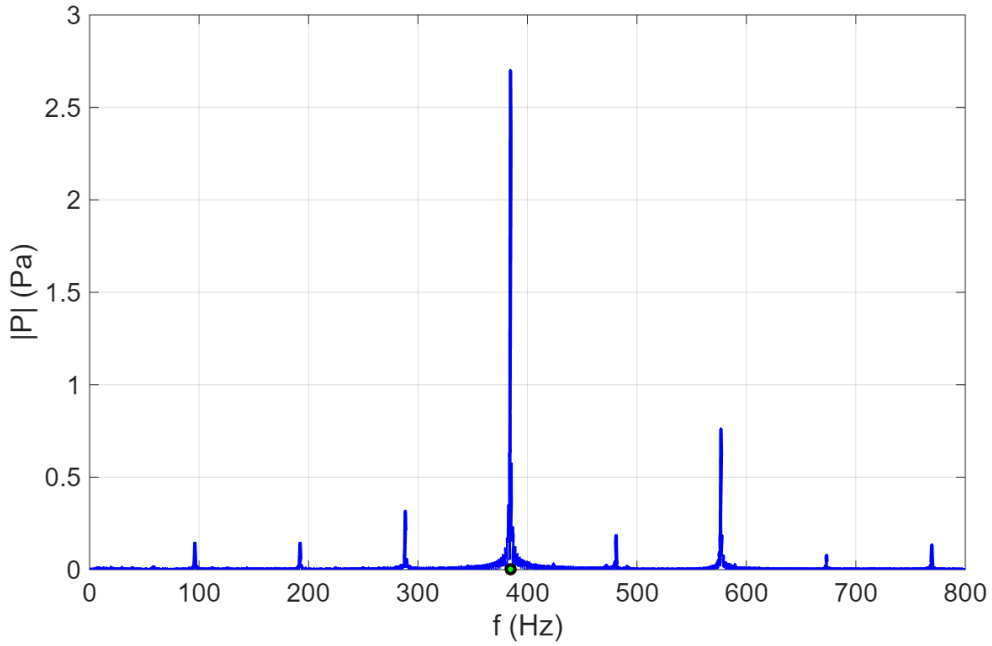


Figure 4.76: Magnitude plot of *p* frequency content for 150 rotations, with f_{tooth} (black circle) identified at 385 Hz.

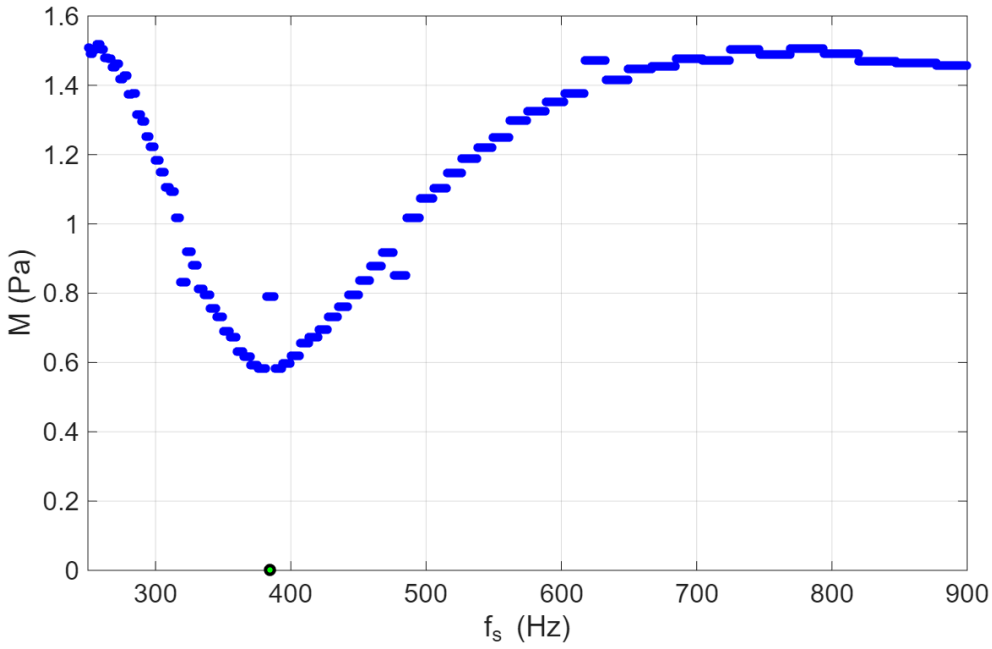


Figure 4.77: Variation in *M* value with periodic f_s. A local minimum occurs at f_{tooth} of 385 Hz (black circle) where M = 0.79 Pa.

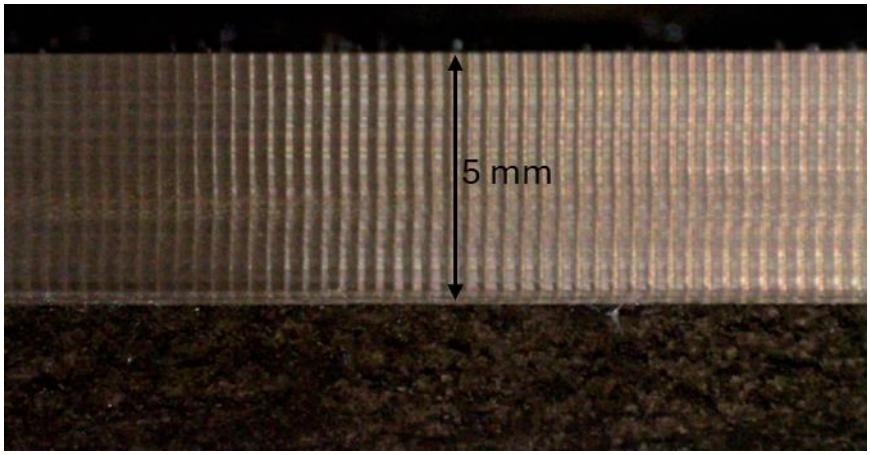


Figure 4.78: Surface of the AISI 4140 steel workpiece with periodic feed marks after the marginally stable cut.

Stable cut: Four-flute endmill on AISI 4140 steel.

Results from tap testing and a stable experimental cut using a four-flute carbide endmill on AISI 4140 steel are presented below. **Table 4.14** shows the modal parameters of the workpiece obtained after tap testing. The tool tip modal parameters presented in **Table 4.9** are retained because, unlike the workpiece which experiences a reduction in mass after cutting, the tool remains unchanged from the previous experimental cut upon inspection.

Table 4.13. Profilometer results from six measured locations on the marginal cut surface of the AISI 4140 steel workpiece.

Location	Ra (μm)	Rq (μm)	Rz (μm)
1	0.813	0.952	3.637
2	0.808	0.966	4.007
3	0.814	0.988	4.336
4	0.969	1.126	4.143
5	1.012	1.155	3.805
6	0.852	0.979	4.067

Figures 4.79 and **4.80** show the frequency response function and the stability lobe diagram, respectively, obtained using the modal parameters. A tangential force coefficient of 2044.5 N/mm^2 and a normal force coefficient of 578.5 N/mm^2 for AISI 4140 steel are selected. A radial depth of cut of 1 mm is selected, and a stable point corresponding to a spindle speed of 5100 rpm and an axial depth of cut of 5 mm is selected on the stability lobe diagram, which achieves the stable cut.

Results from the time domain milling signals of the displacement (x), the acceleration (a), and the sound pressure (p) are presented, including, the total time interval of each signal, the magnified time interval, magnitude plot of the frequency content, and the variation in the M value with the periodic sampling frequency, f_s, which validates chatter detection by periodic sampling of time domain milling signals.

Figures 4.81, **4.85**, and **4.89** show the total time interval of the cut from the CMD, the accelerometer, and the microphone milling signals respectively. **Figures 4.82**, **4.86**, and **4.90** show the magnified time interval of the cut from the CMD, the accelerometer, and the microphone milling signals respectively. **Figures 4.83**, **4.87**, and **4.91** show the magnitude plots of the frequency contents from the CMD, the accelerometer, and the microphone milling signals respectively. It is observed that the tooth passing frequency, f_{tooth}, and its harmonics have the highest peaks in the magnitude plots, indicating stable behavior. In the case of the acceleration and sound pressure milling signals specifically, the 1st harmonic of f_{tooth} have the highest peaks. **Figures 4.84**, **4.88**, and **4.92** show the variations in the M values with the periodic sampling frequency of the time domain milling signals from the CMD, the accelerometer, and the microphone respectively. It is

observed that for the three milling signals, a local minimum in the stability metric occurs at the tooth passing frequency, f_{tooth}, thereby indicating a stable cut. In the case of the acceleration and sound pressure milling signals, local minima occur at f_{tooth} and its 1st harmonic. It is also observed that the M values from the local minima occurring at f_{tooth} are less than those recorded in the previous cuts.

Figure 4.93 shows the surface of the workpiece with periodic feed marks after the cut, indicating the tool tooth trajectory. Even under stable cutting conditions, steel workpieces such as AISI AISI 4140 or AISI 1018 typically exhibit periodic feed marks on the machined surface due to their higher strength, hardness, and strain hardening behavior compared to softer alloys like 6061-T6 aluminum. Surface roughness measurements were conducted at six different locations on the cut surface, yielding a mean Ra value of 0.76 µm with a standard deviation of 0.181 µm, a mean Rq value of 0.91 µm with a standard deviation of 0.195 µm, and a mean Rz value of 3.73 µm with a standard deviation of 0.560 µm. **Table 4.15** shows the Ra, Rq, and Rz values for the six measured locations.

Table 4.14. Workpiece modal parameters of the AISI 4140 steel before the stable cut.

***x*-direction**		
Frequency, f_n (Hz)	**Stiffness, k (N/m)**	**Damping ratio, ζ (-)**
628	1.89×10^7	0.0183
***y*-direction**		
Frequency, f_n (Hz)	**Stiffness, k (N/m)**	**Damping ratio, ζ (-)**
205	6.01×10^8	0.0831
805	2.63×10^9	0.0429
1977	5.39×10^8	0.0120
2130	9.28×10^9	0.0132
2309	3.04×10^8	0.0255
2563	2.11×10^9	0.0085
4019	3.19×10^9	0.0072
4182	3.98×10^9	0.0045

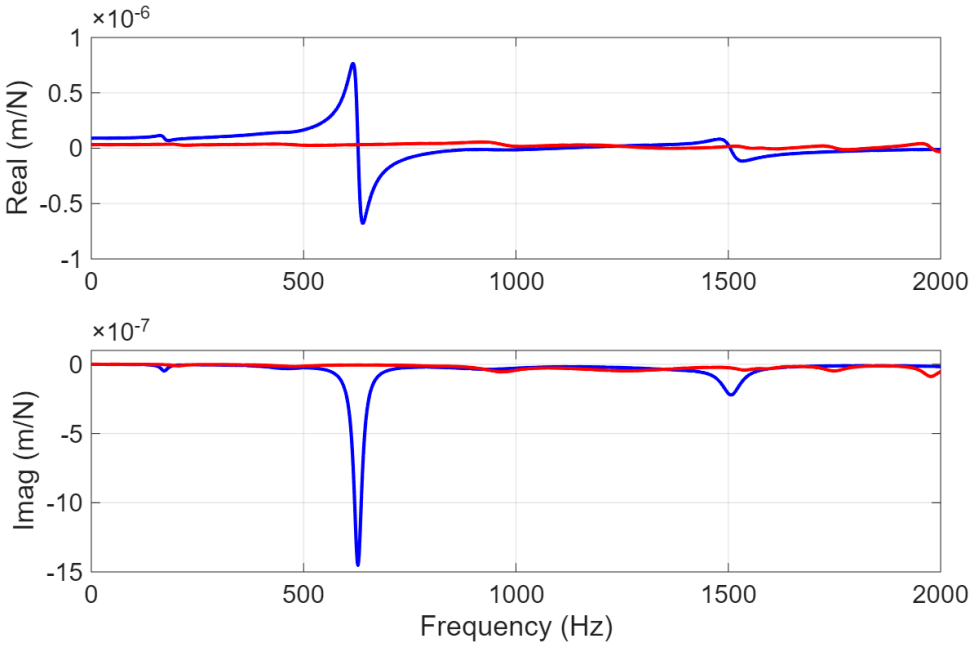


Figure 4.79: Tool tip and workpiece, *x* (blue lines) and *y* (red lines) directions, frequency response function.

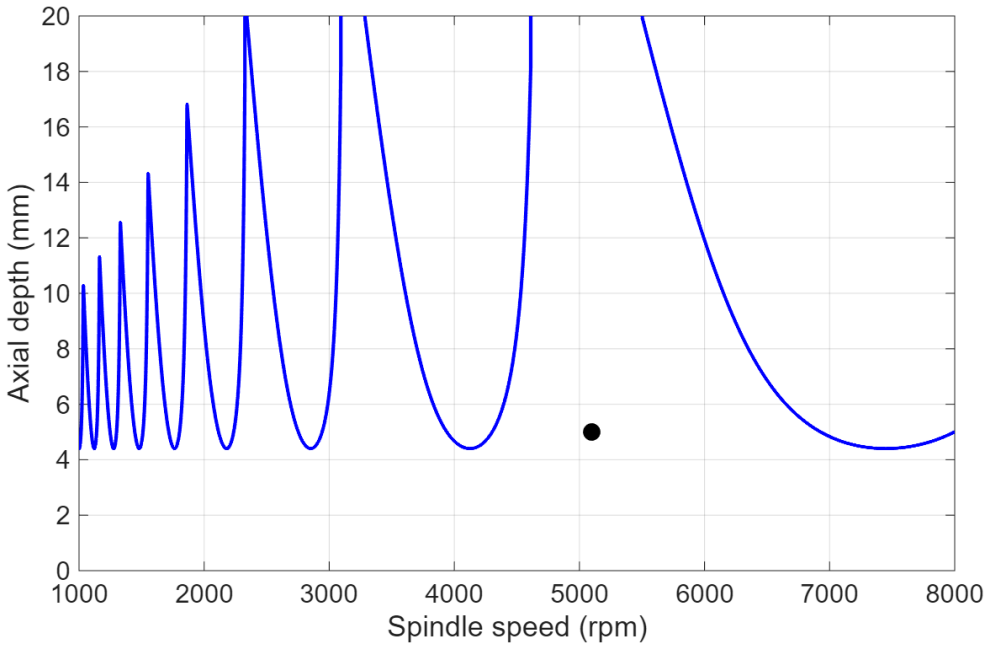


Figure 4.80: Stability lobe diagram with the selected stable point (black dot) corresponding to a spindle speed of 5100 rpm and axial depth of cut of 5 mm.

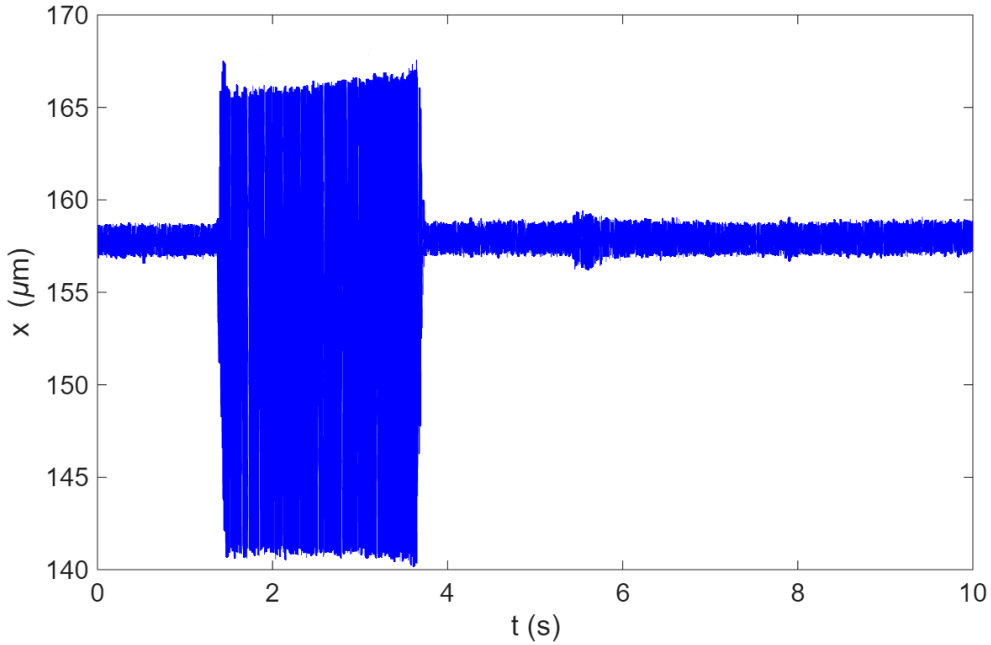


Figure 4.81: The total time interval of the signal from the CMD (displacement signal) showing when the tool interacts with the workpiece.

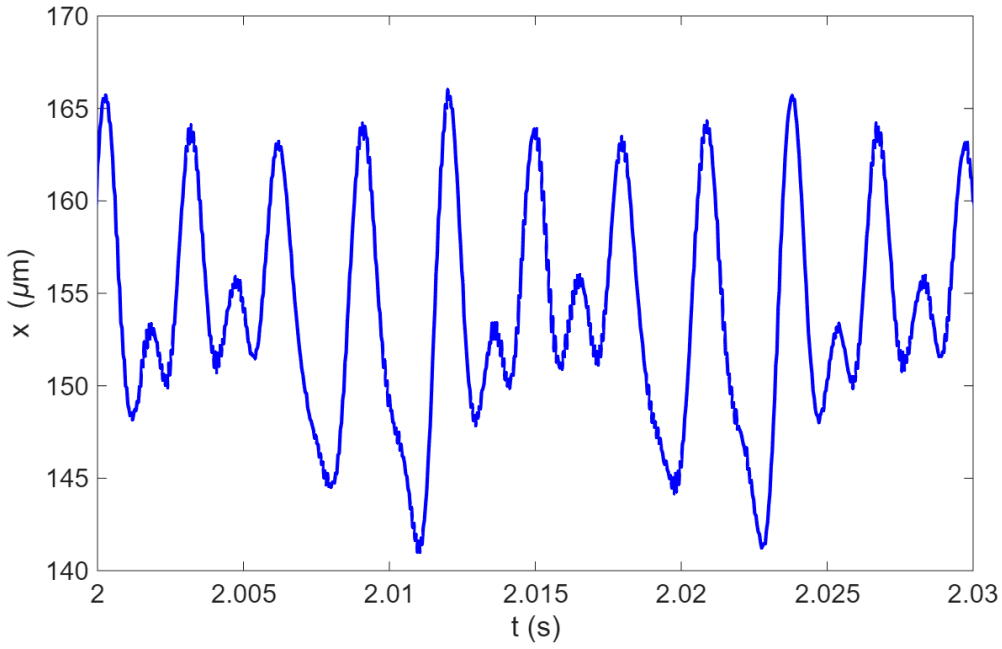


Figure 4.82: The magnified time interval of the signal from the CMD (displacement signal).

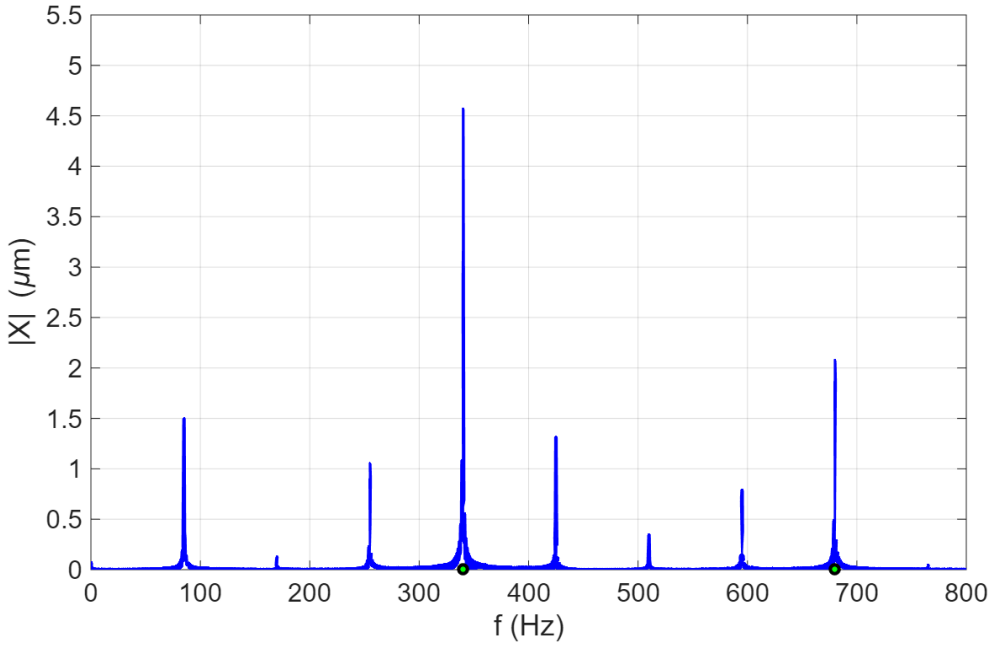


Figure 4.83: Magnitude plot of *x* frequency content for 150 rotations, with f_{tooth} at 340 Hz and its 1st harmonic identified (black circles).

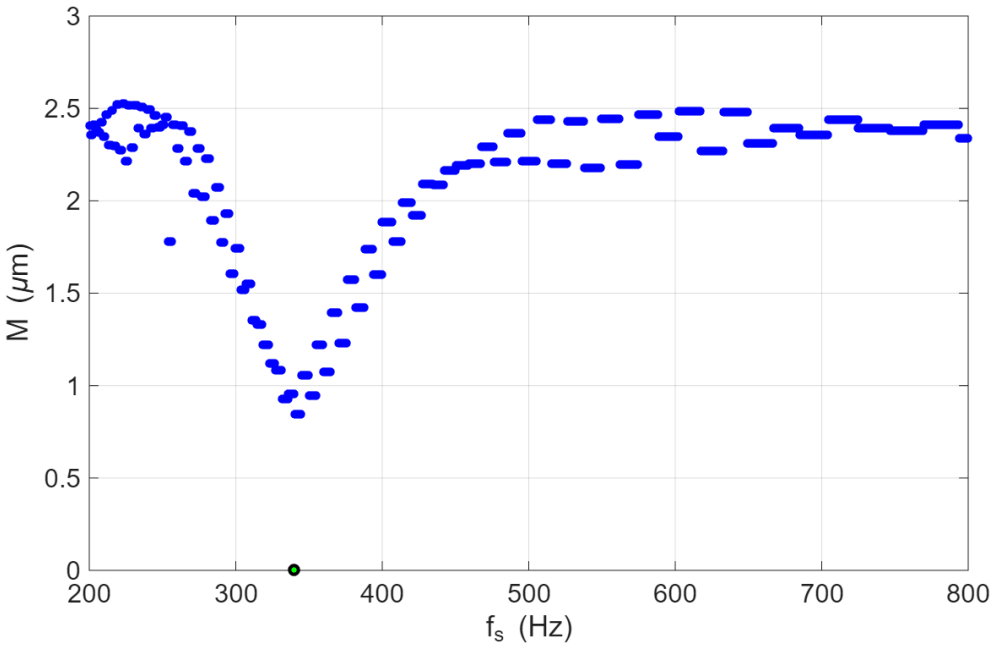


Figure 4.84: Variation in *M* value with periodic f_s. A local minimum occurs at f_{tooth} of 340 Hz (black circle), where M = 0.85 µm.

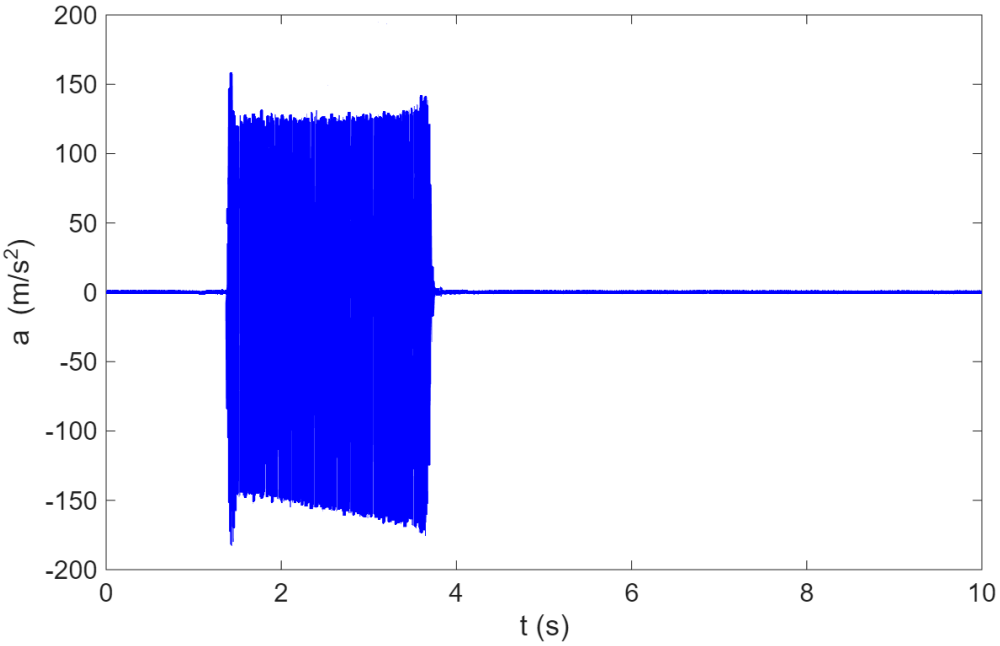


Figure 4.85: The total time interval of the signal from the accelerometer (acceleration signal) showing when the tool interacts with the workpiece.

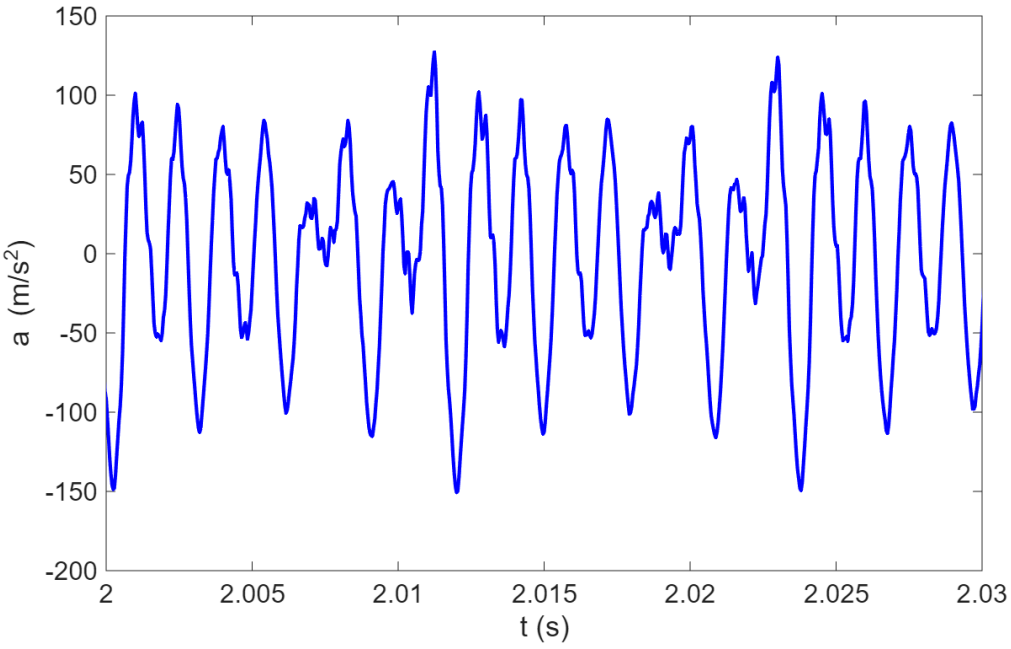


Figure 4.86: The magnified time interval of the signal from the accelerometer (acceleration signal).

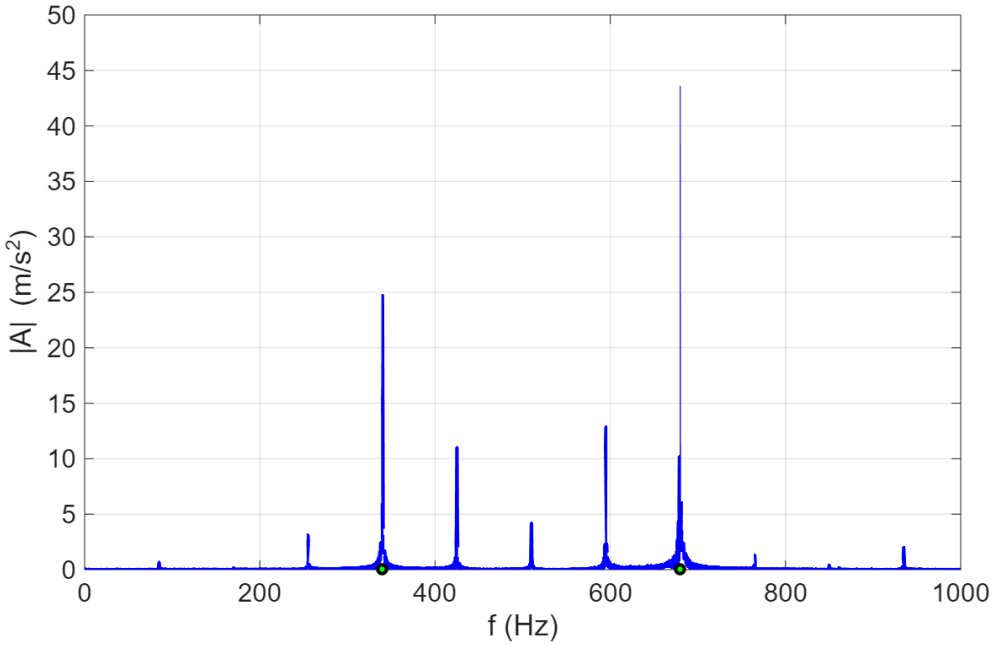


Figure 4.87: Magnitude plot of *a* frequency content for 150 rotations, with f_{tooth} at 340 Hz and its 1st harmonic identified (black circles).

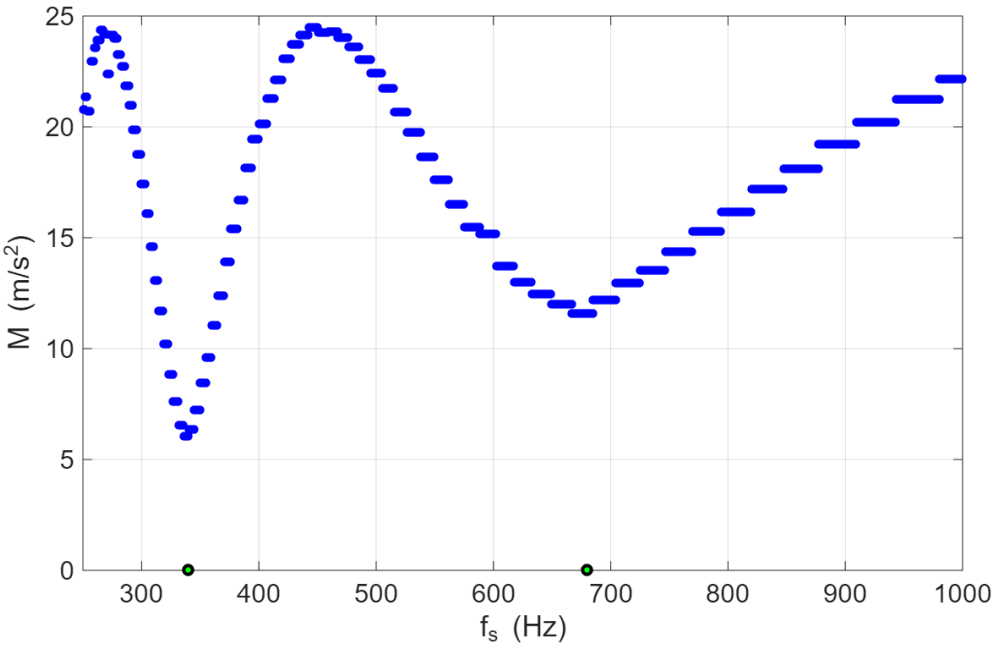


Figure 4.88: Variation in *M* value with periodic f_s. Local minima occur at f_{tooth} of 340 Hz, where M = 6.05 m/s^2, and at its 1st harmonic (black circles).

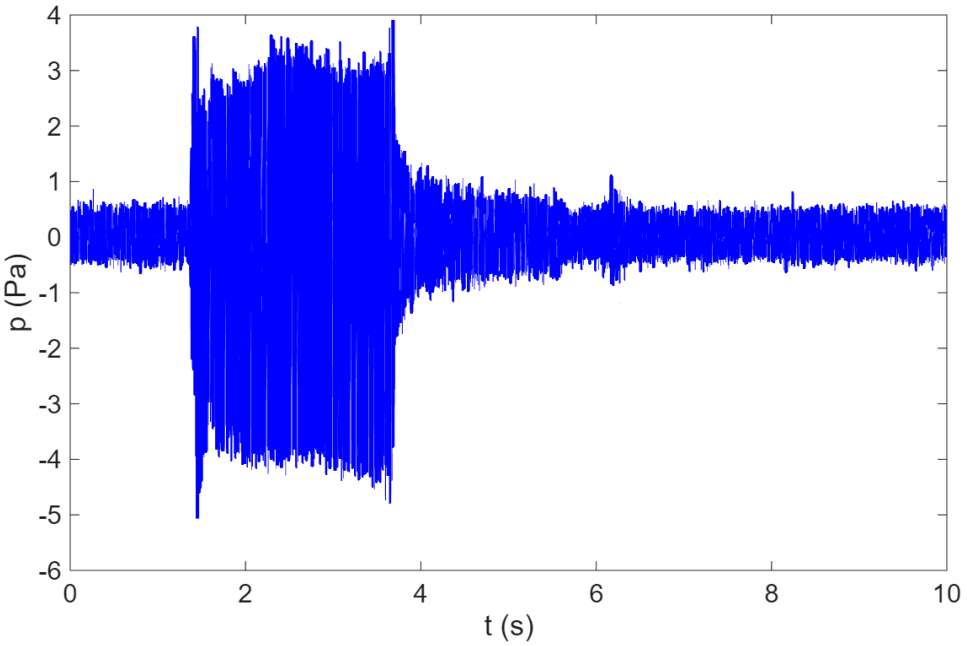


Figure 4.89: The total time interval of the signal from the microphone (sound pressure signal) showing when the tool interacts with the workpiece.

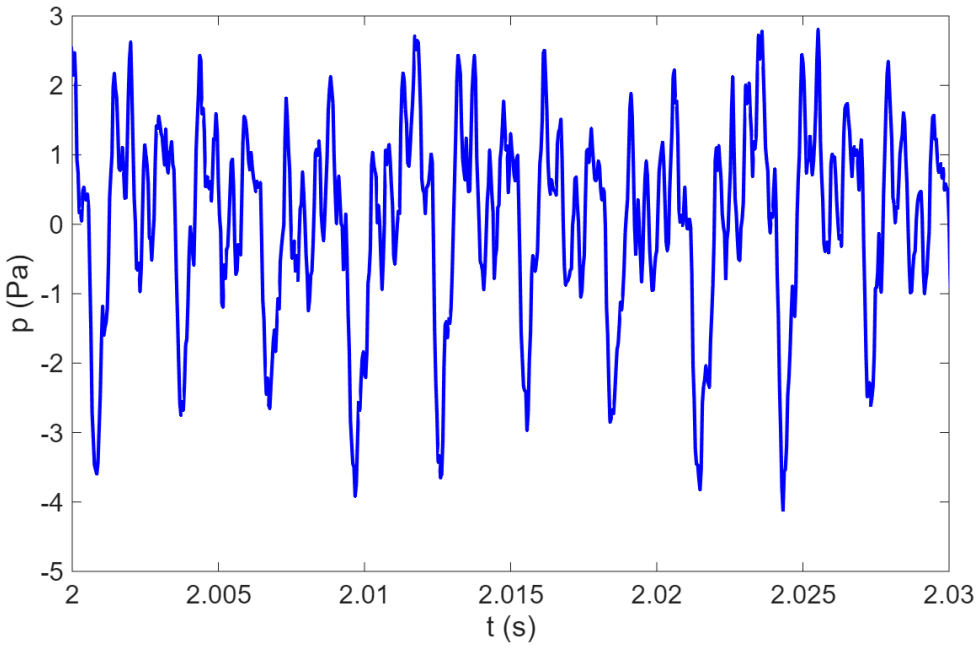


Figure 4.90: The magnified time interval of the signal from the microphone (sound pressure signal).

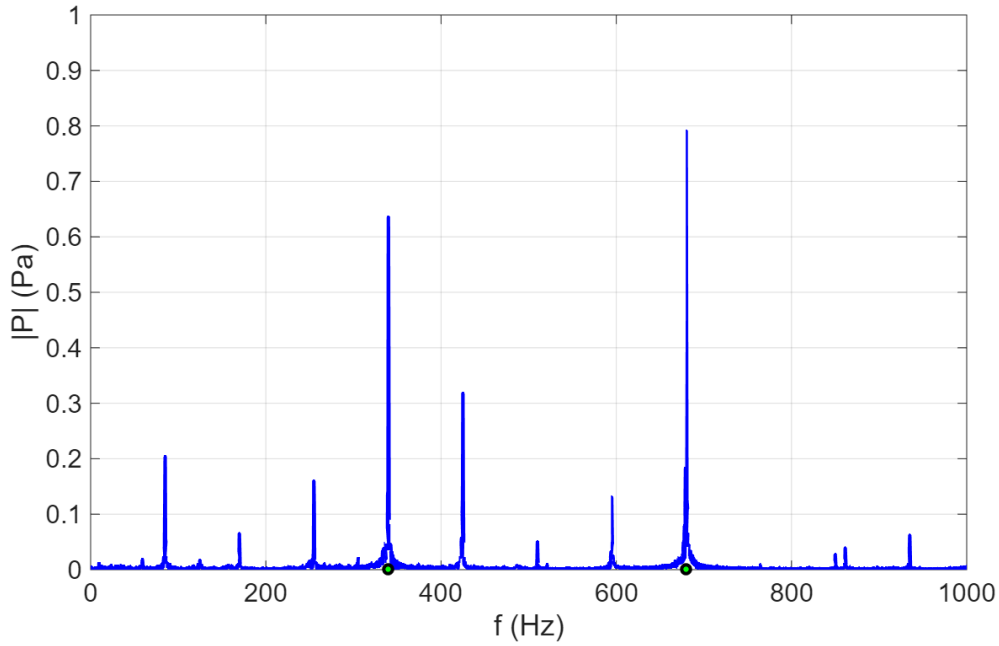


Figure 4.91: Magnitude plot of *p* frequency content for 150 rotations, with f_{tooth} at 340 Hz and its 1st harmonic identified (black circles).

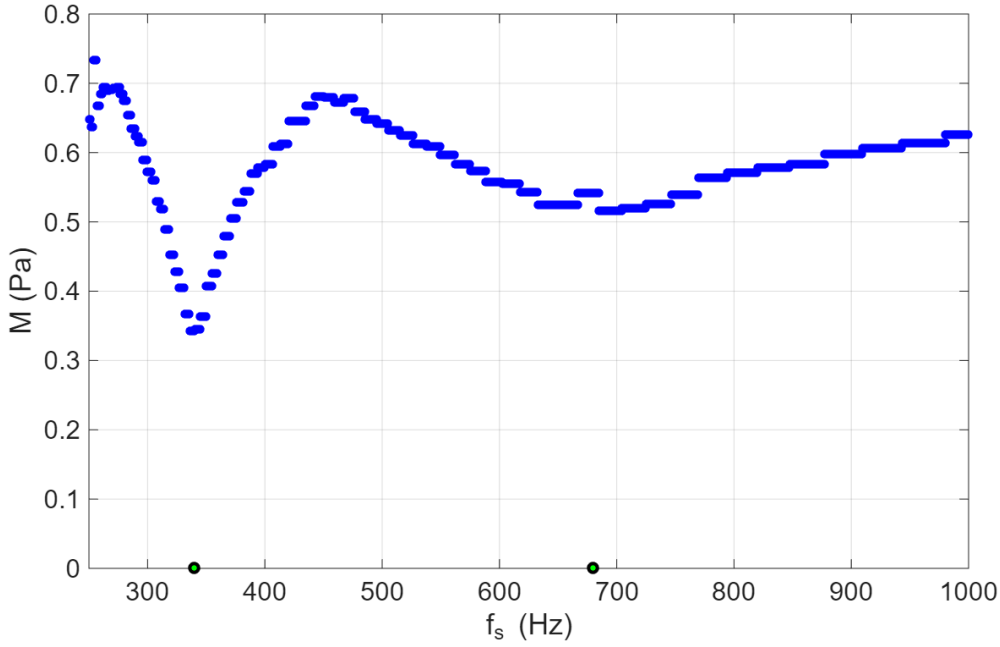


Figure 4.92: Variation in *M* value with periodic f_s. Local minima occur at f_{tooth} of 340 Hz, where M = 0.34 Pa, and at its 1st harmonic (black circles).

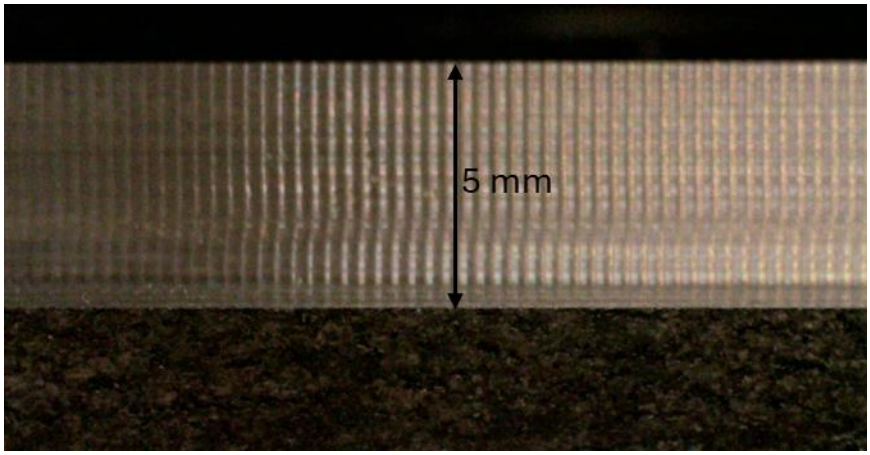


Figure 4.93: Surface of the AISI 4140 steel workpiece with periodic feed marks after the stable cut.

Power sensor results.

Although the power sensor signal could not be used for once-per-revolution sampling, the power sensor measurements for this tool and workpiece combination (four-flute carbide endmill and AISI 4140 steel) also indicate a monotonic rise in spindle power consumption with increasing spindle speed and depth of cut. This trend is consistent with the expected mechanical behavior of the spindle-tool system, where higher rotational speeds and depths of cut demand greater energy input to overcome inertia, friction, and cutting-related resistances.

Table 4.15. Profilometer results from six measured locations on the stable cut surface of the AISI 4140 steel workpiece.

Location	Ra (µm)	Rq (µm)	Rz (µm)
1	0.668	0.816	3.413
2	0.568	0.701	3.058
3	0.810	0.943	3.693
4	0.647	0.786	3.513
5	0.793	0.951	4.052
6	1.080	1.256	4.658

Figures 4.94, **4.95**, and **4.96** show the spindle power consumptions during the unstable, marginally stable, and stable experimental cuts conducted using the four-flute endmill on the AISI 4140 steel workpieces. **Table 4.16** shows the spindle speeds, axial depths of cut, radial depths of cut, and the peak spindle power consumptions for the unstable, marginally stable, and stable experimental cuts.

Table 4.16. Cutting parameters and peak spindle power for the experimental cuts using the four-flute endmill on the AISI 4140 steel workpiece.

Experimental cut	Spindle speed (rpm)	Axial depth (mm)	Radial depth (mm)	Peak spindle power (kW)
Unstable	7000	5	2	2.37
Marginally stable	5770	5	2	1.81
Stable	5100	5	1	1.27

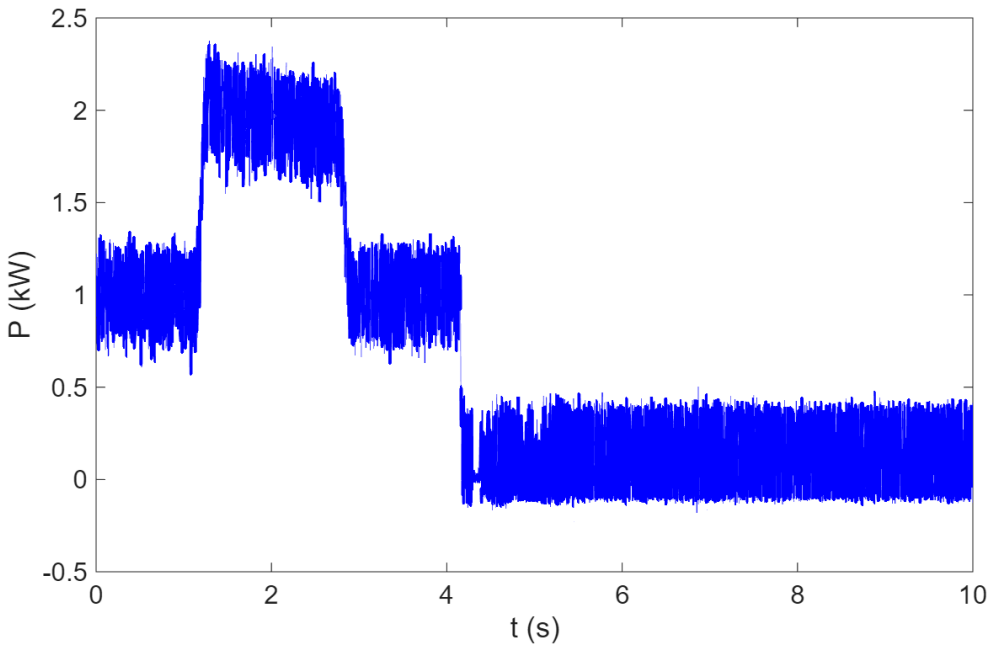


Figure 4.94: Spindle power consumption peaked at 2.37 kW during the unstable cut at a spindle speed of 7000 rpm, axial and radial depths of cut of 5 mm and 2 mm respectively.

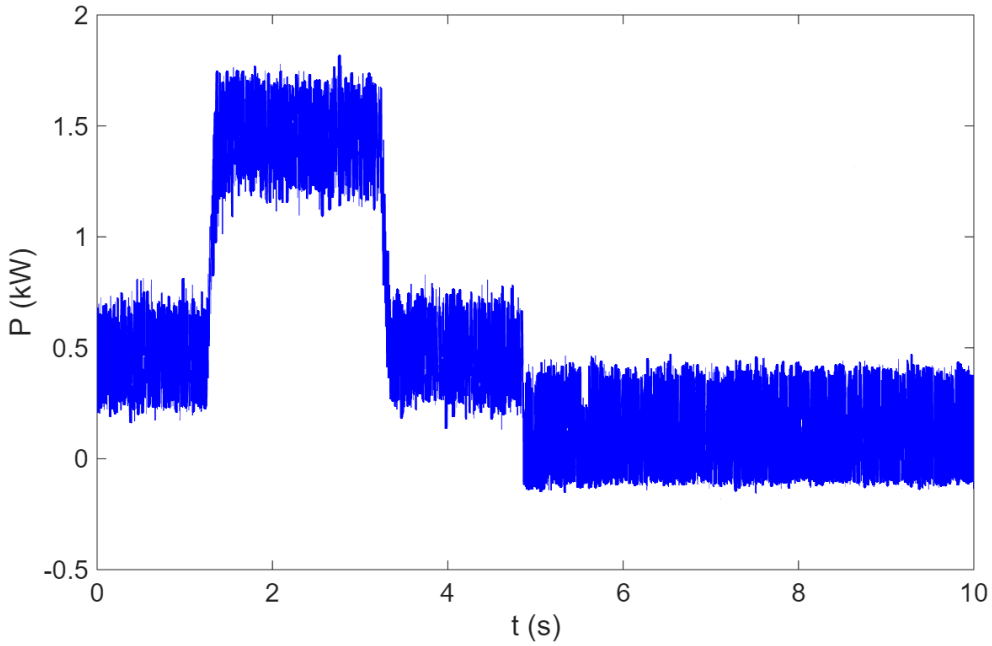


Figure 4.95: Spindle power consumption peaked at 1.81 kW during the marginal cut at a spindle speed of 5770 rpm, axial and radial depths of cut of 5 mm and 2 mm respectively.

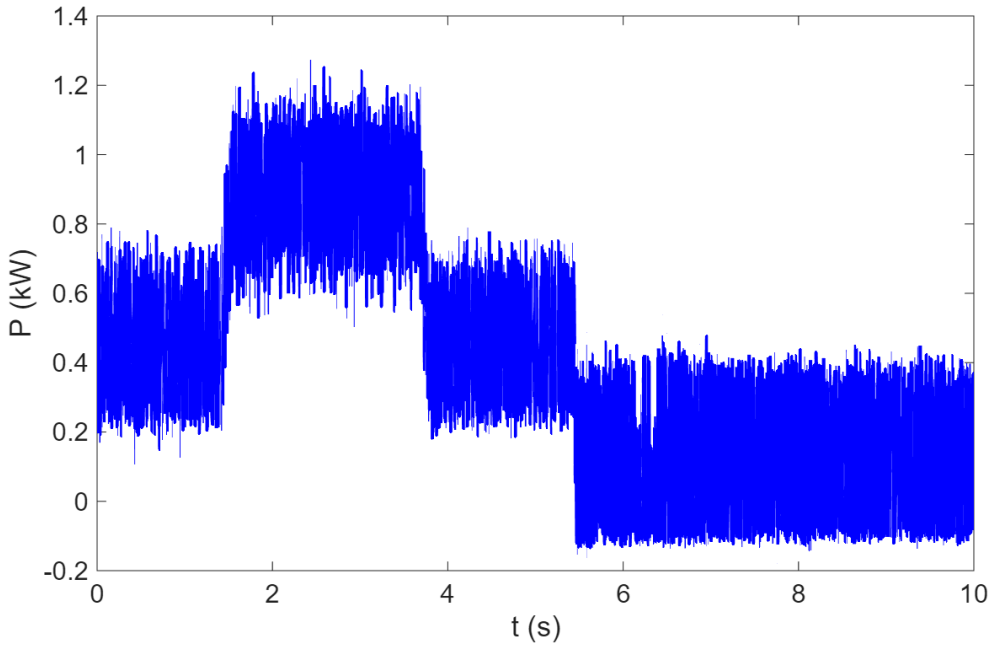


Figure 4.96: Spindle power consumption peaked at 1.27 kW during the stable cut at a spindle speed of 5100 rpm, axial and radial depths of cut of 5 mm and 1 mm respectively.

Unstable cut: Five-flute endmill on AISI 4140 steel

Results from tap testing and an unstable experimental cut using a five-flute carbide endmill on AISI 4140 steel are presented below. **Tables 4.17** and **4.18** show the modal parameters of the tool tip and workpiece respectively, obtained after tap testing, while **Figures 4.97** and **4.98** show the frequency response function and the stability lobe diagram obtained using the modal parameters. A tangential force coefficient of 2044.5 N/mm^2 and a normal force coefficient of 578.5 N/mm^2 for AISI 4140 steel are selected. A radial depth of cut of 1 mm is selected, and an unstable point corresponding to a spindle speed of 6000 rpm and an axial depth of cut of 8 mm is selected on the stability lobe diagram, which achieves an unstable cut.

Results from the time domain milling signals of the displacement (x), the acceleration (a), and the sound pressure (p) are presented, including, the total time interval of each signal, the magnified time interval, magnitude plot of the frequency content, and the variation in the M value with the periodic sampling frequency, f_s. The variation in the M value with the periodic sampling frequency, f_s, validates chatter detection by periodic sampling of time domain milling signals.

Figures 4.99, **4.103**, and **4.107** show the total time interval of the cut from the CMD, the accelerometer, and the microphone milling signals respectively. **Figures 4.100**, **4.104**, and **4.108** show the magnified time interval of the cut from the CMD, the accelerometer, and the microphone milling signals respectively. **Figures 4.101**, **4.105**, and **4.109** show the magnitude plots of the frequency contents from the CMD, the accelerometer, and the microphone milling signals respectively. It is observed that the chatter frequency, f_c, has

the highest peak in the magnitude plots, indicating an unstable cut. **Figures 4.102**, **4.106**, and **4.110** show the variations in the *M* values with the periodic sampling frequency of the time domain milling signals from the CMD, the accelerometer, and the microphone respectively. It is observed that, for the three signals, a local minimum in the stability metric occurs at the chatter frequency, f_c, not at the tooth passing frequency, f_{tooth}, thereby indicating an unstable cut.

Figure 4.111 shows the surface of the workpiece with visible chatter marks after the unstable cut, captured using the Dino-Lite digital microscope. Surface roughness measurements were conducted at six different locations on the cut surface using the Mitutoyo profilometer, yielding a mean Ra value of 1.18 µm with a standard deviation of 0.189 µm, a mean Rq value of 1.40 µm with a standard deviation of 0.219 µm, and a mean Rz value of 5.62 µm with a standard deviation of 0.718 µm. **Table 4.19** shows the Ra, Rq, and Rz values for the six measured locations.

Marginally unstable cut: Five-flute endmill on AISI 4140 steel.

Results from tap testing and a marginally unstable experimental cut using a five-flute carbide endmill on AISI 4140 steel are presented below. Tables 4.20 shows the modal parameters of the workpiece obtained after tap testing. The tool tip modal parameters presented in Table 4.17 are retained because, unlike the workpiece which experiences a reduction in mass after cutting, the tool remains unchanged from the previous experimental cut upon inspection.

Table 4.17. Tool tip modal parameters of the five-flute endmill.

***x*-direction**		
Frequency, f_n (Hz)	**Stiffness, *k* (N/m)**	**Damping ratio, ζ (-)**
172	1.61×10^8	0.0849
942	1.50×10^8	0.1261
1410	1.40×10^8	0.1166
1502	1.68×10^8	0.0167
3530	2.22×10^8	0.1366
10694	7.83×10^8	0.0362
11822	2.76×10^8	0.0261
13489	5.90×10^8	0.0362
15233	1.43×10^9	0.0230
***y*-direction**		
Frequency, f_n (Hz)	**Stiffness, *k* (N/m)**	**Damping ratio, ζ (-)**
971	1.87×10^8	0.0644
1143	3.57×10^8	0.0560
1280	1.85×10^8	0.0392
1526	2.88×10^8	0.0577
1748	5.78×10^8	0.0249
5441	3.10×10^8	0.1237
10856	1.42×10^9	0.0256
11848	4.14×10^8	0.0309
13517	8.20×10^8	0.0370

Table 4.18. Workpiece modal parameters of the AISI 4140 steel before the unstable cut.

***x*-direction**		
Frequency, f_n (Hz)	**Stiffness, *k* (N/m)**	**Damping ratio, ζ (-)**
620	1.86×10^7	0.0198
***y*-direction**		
Frequency, f_n (Hz)	**Stiffness, *k* (N/m)**	**Damping ratio, ζ (-)**
1951	3.71×10^8	0.0111
2068	1.21×10^9	0.0146
2204	4.27×10^8	0.0234
2298	2.27×10^9	0.0083
2548	3.15×10^9	0.0114
3894	7.17×10^8	0.0196
4103	3.70×10^9	0.0149

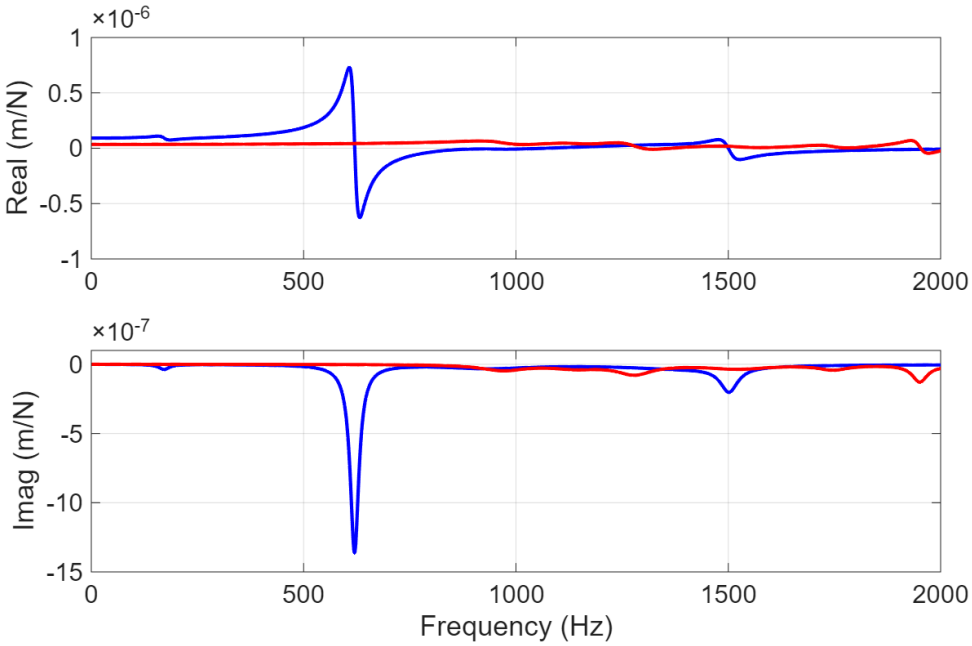


Figure 4.97: Frequency response function of the tool tip and workpiece, *x* (blue lines) and *y* (red lines) directions.

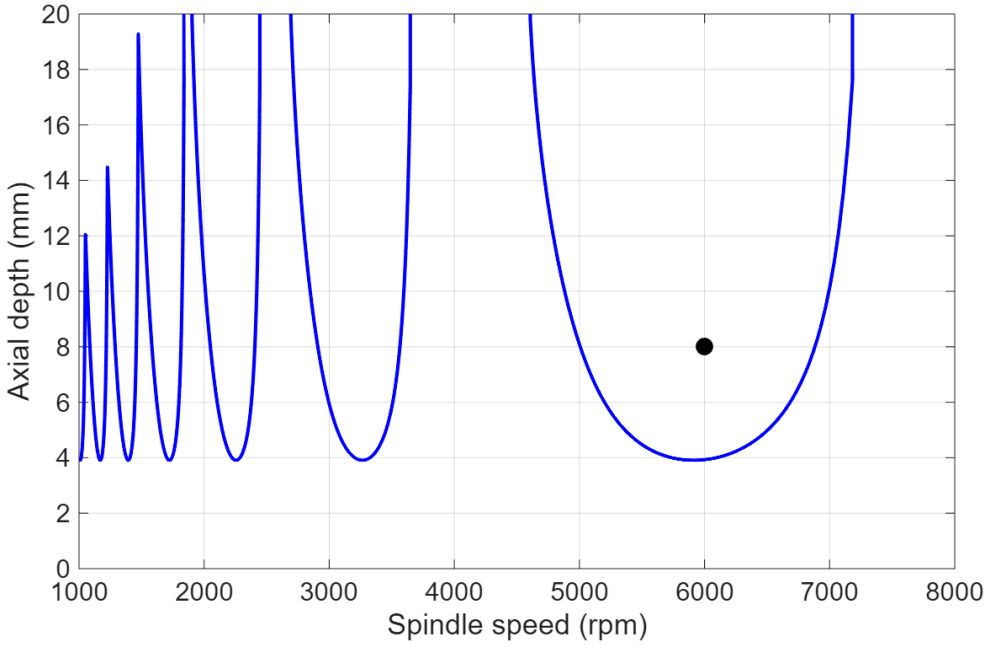


Figure 4.98: Stability lobe diagram with the selected unstable point (black dot) corresponding to a spindle speed of 6000 rpm and axial depth of cut of 8 mm.

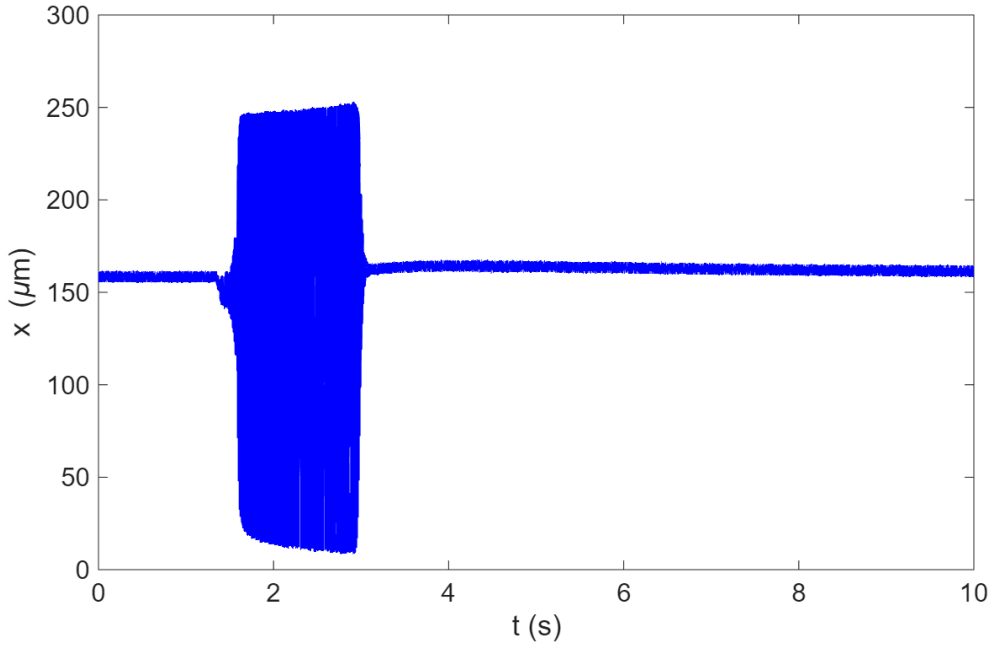


Figure 4.99: The total time interval of the signal from the CMD (displacement signal) showing when the tool interacts with the workpiece.

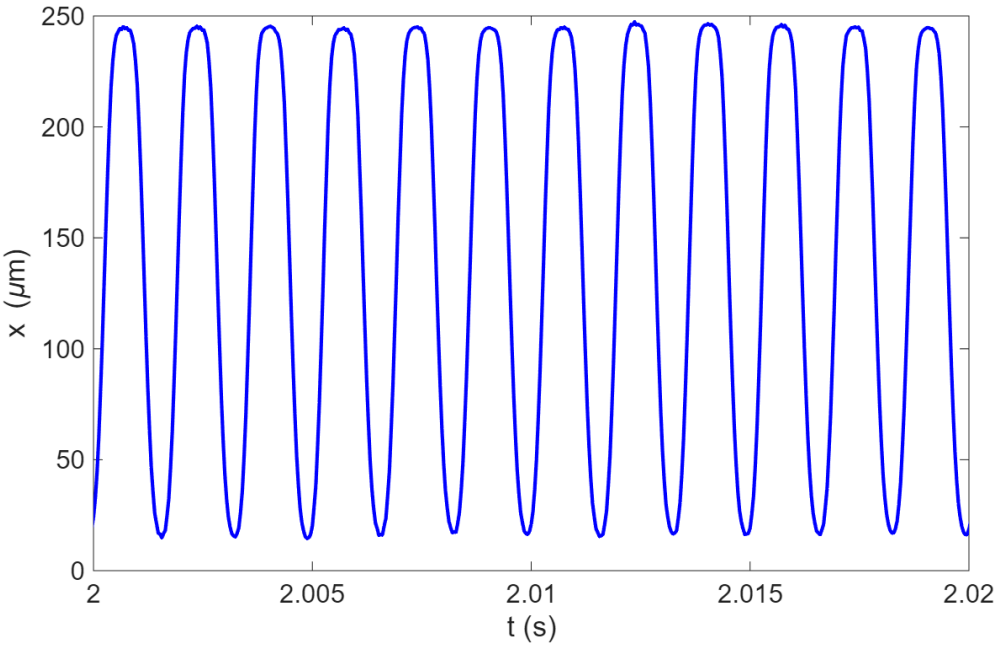


Figure 4.100: The magnified time interval of the signal from the CMD (displacement signal).

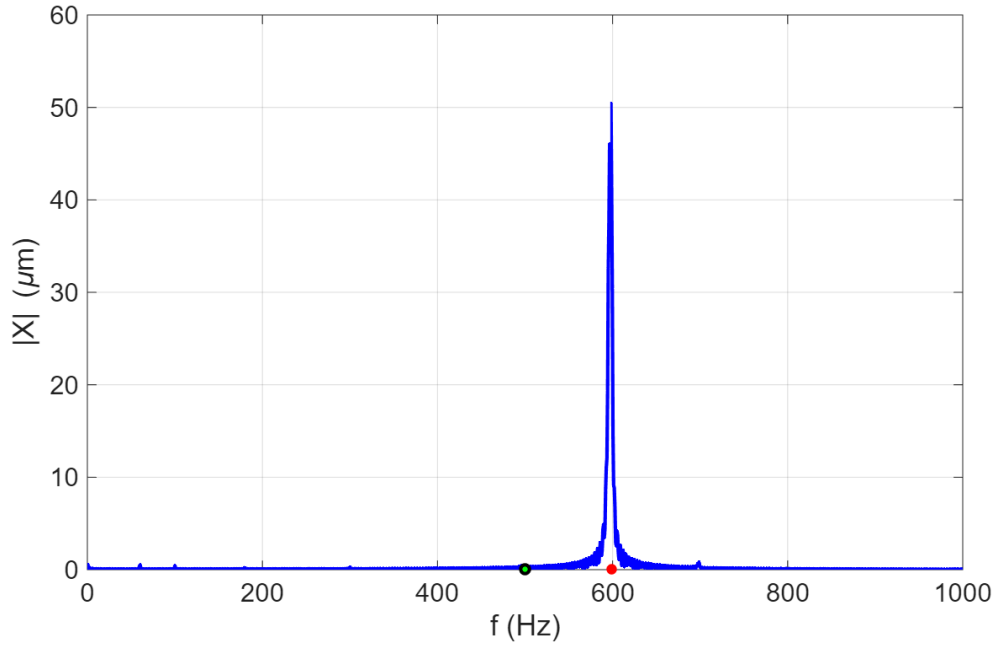


Figure 4.101: Magnitude plot of *x* frequency content for 100 rotations, with f_c (red dot) identified at 599 Hz and f_{tooth} (black circle) at 500 Hz.

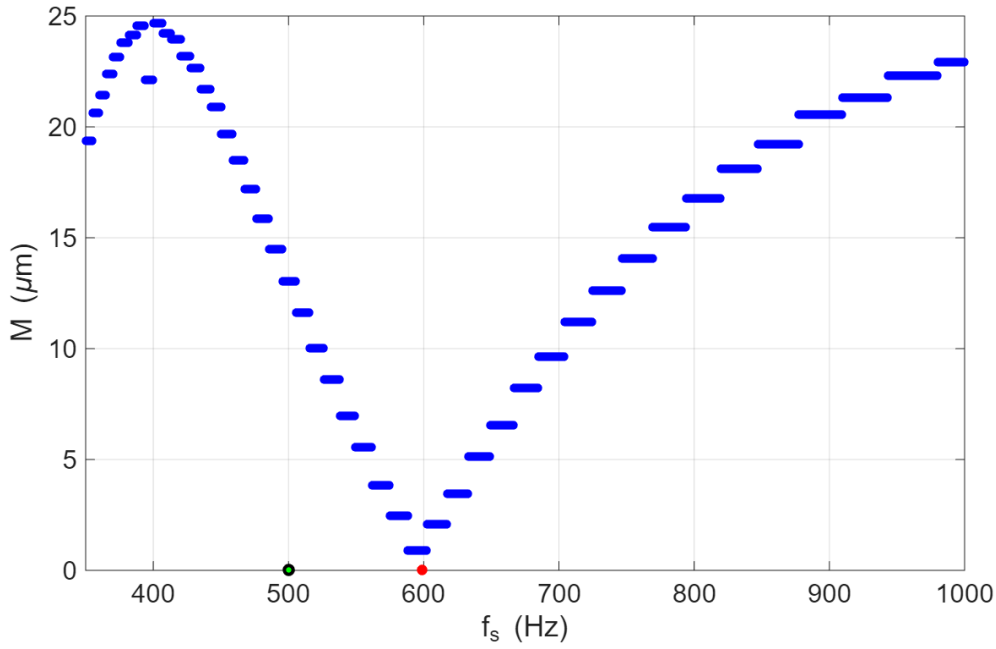


Figure 4.102: Variation in *M* value with periodic f_s. A local minimum occurs at f_c of 599 Hz (red dot) where M = 0.91 µm, not at f_{tooth} (black circle).

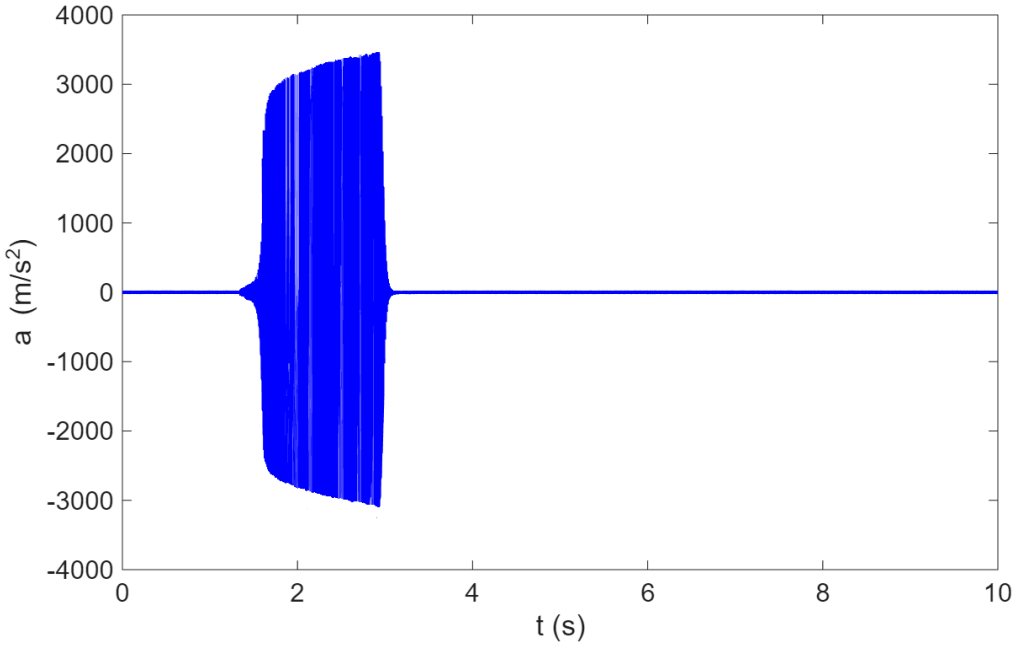


Figure 4.103: The total time interval of the signal from the accelerometer (acceleration signal) showing when the tool interacts with the workpiece.

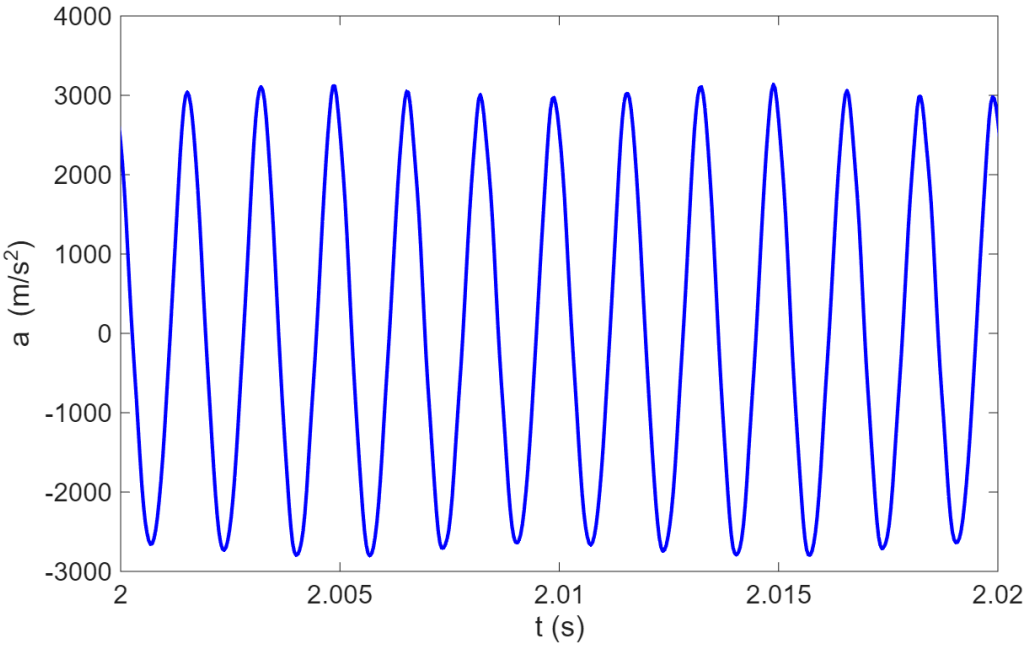


Figure 4.104: The magnified time interval of the signal from the accelerometer (acceleration signal).

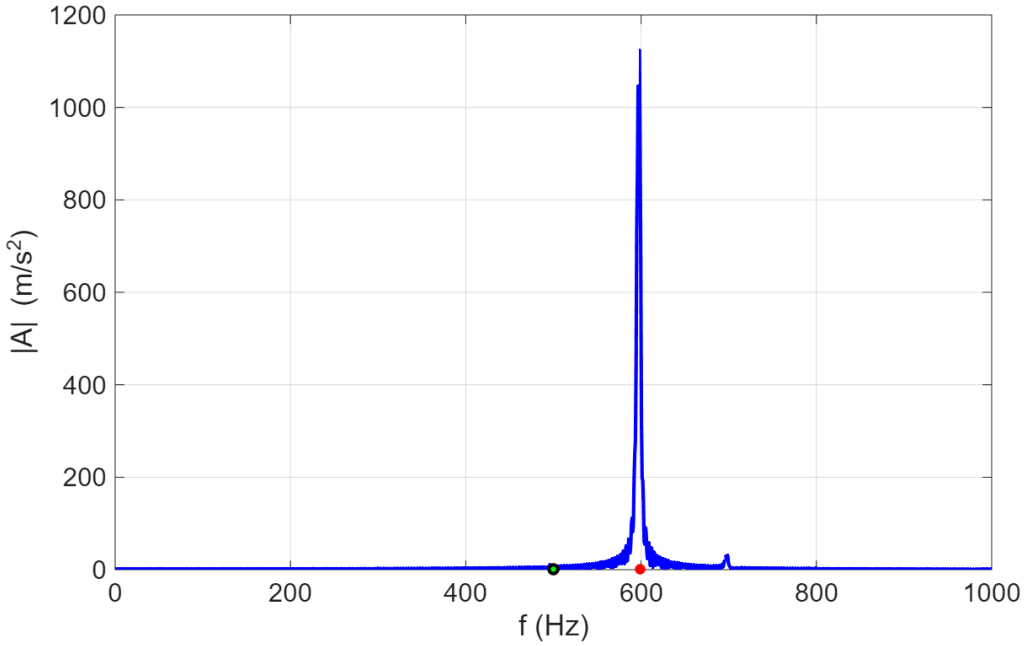


Figure 4.105: Magnitude plot of *a* frequency content for 100 rotations, with f_c (red dot) identified at 599 Hz and f_{tooth} (black circle) at 500 Hz.

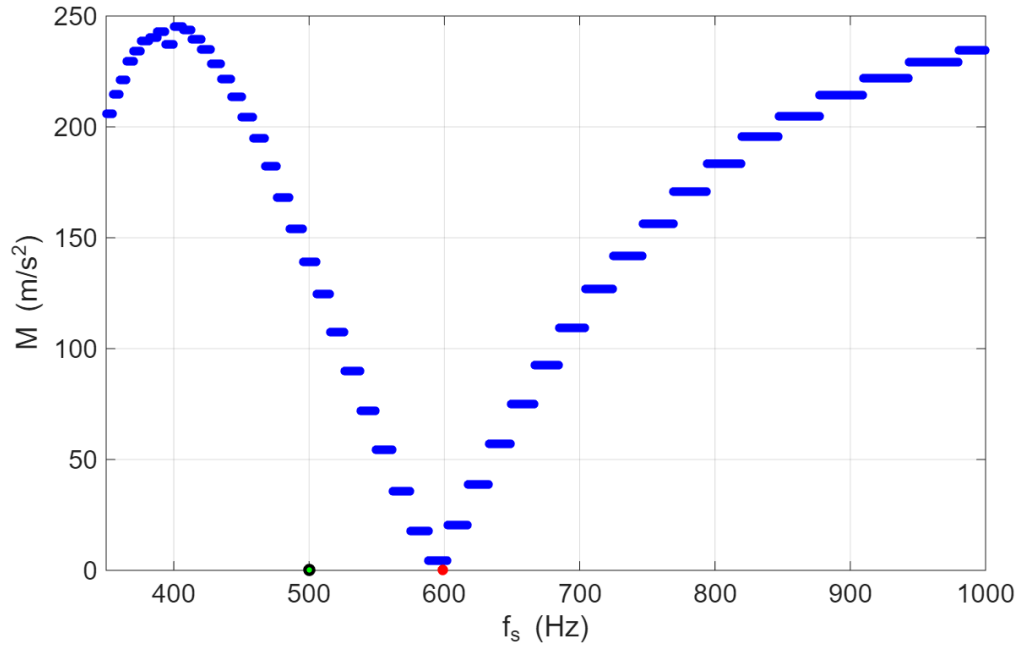


Figure 4.106: Variation in *M* value with periodic f_s. A local minimum occurs at f_c of 599 Hz (red dot) where M = 4.57 m/s^2, not at f_{tooth} (black circle).

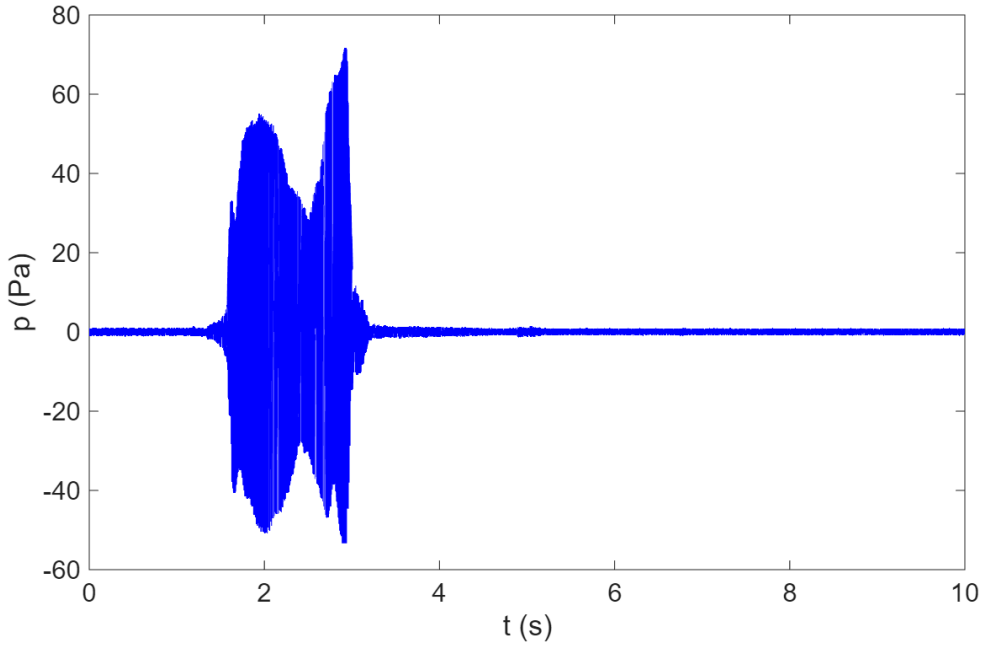


Figure 4.107: The total time interval of the signal from the microphone (sound pressure signal) showing when the tool interacts with the workpiece.

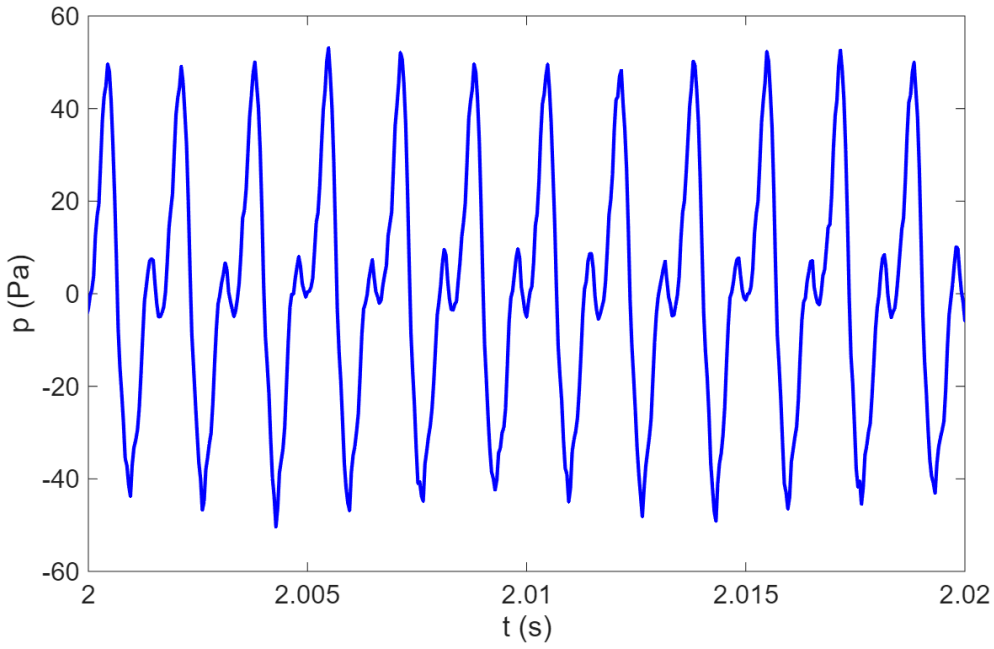


Figure 4.108: The magnified time interval of the signal from the microphone (sound pressure signal).

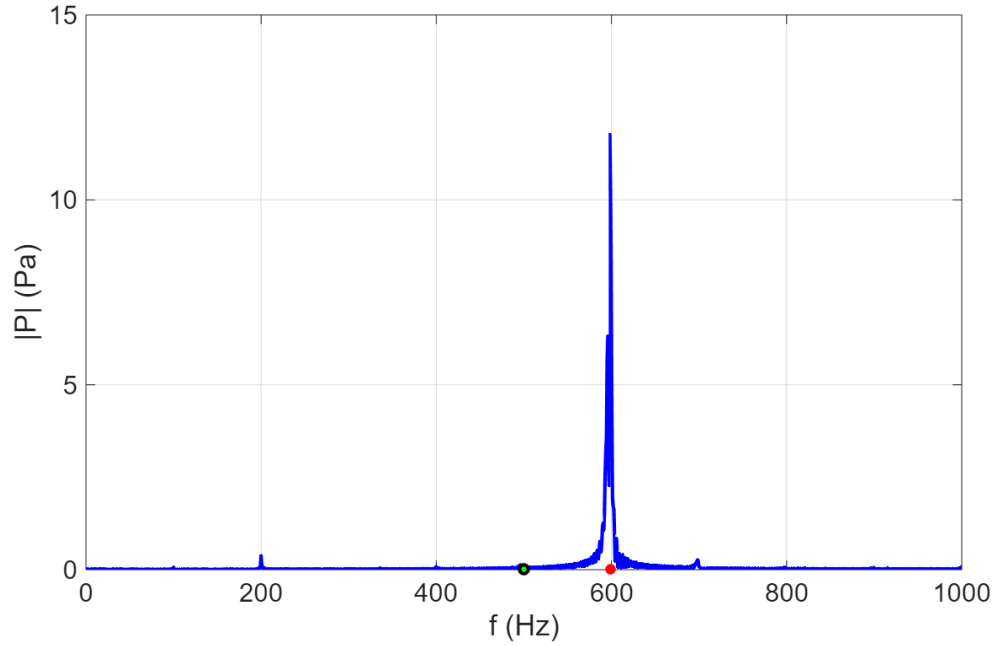


Figure 4.109: Magnitude plot of p frequency content for 100 rotations, with f_c (red dot) identified at 599 Hz and f_{tooth} (black circle) at 500 Hz.

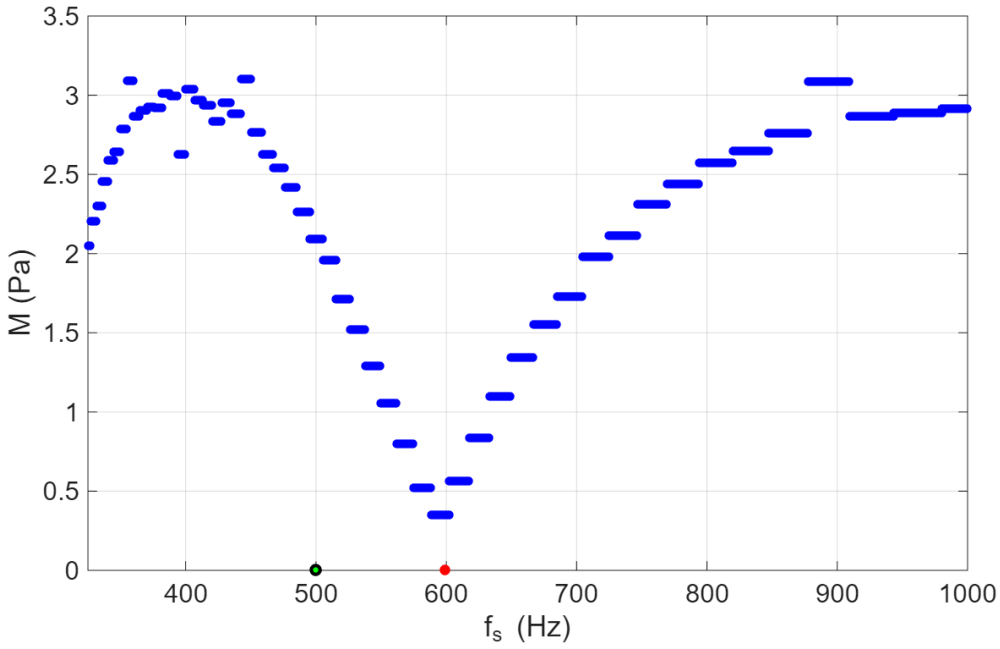


Figure 4.110: Variation in M value with periodic f_s. A local minimum occurs at f_c of 599 Hz (red dot) where 0.35 Pa, not at f_{tooth} (black circle).

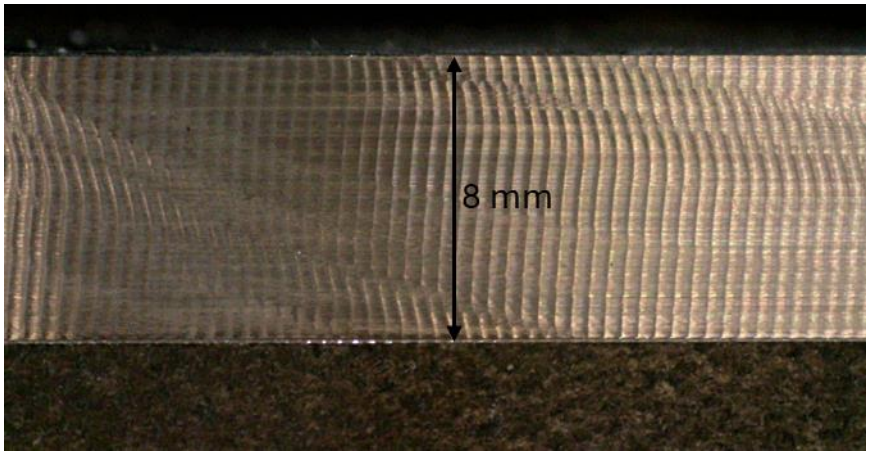


Figure 4.111: Surface of the AISI 4140 steel workpiece with chatter marks after the unstable cut.

Figures 4.112 and **4.113** show the frequency response function and the stability lobe diagram obtained using the modal parameters. A tangential force coefficient of 2044.5 N/mm2 and a normal force coefficient of 578.5 N/mm2 for AISI 4140 steel are selected. A radial depth of cut of 1 mm is selected, and an unstable point corresponding to a spindle speed of 6000 rpm and an axial depth of cut of 4 mm is selected on the stability lobe diagram, which achieves the marginally unstable cut.

Table 4.19. Profilometer results from six measured locations on the unstable cut surface of the AISI 4140 steel workpiece.

Location	Ra (µm)	Rq (µm)	Rz (µm)
1	1.159	1.371	5.520
2	1.188	1.387	4.967
3	1.045	1.229	4.969
4	0.961	1.175	5.774
5	1.231	1.438	5.587
6	1.510	1.797	6.922

Results from the time domain milling signals of the displacement (x), the acceleration (a), and the sound pressure (p) are presented, including, the total time interval of each signal, the magnified time interval, magnitude plot of the frequency content, and the variation in the M value with the periodic sampling frequency, f_s. The variation in the M value with the periodic sampling frequency, f_s, validates chatter detection by periodic sampling of time domain milling signals.

Figures 4.114, **4.118**, and **4.122** show the total time interval of the cut from the CMD, the accelerometer, and the microphone milling signals respectively. **Figures 4.115**, **4.119**, and **4.123** show the magnified time interval of the cut from the CMD, the accelerometer, and the microphone milling signals respectively. **Figures 4.116**, **4.120**, and **4.124** show the magnitude plots of the frequency contents from the CMD, the accelerometer, and the microphone milling signals respectively. It is observed that the chatter frequency, f_c, has the highest peak in the magnitude plots, indicating unstable behavior. **Figures 4.117**, **4.121**, and **4.125** show the variations in the M values with the periodic sampling frequency of the time domain milling signals from the CMD, the accelerometer, and the microphone respectively.

It is observed that, for the three signals, a local minimum in the stability metric occurs at the chatter frequency, f_c, not at the tooth passing frequency, f_{tooth}, thereby indicating an unstable cut. It is also observed that in the case of the displacement, acceleration, and sound signals (**Figure 4.117**, **Figure 4.121,** and **4.125**), although their maximum M values from the variation plots with f_s are less than those recorded in the previous

unstable cut, their minimum M values at the local minima occurring at f_c are higher than those recorded in the previous unstable cut.

Figure 4.126 shows the surface of the workpiece with visible chatter marks after the cut. Surface roughness measurements were conducted at six different locations on the cut surface, yielding a mean Ra value of 0.93 µm with a standard deviation of 0.208 µm, a mean Rq value of 1.11 µm with a standard deviation of 0.232 µm, and a mean Rz value of 4.52 µm with a standard deviation of 0.751 µm. **Table 4.21** shows the Ra, Rq, and Rz values for the six measured locations.

Table 4.20. Workpiece modal parameters of the AISI 4140 steel before the marginal cut.

***x*-direction**		
Frequency, f_n (Hz)	**Stiffness, k (N/m)**	**Damping ratio, ζ (-)**
609	1.79×10^7	0.0201
***y*-direction**		
Frequency, f_n (Hz)	**Stiffness, k (N/m)**	**Damping ratio, ζ (-)**
205	7.29×10^8	0.0711
800	3.72×10^9	0.0209
1953	3.04×10^8	0.0137
2204	2.72×10^8	0.0305
2576	2.10×10^8	0.1340
3896	6.84×10^8	0.0169
4115	9.81×10^8	0.0361

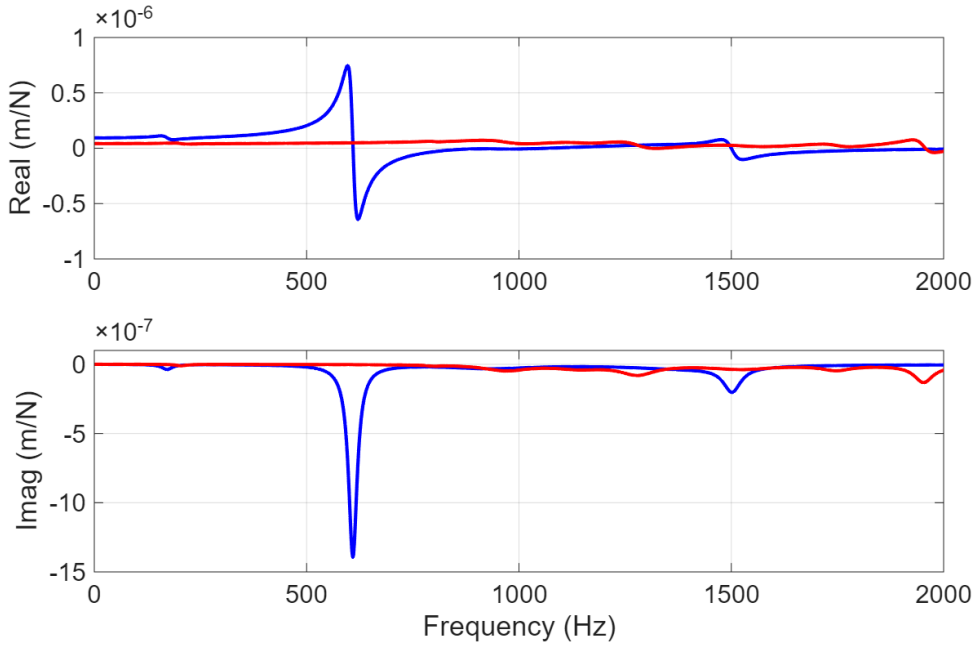


Figure 4.112: Frequency response function of the tool tip and workpiece, *x* (blue lines) and *y* (red lines) directions.

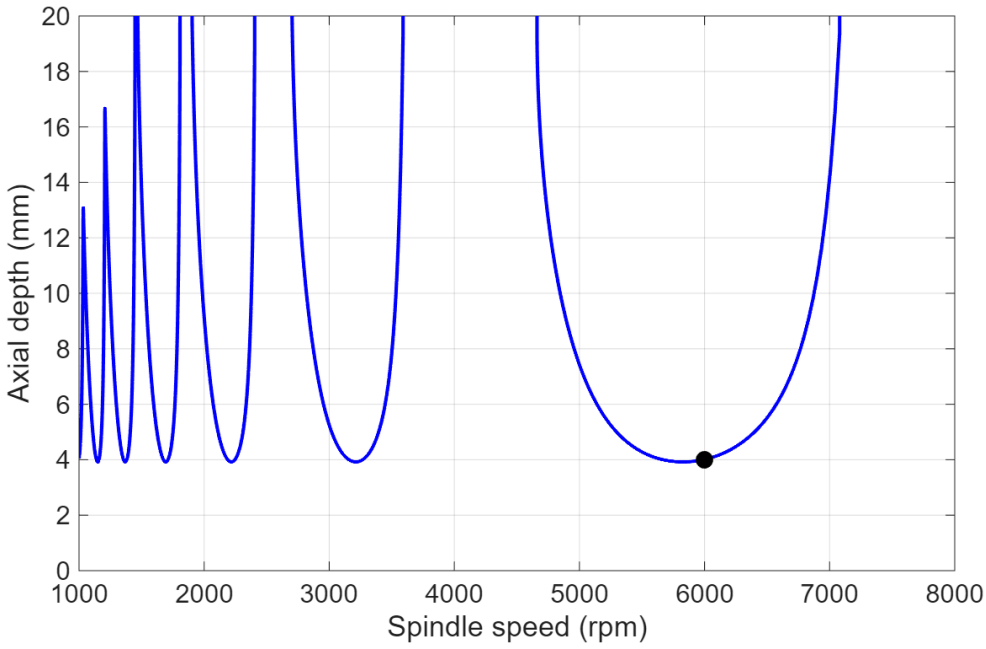


Figure 4.113: Stability lobe diagram with the selected marginal point (black dot) corresponding to a spindle speed of 6000 rpm and axial depth of cut of 4 mm.

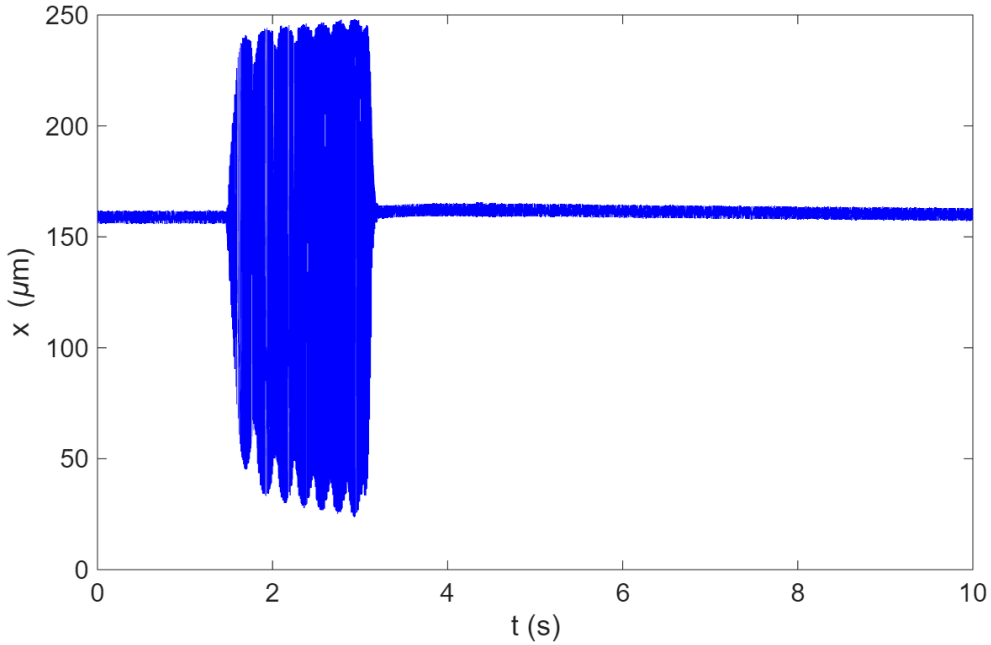


Figure 4.114: The total time interval of the signal from the CMD (displacement signal) showing when the tool interacts with the workpiece.

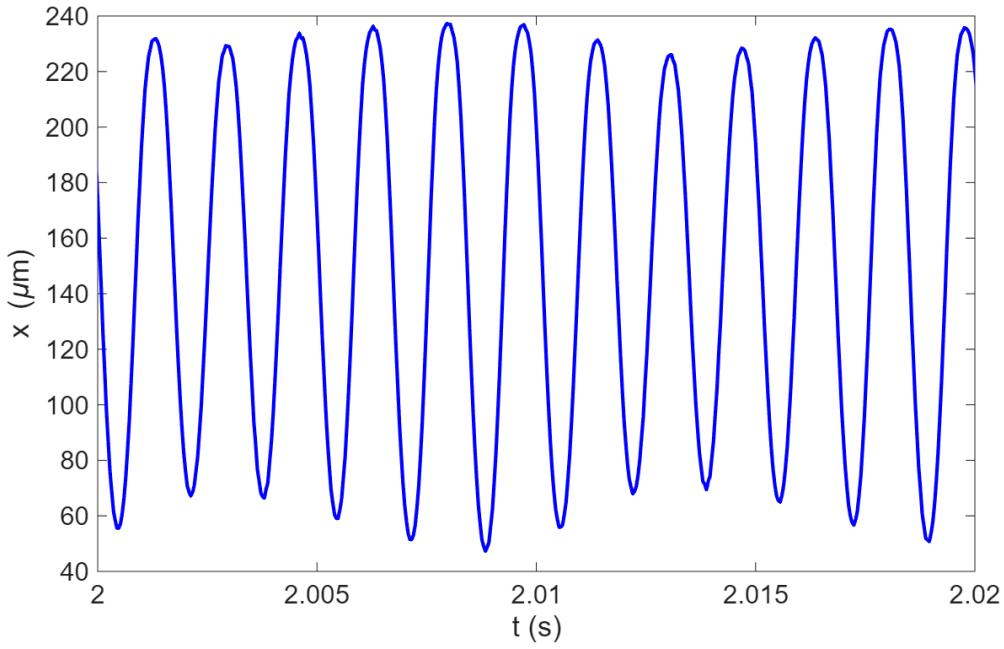


Figure 4.115: The magnified time interval of the signal from the CMD (displacement signal).

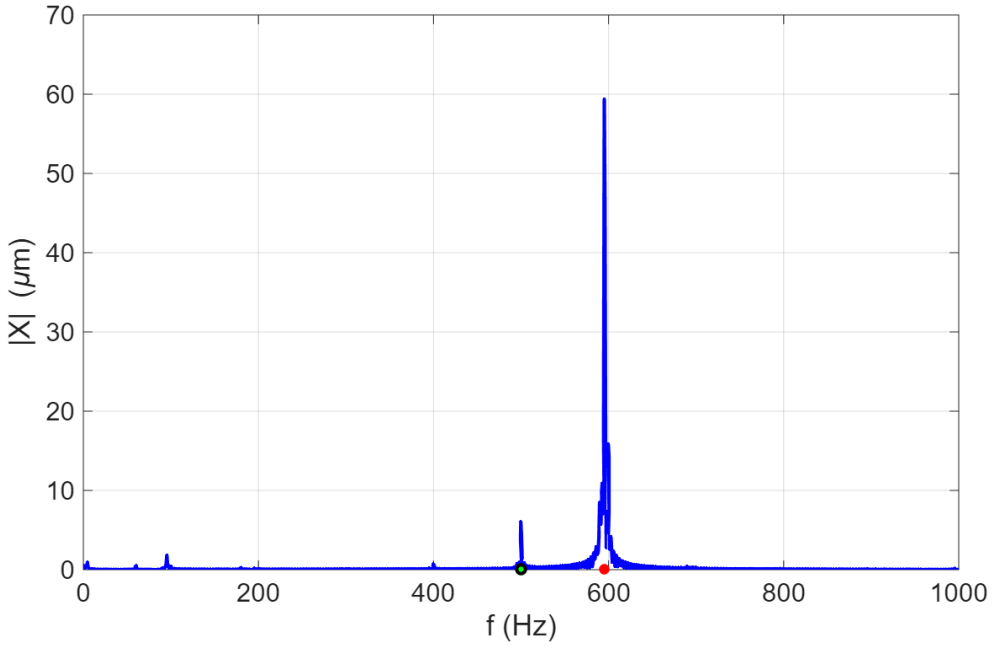


Figure 4.116: Magnitude plot of *x* frequency content for 100 rotations, with f_c (red dot) identified at 595 Hz and f_{tooth} (black circle) at 500 Hz.

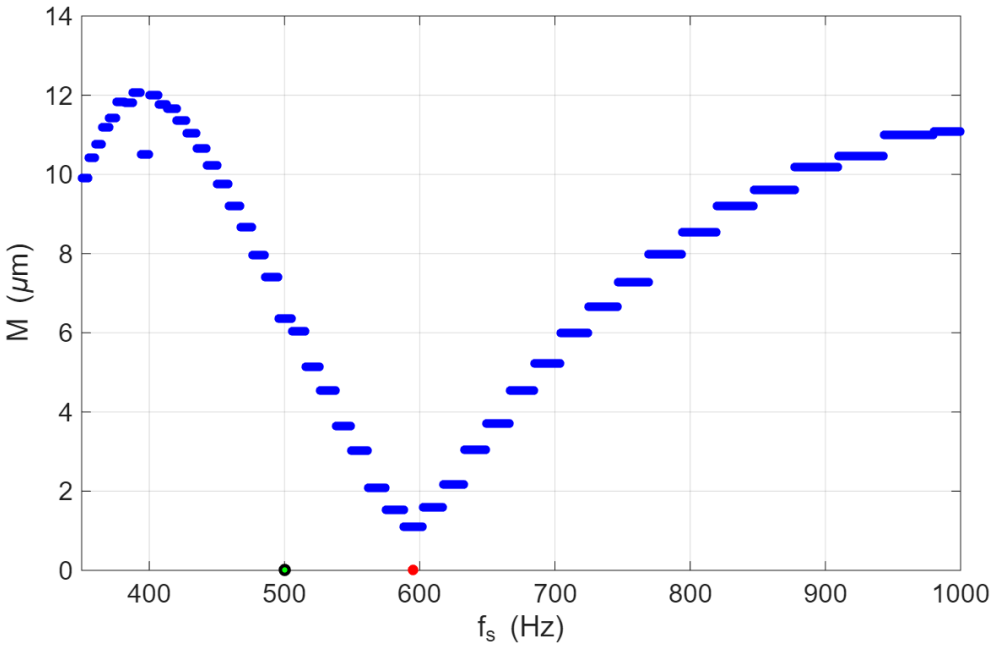


Figure 4.117: Variation in *M* value with periodic f_s. A local minimum occurs at f_c of 595 Hz (red dot) where M = 1.09 µm, not at f_{tooth} (black circle).

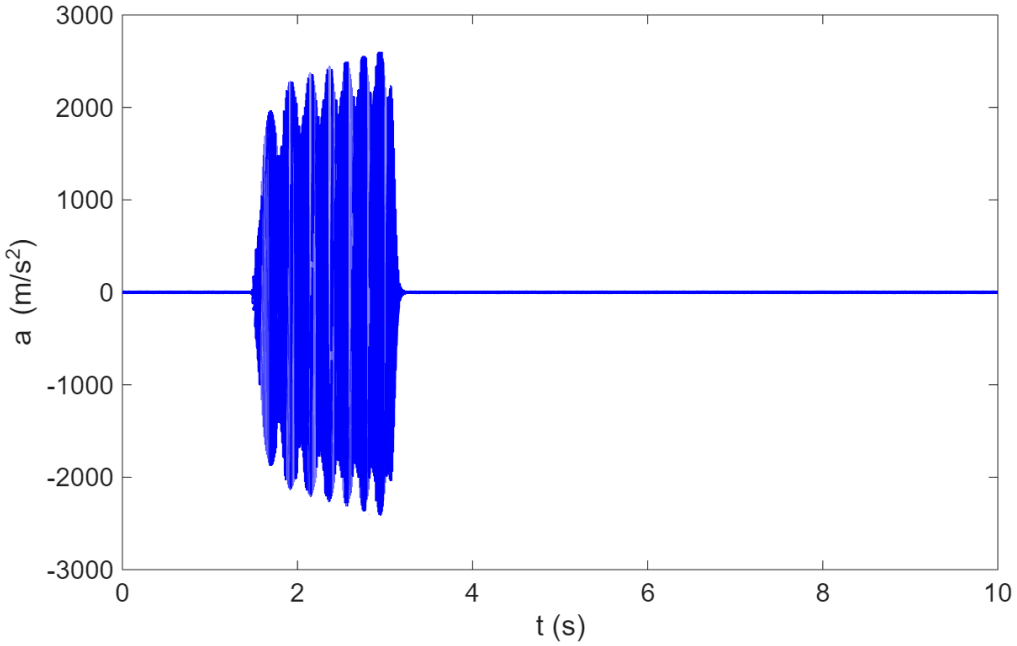


Figure 4.118: The total time interval of the signal from the accelerometer (acceleration signal) showing when the tool interacts with the workpiece.

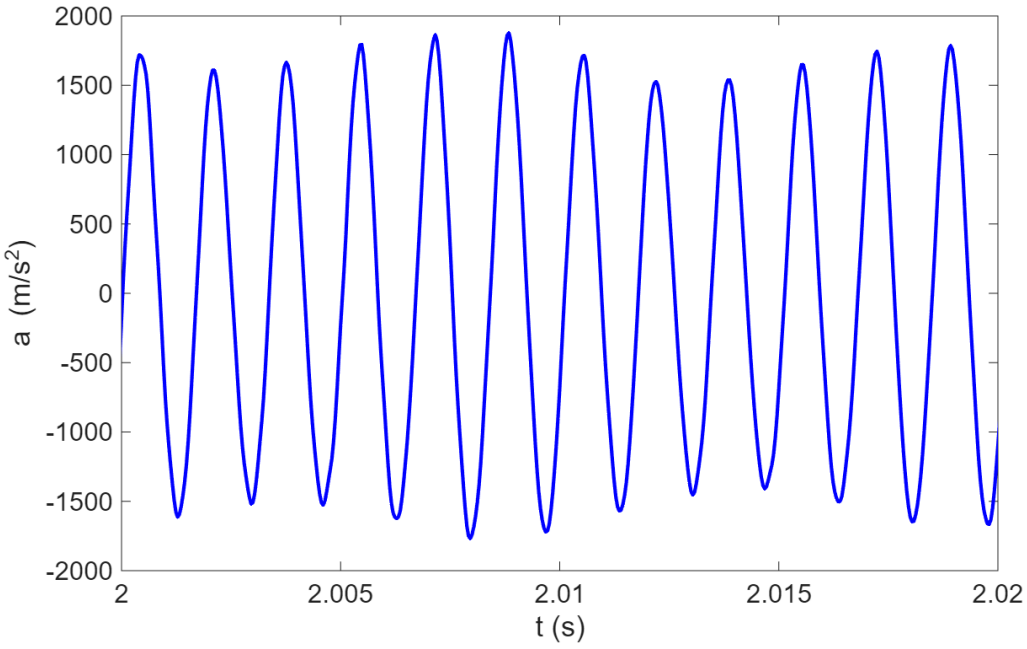


Figure 4.119: The magnified time interval of the signal from the accelerometer (acceleration signal).

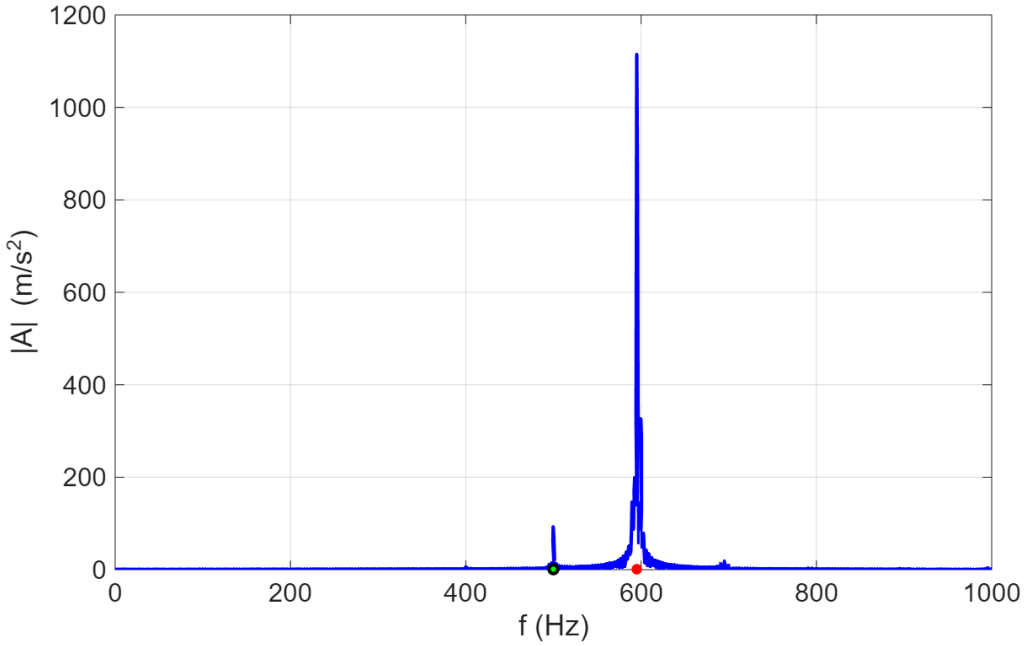


Figure 4.120: Magnitude plot of *a* frequency content for 100 rotations, with f_c (red dot) identified at 595 Hz and f_{tooth} (black circle) at 500 Hz.

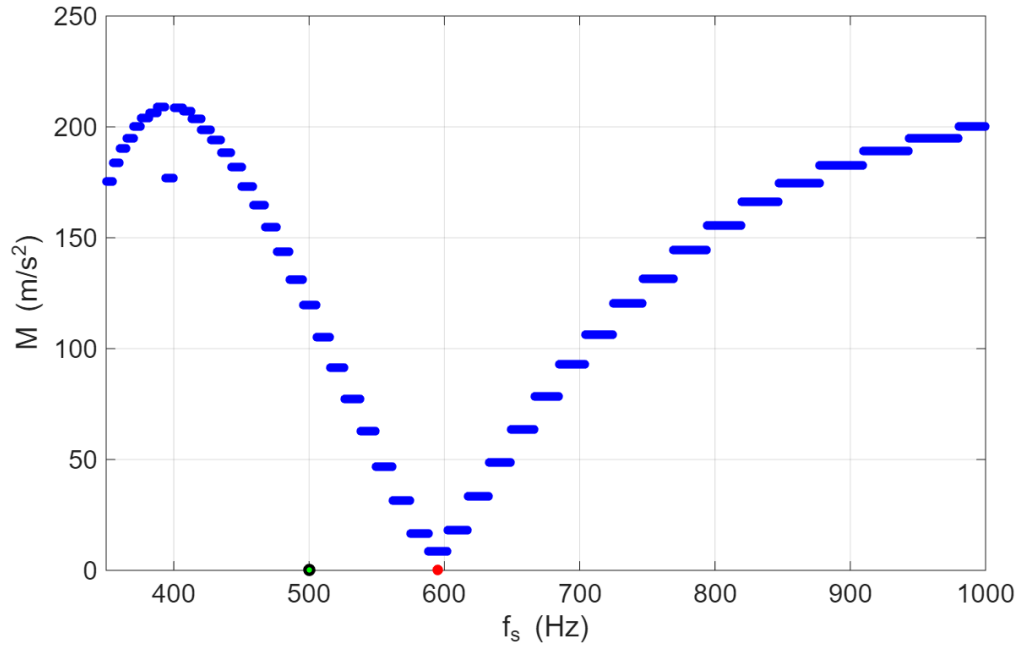


Figure 4.121: Variation in *M* value with periodic f_s. A local minimum occurs at f_c of 595 Hz (red dot) where M = 8.65 m/s^2, not at f_{tooth} (black circle).

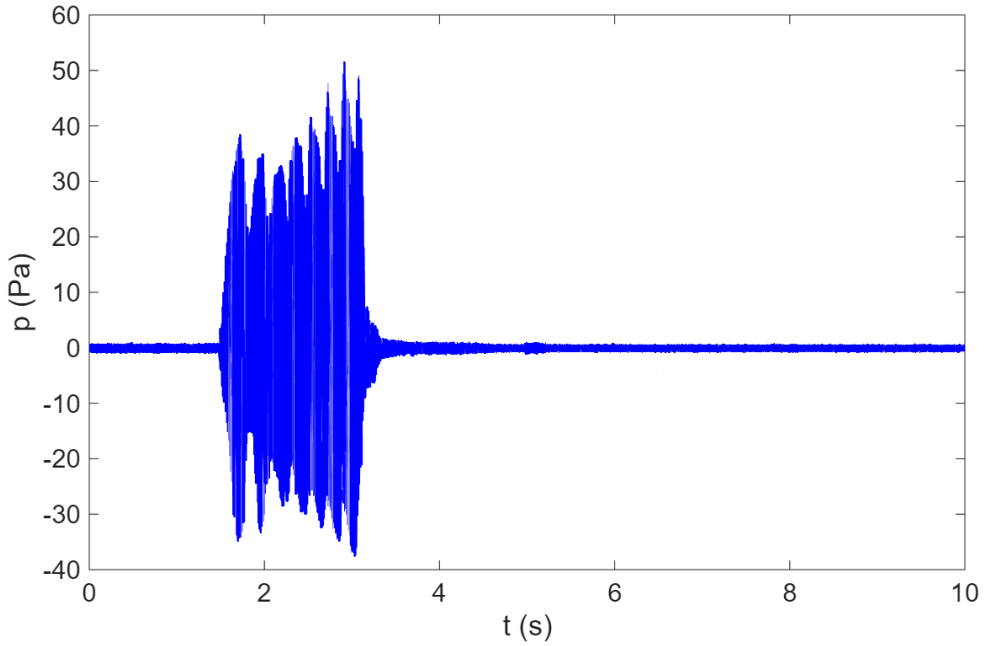


Figure 4.122: The total time interval of the signal from the microphone (sound pressure signal) showing when the tool interacts with the workpiece.

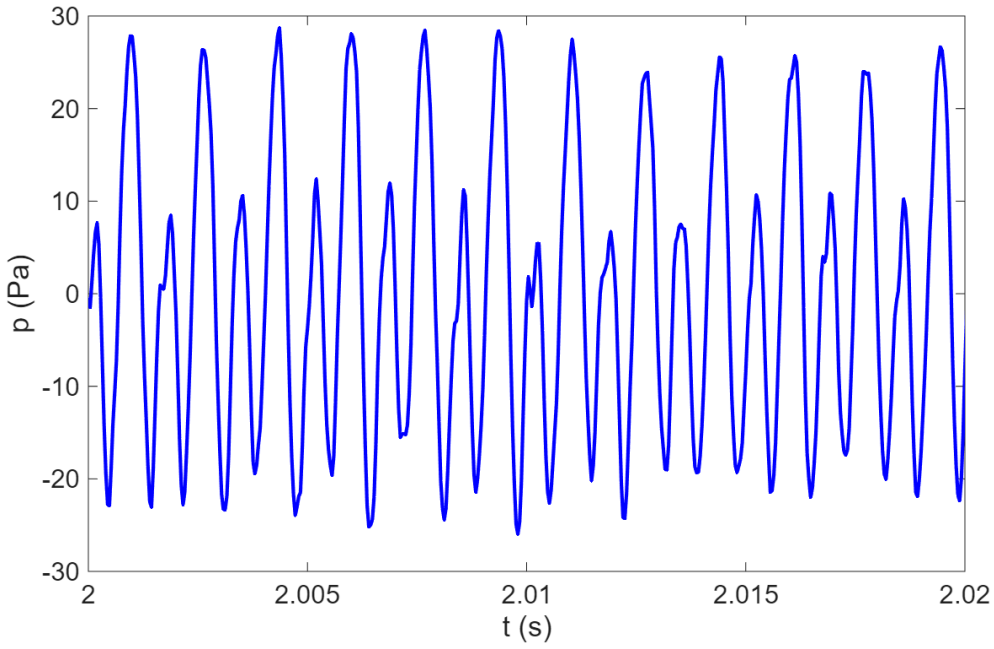


Figure 4.123: The magnified time interval of the signal from the microphone (sound pressure signal).

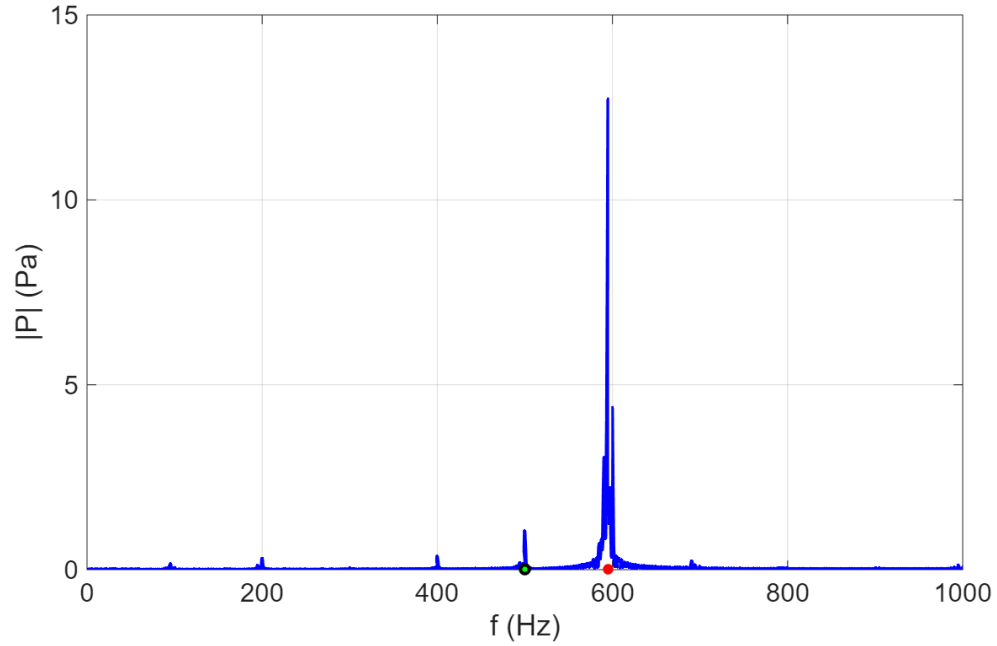


Figure 4.124: Magnitude plot of p frequency content for 100 rotations, with f_c (red dot) identified at 595 Hz and f_{tooth} (black circle) at 500 Hz.

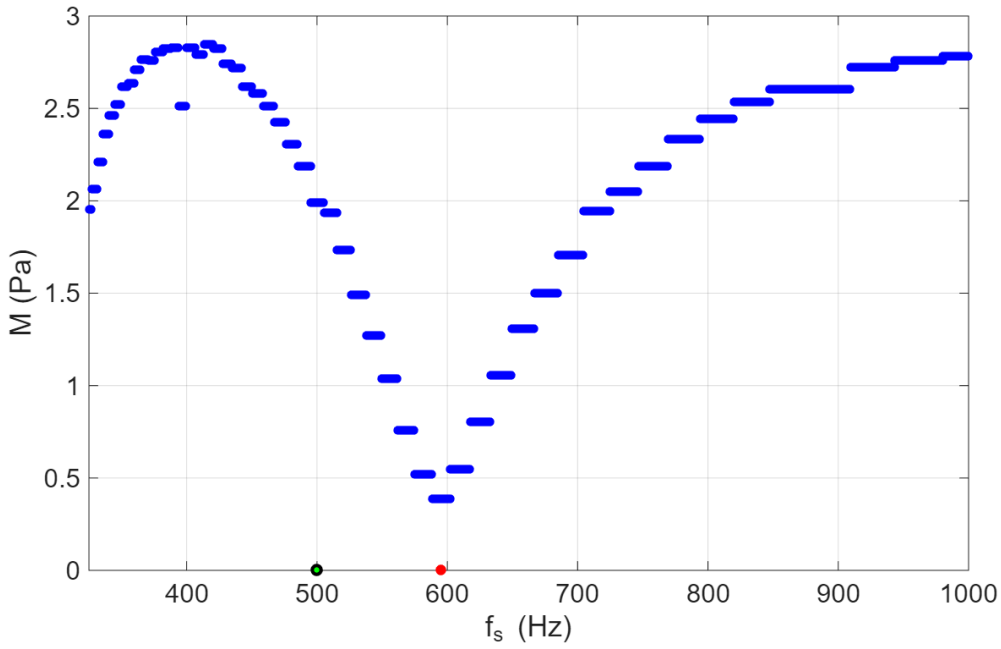


Figure 4.125: Variation in M value with periodic f_s. A local minimum occurs at f_c of 595 Hz (red dot) where M = 0.39 Pa, not at f_{tooth} (black circle).

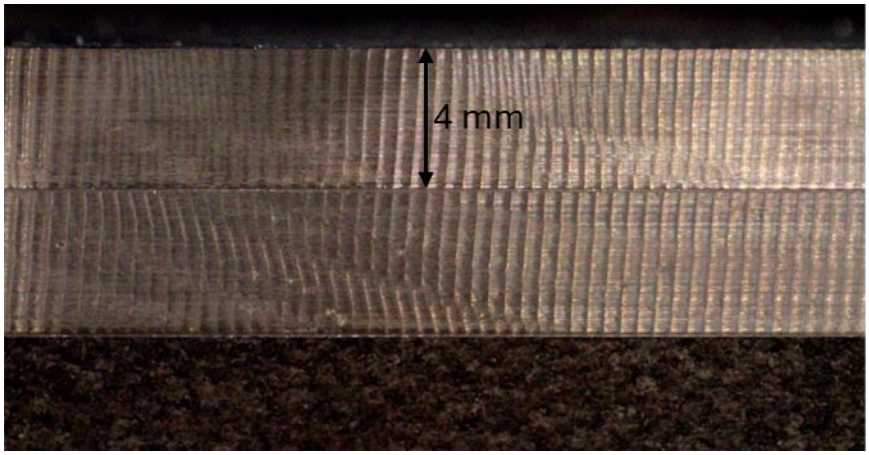


Figure 4.126: Surface of the AISI 4140 steel workpiece with chatter marks after the marginally unstable cut.

Stable cut: Five-flute endmill on AISI 4140 steel.

Results from tap testing and a stable experimental cut using a five-flute carbide endmill on AISI 4140 steel are presented below. **Table 4.22** shows the modal parameters of the workpiece obtained after tap testing. The tool tip modal parameters presented in **Table 4.17** are retained because, unlike the workpiece which experiences a reduction in mass after cutting, the tool remains unchanged from the previous experimental cut upon inspection.

Table 4.21. Profilometer results from six measured locations on the marginal cut surface of the AISI 4140 steel workpiece.

Location	Ra (μm)	Rq (μm)	Rz (μm)
1	0.990	1.186	4.787
2	0.923	1.111	4.532
3	0.609	0.745	3.379
4	1.203	1.391	5.003
5	1.060	1.276	5.453
6	0.796	0.959	3.936

Figures 4.127 and **4.128** show the frequency response function and the stability lobe diagram, respectively, obtained using the modal parameters. A tangential force coefficient of 2044.5 N/mm^2 and a normal force coefficient of 578.5 N/mm^2 for AISI 4140 steel are selected. A radial depth of cut of 1 mm is selected, and a stable point corresponding to a spindle speed of 4000 rpm and an axial depth of cut of 4 mm is selected on the stability lobe diagram, which achieves the stable cut.

Results from the time domain milling signals of the displacement (x), the acceleration (a), and the sound pressure (p) are presented, including, the total time interval of each signal, the magnified time interval, magnitude plot of the frequency content, and the variation in the M value with the periodic sampling frequency, f_s, which validates chatter detection by periodic sampling of time domain milling signals.

Figures 4.129, **4.133**, and **4.137** show the total time interval of the cut from the CMD, the accelerometer, and the microphone milling signals respectively. **Figures 4.130**, **4.134**, and **4.138** show the magnified time interval of the cut from the CMD, the accelerometer, and the microphone milling signals respectively. **Figures 4.131**, **4.135**, and **4.139** show the magnitude plots of the frequency contents from the CMD, the accelerometer, and the microphone milling signals respectively. It is observed that the tooth passing frequency, f_{tooth}, has the highest peak in the magnitude plots, indicating stable behavior. **Figures 4.132**, **4.136**, and **4.140** show the variations in the M values with the periodic sampling frequency of the time domain milling signals from the CMD, the accelerometer, and the microphone respectively. It is observed that for the three milling signals, a local

minimum in the stability metric occurs at the tooth passing frequency, f_{tooth}, thereby indicating a stable cut. It is also observed that the *M* values from the local minima occurring at f_{tooth} are less than those recorded in the previous unstable cuts, except for the case of the displacement signal (**Figure 4.132**) where, although the maximum *M* value from the variation plot with f_s is less than those recorded in the previous two unstable cuts, the minimum *M* value at the local minimum occurring at f_{tooth} has the same value as the one recorded in the first unstable cut (**Figure 4.102**).

Figure 4.141 shows the surface of the workpiece with periodic feed marks after the cut, indicating the tool tooth trajectory. Surface roughness measurements were conducted at six different locations on the cut surface, yielding a mean Ra value of 0.80 µm with a standard deviation of 0.067 µm, a mean Rq value of 0.98 µm with a standard deviation of 0.086 µm, and a mean Rz value of 4.09 µm with a standard deviation of 0.387 µm. **Table 4.23** shows the Ra, Rq, and Rz values for the six measured locations.

Table 4.22. Workpiece modal parameters of the AISI 4140 steel before the stable cut.

***x*-direction**		
Frequency, f_n (Hz)	**Stiffness, *k* (N/m)**	**Damping ratio, ζ (-)**
609	1.83×10^7	0.0201
***y*-direction**		
Frequency, f_n (Hz)	**Stiffness, *k* (N/m)**	**Damping ratio, ζ (-)**
205	6.44×10^8	0.0748
800	4.80×10^9	0.0171
1956	3.57×10^8	0.0133
2207	3.22×10^8	0.0284
2559	5.68×10^8	0.0581
3933	7.97×10^8	0.0180

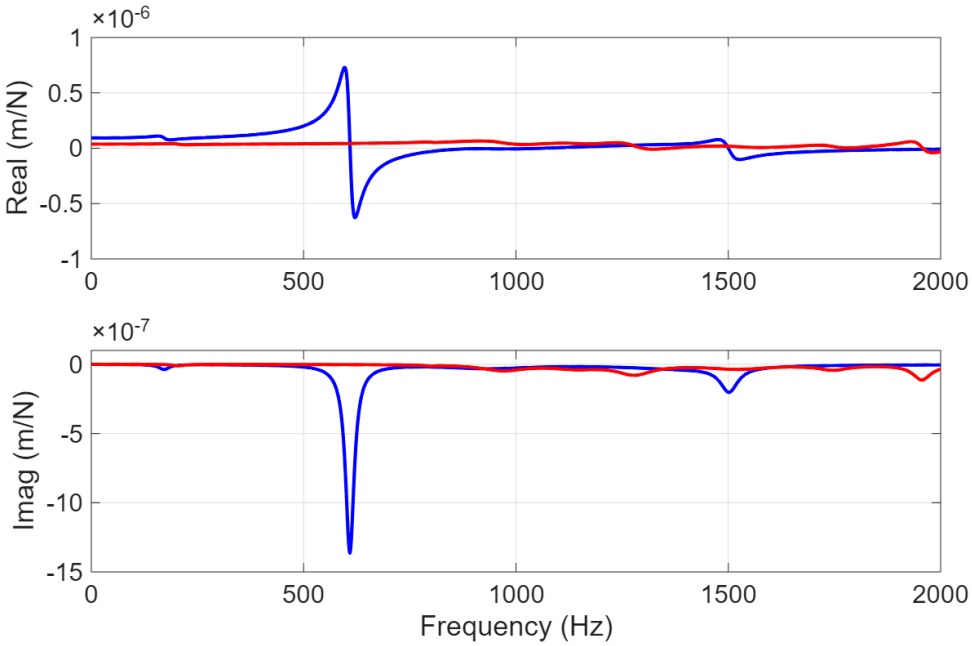


Figure 4.127: Frequency response function of the tool tip and workpiece, *x* (blue lines) and *y* (red lines) directions.

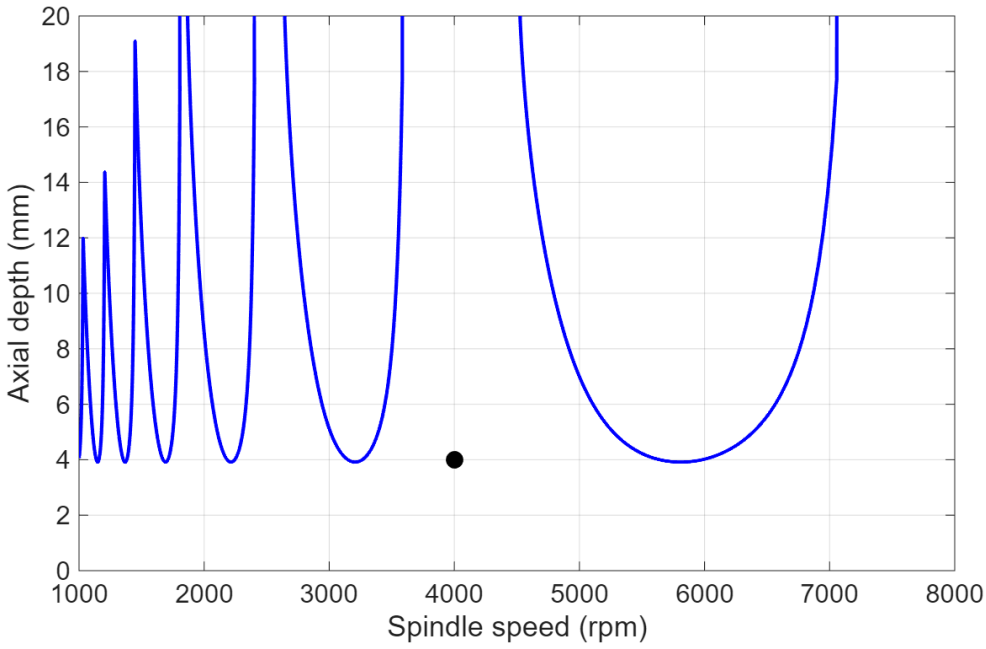


Figure 4.128: Stability lobe diagram with the selected stable point (black dot) corresponding to a spindle speed of 4000 rpm and axial depth of cut of 4 mm.

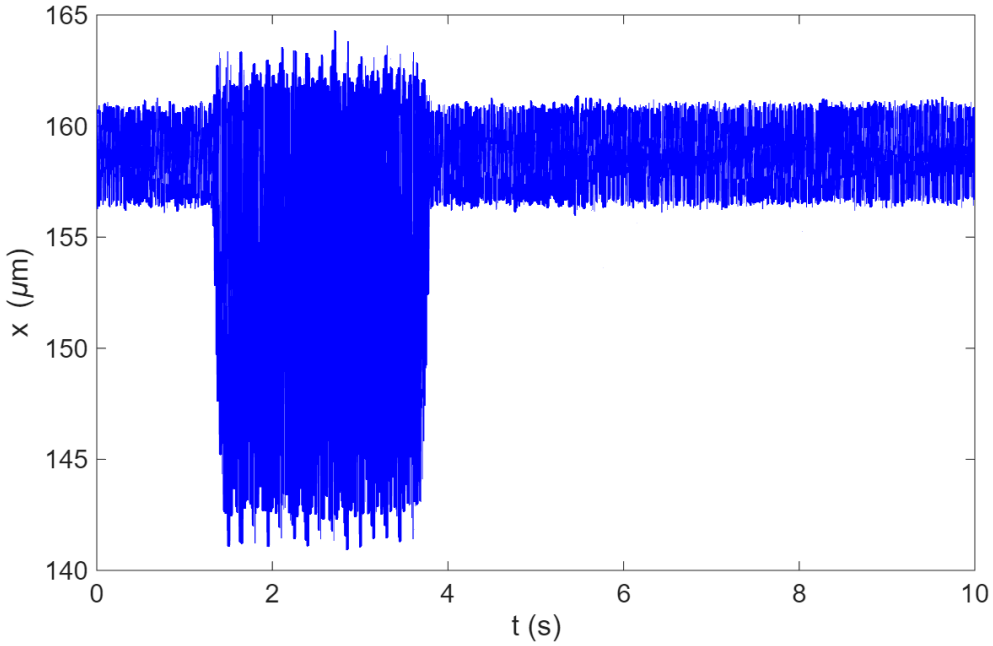


Figure 4.129: The total time interval of the signal from the CMD (displacement signal) showing when the tool interacts with the workpiece.

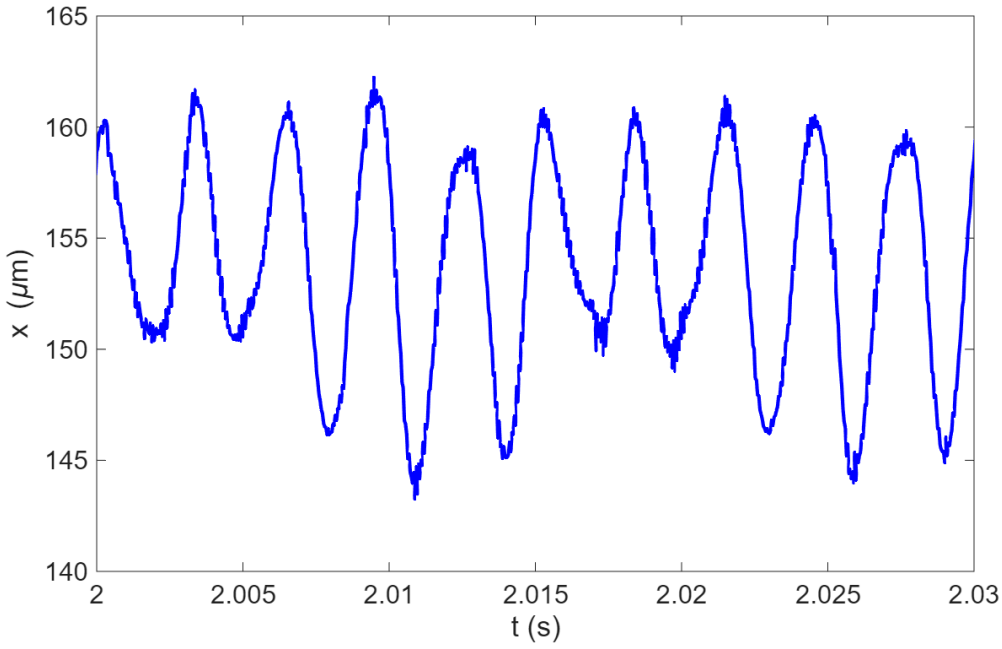


Figure 4.130: The magnified time interval of the signal from the CMD (displacement signal).

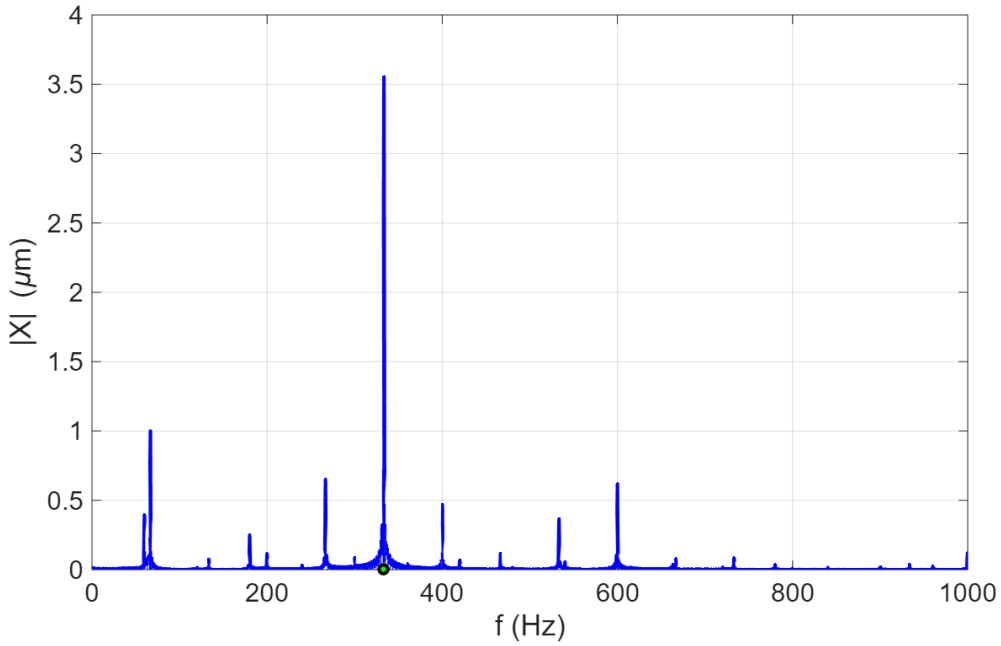


Figure 4.131: Magnitude plot of *x* frequency content for 100 rotations, with f_{tooth} identified at 333 Hz (black circles).

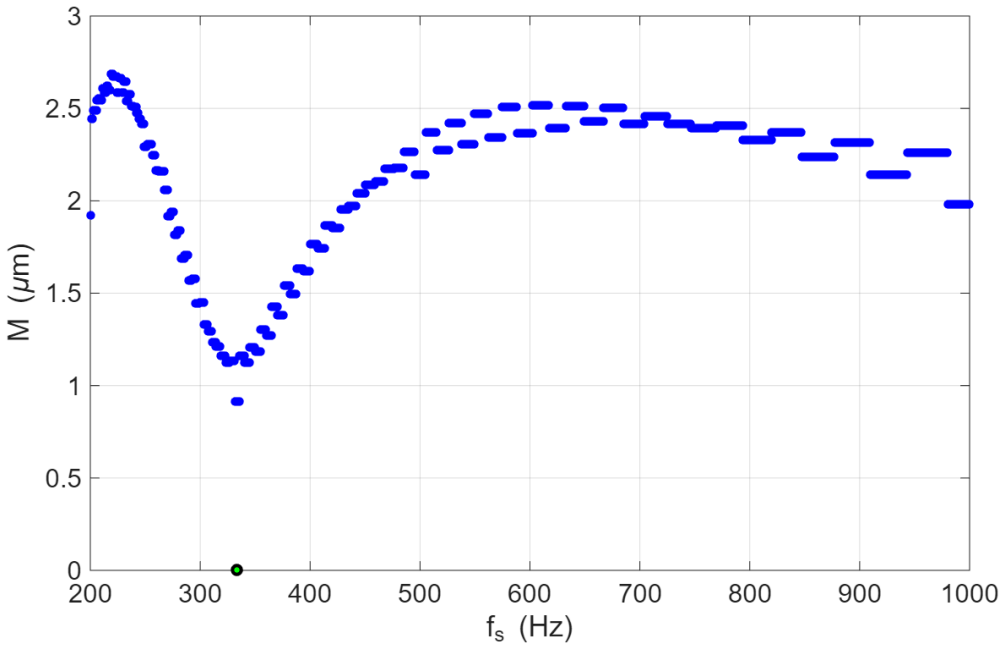


Figure 4.132: Variation in *M* value with periodic f_s. A local minimum occurs at f_{tooth} of 333 Hz (black circle), where M = 0.91 µm.

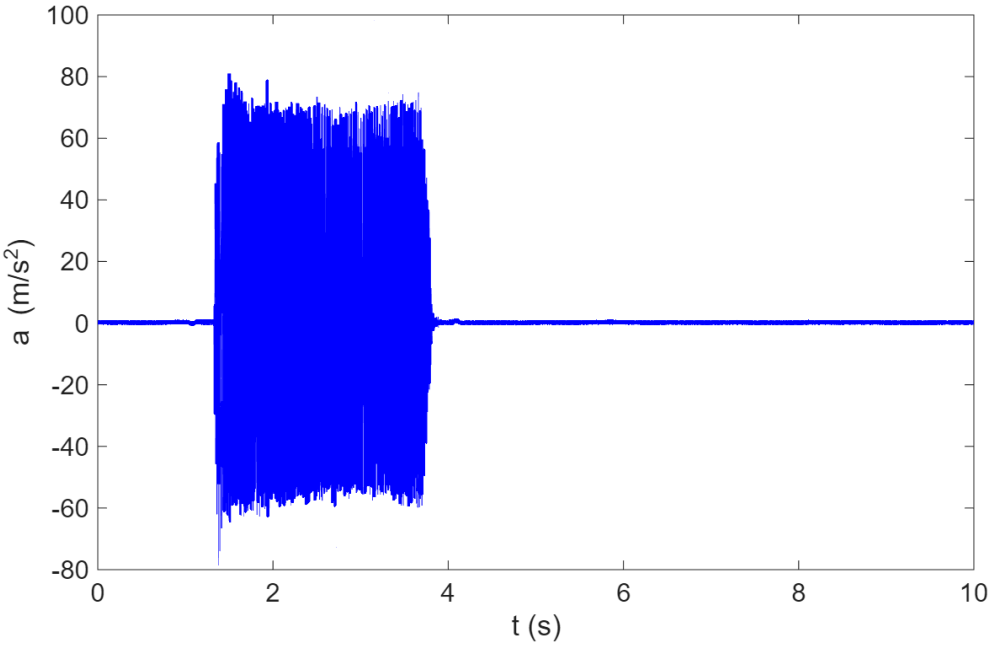


Figure 4.133: The total time interval of the signal from the accelerometer (acceleration signal) showing when the tool interacts with the workpiece.

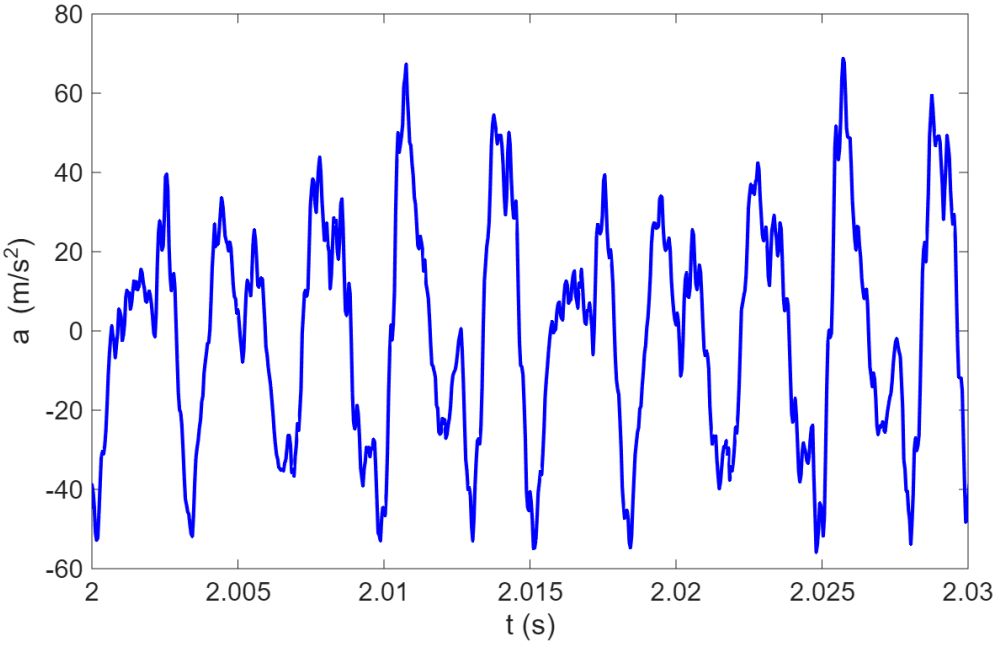


Figure 4.134: The magnified time interval of the signal from the accelerometer (acceleration signal).

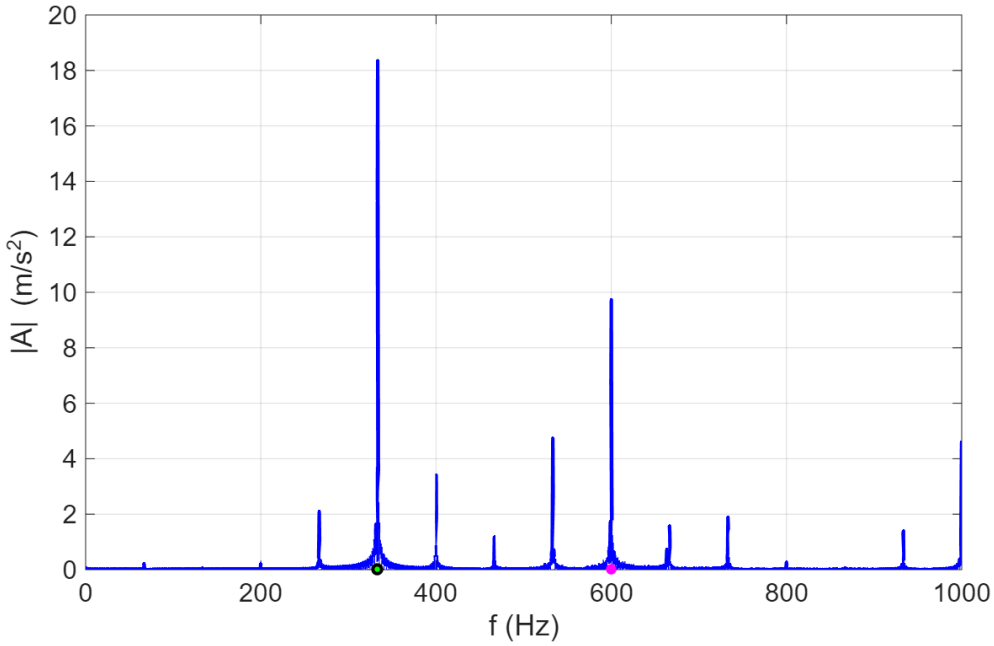


Figure 4.135: Magnitude plot of *a* frequency content for 100 rotations, with f_{tooth} (black circle) identified at 333 Hz and a runout frequency (magenta dot) also identified.

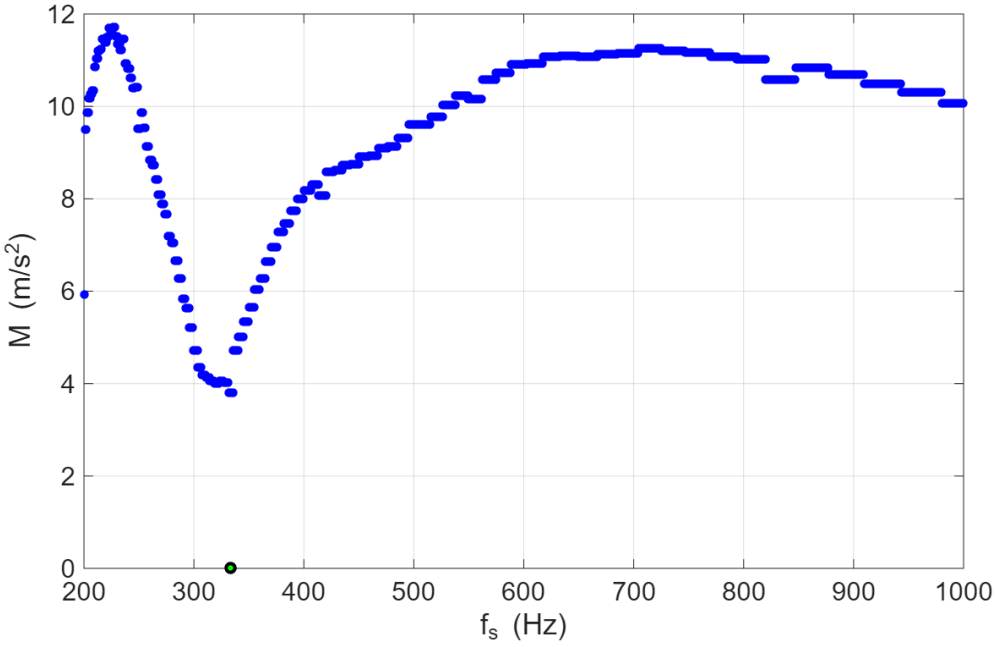


Figure 4.136: Variation in *M* value with periodic f_s. A local minimum occurs at f_{tooth} of 333 Hz (black circle), where M = 3.79 m/s^2.

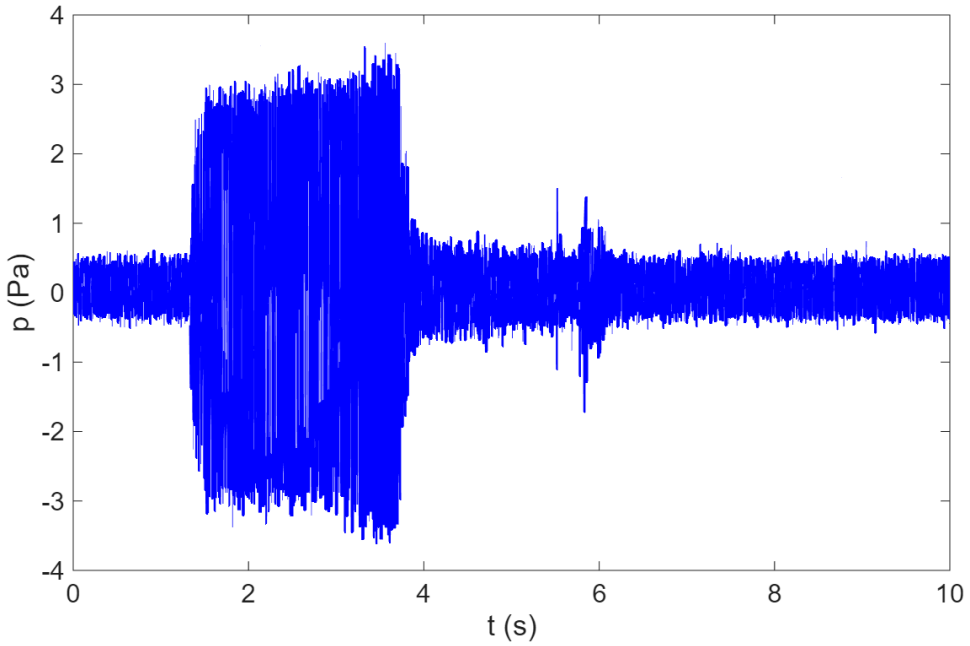


Figure 4.137: The total time interval of the signal from the microphone (sound pressure signal) showing when the tool interacts with the workpiece.

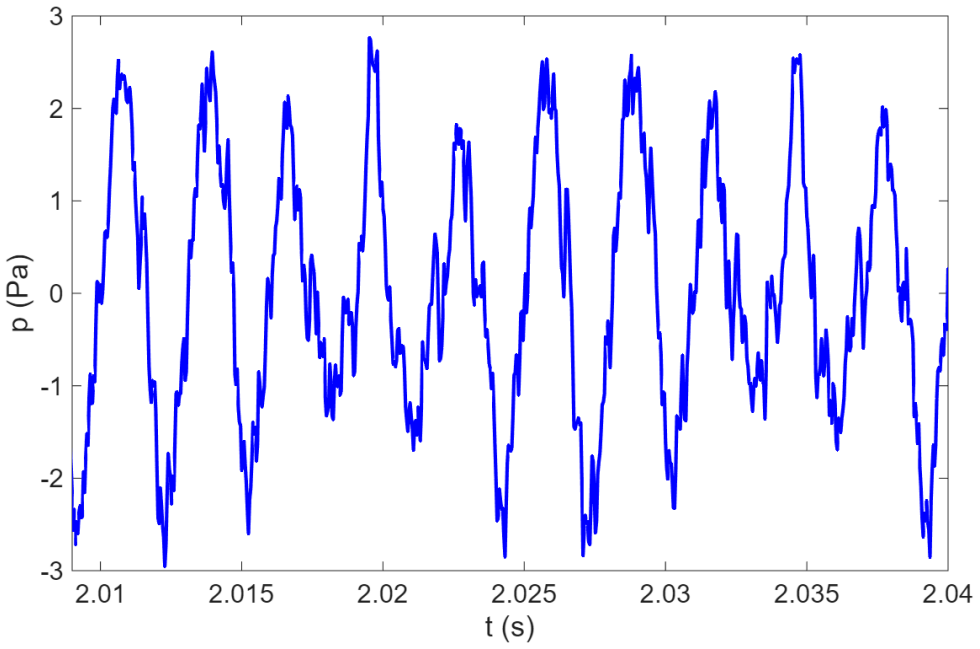


Figure 4.138: The magnified time interval of the signal from the microphone (sound pressure signal).

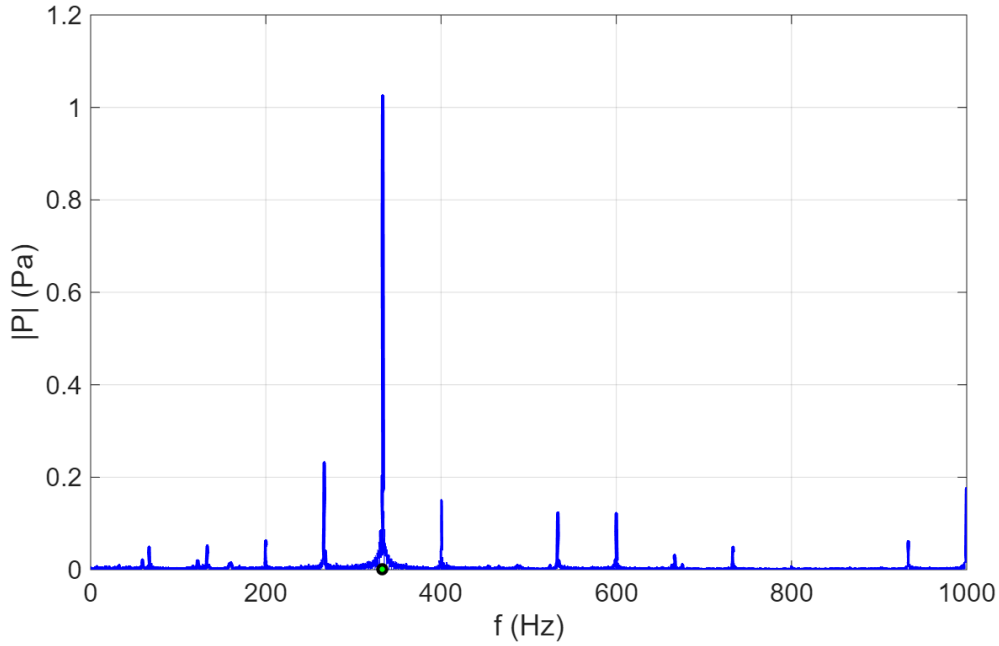


Figure 4.139: Magnitude plot of *p* frequency content for 100 rotations, with f_{tooth} (black circle) identified at 333 Hz.

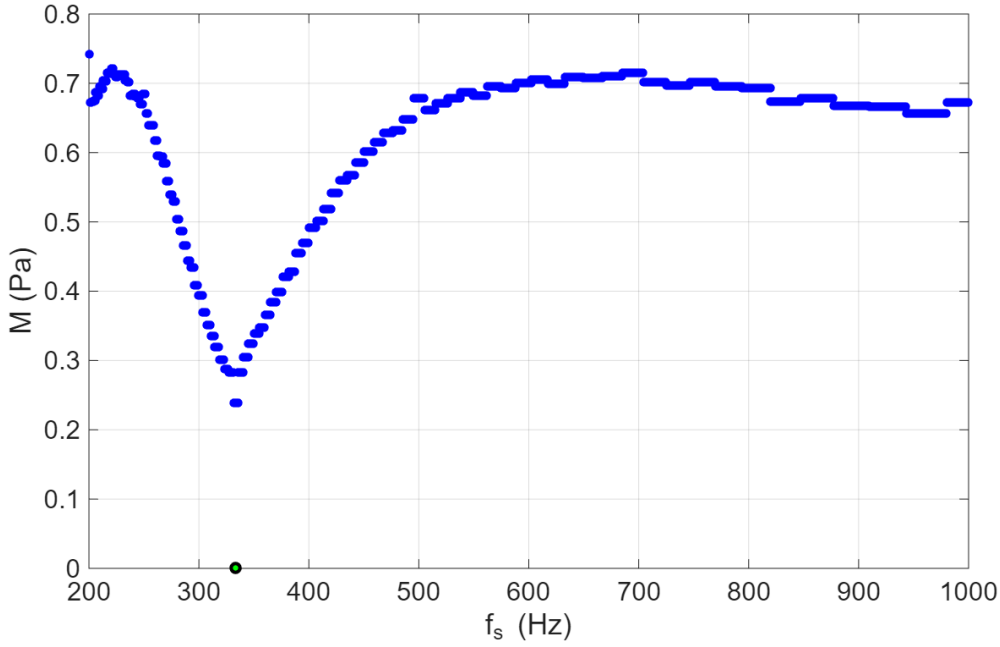


Figure 4.140: Variation in *M* value with periodic f_s. A local minimum occurs at f_{tooth} of 333 Hz (black circle), where M = 0.24 Pa.

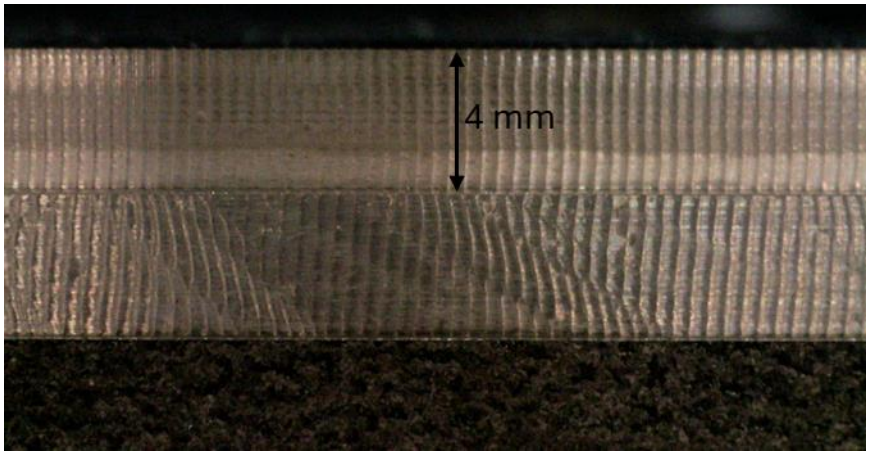


Figure 4.141: Surface of the AISI 4140 steel workpiece with periodic feed marks after the stable cut.

Power sensor results.

The power sensor measurements for this tool and workpiece combination (five-flute carbide endmill and AISI 4140 steel) also indicate a monotonic rise in spindle power consumption with increasing spindle speed and depths of cut. This trend is consistent with the expected mechanical behavior of the spindle-tool system, where higher rotational speeds and depths of cut demand greater energy input to overcome inertia, friction, and cutting-related resistances.

Table 4.23. Profilometer results from six measured locations on the stable cut surface of the AISI 4140 steel workpiece.

Location	Ra (µm)	Rq (µm)	Rz (µm)
1	0.763	0.934	3.954
2	0.883	1.046	4.189
3	0.695	0.852	3.969
4	0.824	0.960	3.581
5	0.847	1.095	4.759
6	0.783	0.963	4.099

Figures 4.142, **4.143**, and **4.144** show the spindle power consumptions during the unstable, marginally unstable, and stable experimental cuts conducted using the five-flute endmill on the AISI 4140 steel workpieces. **Table 4.24** shows the spindle speeds, axial depths of cut, radial depths of cut, and the peak spindle power consumptions for the unstable, marginally unstable, and stable experimental cuts. It is observed that although the unstable and marginally stable cuts are conducted at the same spindle speed, the unstable cut has a higher axial depth of cut which leads to a higher spindle power consumption.

Spindle Speed Selection

Using a four-flute endmill on AISI 4140 steel, an unstable experimental cut is conducted, after which the chatter frequency is used to calculate a new spindle speed based on **Equation 2**. The new spindle speed is then used to achieve a stable experimental cut.

$$\Omega = \frac{60 f_c}{j N_t} \text{ , } j = 1, 2, 3, \ldots \quad (2)$$

Unstable cut: Four-flute endmill on AISI 4140 steel

Results from tap testing and an unstable experimental cut using a four-flute carbide endmill on AISI 4140 steel are presented below. **Tables 4.25** and **4.26** show the modal parameters of the tool tip and workpiece respectively, obtained after tap testing, while **Figures 4.145** and **4.146** show the frequency response function and the stability lobe diagram obtained using the modal parameters. A tangential force coefficient of 2044.5 N/mm^2 and a normal force coefficient of 578.5 N/mm^2 for AISI 4140 steel are selected.

Table 4.24. Cutting parameters and peak spindle power for the experimental cuts using the five-flute endmill on the AISI 4140 steel workpiece.

Experimental cut	Spindle speed (rpm)	Axial depth (mm)	Radial depth (mm)	Peak spindle power (kW)
Unstable	6000	8	1	1.84
Marginally unstable	6000	4	1	1.41
Stable	4000	4	1	1.19

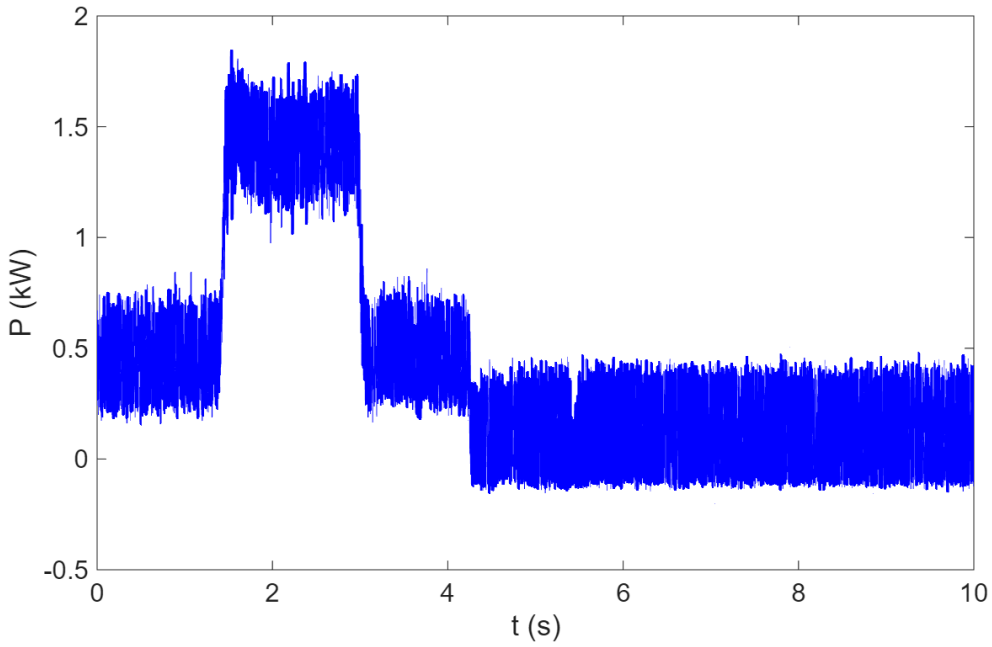


Figure 4.142: Spindle power consumption peaked at 1.84 kW during the unstable cut at a spindle speed of 6000 rpm, axial and radial depths of cut of 8 mm and 1 mm respectively.

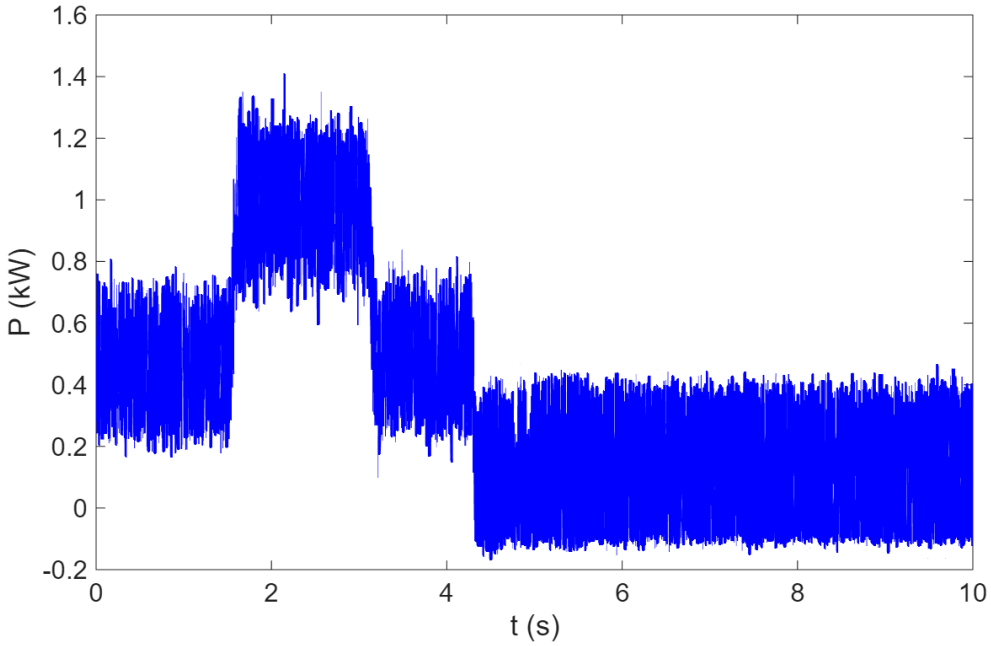


Figure 4.143: Spindle power consumption peaked at 1.41 kW during the unstable cut at a spindle speed of 6000 rpm, axial and radial depths of cut of 4 mm and 1 mm respectively.

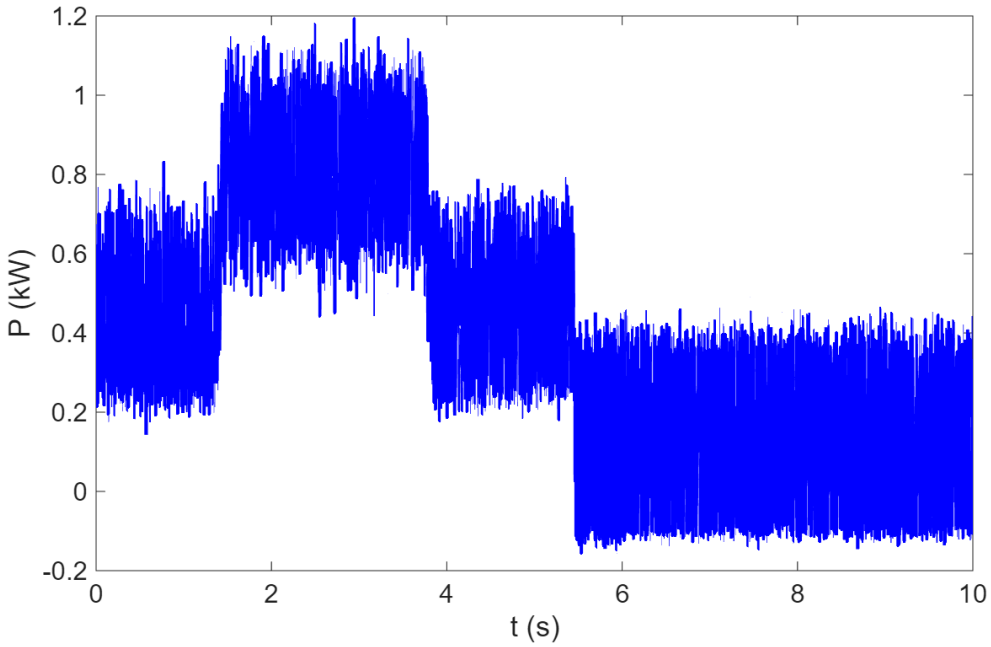


Figure 4.144: Spindle power consumption peaked at 1.19 kW during the unstable cut at a spindle speed of 4000 rpm, axial and radial depths of cut of 4 mm and 1 mm respectively.

A radial depth of cut of 2 mm is selected, and an unstable point corresponding to a spindle speed of 6800 rpm and an axial depth of cut of 5 mm is selected on the stability lobe diagram, which achieves an unstable cut.

Results from the time domain milling signals of the displacement (x), the acceleration (a), and the sound pressure (p) are presented, including, the total time interval of each signal, the magnified time interval, magnitude plot of the frequency content, and the variation in the M value with the periodic sampling frequency, f_s. As stated earlier, the variation in the M value with the periodic sampling frequency, f_s, validates chatter detection by periodic sampling of time domain milling signals.

Figures 4.147, **4.151**, and **4.155** show the total time interval of the cut from the CMD, the accelerometer, and the microphone milling signals respectively. **Figures 4.148**, **4.152**, and **4.156** show the magnified time interval of the cut from the CMD, the accelerometer, and the microphone milling signals respectively. **Figures 4.149**, **4.153**, and **4.157** show the magnitude plots of the frequency contents from the CMD, the accelerometer, and the microphone milling signals respectively. It is observed that the chatter frequency, f_c, has the highest peak in the magnitude plots, indicating an unstable cut. **Figures 4.150**, **4.154**, and **4.158** show the variations in the M values with the periodic sampling frequency of the time domain milling signals from the CMD, the accelerometer, and the microphone respectively. It is observed that a local minimum in the stability metric occurs at the chatter frequency, f_c, not at the tooth passing frequency, f_{tooth}, thereby indicating an unstable cut.

Figure 4.159 shows the surface of the workpiece with visible chatter marks after the unstable cut, captured using the Dino-Lite digital microscope. Surface roughness measurements were conducted at six different locations on the cut surface using the Mitutoyo profilometer, yielding a mean Ra value of 0.92 µm with a standard deviation of 0.034 µm, a mean Rq value of 1.11 µm with a standard deviation of 0.043 µm, and a mean Rz value of 4.83 µm with a standard deviation of 0.288 µm. **Table 4.27** shows the Ra, Rq, and Rz values for the six measured locations.

The identified chatter frequency of 551 Hz is used in **Equation 2** to calculate a new spindle speed of 4133 rpm, where $N_t = 4$ and $j = 2$.

Table 4.25. Tool tip modal parameters of the four-flute endmill.

***x*-direction**		
Frequency, f_n (Hz)	**Stiffness, *k* (N/m)**	**Damping ratio, ζ (-)**
173	1.82×10^8	0.0746
444	1.80×10^8	0.1421
960	1.14×10^8	0.1463
1410	1.37×10^8	0.1166
1505	1.33×10^8	0.0167
3554	5.07×10^8	0.0669
4391	9.07×10^8	0.0300
5327	2.36×10^8	0.0784
10208	1.19×10^8	0.0459
11044	4.64×10^8	0.0230
***y*-direction**		
Frequency, f_n (Hz)	**Stiffness, *k* (N/m)**	**Damping ratio, ζ (-)**
475	4.30×10^8	0.0669
968	2.56×10^8	0.0493
1129	1.44×10^8	0.1098
1287	1.81×10^8	0.0309
1562	3.06×10^8	0.0408
1748	4.26×10^8	0.0239
5377	2.65×10^8	0.0754
10365	1.00×10^8	0.0528
11043	5.08×10^8	0.0219

Table 4.26. Workpiece modal parameters of the AISI 4140 steel before the unstable cut.

***x*-direction**		
Frequency, f_n (Hz)	**Stiffness, *k* (N/m)**	**Damping ratio, ζ (-)**
569	1.49×10^7	0.0282
***y*-direction**		
Frequency, f_n (Hz)	**Stiffness, *k* (N/m)**	**Damping ratio, ζ (-)**
1880	1.42×10^8	0.0114
2062	6.30×10^8	0.0180
3124	4.41×10^9	0.0093
3611	7.10×10^8	0.0150
3769	2.13×10^8	0.0991

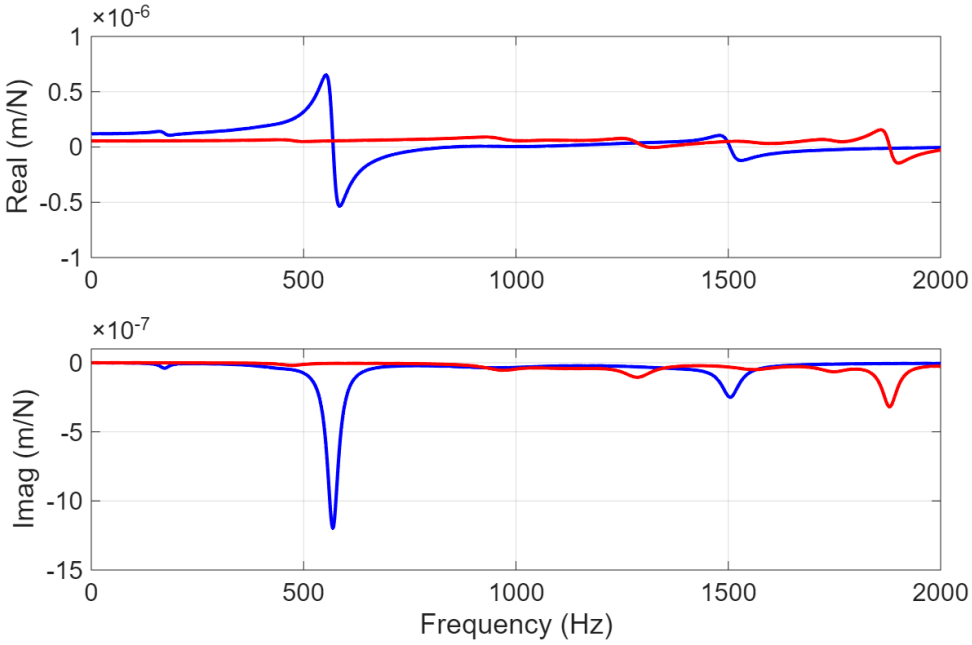


Figure 4.145: Frequency response function of the tool tip and workpiece, *x* (blue lines) and *y* (red lines) directions.

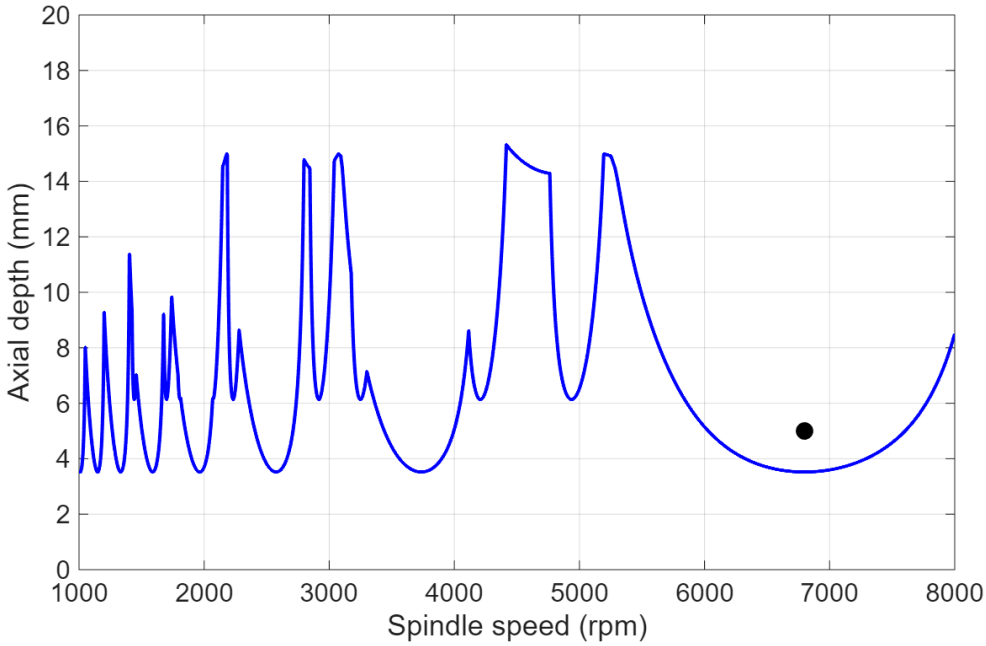


Figure 4.146: Stability lobe diagram with the selected unstable point (black dot) corresponding to a spindle speed of 6800 rpm and axial depth of cut of 5 mm.

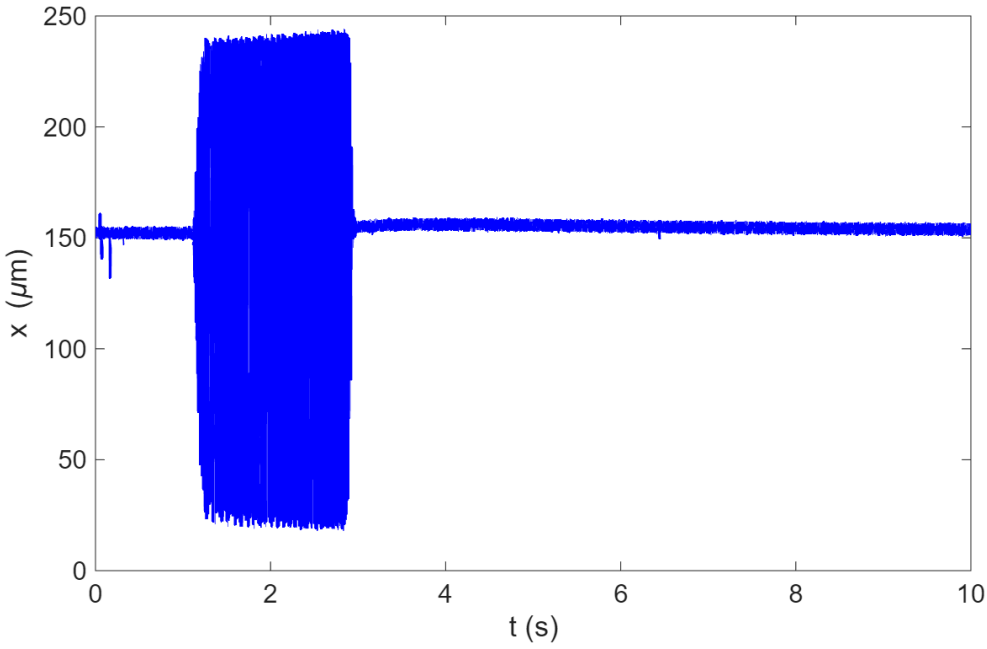


Figure 4.147: The total time interval of the signal from the CMD (displacement signal) showing when the tool interacts with the workpiece.

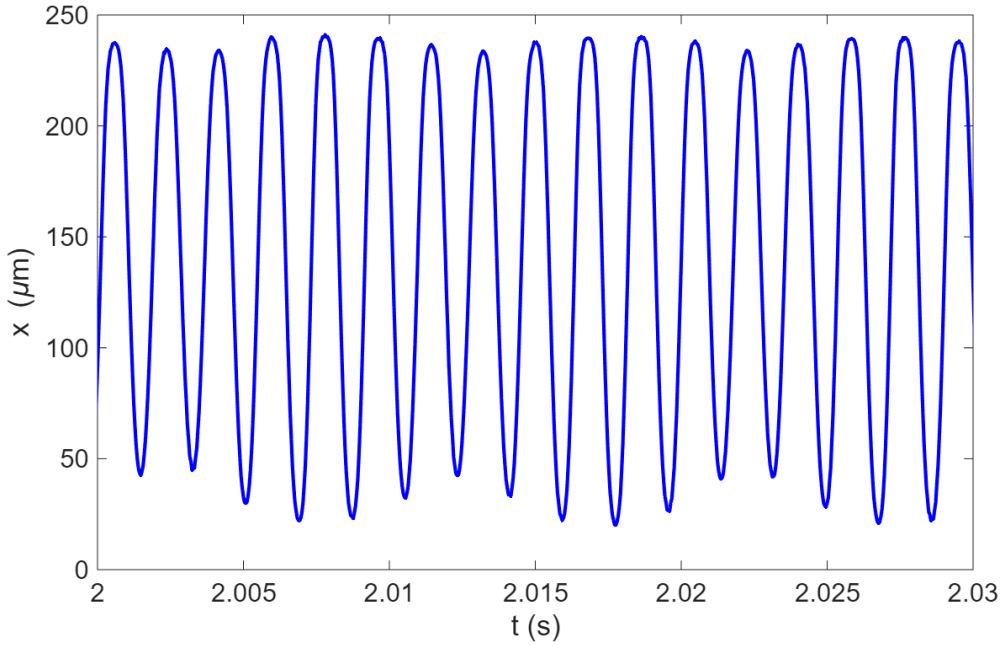


Figure 4.148: The magnified time interval of the signal from the CMD (displacement signal).

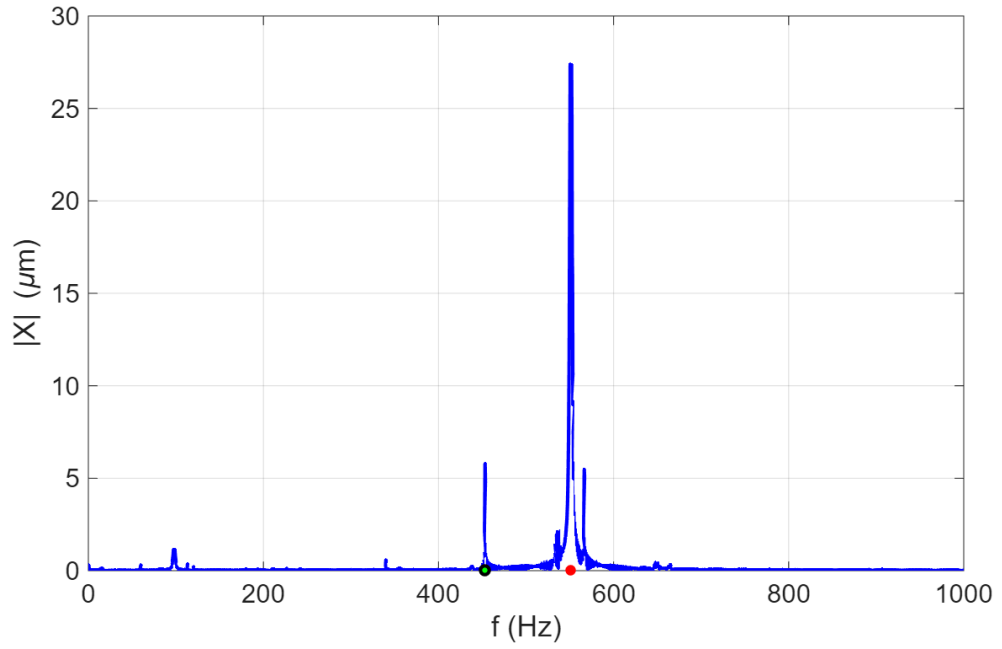


Figure 4.149: Magnitude plot of x frequency content for 150 rotations, with f_c (red dot) identified at 551 Hz and f_{tooth} (black circle) at 453 Hz.

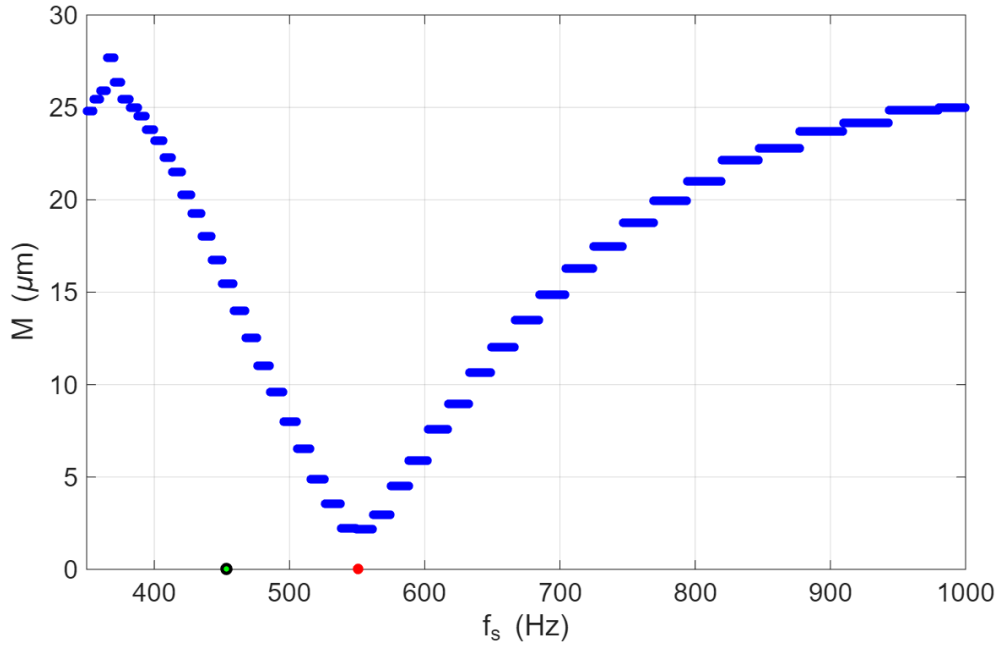


Figure 4.150: Variation in M value with periodic f_s. A local minimum occurs at f_c of 551 Hz (red dot) where M = 2.17 µm, not at f_{tooth} (black circle).

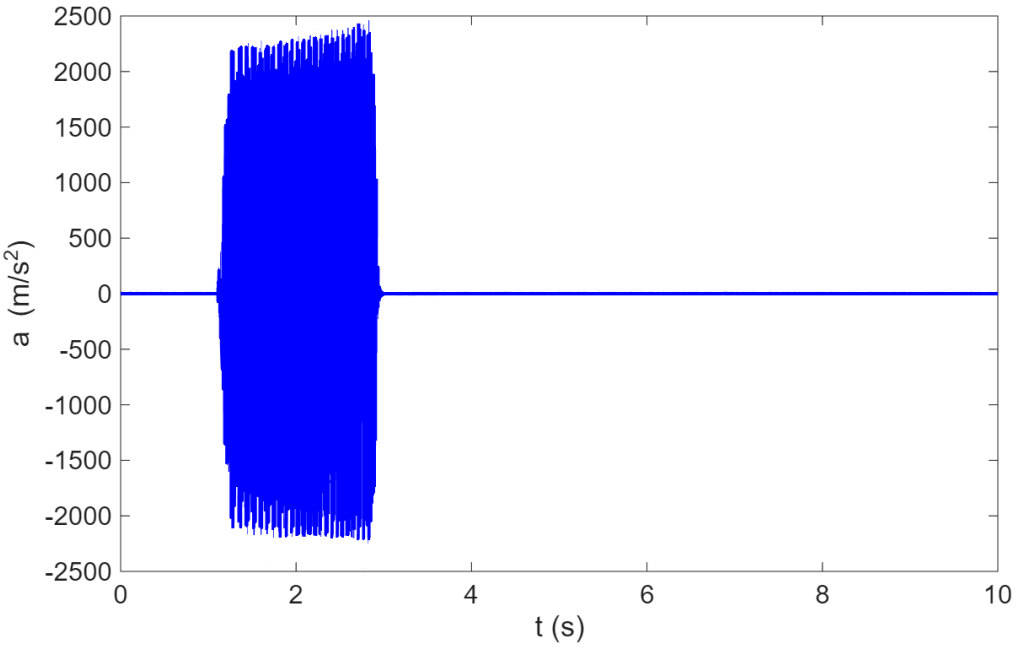


Figure 4.151: The total time interval of the signal from the accelerometer (acceleration signal) showing when the tool interacts with the workpiece.

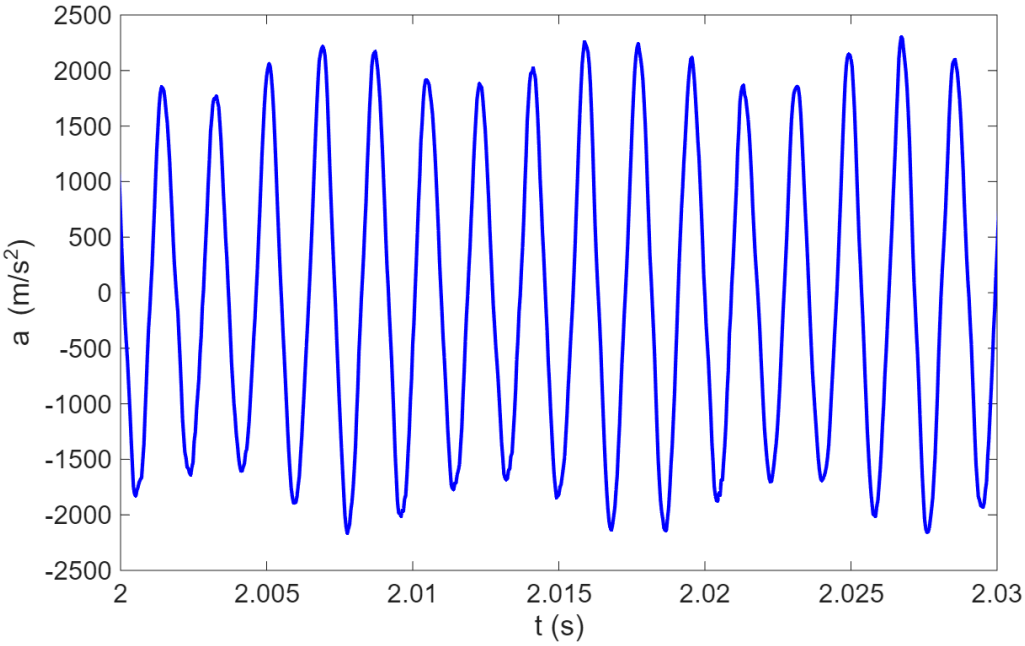


Figure 4.152: The magnified time interval of the signal from the accelerometer (acceleration signal).

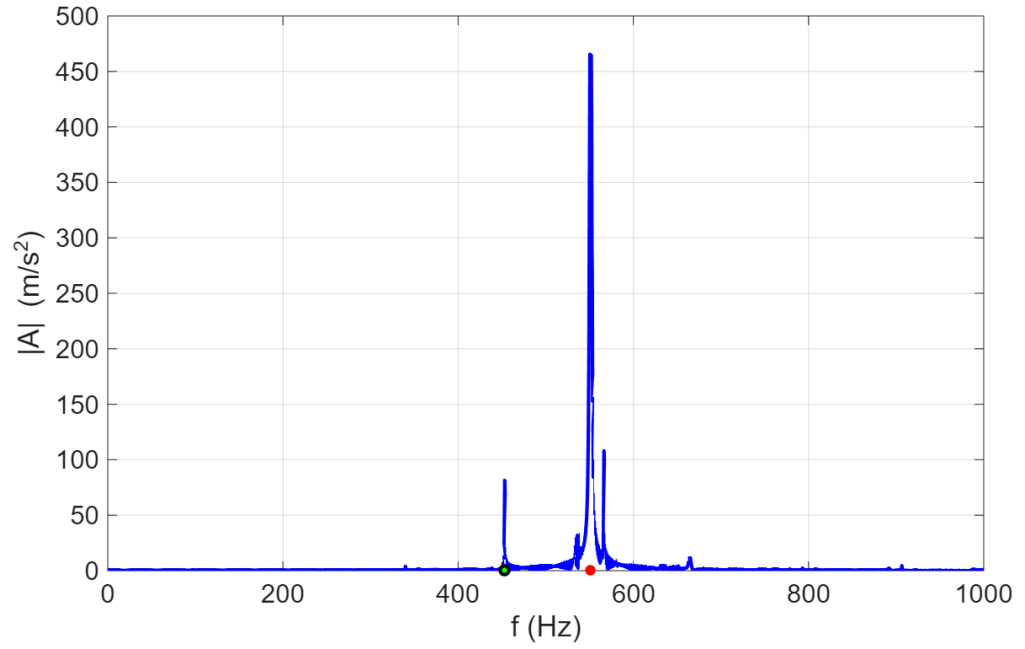


Figure 4.153: Magnitude plot of *a* frequency content for 150 rotations, with f_c (red dot) identified at 551 Hz and f_{tooth} (black circle) at 453 Hz.

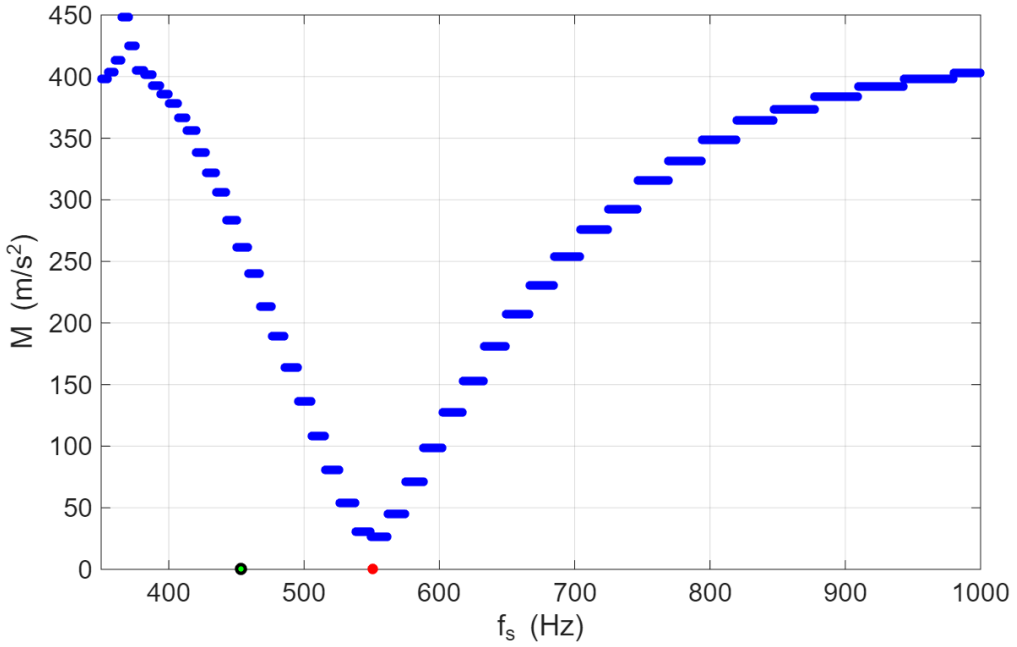


Figure 4.154: Variation in M value with periodic f_s. A local minimum occurs at f_c of 551 Hz (red dot) where M = 26.34 m/s^2, not at f_{tooth} (black circle).

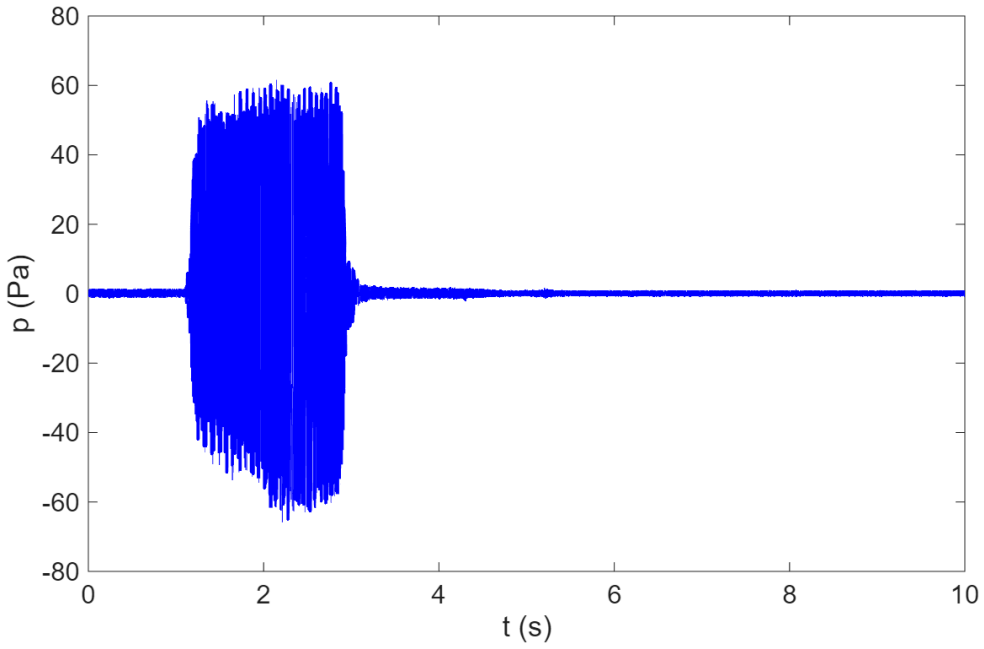


Figure 4.155: The total time interval of the signal from the microphone (sound pressure signal) showing when the tool interacts with the workpiece.

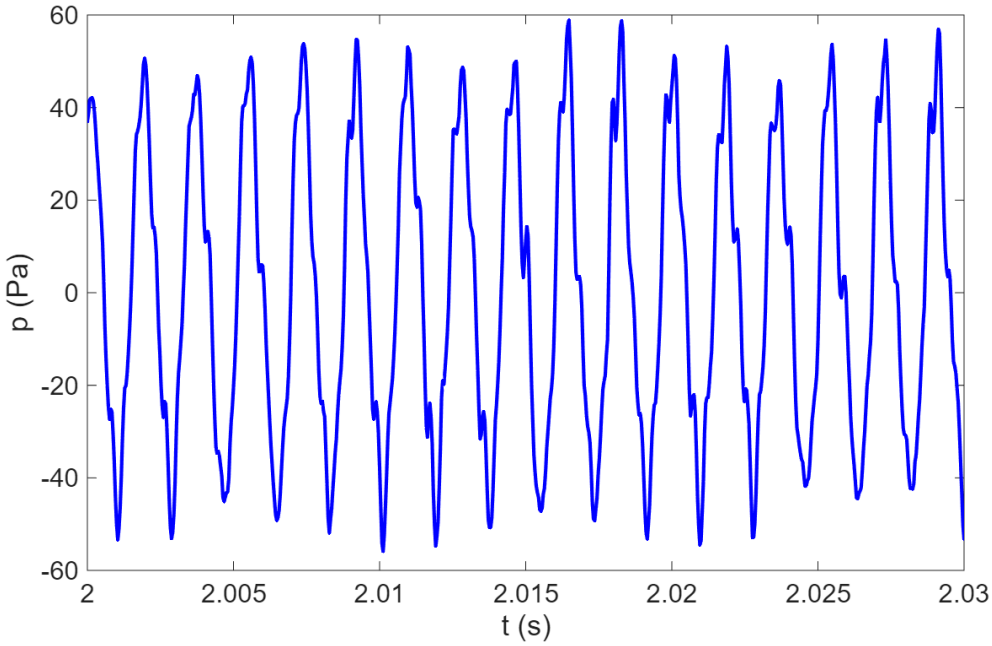


Figure 4.156: The magnified time interval of the signal from the microphone (sound pressure signal).

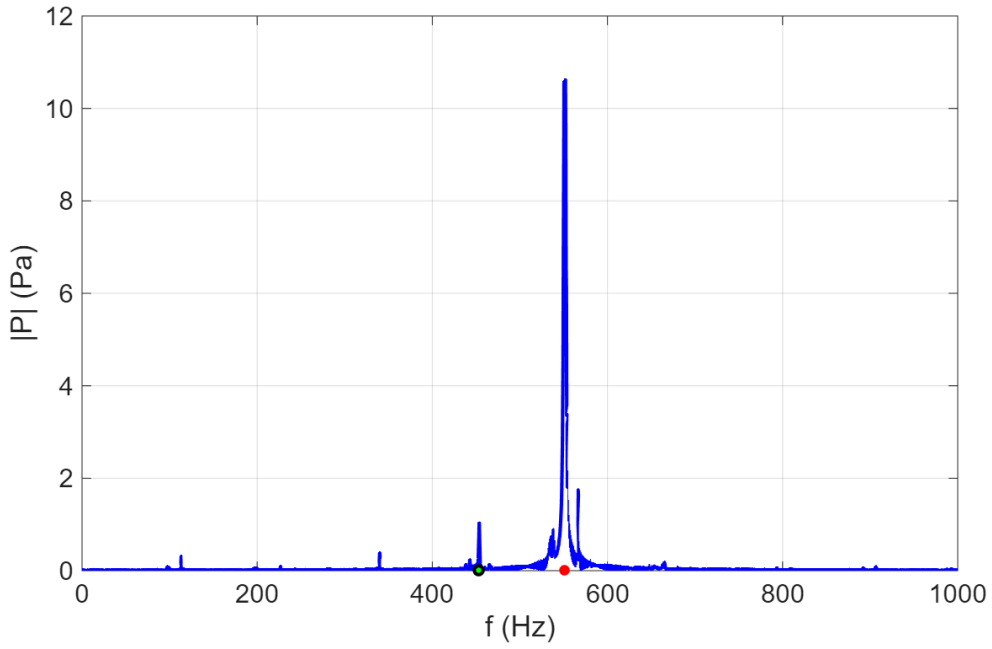


Figure 4.157: Magnitude plot of p frequency content for 150 rotations, with f_c (red dot) identified at 551 Hz and f_{tooth} (black circle) at 453 Hz.

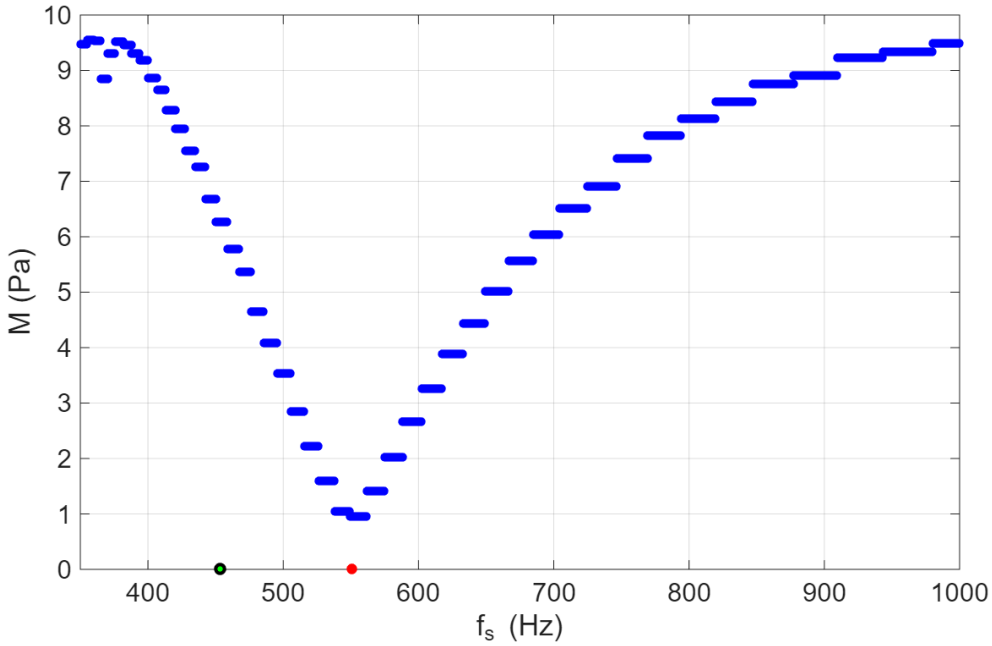


Figure 4.158: Variation in M value with periodic f_s. A local minimum occurs at f_c of 551 Hz (red dot) where M = 0.95 Pa, not at f_{tooth} (black circle).

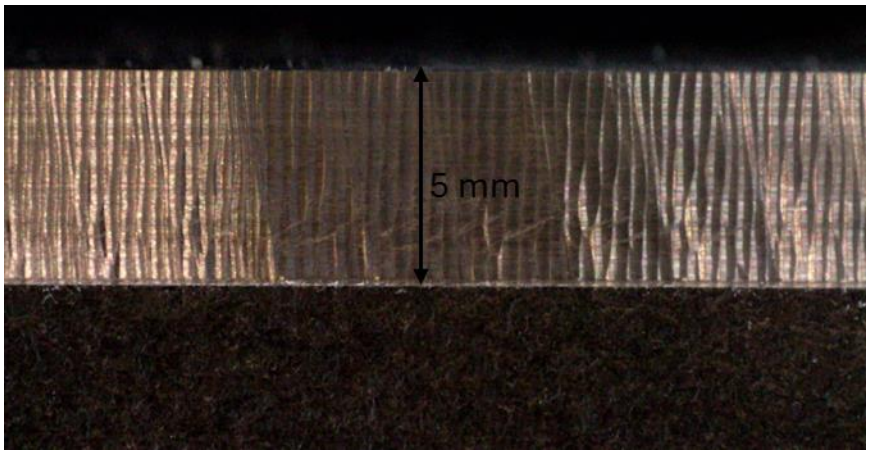


Figure 4.159: Surface of the AISI 4140 steel workpiece with chatter marks after the unstable cut.

Stable cut with new spindle speed: Four-flute endmill on AISI 4140 steel

The identified chatter frequency of 551 Hz from the previous unstable cut is used in **Equation 2** to calculate a new spindle speed of 4133 rpm, where $N_t = 4$ and $j = 2$. The new spindle speed and the resulting feed rate are the only operating parameters changed in the CNC machine to achieve a stable cut. Results from tap testing and the stable experimental cut using a four-flute carbide endmill on AISI 4140 steel are presented below. **Table 4.28** shows the modal parameters of the workpiece obtained after tap testing. The tool tip modal parameters presented in **Table 4.25** are retained because, unlike the workpiece which experiences a reduction in mass after cutting, the tool remains unchanged from the previous experimental cut upon inspection. **Figures 4.160** and **4.161** show the frequency response function and the stability lobe diagram obtained using the modal parameters. The tangential and normal force coefficients of 2044.5 N/mm^2 and 578.5 N/mm^2 respectively are retained, as well as the radial depth of cut of 2 mm. A stable point corresponding to the new spindle speed of 4133 rpm and the retained axial depth of cut of 5 mm is selected on the stability lobe diagram, which achieves a stable cut.

Table 4.27. Profilometer results from six measured locations on the unstable cut surface of the AISI 4140 steel workpiece.

Location	Ra (μm)	Rq (μm)	Rz (μm)
1	0.930	1.107	4.424
2	0.907	1.090	5.193
3	0.884	1.068	4.642
4	0.968	1.189	5.008
5	0.894	1.091	4.684
6	0.954	1.132	5.004

Results from the time domain milling signals of the displacement (x), the acceleration (a), and the sound pressure (p) are presented, including, the total time interval of each signal, the magnified time interval, magnitude plot of the frequency content, and the variation in the M value with the periodic sampling frequency, f_s.

Figures 4.162, **4.166**, and **4.170** show the total time interval of the cut from the CMD, the accelerometer, and the microphone milling signals respectively. **Figures 4.163**, **4.167**, and **4.171** show the magnified time interval of the cut from the CMD, the accelerometer, and the microphone milling signals respectively. **Figures 4.164**, **4.168**, and **4.172** show the magnitude plots of the frequency contents from the CMD, the accelerometer, and the microphone milling signals respectively. It is observed that the tooth passing frequency, f_{tooth}, or its harmonics have the highest peak in the magnitude plots, indicating a stable cut. **Figures 4.165**, **4.169**, and **4.173** show the variations in the M values with the periodic sampling frequency of the time domain milling signals from the CMD, the accelerometer, and the microphone respectively. It is observed that a local minimum in the stability metric occurs at the tooth passing frequency, f_{tooth}, also indicating a stable cut. **Figure 4.174** shows the surface of the workpiece with periodic feed marks after the cut, indicating the tool tooth trajectory. Surface roughness measurements were conducted at six different locations on the cut surface using the Mitutoyo profilometer, yielding a mean Ra value of 0.73 µm with a standard deviation of 0.087 µm, a mean Rq value of 0.87 µm with a standard deviation of 0.083 µm, and a mean Rz value of 3.71 µm with a standard deviation of 0.217 µm. **Table 4.29** shows the Ra, Rq, and Rz values for the six measured locations.

Table 4.28. Workpiece modal parameters of the AISI 4140 steel before the stable cut.

***x*-direction**		
Frequency, f_n (Hz)	**Stiffness, *k* (N/m)**	**Damping ratio, ζ (-)**
566	1.45×10^7	0.0325
***y*-direction**		
Frequency, f_n (Hz)	**Stiffness, *k* (N/m)**	**Damping ratio, ζ (-)**
1895	1.35×10^8	0.0125
2069	5.31×10^8	0.0169
3624	1.46×10^9	0.0090
3762	1.28×10^9	0.0149

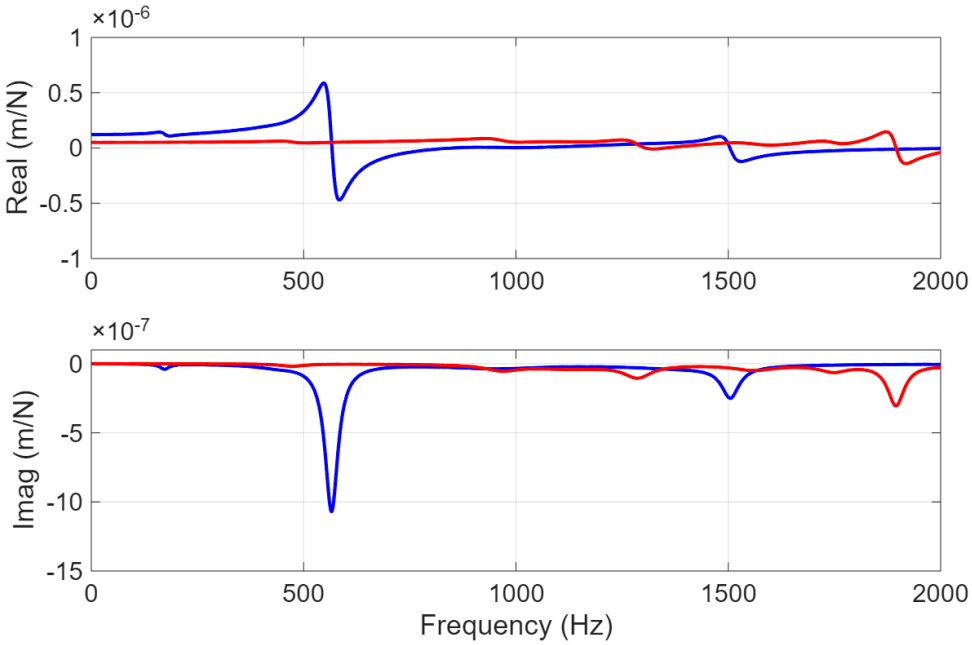


Figure 4.160: Frequency response function of the tool tip and workpiece, *x* (blue lines) and *y* (red lines) directions.

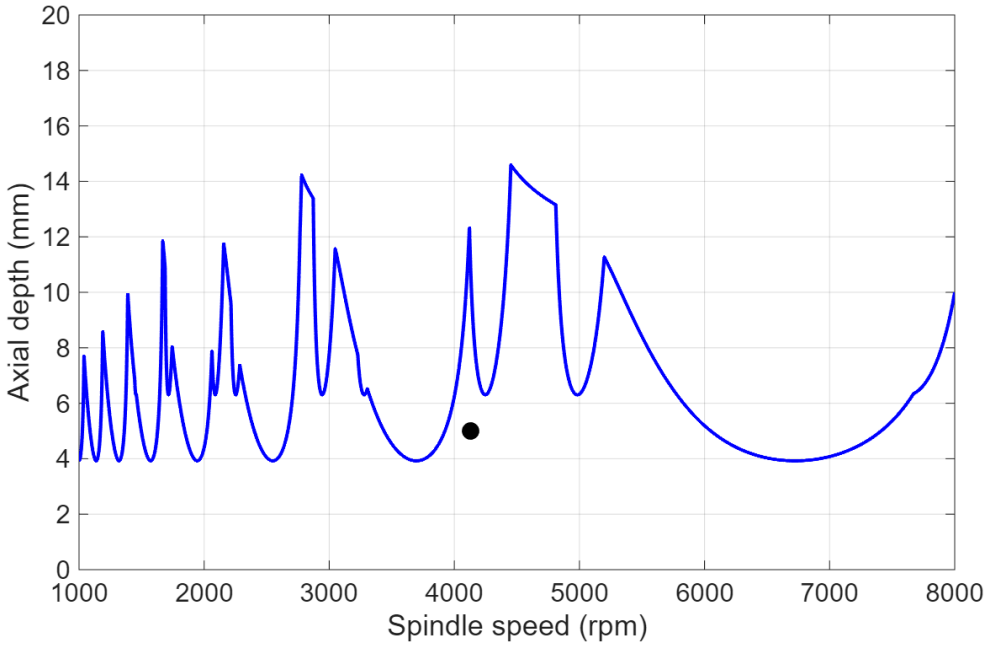


Figure 4.161: Stability lobe diagram with the selected stable point (black dot) corresponding to a spindle speed of 4133 rpm and axial depth of cut of 5 mm.

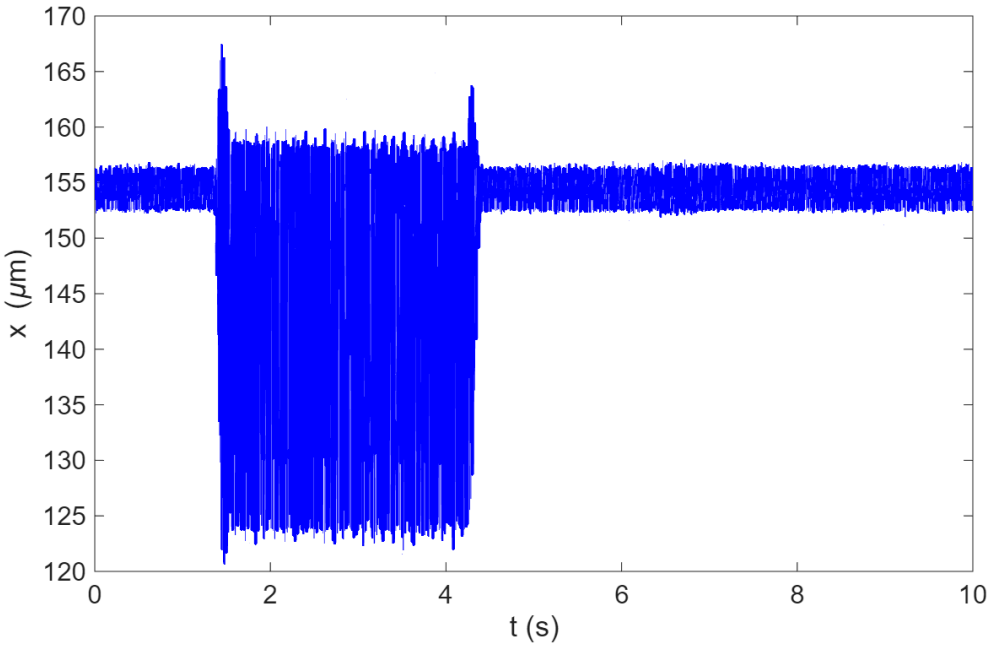


Figure 4.162: The total time interval of the signal from the CMD (displacement signal) showing when the tool interacts with the workpiece.

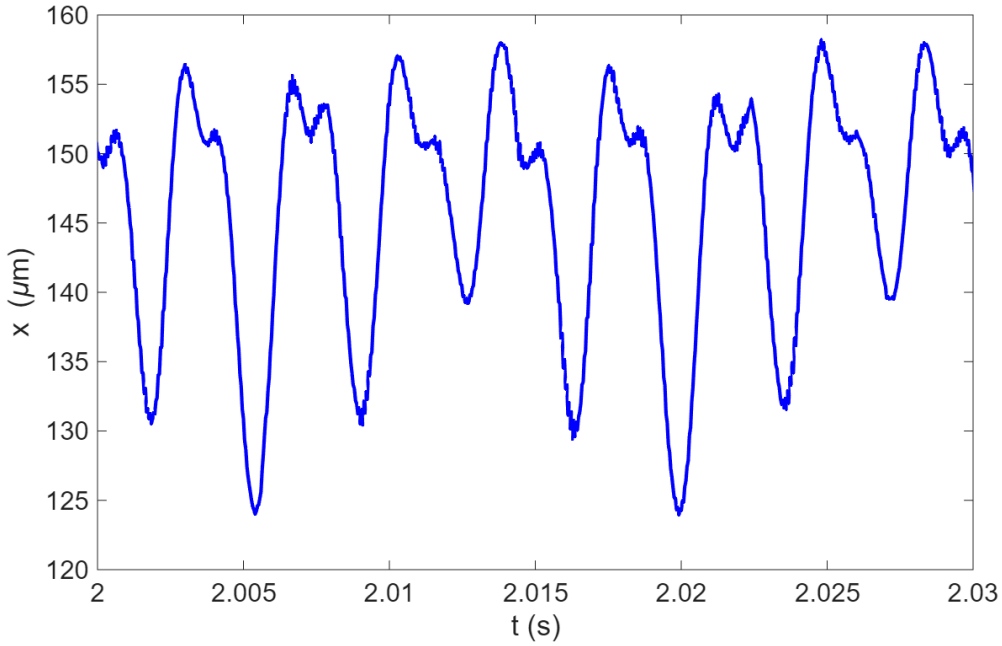


Figure 4.163: The magnified time interval of the signal from the CMD (displacement signal).

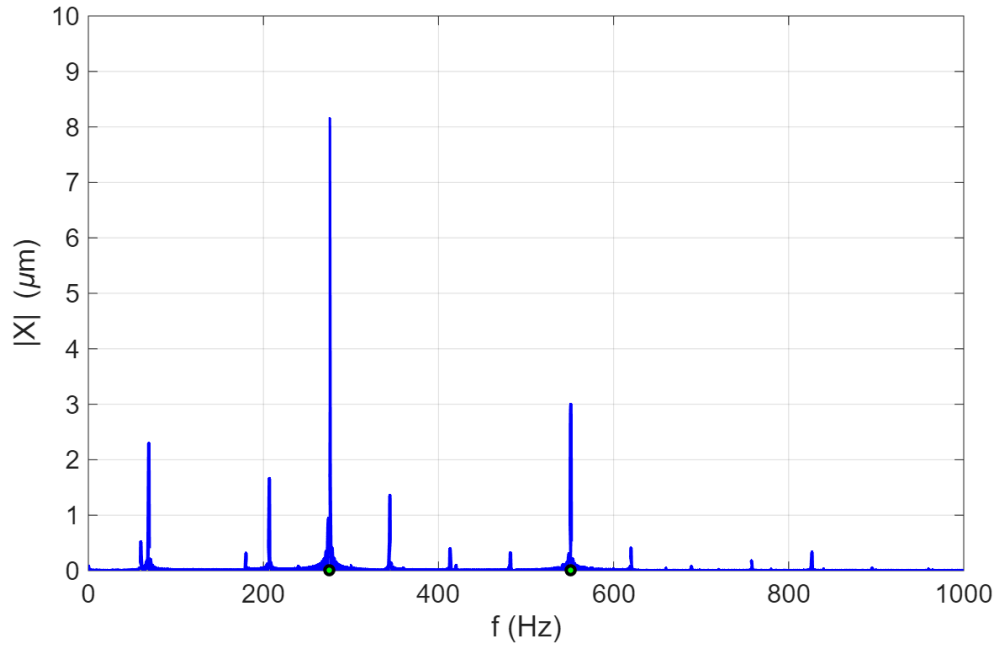


Figure 4.164: Magnitude plot of *x* frequency content for 150 rotations, with f_{tooth} at 276 Hz and its 1st harmonic (black circles) identified.

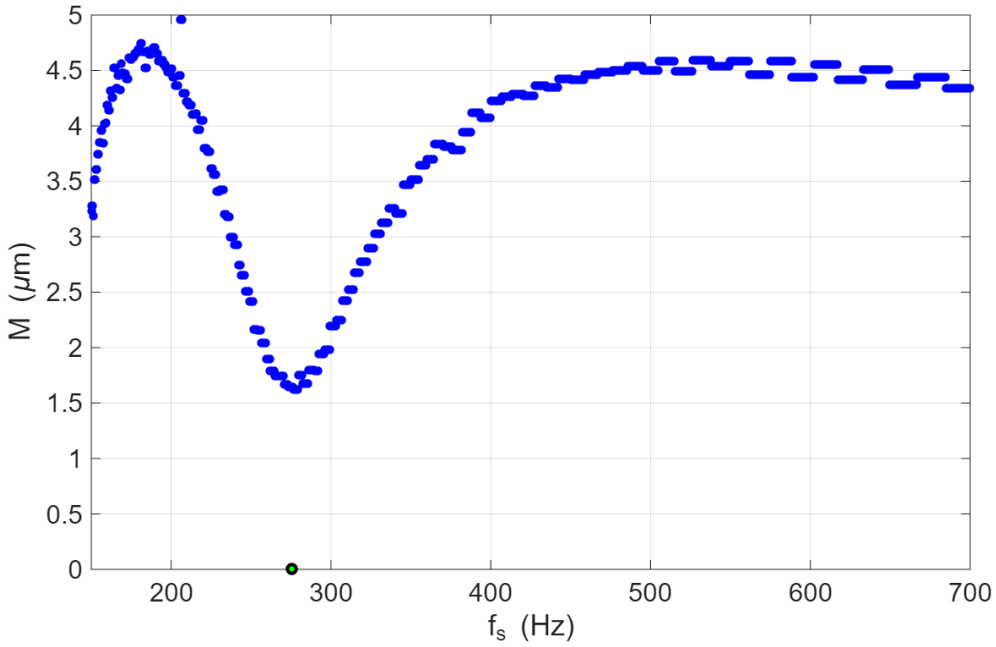


Figure 4.165: Variation in M value with periodic f_s. A local minimum occurs at f_{tooth} of 276 Hz (black circle), where M = 1.64 µm.

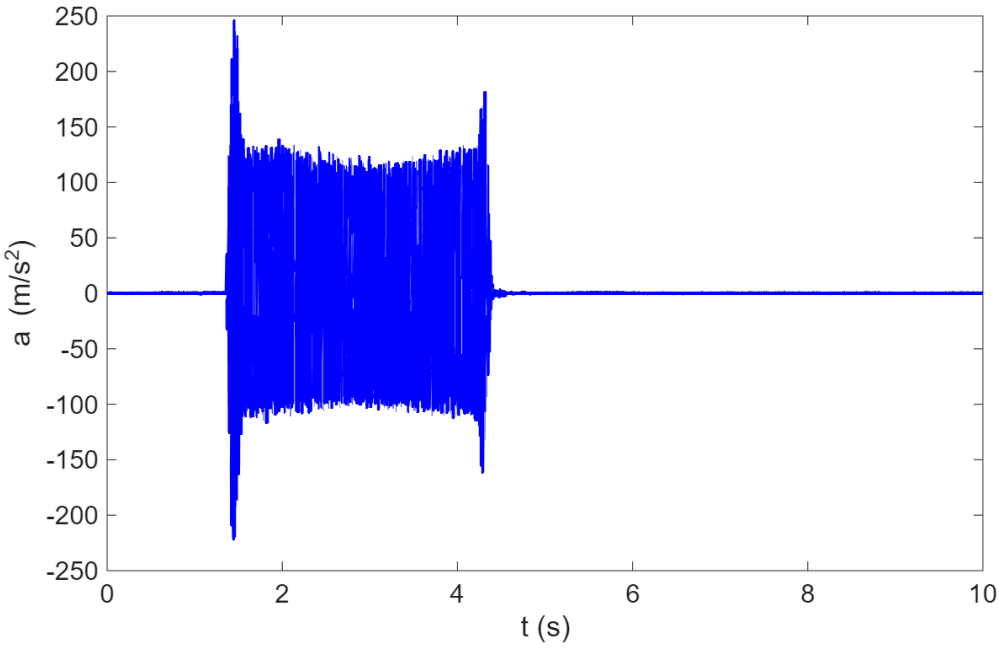


Figure 4.166: The total time interval of the signal from the accelerometer (acceleration signal) showing when the tool interacts with the workpiece.

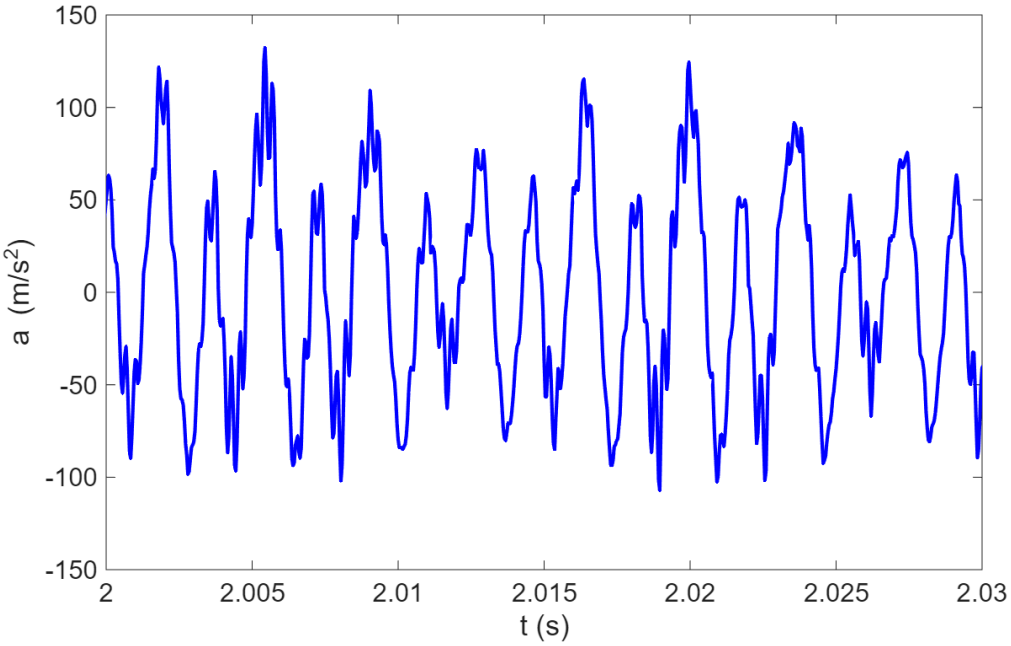


Figure 4.167: The magnified time interval of the signal from the accelerometer (acceleration signal).

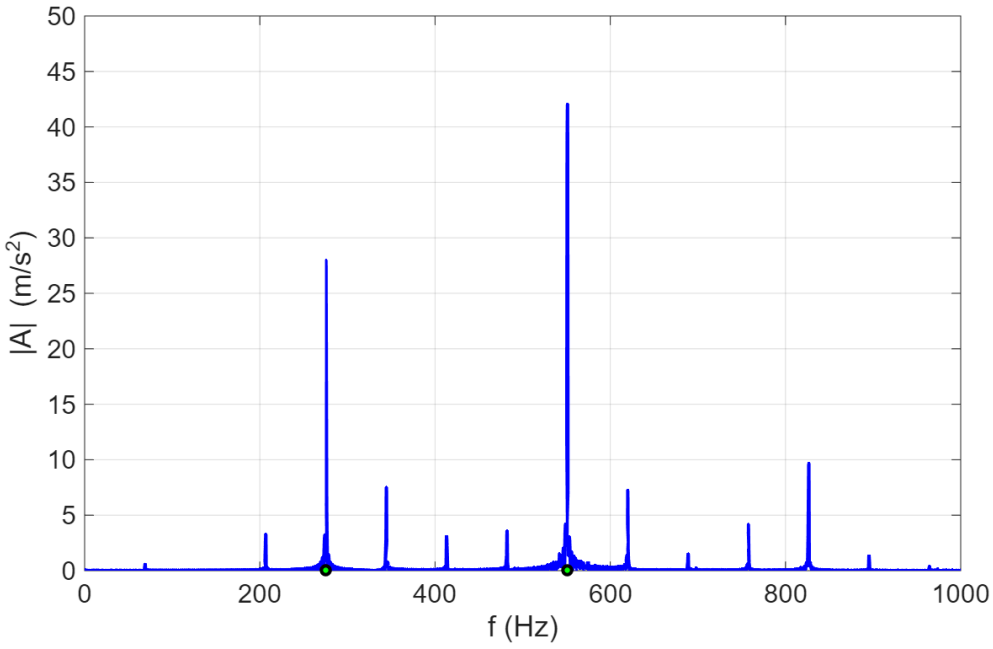


Figure 4.168: Magnitude plot of *a* frequency content for 150 rotations, with f_{tooth} at 276 Hz and its 1st harmonic (black circles) identified.

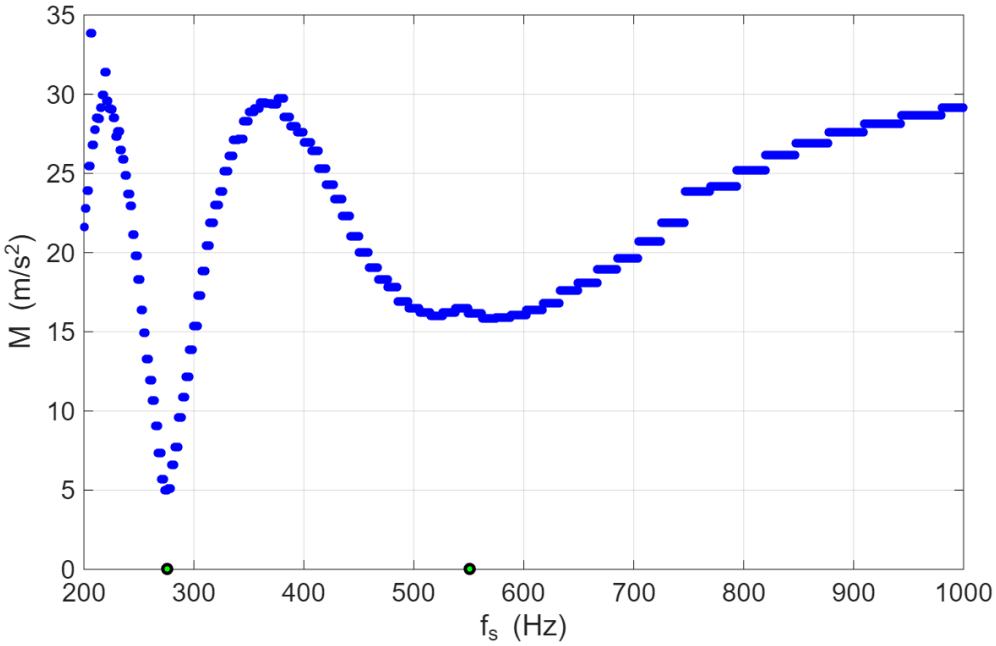


Figure 4.169: Variation in M value with periodic f_s. Local minima occur at f_{tooth} of 276 Hz and its first harmonic (black circles), where M = 5 m/s^2.

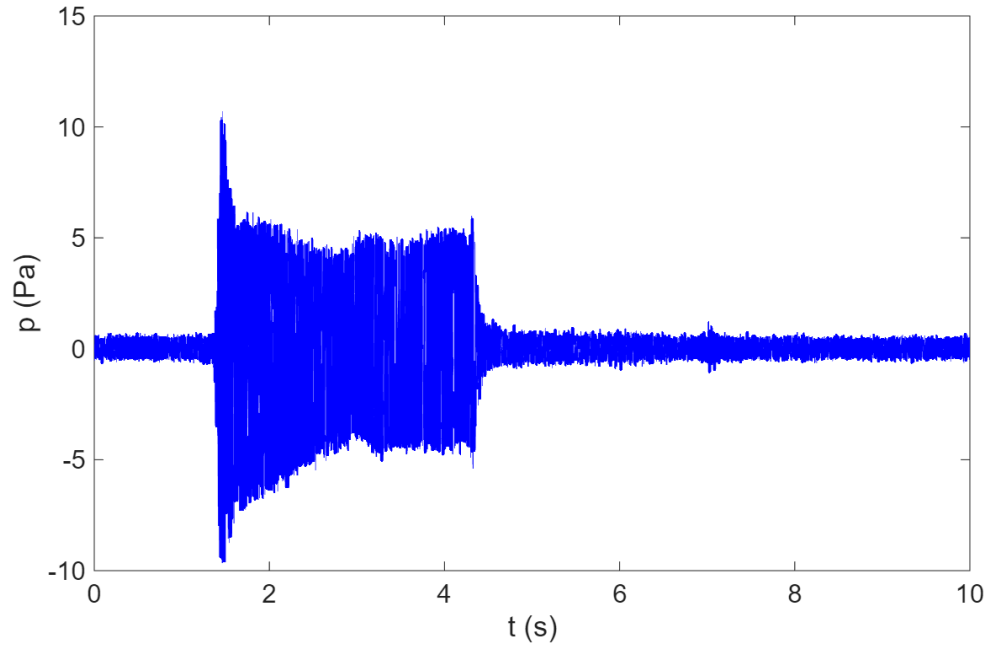


Figure 4.170: The total time interval of the signal from the microphone (sound pressure signal) showing when the tool interacts with the workpiece.

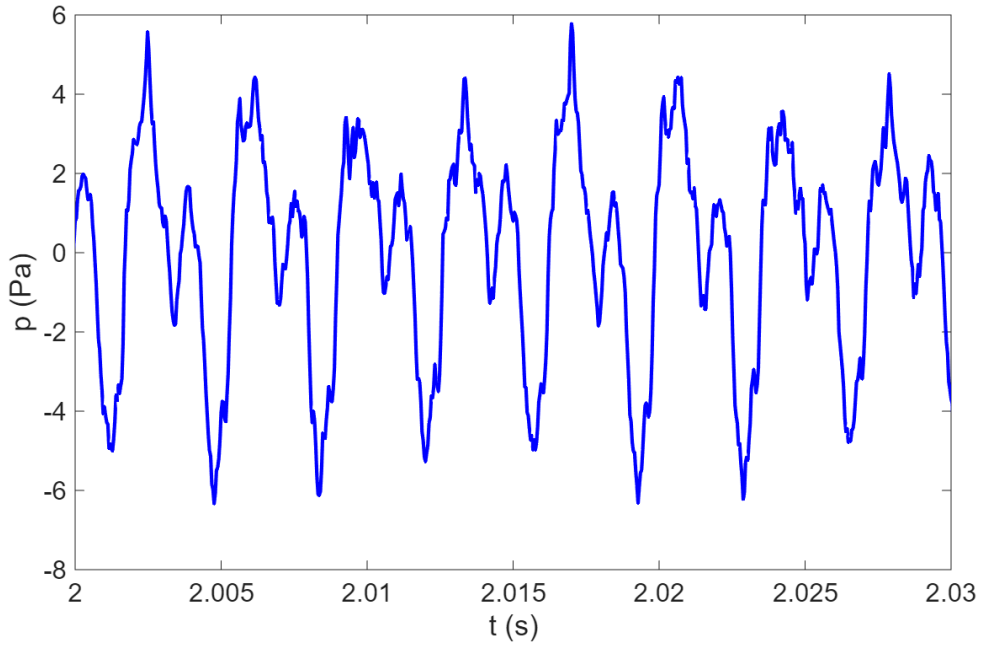


Figure 4.171: The magnified time interval of the signal from the microphone (sound pressure signal).

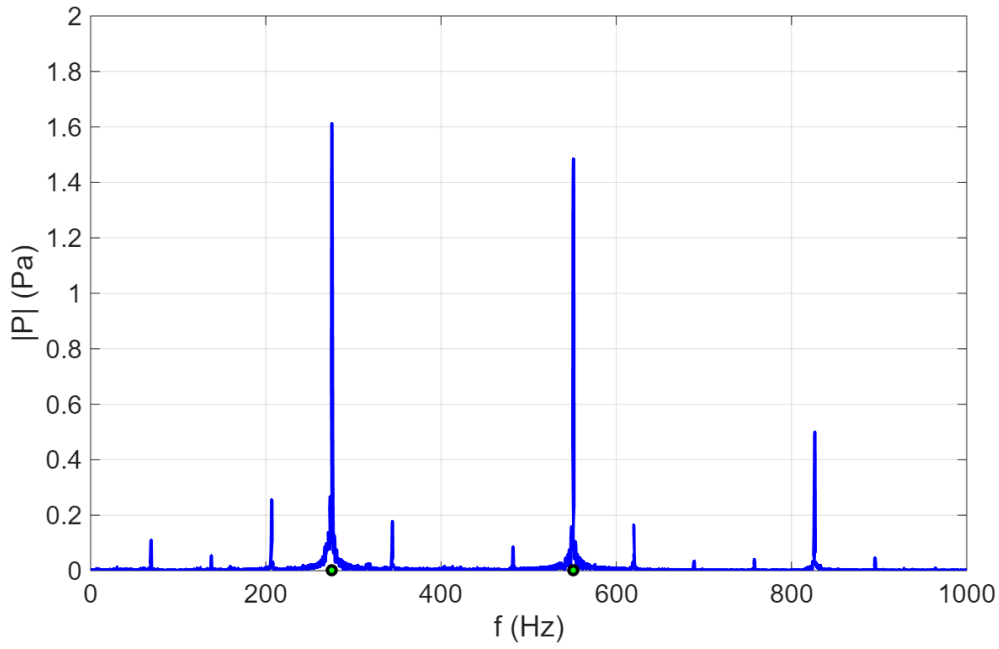


Figure 4.172: Magnitude plot of p frequency content for 150 rotations, with f_{tooth} at 276 Hz and its 1st harmonic (black circles) identified.

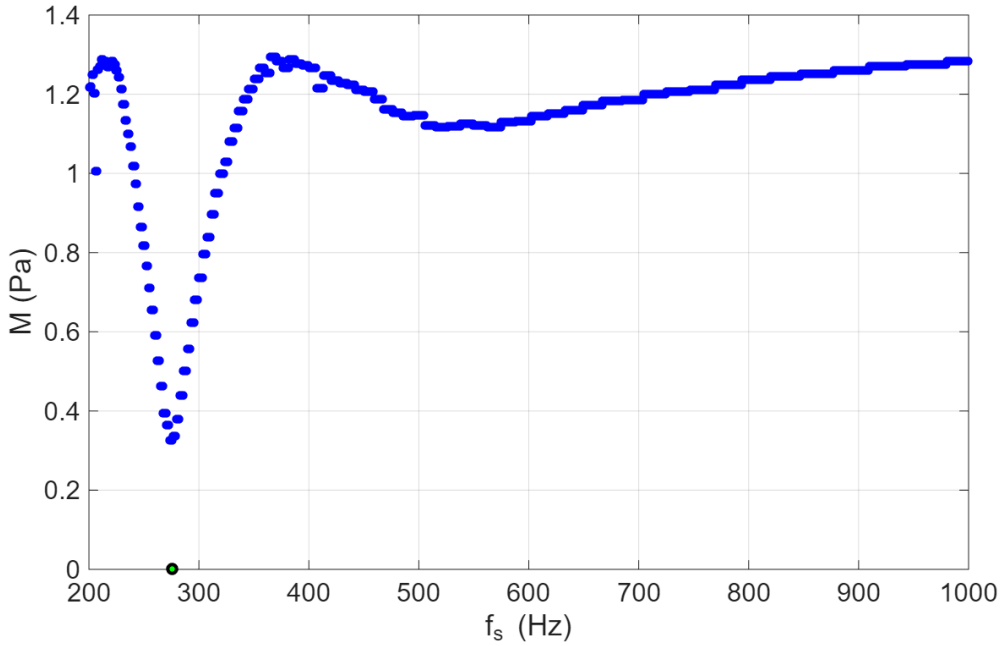


Figure 4.173: Variation in M value with periodic f_s. A local minimum occurs at f_{tooth} of 276 Hz (black circle), where M = 0.33 Pa.

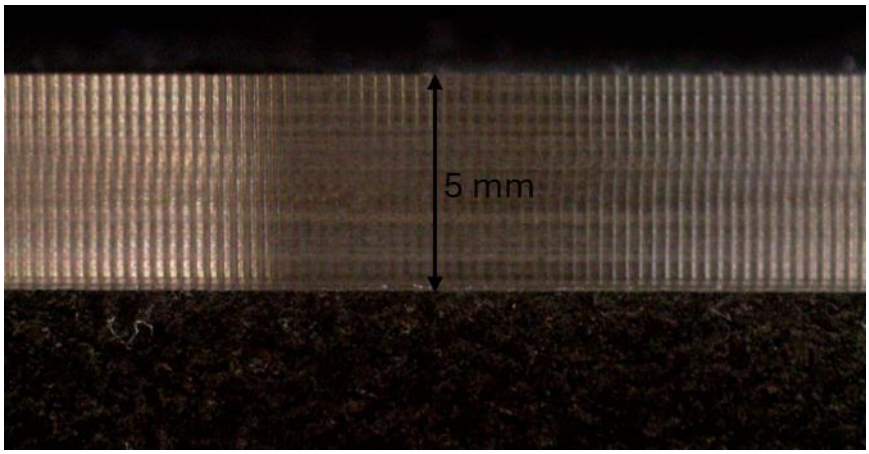


Figure 4.174: Surface of the AISI 4140 steel workpiece with periodic feed marks after the stable cut.

Closed Loop Feasibility Study

As stated in chapter 3, the MATLAB code [Appendix A] for in situ, low-latency chatter detection and spindle speed selection by scanned periodic sampling frequency is applied using the NI data acquisition device, the accelerometer, and microphone. The MATLAB code follows the closed loop algorithm shown in **Figure 3.7**. The five-flute carbide endmill is used to conduct experimental cuts on the AISI 1018 steel workpiece. The average computation time for the MATLAB code to categorize a cut as stable or unstable, after data collection (after "t1" from Appendix A. t1 represents the user defined time required to complete the cut while the milling signals are collected and processed simultaneously), is 1.37 s.

Marginal cut 1: Five-flute endmill on AISI 1018 steel

Results from the acceleration signal during an experimental cut using a five-flute carbide endmill on AISI 1018 steel are presented below. **Tables 4.30** and **4.31** show the modal parameters of the tool tip and workpiece respectively, obtained after tap testing, while **figures 4.175** and **4.176** show the frequency response function and the stability lobe diagram obtained using the modal parameters.

Table 4.29. Profilometer results from six measured locations on the stable cut surface of the AISI 4140 steel workpiece.

Location	Ra (μm)	Rq (μm)	Rz (μm)
1	0.799	0.949	4.036
2	0.754	0.903	3.705
3	0.789	0.906	3.469
4	0.750	0.896	3.877
5	0.563	0.712	3.510
6	0.712	0.861	3.662

A tangential and normal force coefficient of 1742.8 N/mm^2 and 528.4 N/mm^2 respectively [53] for AISI 1018 steel are selected. A radial depth of cut of 2 mm is selected, and a marginal point corresponding to a spindle speed of 4650 rpm and an axial depth of cut of 8 mm is selected on the stability lobe diagram.

Because a local minimum does not occur at the tooth passing frequency, f_{tooth}, the algorithm categorizes the cut as unstable, it then uses FFT to determine the chatter frequency, f_c, and recommends new spindle speeds. A spindle speed of 4942 rpm is selected from the recommended list to be used in achieving a stable cut. **Figures 4.177** shows the total time interval of the cut from the acceleration signal. **Figures 4.178** shows the magnified time interval of the cut. **Figures 4.179** shows the magnitude plot of the frequency content from the accelerometer. It is observed that the chatter frequency, f_c, has the highest peak in the magnitude plot, indicating an unstable cut. **Figures 4.180** shows the variation in the M value with the periodic sampling frequency f_s of the time domain milling signal from the accelerometer. It is observed that a local minimum in the stability metric occurs at the chatter frequency, f_c, not at the tooth passing frequency, f_{tooth}, thereby indicating an unstable cut.

Figure 4.181 shows the surface of the workpiece after the cut, captured using the Dino-Lite digital microscope. Without periodic sampling of the time domain milling signals using techniques such as the variation of the M values with f_s, such marginal cuts can be wrongly categorized as stable due to the stable-looking periodic feed marks on the cut surface. Surface roughness measurements were conducted at six different locations on the cut surface using the Mitutoyo profilometer, yielding a mean Ra value of 1.16 µm with a

standard deviation of 0.061 μm, a mean Rq value of 1.39 μm with a standard deviation of 0.076 μm, and a mean Rz value of 5.73 μm with a standard deviation of 0.444 μm. **Table 4.32** shows the Ra, Rq, and Rz values for the six measured locations.

Table 4.30. Tool tip modal parameters of the five-flute endmill.

***x*-direction**		
Frequency, f_n (Hz)	**Stiffness, *k* (N/m)**	**Damping ratio, ζ (-)**
172	1.33×10^8	0.0848
474	2.14×10^8	0.1213
938	1.26×10^8	0.1352
1493	1.05×10^8	0.0289
4337	5.72×10^8	0.0669
10734	4.20×10^8	0.0493
11738	2.28×10^8	0.0239
13005	6.31×10^8	0.0377
***y*-direction**		
Frequency, f_n (Hz)	**Stiffness, *k* (N/m)**	**Damping ratio, ζ (-)**
483	3.53×10^8	0.1056
959	2.90×10^8	0.0408
1288	8.01×10^7	0.1154
1571	8.42×10^8	0.0217
1751	5.41×10^8	0.0232
3345	3.67×10^8	0.1237
10657	3.31×10^8	0.0577
11293	1.52×10^9	0.0202
11756	2.52×10^8	0.0196
13326	5.36×10^8	0.0392

Table 4.31. Workpiece modal parameters of the AISI 1018 steel before the marginal cut.

***x*-direction**		
Frequency, f_n (Hz)	**Stiffness, k (N/m)**	**Damping ratio, ζ (-)**
839	7.53×10^7	0.0100
***y*-direction**		
Frequency, f_n (Hz)	**Stiffness, k (N/m)**	**Damping ratio, ζ (-)**
219	7.41×10^8	0.0937
2413	4.09×10^9	0.0244
3080	8.22×10^8	0.0478
3182	1.76×10^{10}	0.0042
3447	1.48×10^9	0.0077
3637	1.91×10^{10}	0.0036
6302	6.49×10^9	0.0074
17517	1.76×10^{10}	0.0149

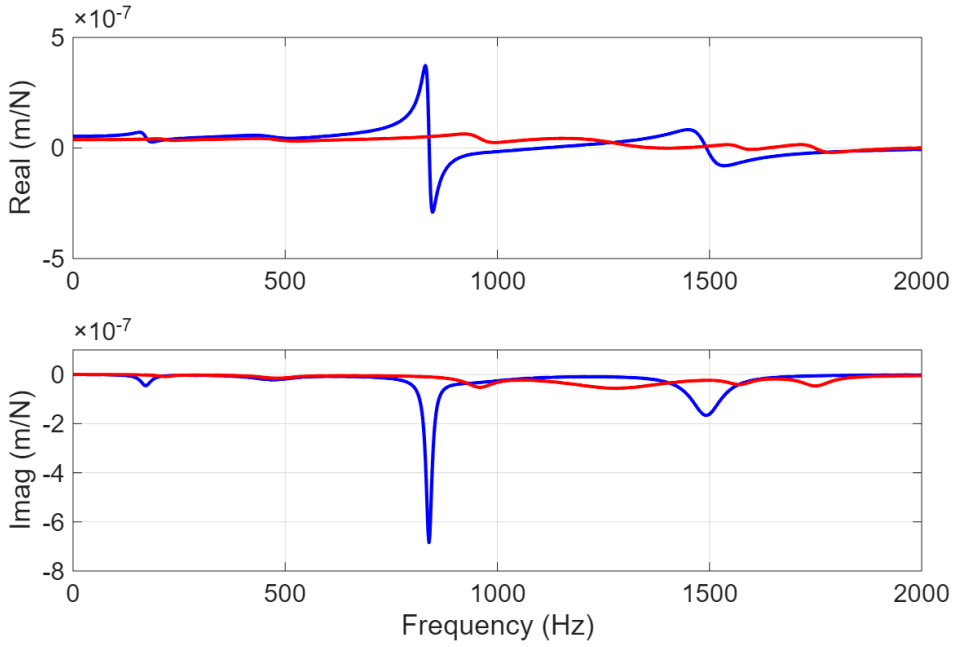


Figure 4.175: Frequency response function of the tool tip and workpiece, *x* (blue lines) and *y* (red lines) directions.

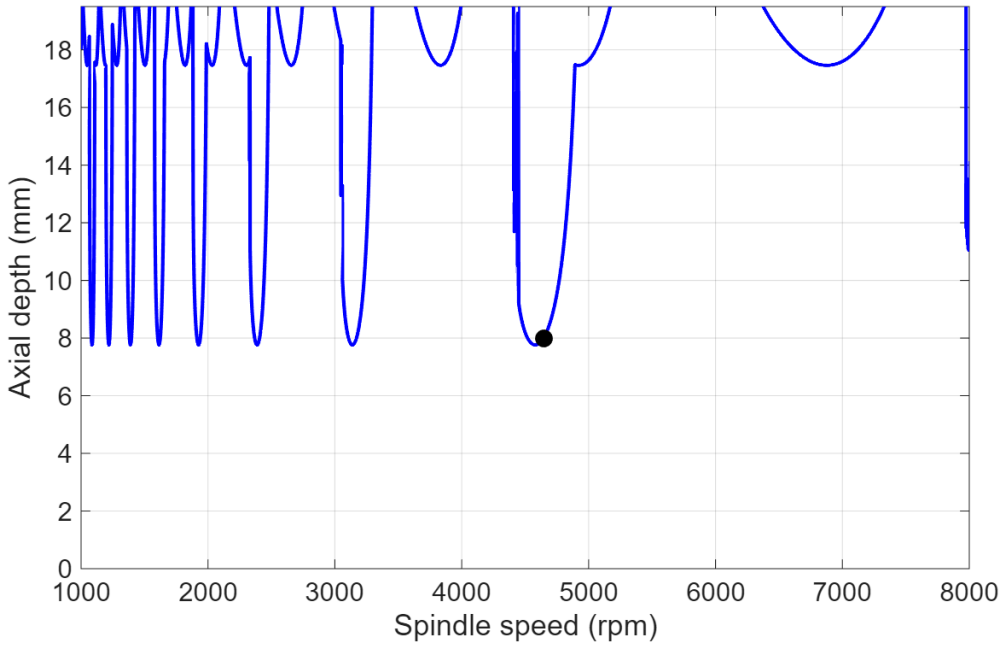


Figure 4.176: Stability lobe diagram with the selected marginal point (black dot) corresponding to a spindle speed of 4650 rpm and axial depth of cut of 8 mm.

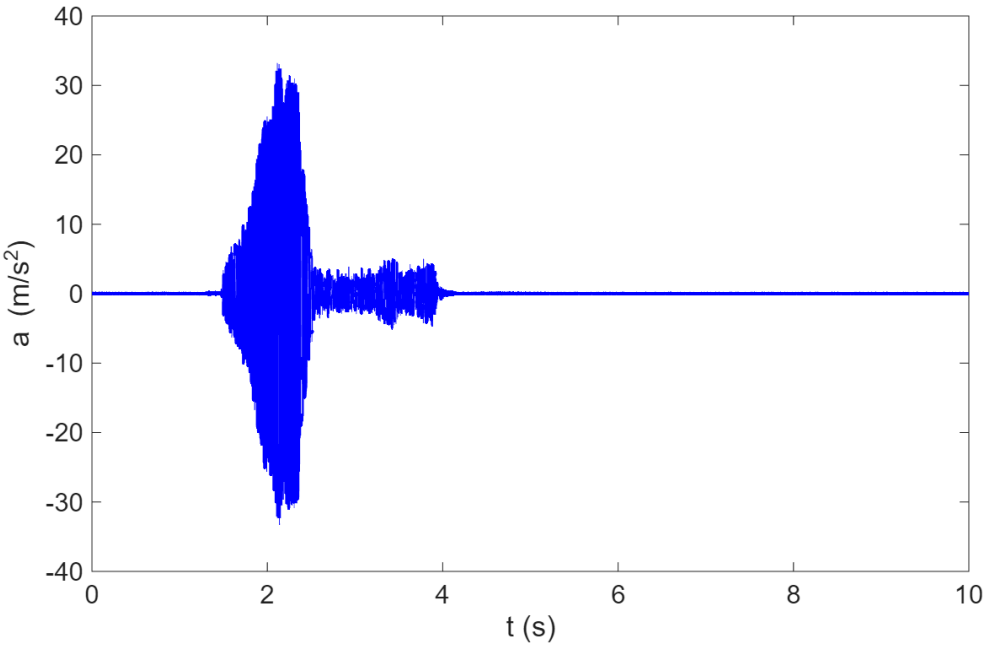


Figure 4.177: The total time interval of the signal from the accelerometer (acceleration signal) showing when the tool interacts with the workpiece.

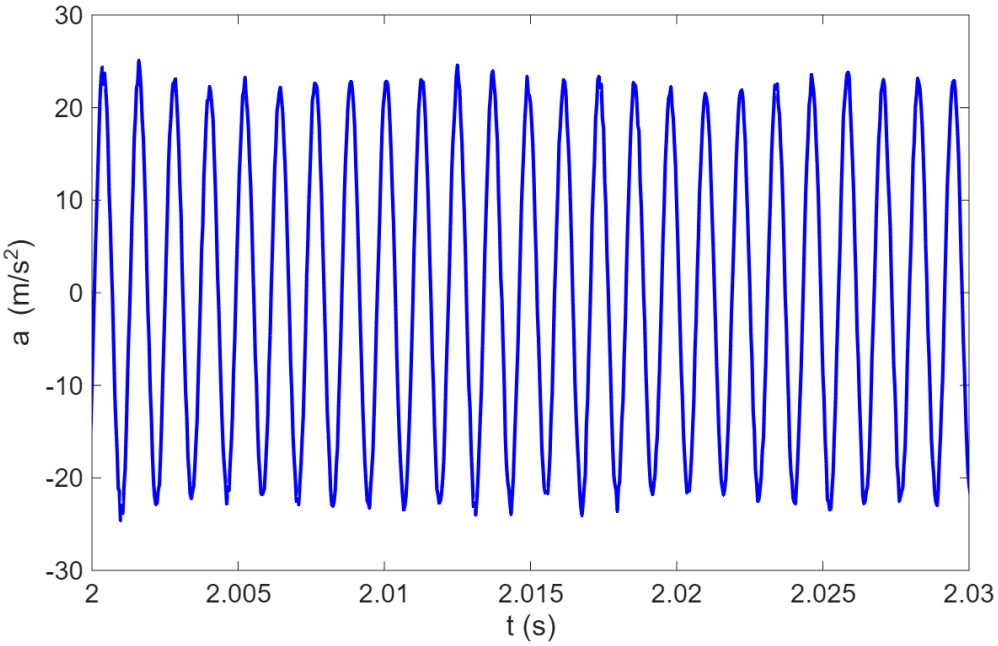


Figure 4.178: The magnified time interval of the signal from the accelerometer (acceleration signal).

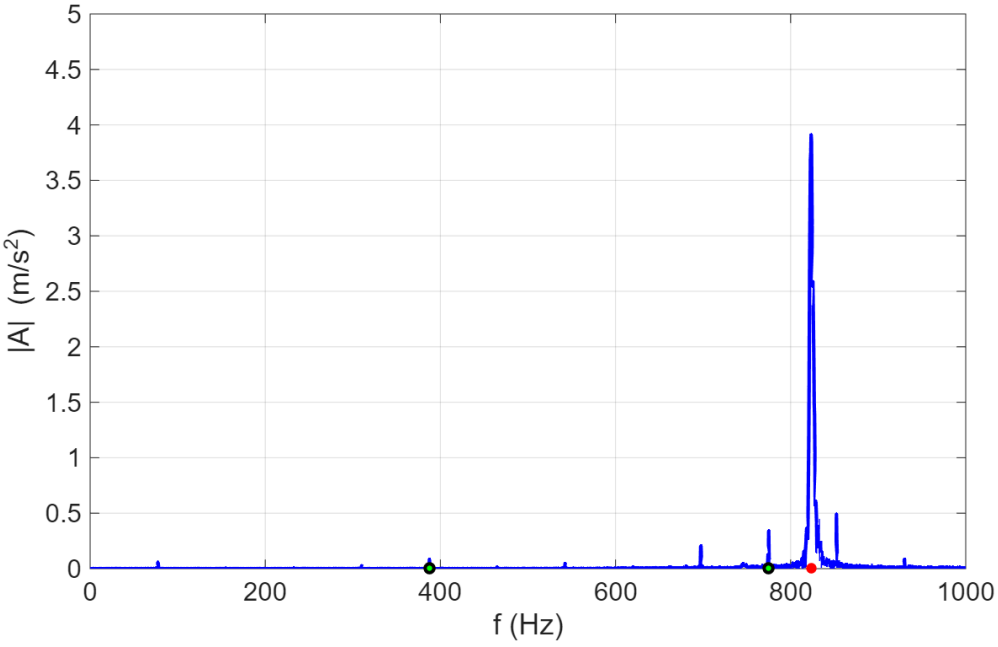


Figure 4.179: Magnitude plot of *a* frequency content for 150 rotations, identifying f_c (red dot) at 824 Hz, and f_{tooth} (black circle) at 388 Hz with its 1st harmonic (black circle).

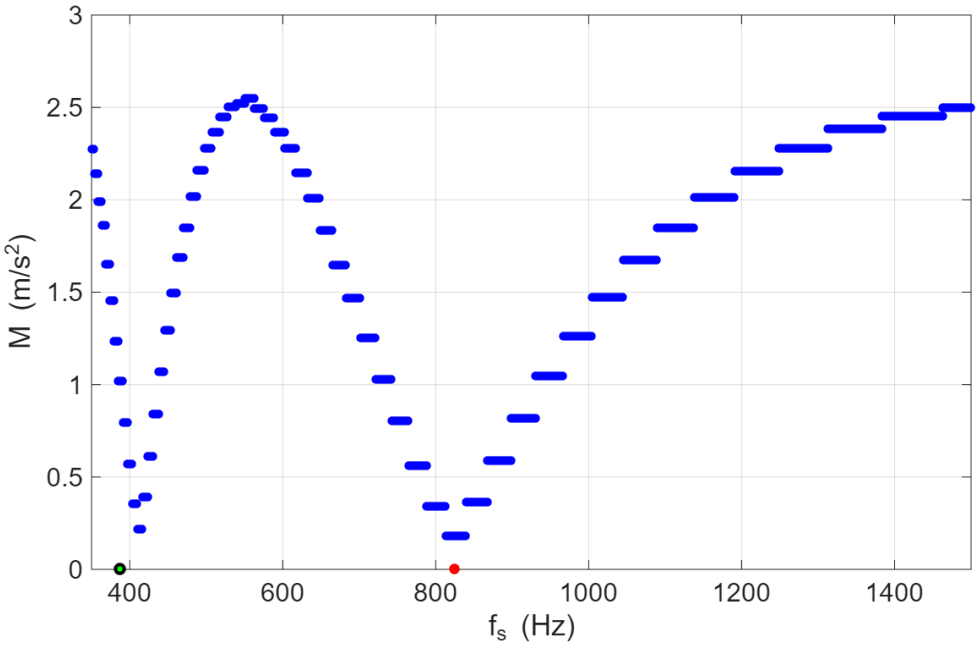


Figure 4.180: Variation in M value with periodic f_s. A local minimum occurs at f_c of 824 Hz (red dot) where M = 0.18 m/s^2, not at f_{tooth} (black circle).

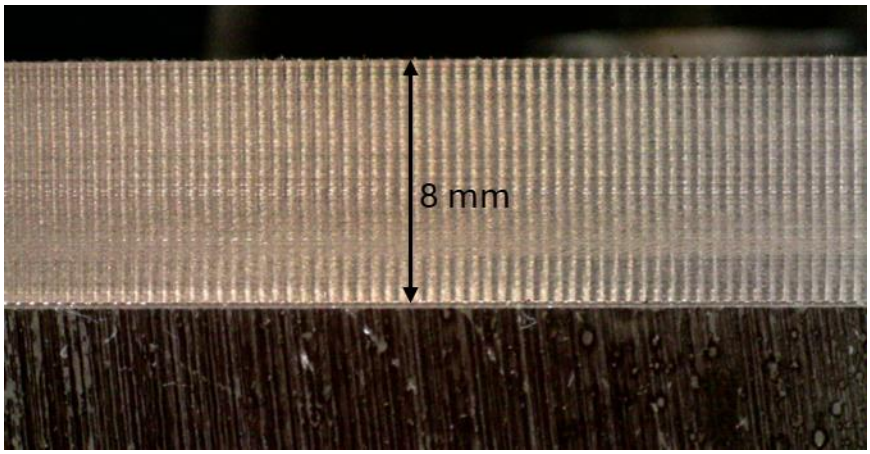


Figure 4.181: Surface of the AISI 1018 steel workpiece after the marginal cut.

Stable cut 1: Five-flute endmill on AISI 1018 steel

Results from the acceleration signal during the resulting stable experimental cut, after the previous marginal cut, using the five-flute carbide endmill on AISI 1018 steel are presented below. **Tables 4.33** shows the modal parameters of the workpiece obtained after tap testing. The tool tip modal parameters presented in **Table 4.30** are retained because, unlike the workpiece which experiences a reduction in mass after cutting, the tool remains unchanged from the previous experimental cut upon inspection. **Figures 4.182** and **4.183** show the frequency response function and the stability lobe diagram obtained using the modal parameters. The tangential and normal force coefficients of 1742.8 N/mm^2 and 528.4 N/mm^2 respectively are retained, as well as the radial depth of cut of 2 mm. A stable point corresponding to the new spindle speed of 4942 rpm recommended by the algorithm and the retained axial depth of cut of 8 mm is selected on the stability lobe diagram, which achieves a stable cut.

Because a local minimum occurs at the tooth passing frequency, f_{tooth}, the algorithm categorizes the cut as stable. **Figures 4.184** shows the total time interval of the cut from the acceleration signal. **Figures 4.185** shows the magnified time interval of the cut.

Table 4.32. Profilometer results from six measured locations on the marginal cut surface of the AISI 1018 steel workpiece.

Location	Ra (µm)	Rq (µm)	Rz (µm)
1	1.217	1.494	6.501
2	1.189	1.411	5.829
3	1.054	1.279	5.177
4	1.149	1.353	5.481
5	1.211	1.443	5.626
6	1.135	1.357	5.788

Figures 4.186 shows the magnitude plot of the frequency content from the accelerometer. It is observed that the 1st harmonic of the tooth passing frequency, f_{tooth}, is the highest peak in the magnitude plot, indicating a stable cut. **Figures 4.187** shows the variation in the *M* value with the periodic sampling frequency of the time domain milling signal from the accelerometer. It is observed that local minima in the stability metric occur at the tooth passing frequency, f_{tooth}, and its harmonic, indicating a stable cut.

Figure 4.188 shows the surface of the workpiece with periodic feed marks after the cut, indicating the tool tooth trajectory. Surface roughness measurements were conducted at six different locations on the cut surface using the Mitutoyo profilometer, yielding a mean Ra value of 0.74 µm with a standard deviation of 0.102 µm, a mean Rq value of 0.92 µm with a standard deviation of 0.089 µm, and a mean Rz value of 4.24 µm with a standard deviation of 0.227 µm. The surface roughness measurements reiterate the unstable behavior of the previous marginal cut. **Table 4.34** shows the Ra, Rq, and Rz values for the six measured locations.

Table 4.33. Workpiece modal parameters of the AISI 4140 steel before the stable cut.

***x*-direction**		
Frequency, f_n (Hz)	**Stiffness, *k* (N/m)**	**Damping ratio, ζ (-)**
839	8.23×10^7	0.0100
***y*-direction**		
Frequency, f_n (Hz)	**Stiffness, *k* (N/m)**	**Damping ratio, ζ (-)**
204	5.93×10^8	0.0843
2417	4.23×10^9	0.0180
3189	9.12×10^8	0.0307
3456	1.49×10^9	0.0073
6310	5.60×10^9	0.0059
9236	7.81×10^9	0.0170
17877	5.44×10^{10}	0.0009

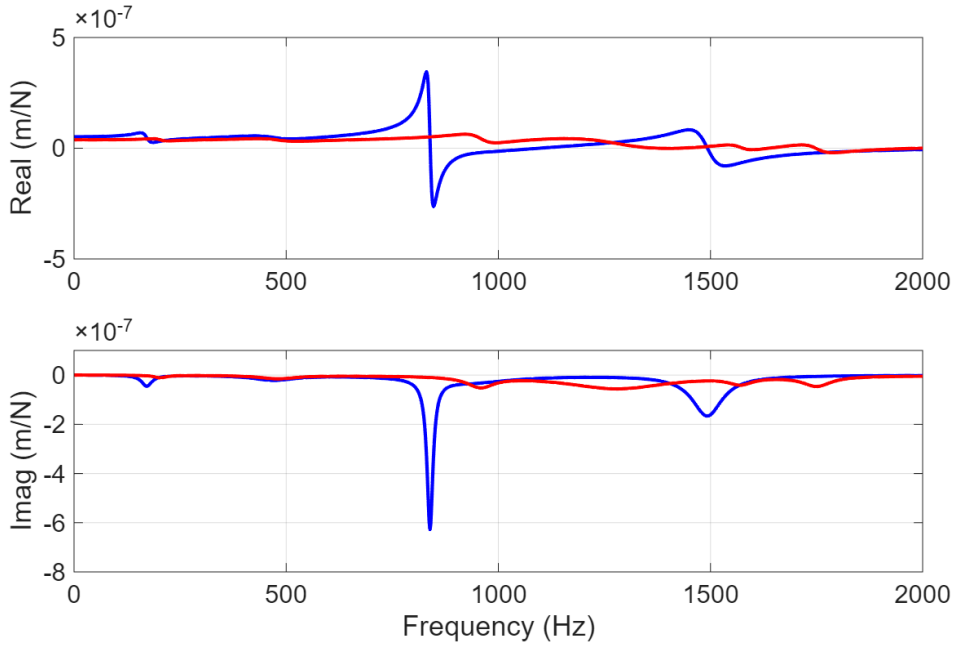


Figure 4.182: Frequency response function of the tool tip and workpiece, *x* (blue lines) and *y* (red lines) directions.

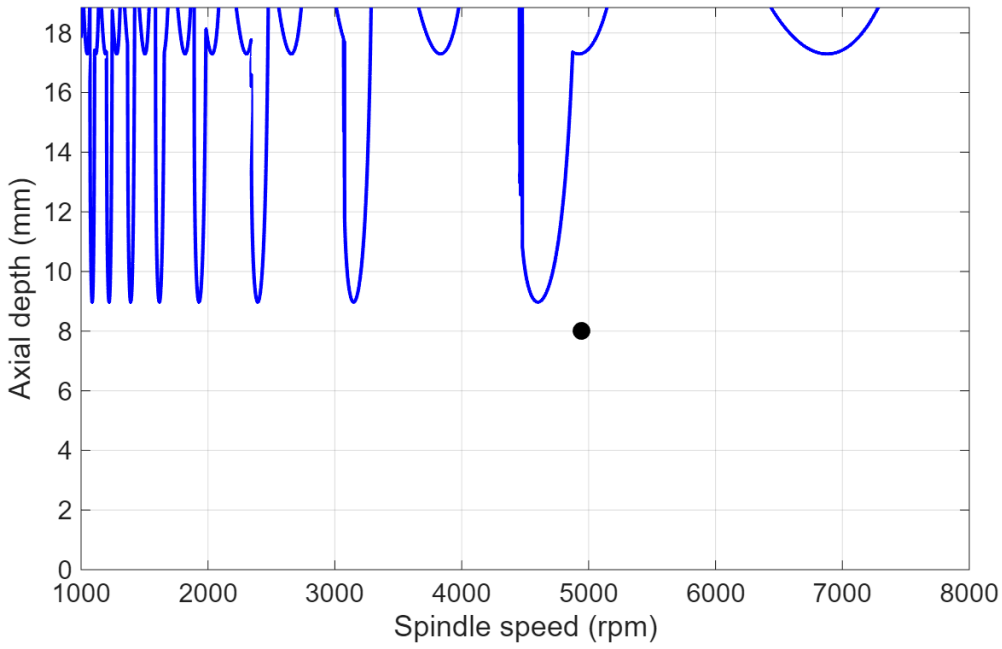


Figure 4.183: Stability lobe diagram with the recommended stable point (black dot) corresponding to a spindle speed of 4942 rpm and axial depth of cut of 8 mm.

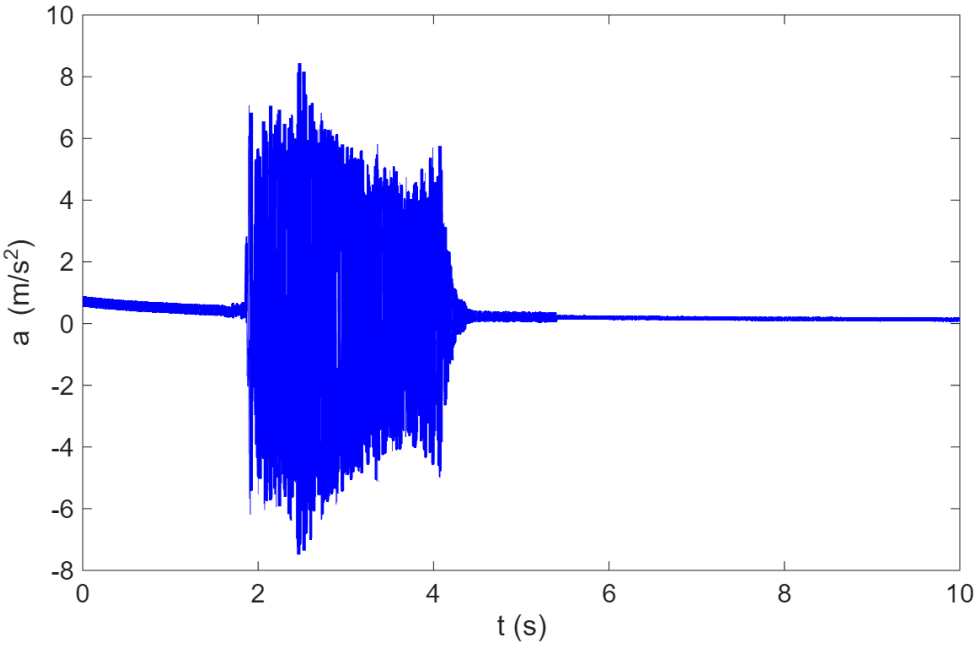


Figure 4.184: The total time interval of the signal from the accelerometer (acceleration signal) showing when the tool interacts with the workpiece.

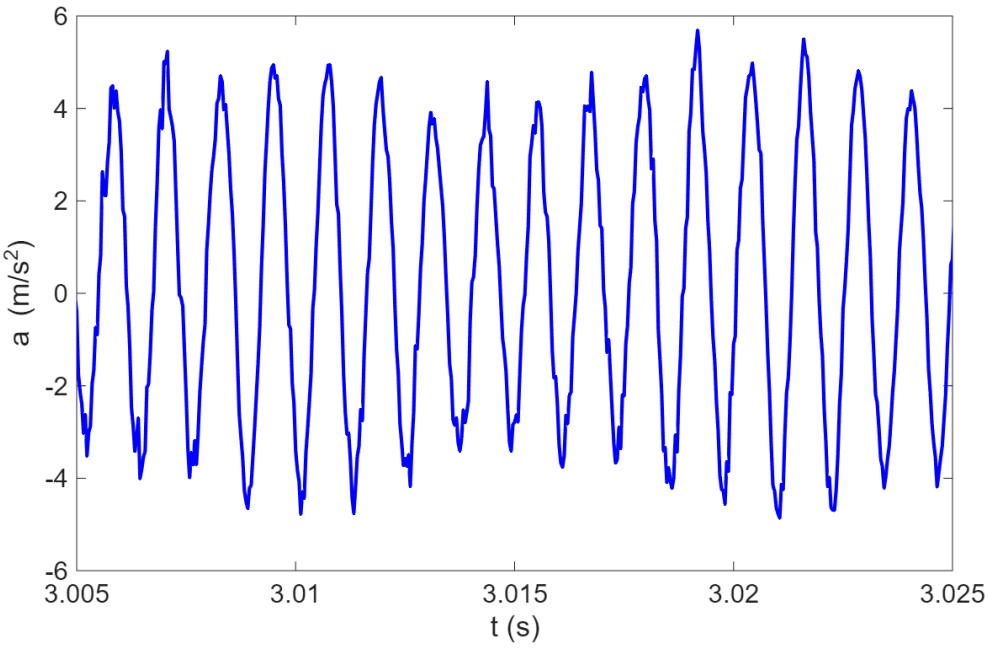


Figure 4.185: The magnified time interval of the signal from the accelerometer (acceleration signal).

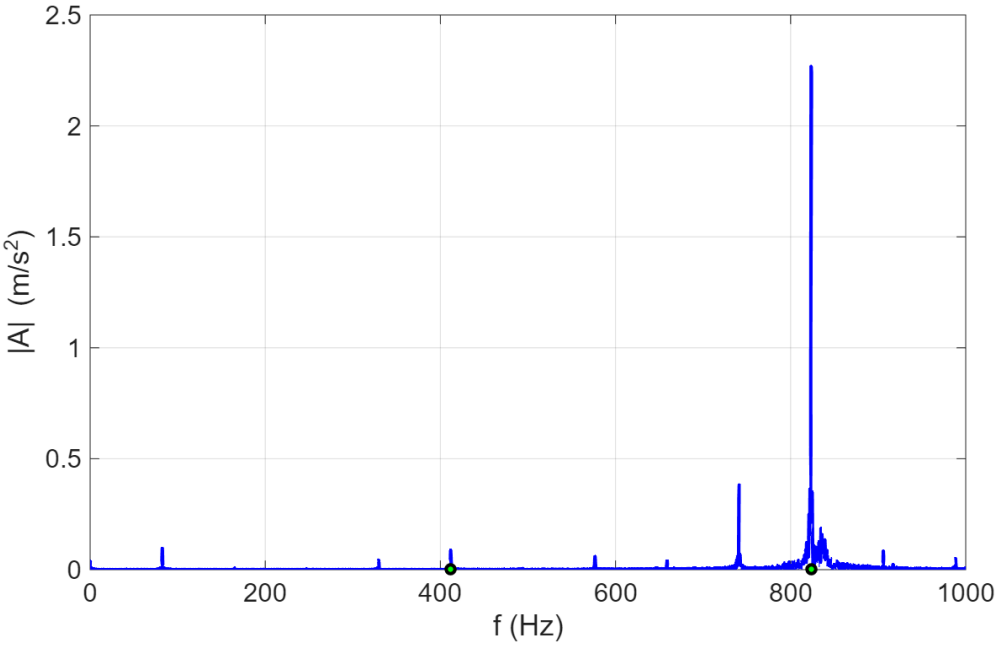


Figure 4.186: Magnitude plot of *a* frequency content for 150 rotations, with f_{tooth} at 412 Hz and its 1st harmonic at 824 Hz (black circles) identified.

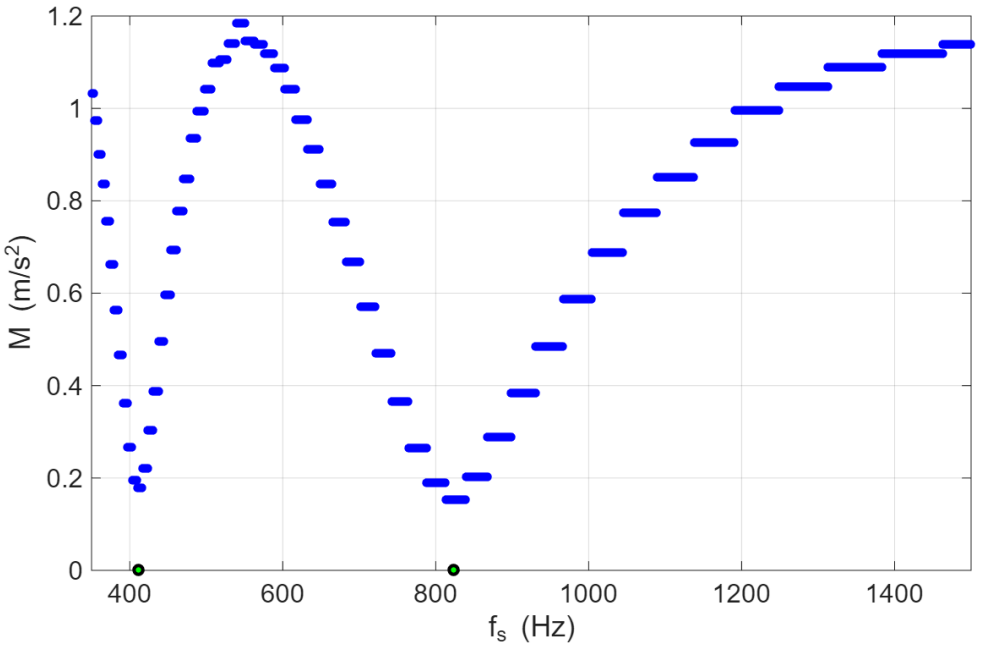


Figure 4.187: Variation in *M* with periodic f_s. Local minima occur at f_{tooth} of 412 Hz (black circle) where M = 0.18 m/s^2 and its first harmonic (black circle) at M = 0.15 m/s^2.

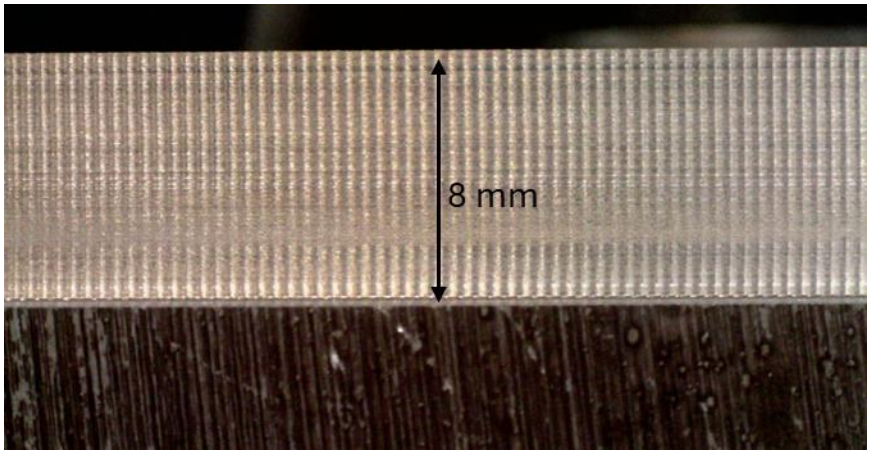


Figure 4.188: Surface of the AISI 1018 steel workpiece with periodic feed marks after the stable cut.

Unstable cut 2: Five-flute endmill on AISI 1018 steel

Results from the microphone sound pressure signal during an unstable experimental cut using a five-flute carbide endmill on AISI 1018 steel are presented below. **Tables 4.35** shows the modal parameters of the workpiece obtained after tap testing. The tool tip modal parameters presented in **Table 4.30** are retained because, unlike the workpiece which experiences a reduction in mass after cutting, the tool remains unchanged from the previous experimental cut upon inspection.

Table 4.34. Profilometer results from six measured locations on the stable cut surface of the AISI 1018 steel workpiece.

Location	Ra (µm)	Rq (µm)	Rz (µm)
1	0.620	0.821	4.016
2	0.771	0.948	4.306
3	0.606	0.796	4.018
4	0.837	1.016	4.633
5	0.828	0.984	4.245
6	0.772	0.940	4.221

Figures 4.189 and **4.190** show the frequency response function and the stability lobe diagram obtained using the modal parameters. A tangential and normal force coefficient of 1742.8 N/mm^2 and 528.4 N/mm^2 respectively for AISI 1018 steel are selected. A radial depth of cut of 2.5 mm is selected, and an unstable point corresponding to a spindle speed of 4700 rpm and an axial depth of cut of 8 mm is selected on the stability lobe diagram, which achieves an unstable cut.

Because a local minimum does not occur at the tooth passing frequency, f_{tooth}, the algorithm categorizes the cut as unstable, it then uses FFT to determine the chatter frequency, f_c, and recommends new spindle speeds. A spindle speed of 4998 rpm is selected from the recommended list to be used in achieving a stable cut. **Figures 4.191** shows the total time interval of the cut from the microphone signal. **Figures 4.192** shows the magnified time interval of the cut. **Figures 4.193** shows the magnitude plot of the frequency content from the microphone sound pressure signal. It is observed that the chatter frequency, f_c, has the highest peak in the magnitude plot, indicating an unstable cut. **Figures 4.194** shows the variation in the M value with the periodic sampling frequency of the time domain milling signal from the microphone. It is observed that a local minimum in the stability metric occurs at the chatter frequency, f_c, not at the tooth passing frequency, f_{tooth}, thereby indicating an unstable cut.

Table 4.35. Workpiece modal parameters of the AISI 1018 steel before the unstable cut.

***x*-direction**		
Frequency, f_n (Hz)	**Stiffness, k (N/m)**	**Damping ratio, ζ (-)**
842	8.14×10^7	0.0091
***y*-direction**		
Frequency, f_n (Hz)	**Stiffness, k (N/m)**	**Damping ratio, ζ (-)**
203	7.95×10^8	0.0620
808	2.75×10^9	0.0455
1285	6.92×10^9	0.0231
2020	1.32×10^{10}	0.0098
2419	4.58×10^9	0.0192
3189	9.51×10^8	0.0312
3458	1.39×10^9	0.0075
5358	8.71×10^9	0.0114
6314	4.96×10^9	0.0071
8276	1.61×10^9	0.0651
17865	4.49×10^{10}	0.0009

Figure 4.195 shows the surface of the workpiece with visible chatter marks after the unstable cut, captured using the Dino-Lite digital microscope. Surface roughness measurements were conducted at six different locations on the cut surface using the Mitutoyo profilometer, yielding a mean Ra value of 1.50 µm with a standard deviation of 0.515 µm, a mean Rq value of 1.78 µm with a standard deviation of 0.580 µm, and a mean Rz value of 7.12 µm with a standard deviation of 1.861 µm. **Table 4.36** shows the Ra, Rq, and Rz values for the six measured locations.

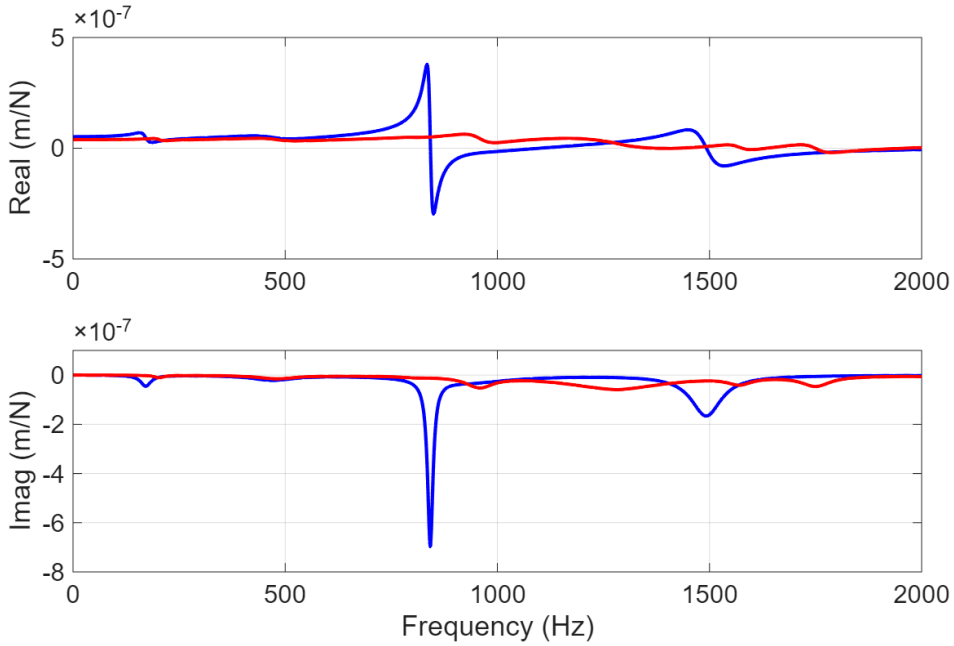


Figure 4.189: Frequency response function of the tool tip and workpiece, *x* (blue lines) and *y* (red lines) directions.

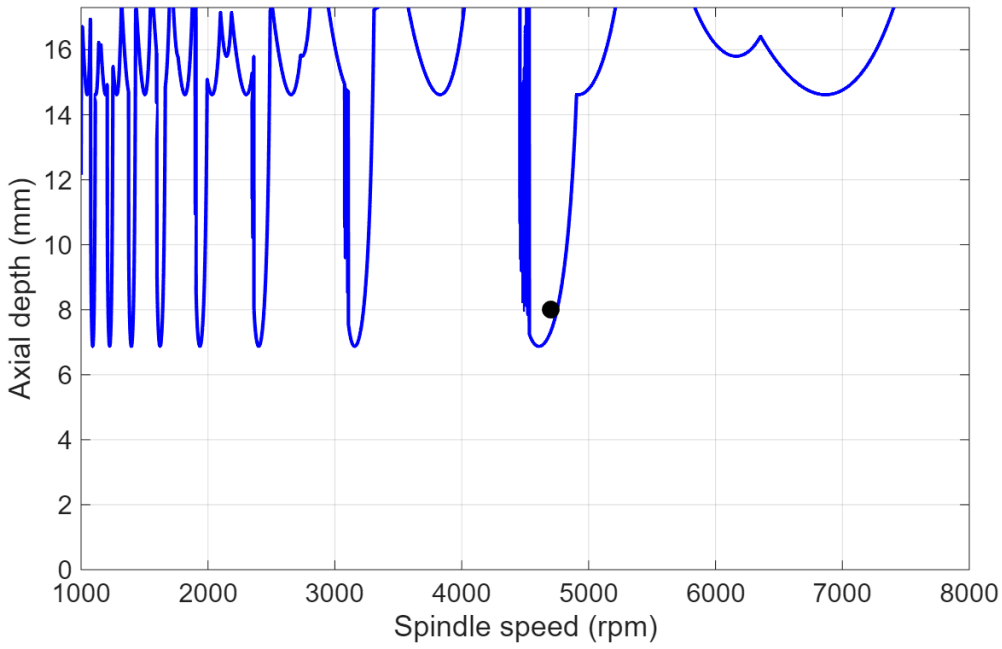


Figure 4.190: Stability lobe diagram with the selected unstable point (black dot) corresponding to a spindle speed of 4700 rpm and axial depth of cut of 8 mm.

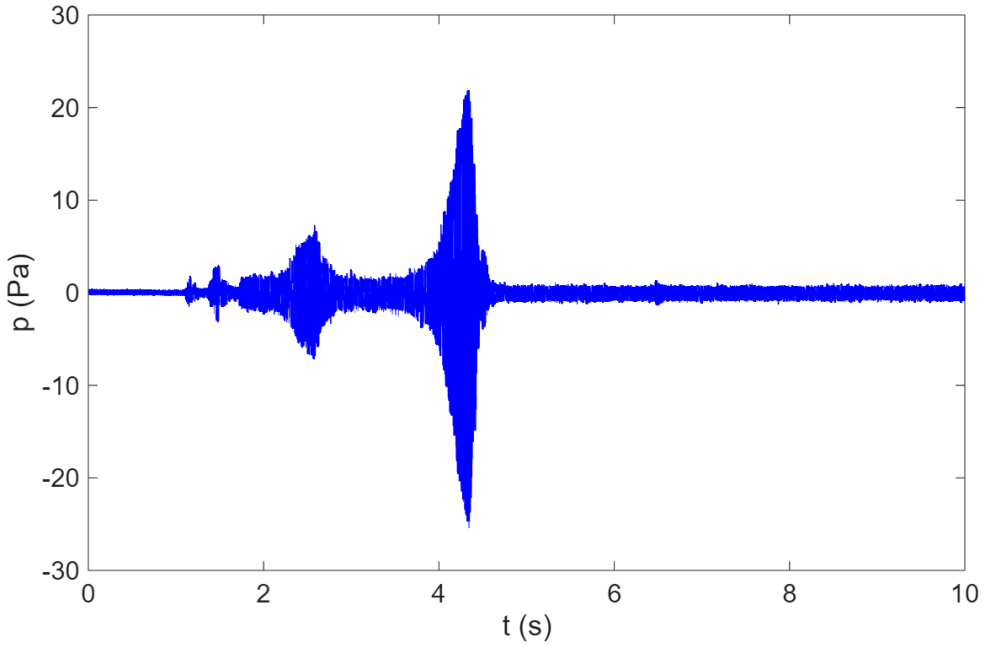


Figure 4.191: The total time interval of the signal from the microphone (sound pressure signal) showing when the tool interacts with the workpiece.

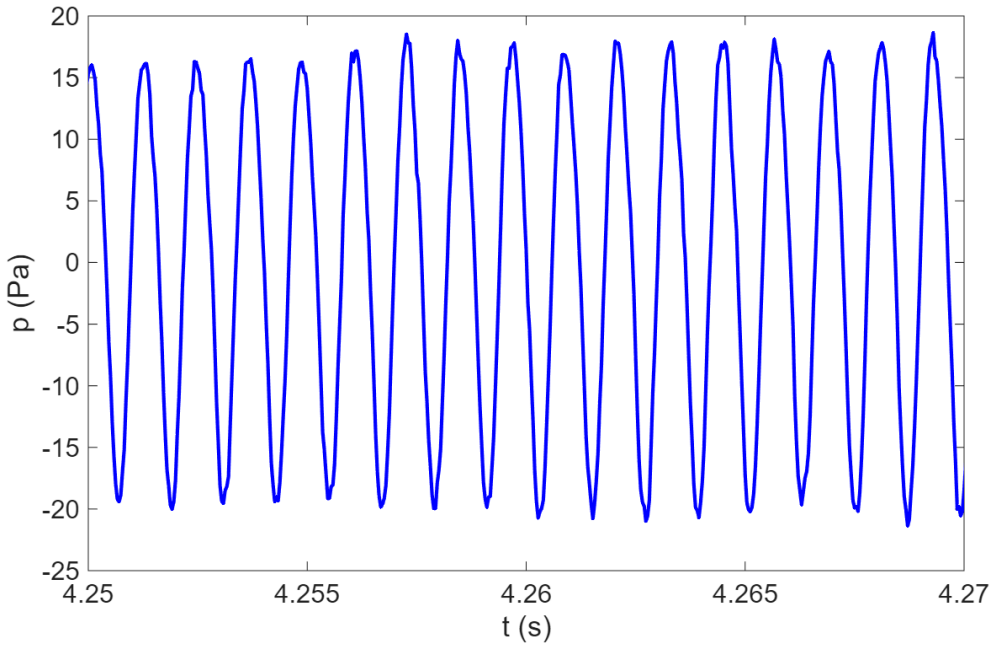


Figure 4.192: The magnified time interval of the signal from the microphone (sound pressure signal).

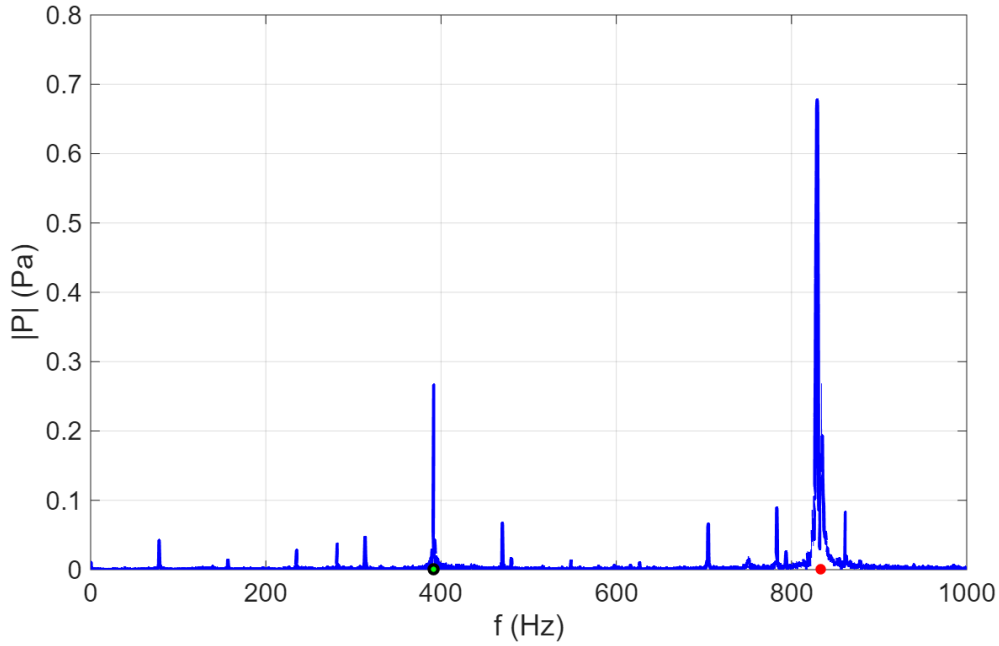


Figure 4.193: Magnitude plot of p frequency content for 150 rotations, identifying f_c (red dot) at 833 Hz, and f_{tooth} (black circle) at 392 Hz.

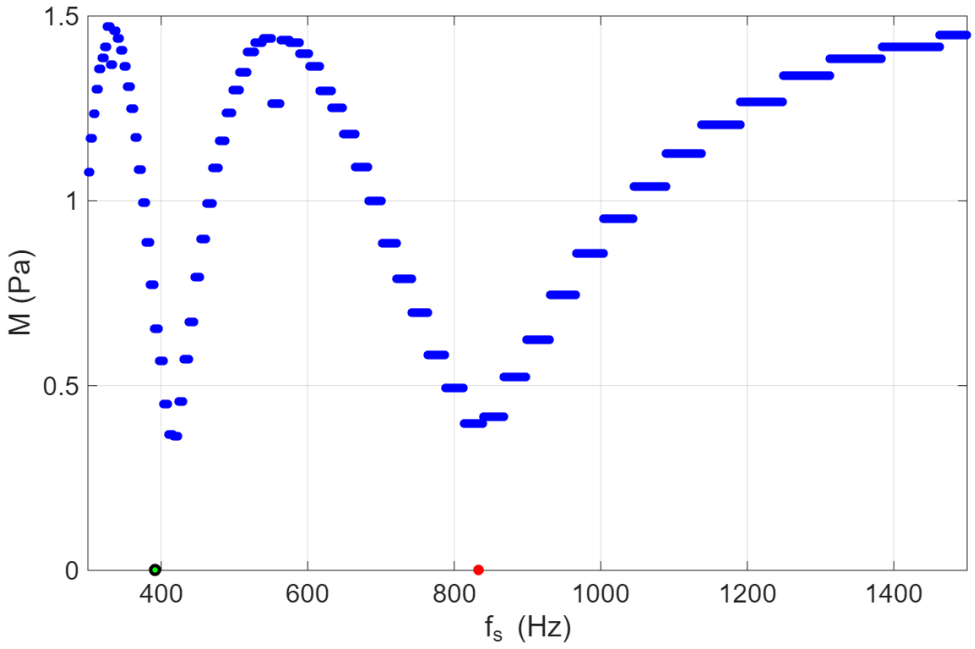


Figure 4.194: Variation in M value with periodic f_s. A local minimum occurs at f_c of 833 Hz (red dot) where M = 0.40 Pa, not at f_{tooth} (black circle).

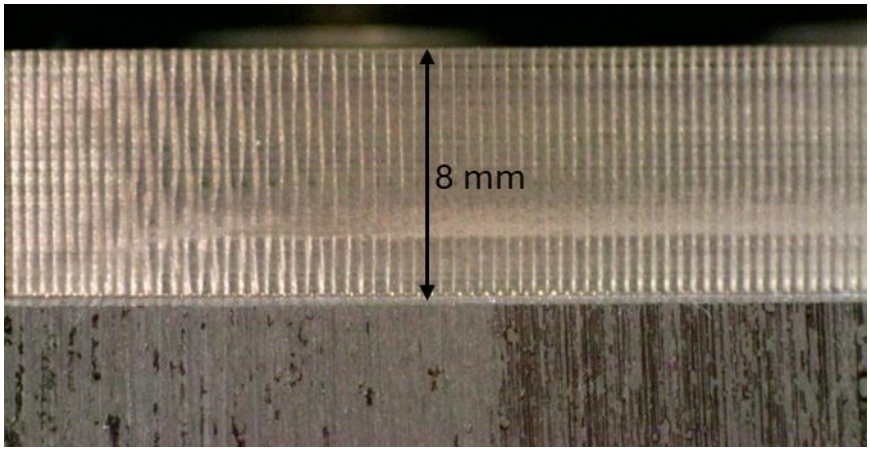


Figure 4.195: Surface of the AISI 1018 steel workpiece with visible chatter marks after the unstable cut.

Stable cut 2: Five-flute endmill on AISI 1018 steel

Results from the microphone sound pressure signal during the resulting stable experimental cut using a five-flute carbide endmill on AISI 1018 steel are presented below. **Tables 4.37** shows the modal parameters of the workpiece obtained after tap testing. The tool tip modal parameters presented in **Table 4.30** are retained because, unlike the workpiece which experiences a reduction in mass after cutting, the tool remains unchanged from the previous experimental cut upon inspection.

Table 4.36. Profilometer results from six measured locations on the unstable cut surface of the AISI 1018 steel workpiece.

Location	Ra (μm)	Rq (μm)	Rz (μm)
1	1.183	1.388	5.557
2	1.393	1.635	6.242
3	1.074	1.337	6.063
4	2.197	2.547	8.930
5	2.094	2.483	9.991
6	1.061	1.301	5.909

Figures 4.196 and **4.197** show the frequency response function and the stability lobe diagram obtained using the modal parameters. The tangential and normal force coefficients of 1742.8 N/mm^2 and 528.4 N/mm^2 respectively are retained, as well as the radial depth of cut of 2.5 mm. A stable point corresponding to the new spindle speed of 4998 rpm recommended by the algorithm and the retained axial depth of cut of 8 mm is selected on the stability lobe diagram, which achieves a stable cut. Because a local minimum occurs at the tooth passing frequency, f_{tooth}, the algorithm categorizes the cut as stable. **Figures 4.198** shows the total time interval of the cut from the microphone signal. **Figures 4.199** shows the magnified time interval of the cut. **Figures 4.200** shows the magnitude plot of the frequency content from the microphone sound pressure signal. It is observed that the 1st harmonic of the tooth passing frequency, f_{tooth}, has the highest peak in the magnitude plot, indicating a stable cut. **Figures 4.201** shows the variation in the *M* value with the periodic sampling frequency of the time domain milling signal from the microphone. It is observed that local minima in the stability metric occur at the tooth passing frequency, f_{tooth}, and its harmonic indicating a stable cut.

Figure 4.202 shows the surface of the workpiece with periodic feed marks after the cut, indicating the tool tooth trajectory. Surface roughness measurements were conducted at six different locations on the cut surface using the Mitutoyo profilometer, yielding a mean Ra value of 0.94 µm with a standard deviation of 0.085 µm, a mean Rq value of 1.13 µm with a standard deviation of 0.101 µm, and a mean Rz value of 4.94 µm with a standard deviation of 0.723 µm. **Table 4.38** shows the Ra, Rq, and Rz values for the six measured locations.

Table 4.37. Workpiece modal parameters of the AISI 1018 steel before the stable cut.

***x*-direction**		
Frequency, f_n (Hz)	**Stiffness, k (N/m)**	**Damping ratio, ζ (-)**
844	7.94×10^7	0.0090
***y*-direction**		
Frequency, f_n (Hz)	**Stiffness, k (N/m)**	**Damping ratio, ζ (-)**
205	7.91×10^8	0.0693
811	3.04×10^9	0.0483
1284	7.60×10^9	0.0207
2422	4.79×10^9	0.0195
3192	9.54×10^8	0.0304
3467	1.42×10^9	0.0070
5370	8.29×10^9	0.0113
6322	4.67×10^9	0.0078
8261	3.31×10^9	0.0252
17856	4.41×10^{10}	0.0009

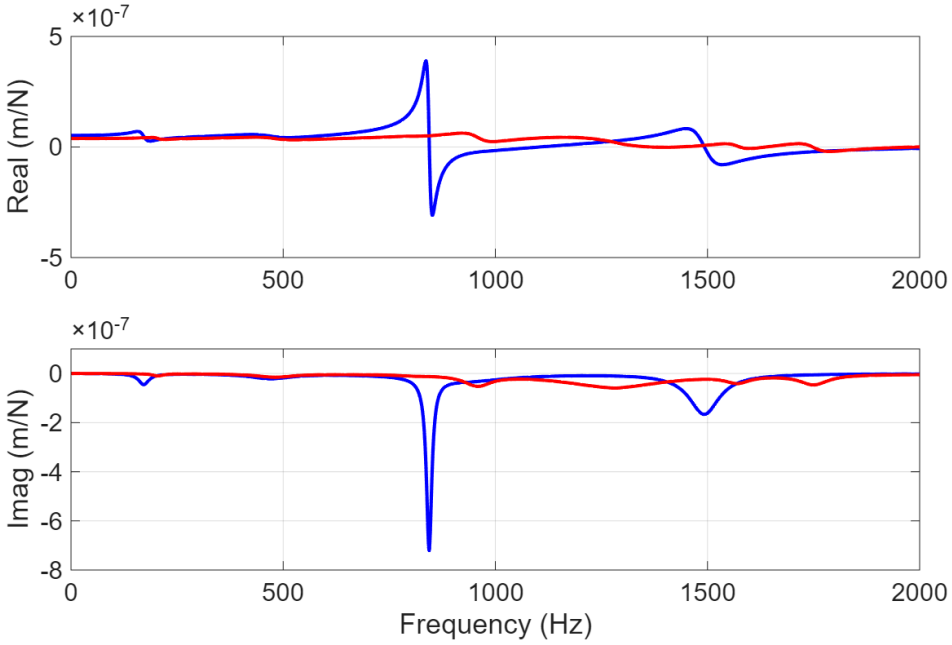


Figure 4.196: Frequency response function of the tool tip and workpiece, *x* (blue lines) and *y* (red lines) directions.

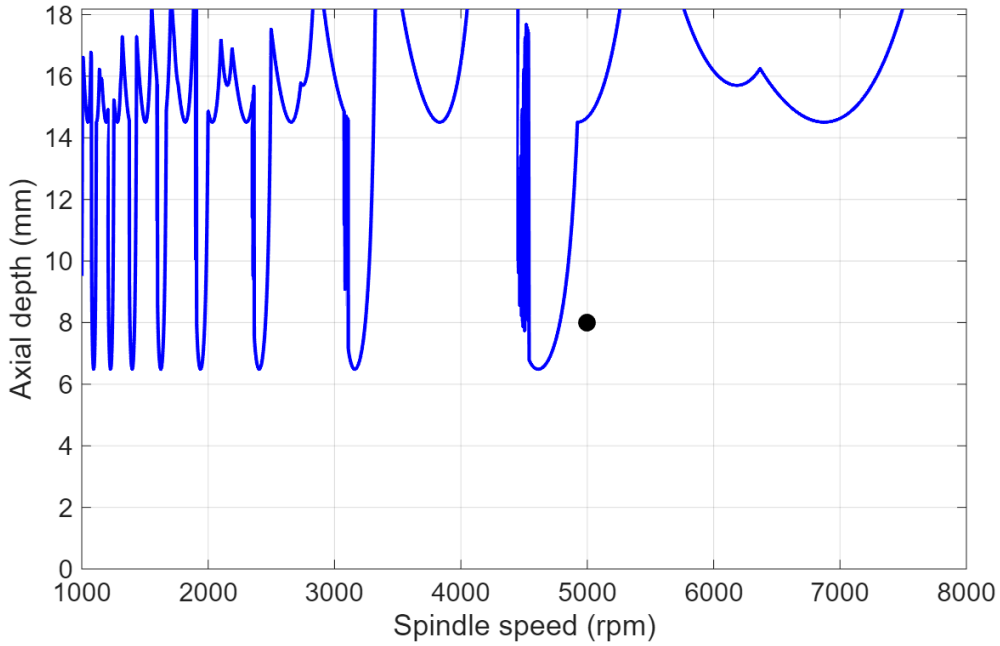


Figure 4.197: Stability lobe diagram with the recommended stable point (black dot) corresponding to a spindle speed of 4998 rpm and axial depth of cut of 8 mm.

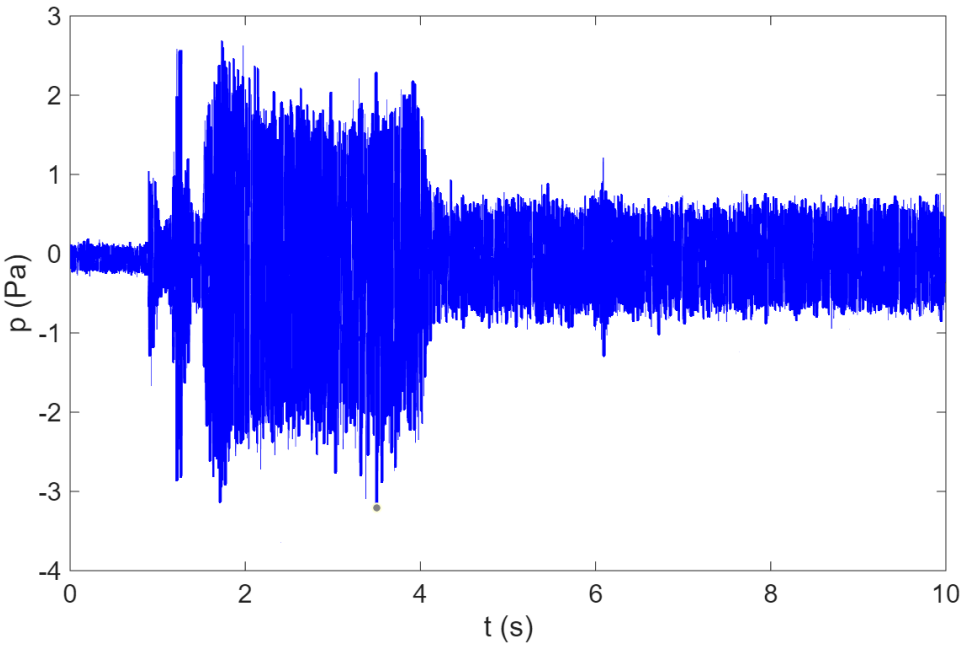


Figure 4.198: The total time interval of the signal from the microphone (sound pressure signal) showing when the tool interacts with the workpiece.

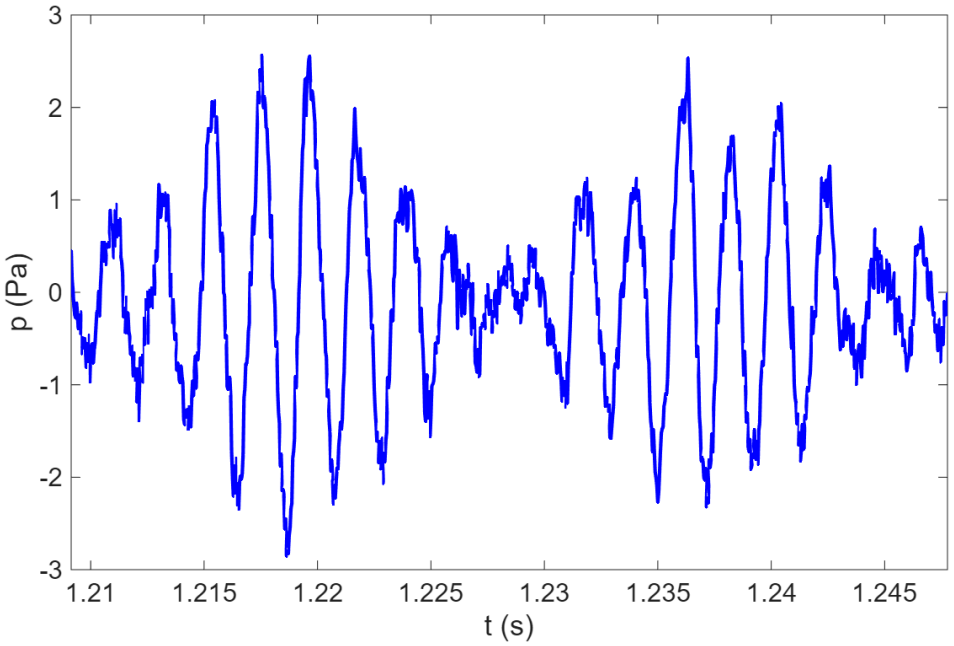


Figure 4.199: The magnified time interval of the signal from the microphone (sound pressure signal).

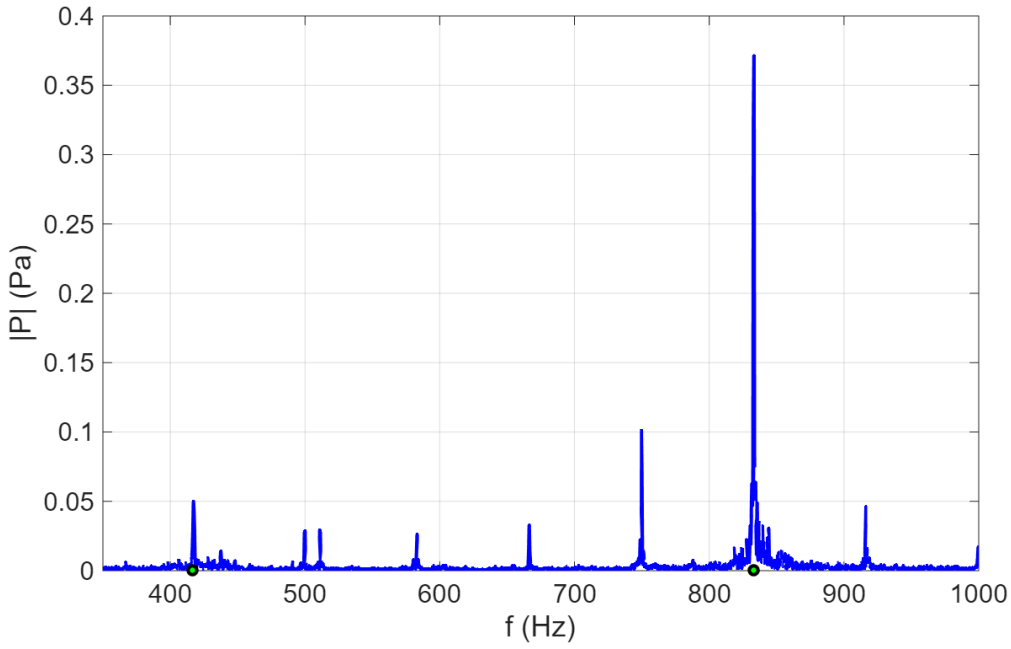


Figure 4.200: Magnitude plot of p frequency content for 150 rotations, with f_{tooth} at 417 Hz and its 1st harmonic at 834 Hz (black circles) identified.

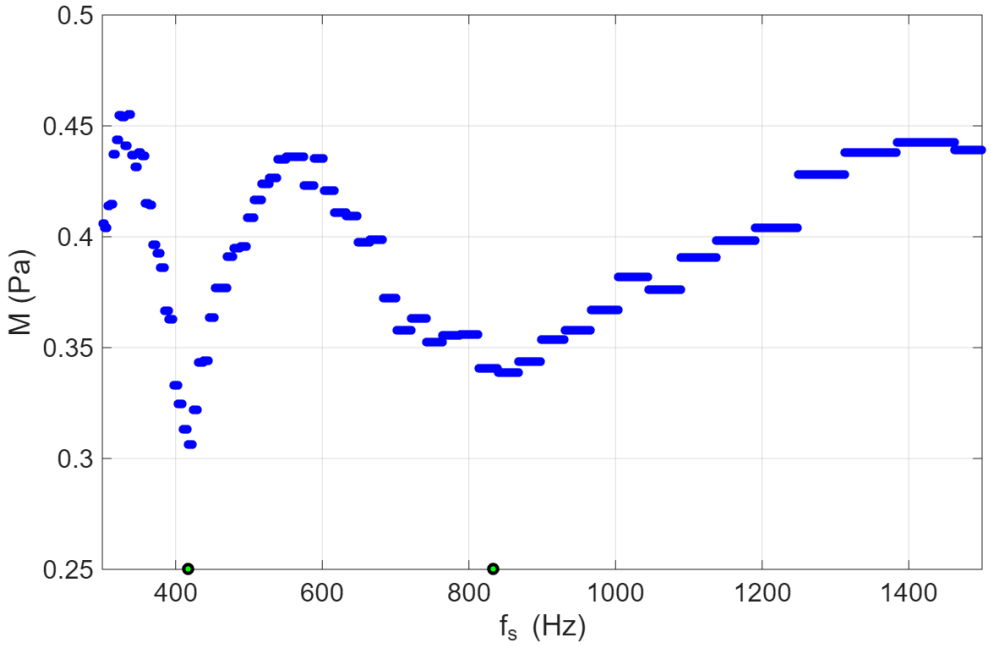


Figure 4.201: Variation in M with periodic f_s. Local minima occur at f_{tooth} of 417 Hz (black circle) where M = 0.31 Pa and its first harmonic (black circle).

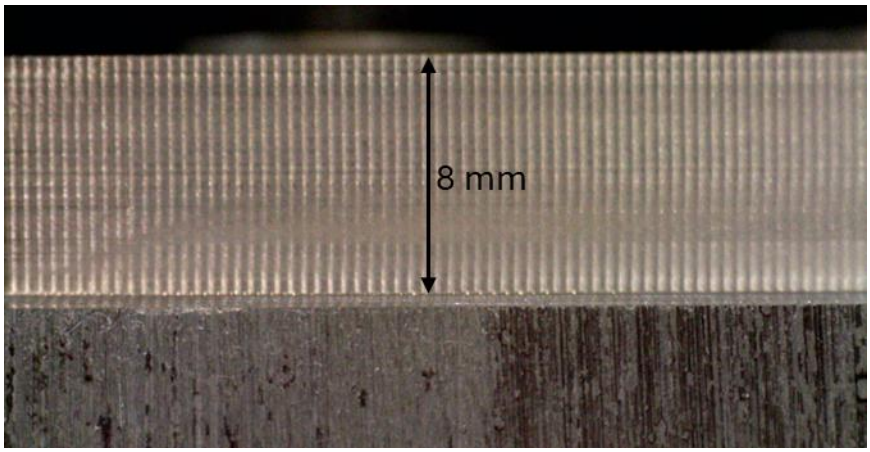


Figure 4.202: Surface of the AISI 1018 steel workpiece with periodic feed marks after the stable cut.

Unstable cut 3: Five-flute endmill on AISI 1018 steel

Results from the acceleration signal during an unstable experimental cut using a five-flute carbide endmill on AISI 1018 steel are presented below. **Tables 4.39** shows the modal parameters of the workpiece obtained after tap testing. The tool tip modal parameters presented in **Table 4.30** are retained because, unlike the workpiece which experiences a reduction in mass after cutting, the tool remains unchanged from the previous experimental cut upon inspection. **Figures 4.203** and **4.204** show the frequency response function and the stability lobe diagram obtained using the modal parameters. A tangential and normal force coefficient of 1742.8 N/mm^2 and 528.4 N/mm^2 respectively for AISI 1018 steel are selected. A radial depth of cut of 3 mm is selected, and an unstable point corresponding to a spindle speed of 4780 rpm and an axial depth of cut of 8 mm is selected on the stability lobe diagram, which achieves an unstable cut.

Because a local minimum does not occur at the tooth passing frequency, f_{tooth}, the algorithm categorizes the cut as unstable, it then uses FFT to determine the exact chatter frequency, f_c, and recommends new spindle speeds.

Table 4.38. Profilometer results from six measured locations on the stable cut surface of the AISI 1018 steel.

Location	Ra (µm)	Rq (µm)	Rz (µm)
1	1.017	1.219	5.267
2	0.979	1.204	6.133
3	0.807	0.979	4.036
4	1.023	1.214	4.898
5	0.918	1.089	4.903
6	0.881	1.052	4.428

A spindle speed of 5027 rpm is selected from the recommended list to be used in achieving a stable cut. **Figures 4.205** shows the total time interval of the cut from the acceleration signal. **Figures 4.206** shows the magnified time interval of the cut. **Figures 4.207** shows the magnitude plot of the frequency content from the accelerometer. It is observed that the chatter frequency, f_c, has the highest peak in the magnitude plot, indicating an unstable cut. **Figures 4.208** shows the variation in the *M* value with the periodic sampling frequency of the time domain milling signal from the accelerometer. It is observed that a local minimum in the stability metric occurs at the chatter frequency, f_c, not at the tooth passing frequency, f_{tooth}, thereby indicating an unstable cut.

Figure 4.209 shows the surface of the workpiece with visible chatter marks after the unstable cut, captured using the Dino-Lite digital microscope. Surface roughness measurements were conducted at six different locations on the cut surface using the Mitutoyo profilometer, yielding a mean Ra value of 1.25 µm with a standard deviation of 0.142 µm, a mean Rq value of 1.49 µm with a standard deviation of 0.158 µm, and a mean Rz value of 6.25 µm with a standard deviation of 0.533 µm. **Table 4.40** shows the Ra, Rq, and Rz values for the six measured locations.

Table 4.39. Workpiece modal parameters of the AISI 1018 steel before the unstable cut.

***x*-direction**		
Frequency, f_n (Hz)	**Stiffness, *k* (N/m)**	**Damping ratio, ζ (-)**
851	6.91×10^7	0.0098
***y*-direction**		
Frequency, f_n (Hz)	**Stiffness, *k* (N/m)**	**Damping ratio, ζ (-)**
203	8.06×10^8	0.0649
819	2.88×10^9	0.0498
2428	4.69×10^9	0.0247

Table 4.39. continued: Workpiece modal parameters of the AISI 1018 steel before the unstable cut.

Frequency, f_n (Hz)	Stiffness, k (N/m)	Damping ratio, ζ (-)
3252	4.75×10^9	0.0126
3484	1.96×10^9	0.0075
3642	6.38×10^9	0.0044
6375	1.27×10^{10}	0.0080
11136	1.33×10^{10}	0.0086
17558	6.99×10^{10}	0.0025

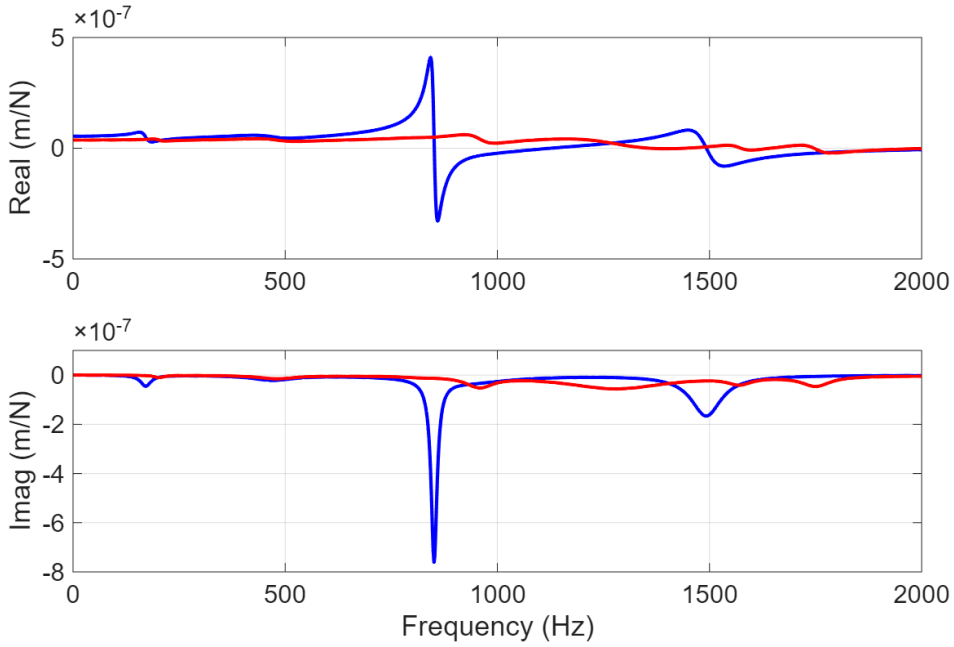


Figure 4.203: Frequency response function of the tool tip and workpiece, *x* (blue lines) and *y* (red lines) directions.

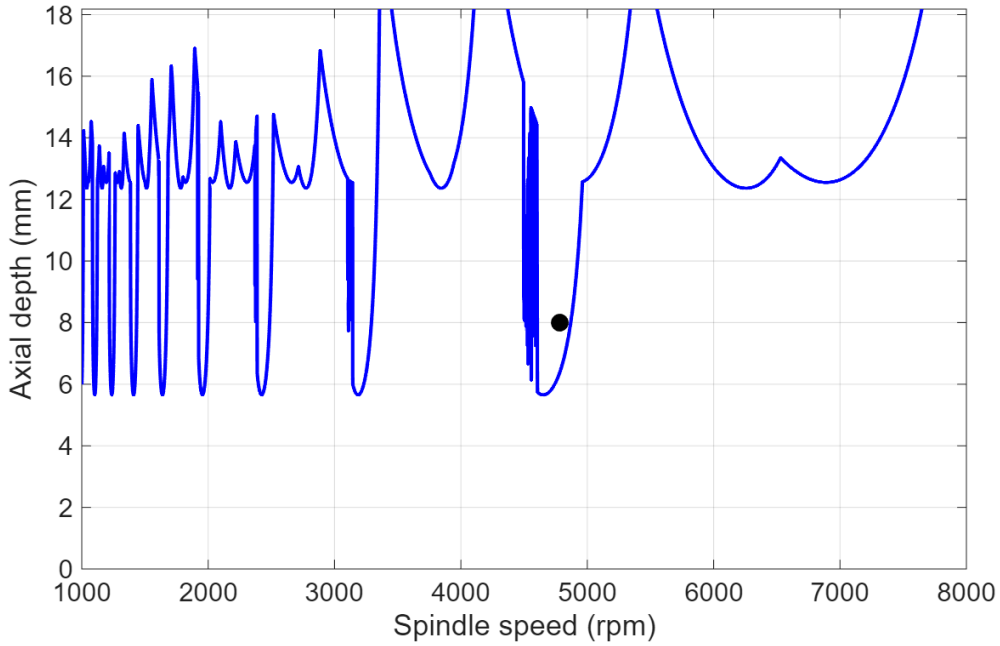


Figure 4.204: Stability lobe diagram with the selected unstable point (black dot) corresponding to a spindle speed of 4780 rpm and axial depth of cut of 8 mm.

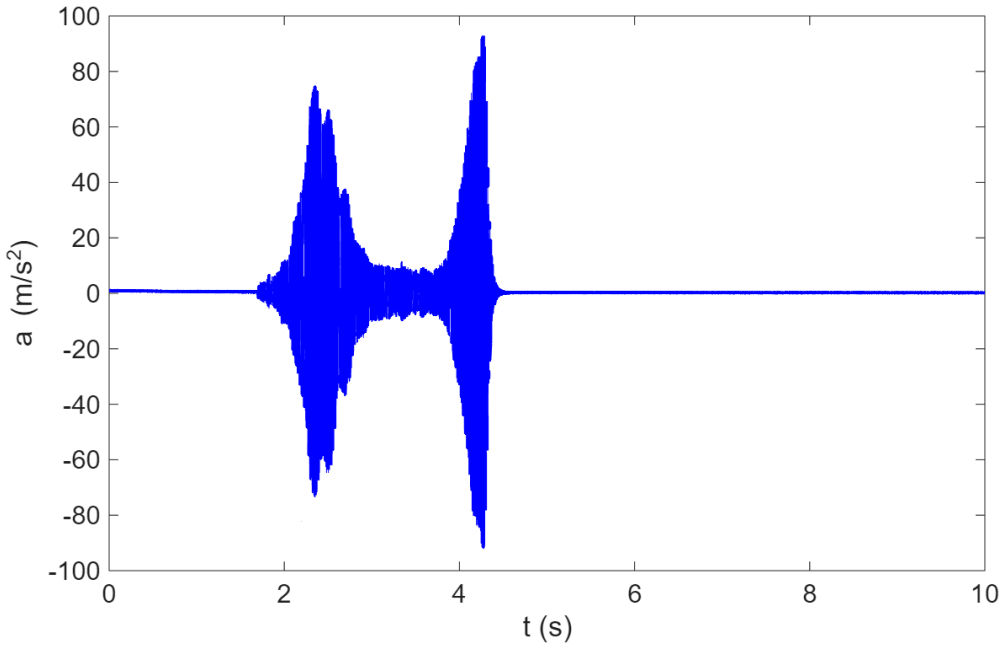


Figure 4.205: The total time interval of the signal from the accelerometer (acceleration signal) showing when the tool interacts with the workpiece.

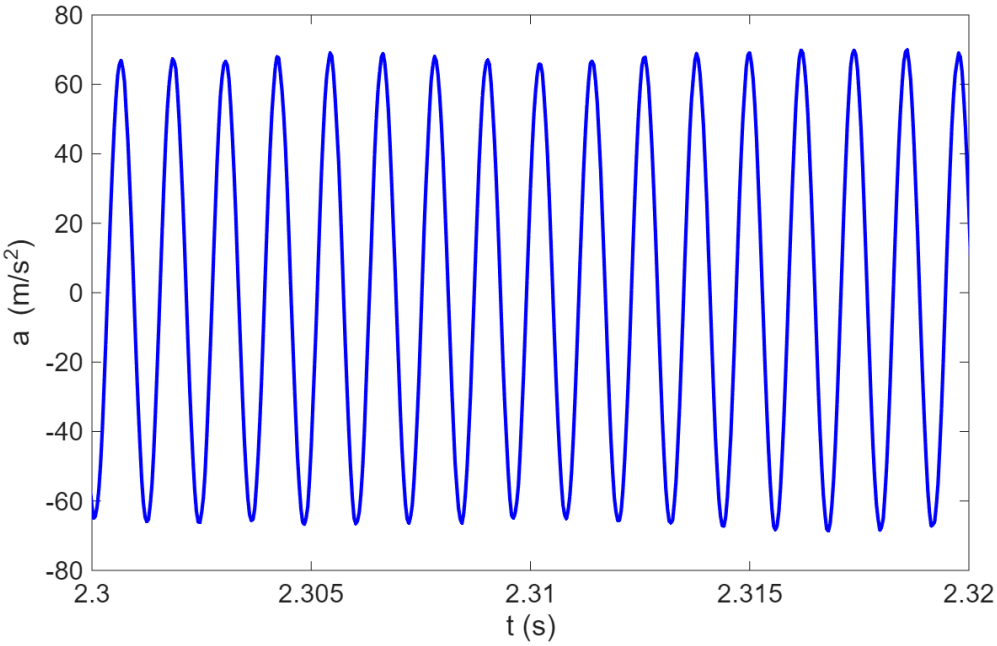


Figure 4.206: The magnified time interval of the signal from the accelerometer (acceleration signal).

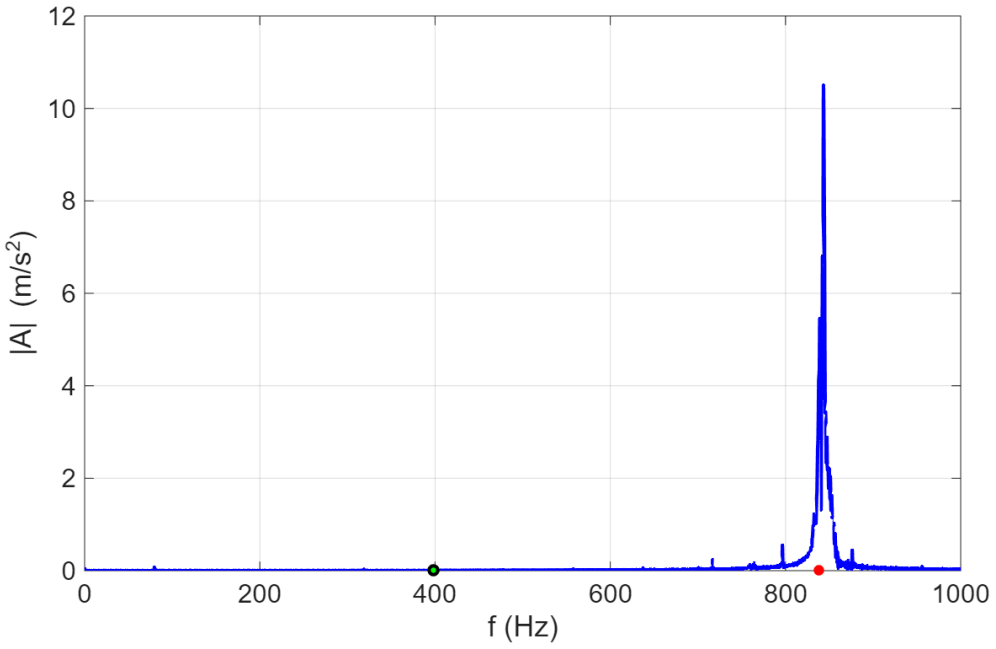


Figure 4.207: Magnitude plot of *a* frequency content for 150 rotations, identifying f_c (red dot) at 838 Hz, and f_{tooth} (black circle) at 398 Hz with its 1st harmonic (black circle).

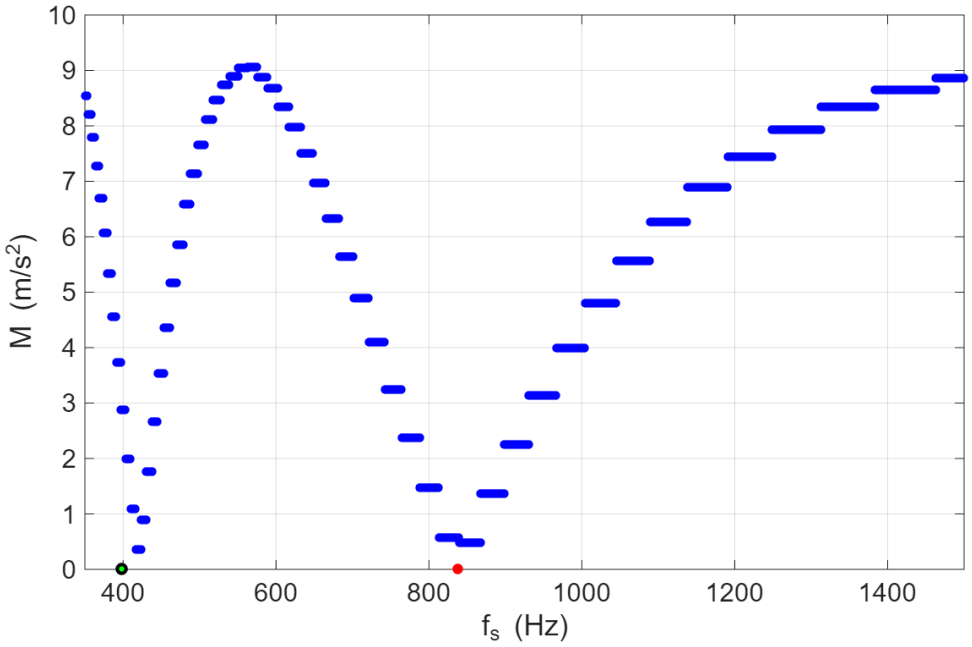


Figure 4.208: Variation in M value with periodic f_s. A local minimum occurs at f_c of 838 Hz (red dot) where M = 0.57 m/s^2, not at f_{tooth} (black circle).

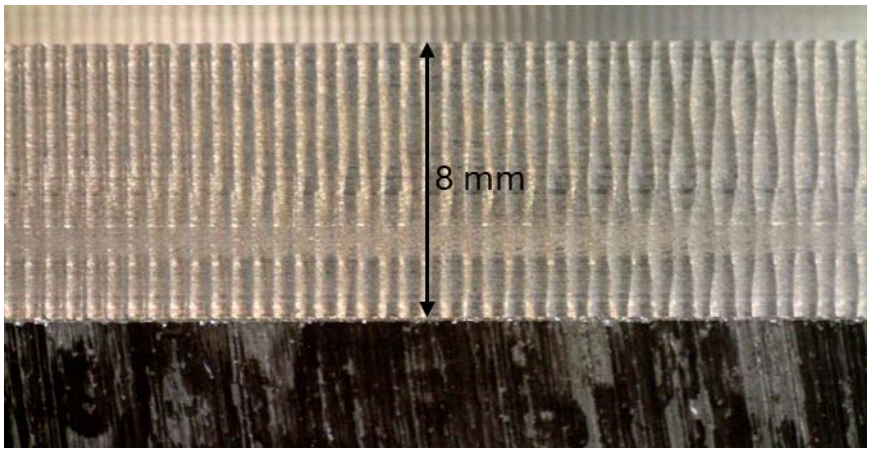


Figure 4.209: Surface of the AISI 1018 steel workpiece with visible chatter marks after the unstable cut.

Stable cut 3: Five-flute endmill on AISI 1018 steel

Results from the acceleration signal during the stable experimental cut using a five-flute carbide endmill on AISI 1018 steel are presented below. **Tables 4.41** shows the modal parameters of the workpiece obtained after tap testing. The tool tip modal parameters presented in **Table 4.30** are retained because, unlike the workpiece which experiences a reduction in mass after cutting, the tool remains unchanged from the previous experimental cut upon inspection. **Figures 4.210** and **4.211** show the frequency response function and the stability lobe diagram obtained using the modal parameters. The tangential and normal force coefficients of 1742.8 N/mm^2 and 528.4 N/mm^2 respectively are retained, as well as the radial depth of cut of 3 mm. A stable point corresponding to the new spindle speed of 5027 rpm recommended by the algorithm and the retained axial depth of cut of 8 mm is selected on the stability lobe diagram, which achieves a stable cut.

Table 4.40. Profilometer results from six measured locations on the unstable cut surface of the AISI 1018 steel.

Location	Ra (µm)	Rq (µm)	Rz (µm)
1	1.150	1.354	6.024
2	1.500	1.780	7.033
3	1.346	1.564	6.214
4	1.139	1.380	5.440
5	1.195	1.437	6.563
6	1.190	1.442	6.234

Because a local minimum occurs at the tooth passing frequency, f_{tooth}, the algorithm categorizes the cut as stable. **Figures 4.212** shows the total time interval of the cut from the acceleration signal. **Figures 4.213** shows the magnified time interval of the cut. **Figures 4.214** shows the magnitude plot of the frequency content from the accelerometer. It is observed that the tooth passing frequency, f_{tooth}, has the highest peak in the magnitude plot, indicating a stable cut. **Figures 4.215** shows the variation in the *M* value with the periodic sampling frequency of the time domain milling signal from the accelerometer. It is observed that a local minimum in the stability metric occurs at the tooth passing frequency, f_{tooth}, indicating a stable cut.

Figure 4.216 shows the surface of the workpiece with periodic feed marks after the cut, indicating the tool tooth trajectory. Surface roughness measurements were conducted at six different locations on the cut surface using the Mitutoyo profilometer, yielding a mean Ra value of 0.88 µm with a standard deviation of 0.128 µm, a mean Rq value of 1.06 µm with a standard deviation of 0.142 µm, and a mean Rz value of 4.56 µm with a standard deviation of 0.492 µm. **Table 4.42** shows the Ra, Rq, and Rz values for the six measured locations.

Table 4.41. Workpiece modal parameters of the AISI 1018 steel before the stable cut.

***x*-direction**		
Frequency, f_n (Hz)	**Stiffness, *k* (N/m)**	**Damping ratio, ζ (-)**
855	6.68×10^7	0.0116
***y*-direction**		
Frequency, f_n (Hz)	**Stiffness, *k* (N/m)**	**Damping ratio, ζ (-)**
203	7.84×10^8	0.0693
811	4.27×10^9	0.0309
2437	5.13×10^9	0.0219

Table 4.41. continued: Workpiece modal parameters of the AISI 1018 steel before the stable cut.

Frequency, f_n (Hz)	Stiffness, k (N/m)	Damping ratio, ζ (-)
3254	3.22×10^9	0.0170
3487	1.71×10^9	0.0079
3644	6.45×10^9	0.0042
5399	1.17×10^{10}	0.0112
6385	8.15×10^9	0.0105
11129	5.49×10^9	0.0248

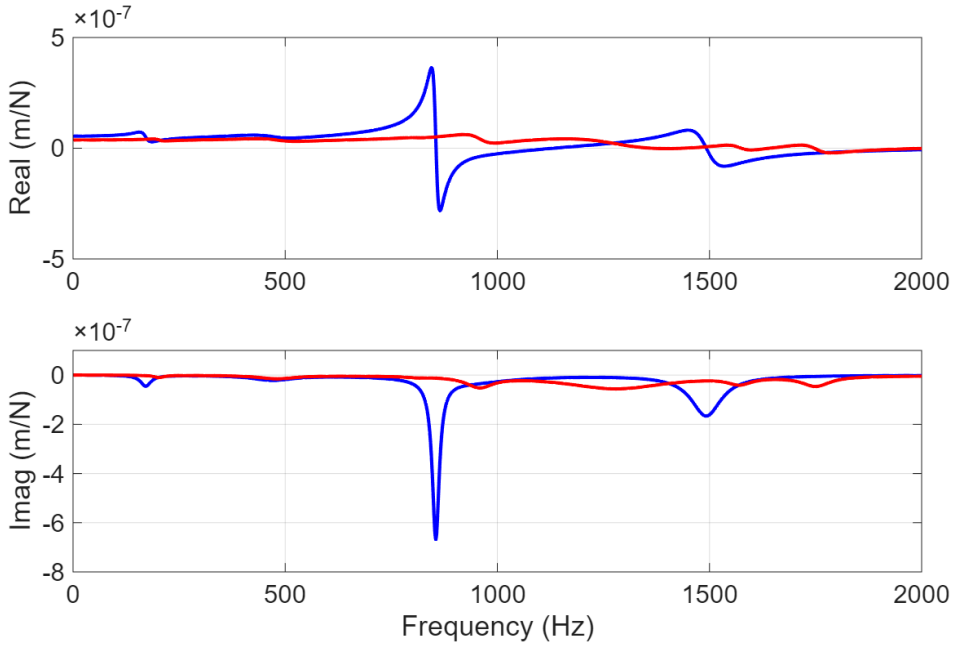


Figure 4.210: Frequency response function of the tool tip and workpiece, *x* (blue lines) and *y* (red lines) directions.

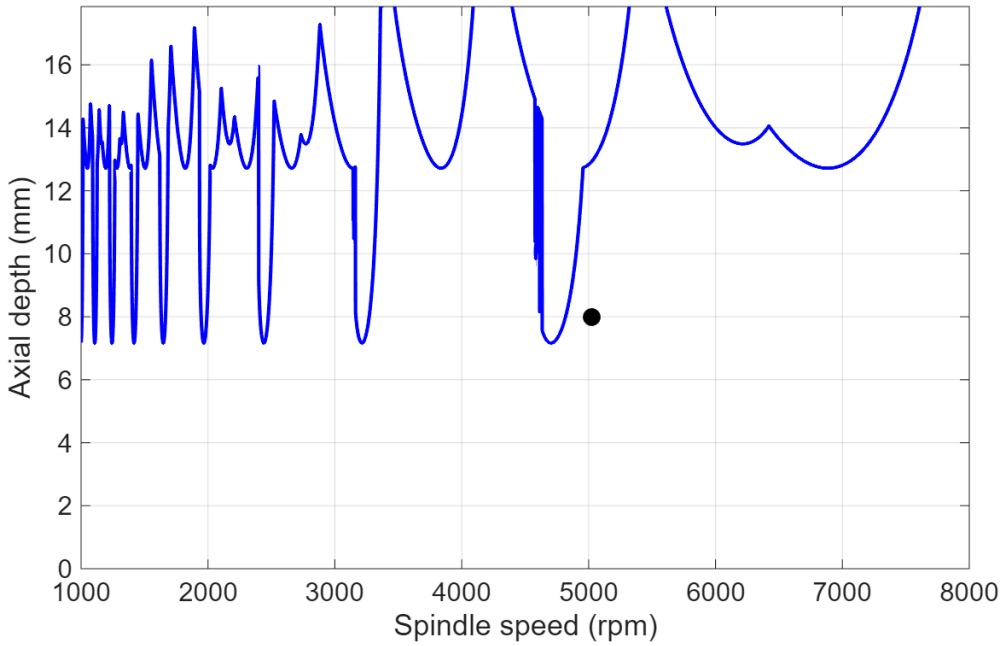


Figure 4.211: Stability lobe diagram with the selected stable point (black dot) corresponding to a spindle speed of 5027 rpm and axial depth of cut of 8 mm.

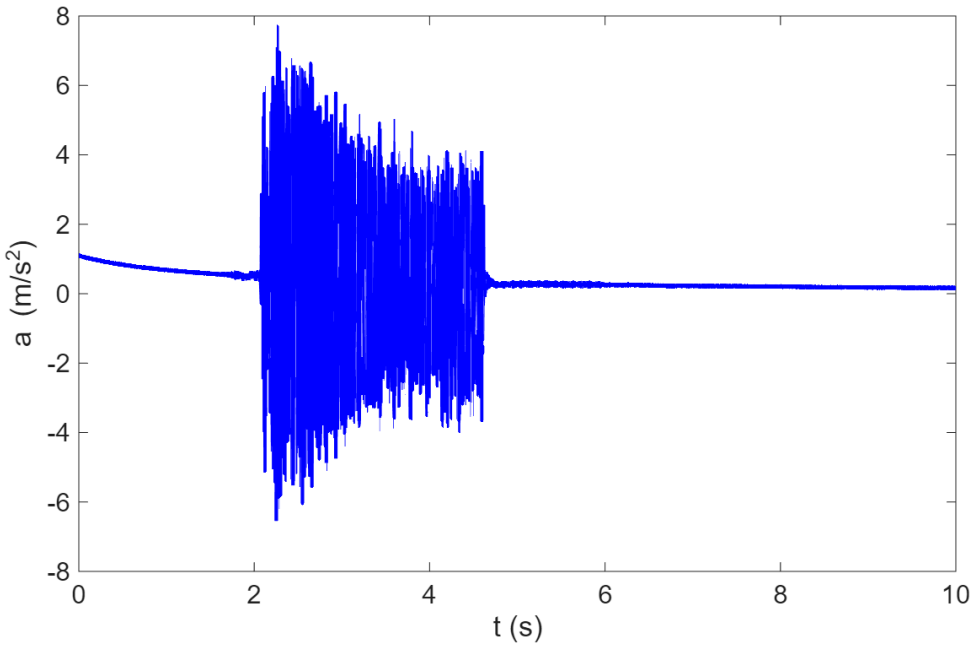


Figure 4.212: The total time interval of the signal from the accelerometer (acceleration signal) showing when the tool interacts with the workpiece.

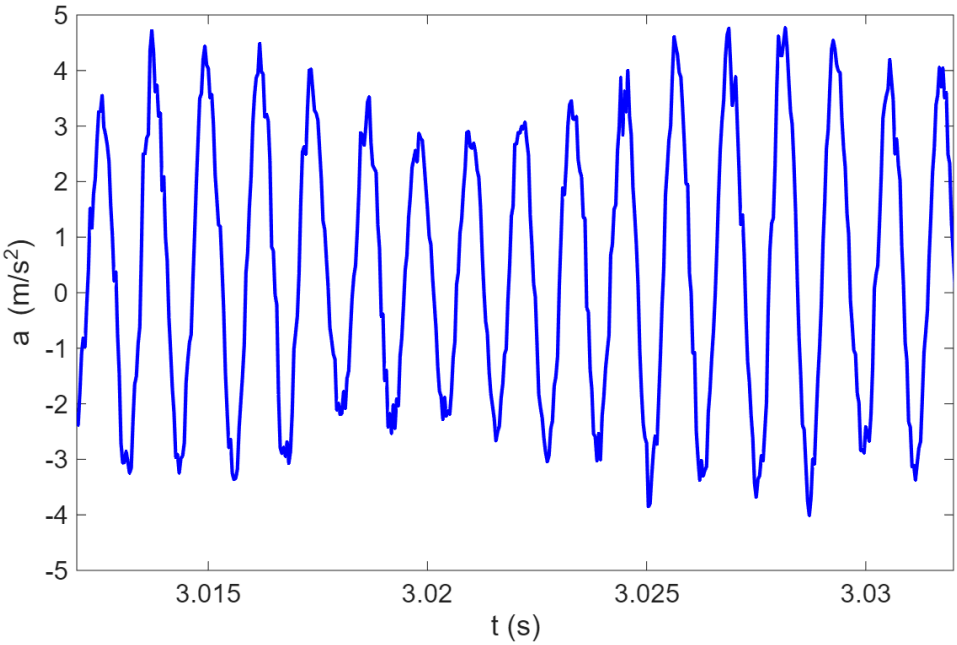


Figure 4.213: The magnified time interval of the signal from the accelerometer (acceleration signal).

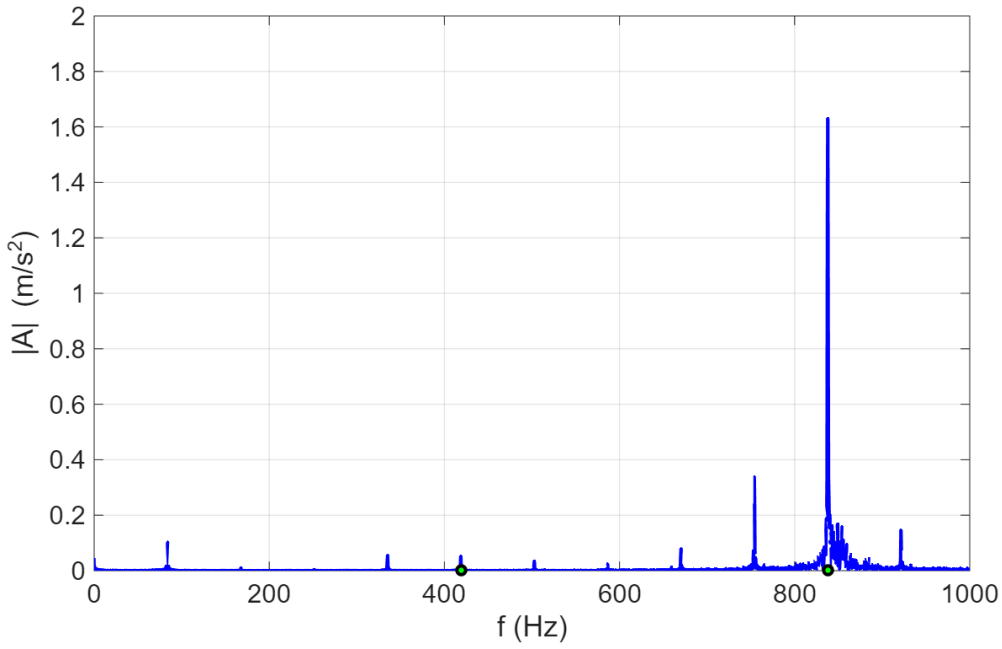


Figure 4.214: Magnitude plot of *a* frequency content for 150 rotations, with f_{tooth} at 419 Hz and its 1st harmonic at 838 Hz (black circles) identified.

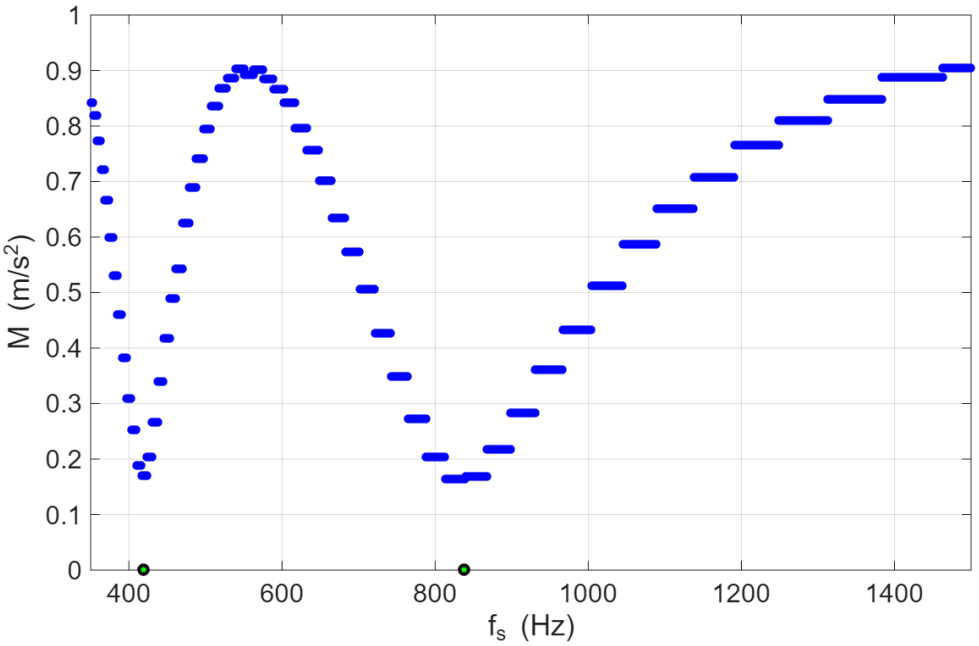


Figure 4.215: Variation in M with periodic f_s. Local minima occur at f_{tooth} of 419 Hz (black circle) where M = 0.17 m/s^2 and its first harmonic.

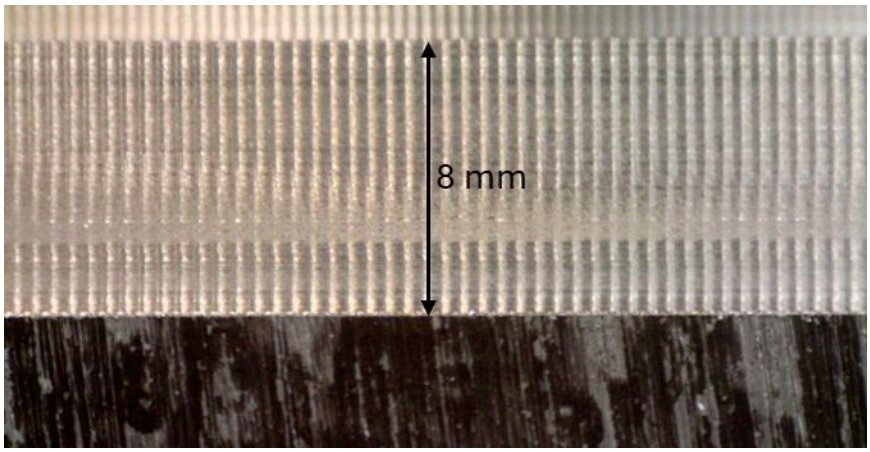


Figure 4.216: Surface of the AISI 1018 steel workpiece with periodic feed marks after the stable cut.

Figures 4.217, **4.218**, and **4.219** show the changes in the minimum and maximum *M* values for the stable, marginal, and unstable cuts from the 2-flute endmill on 6061 aluminum displacement signals, 4-flute endmill on 4140 steel acceleration signals, and 5-flute endmill on 4140 steel sound pressure signals respectively, all from the first experimental phase. This highlights the reduction in the magnitude of the stability metric during stable cutting conditions compared to less stable and unstable conditions.

Table 4.42. Profilometer results from six measured locations on the stable cut surface of the AISI 1018 steel workpiece.

Location	Ra (μm)	Rq (μm)	Rz (μm)
1	0.923	1.077	4.283
2	0.804	0.951	4.028
3	1.080	1.292	5.446
4	0.810	0.957	4.400
5	0.943	1.131	4.726
6	0.719	0.919	4.455

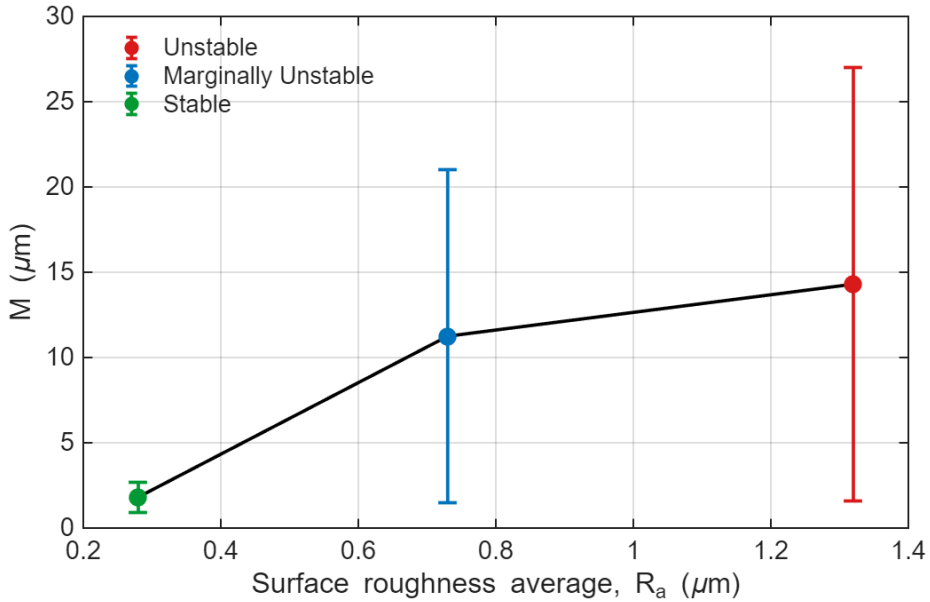


Figure 4.217: Minimum and maximum *M* values for the stable, marginally unstable, and unstable cuts from the 2-flute endmill on 6061 aluminum displacement signals.

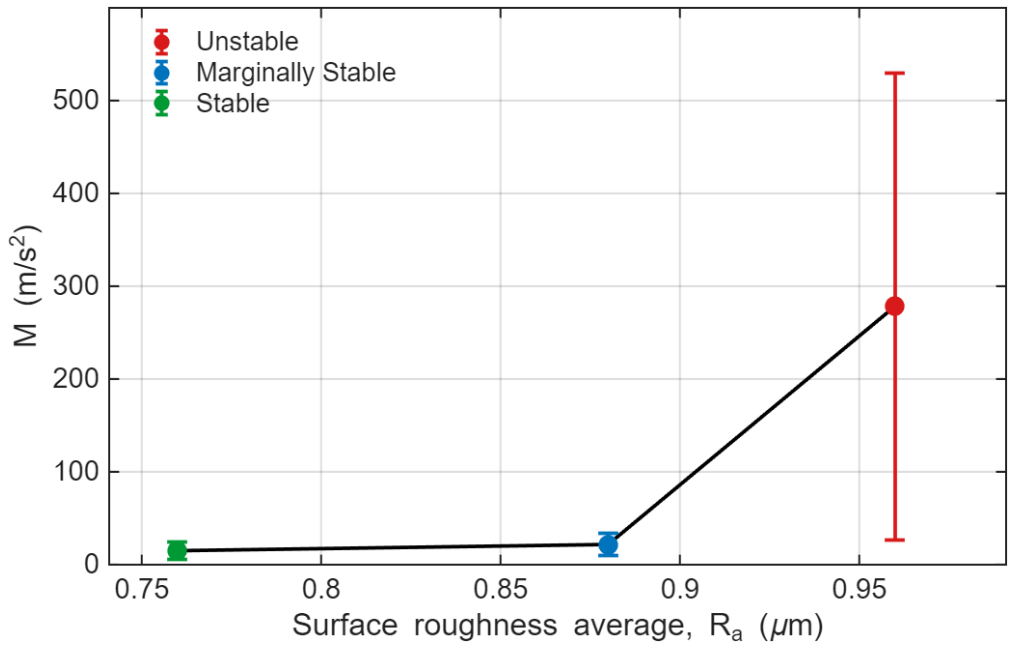


Figure 4.218: Minimum and maximum *M* values for the stable, marginally stable, and unstable cuts from the 4-flute endmill on 4140 steel acceleration signals.

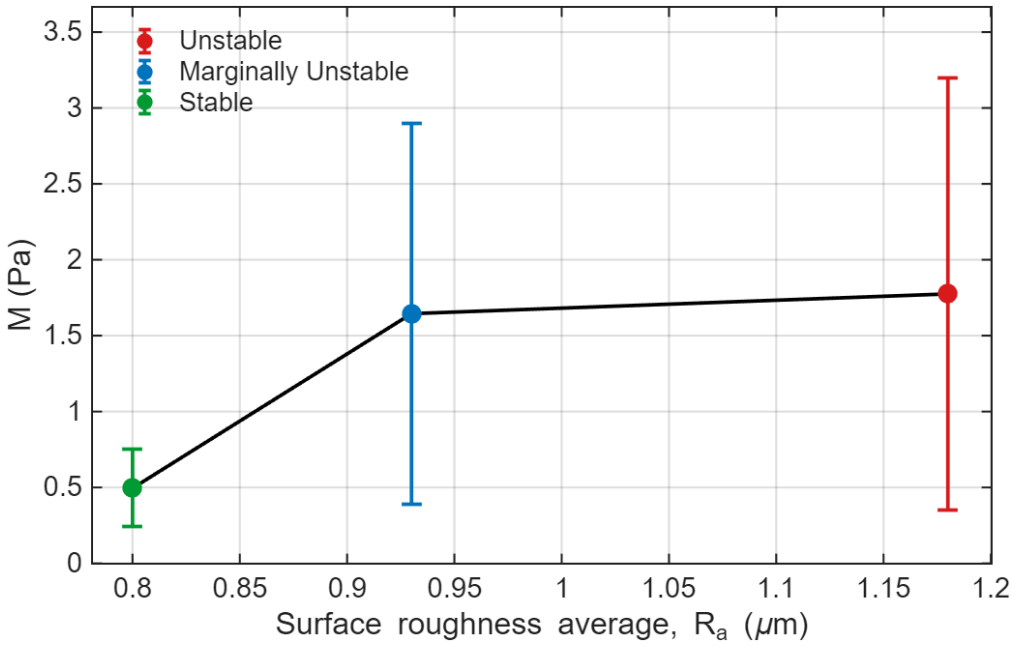


Figure 4.219: Minimum and maximum *M* values for the stable, marginally unstable, and unstable cuts from the 5-flute endmill on 4140 steel sound pressure signals.

CHAPTER FIVE

CONCLUSIONS AND RECOMMENDATIONS FOR FUTURE WORKS

This study presented an experimental evaluation and validation of a novel, in situ method for chatter detection in milling operations by periodic sampling of time domain milling signals. The method operates by scanning a preselected range of periodic sampling frequencies and computing a stability metric for each sampled frequency. The stability metric, *M*, is based on the normalized sum of the absolute value of the differences between adjacent samples for each sampling frequency. For stable cutting conditions, a local minimum in the stability metric occurred at the tooth passing frequency, while for unstable cutting conditions, a local minimum in the stability metric occurred at or near the chatter frequency. It was also observed that the value of the stability metric is lower at stable cutting conditions, where only forced vibrations are present, that it is for unstable cutting conditions, where both forced and self-excited vibrations are present. The difference in *M* value magnitude further validates the use of this method for determining the level of severity for unstable cutting conditions or the level of stability for stable cutting conditions in situ.

The method was experimentally validated over three phases of testing using a Haas VF-4 CNC vertical milling machine, three solid carbide endmills with different flute geometries and coatings, and three workpiece materials. Milling signals were acquired using a constrained motion dynamometer (CMD), accelerometers, and a microphone, while surface finish inspections were done using a digital microscope and a profilometer. In the three phases, the plots showing the variation in the *M* value with the sampling

frequency were used to determine whether a cut was stable or unstable, thereby validating the chatter detection approach. In other words, the location of a local minimum in the stability metric with respect to the tooth passing frequency and the chatter frequency was used to determine whether a cut was stable or unstable. In the first phase, stable, marginal, and unstable experimental cuts were performed using the two-flute, four-flute, and five-flute carbide endmills on 6061-T6 aluminum and AISI 4140 steel workpieces. In the second phase, unstable experimental cuts were conducted to determine chatter frequencies, after which the chatter frequencies were used to calculate new spindle speeds. The new spindle speeds and corresponding feed rates were applied to achieve stable cuts under the same cutting parameters and conditions, thereby demonstrating the effectiveness of spindle speed selection for chatter suppression. In the third phase, the method was implemented for closed loop applicability. A MATLAB code was developed and used, together with an NI data acquisition device, for low-latency, in situ chatter detection and spindle speed selection using the scanned periodic sampling frequency approach. The code, following the algorithm in **Figure 3.7** was run simultaneously with experimental cuts using the five-flute endmill on AISI 1018 steel. This phase confirmed that the method can be applied with low-latency for practical manufacturing use.

Thus, across all experimental phases, the results demonstrate that:

- The novel chatter detection approach using scanned periodic sampling frequency and time domain milling signals is valid and repeatable for detecting chatter in situ.

- The location of the local minimum in the stability metric provides a clear and consistent indicator for distinguishing between stable and unstable cutting conditions.
- For the same experimental setup, the magnitude of the stability metric is lower during stable cutting conditions than during unstable conditions. Thus, the stability metric can be used to ascertain the severity of chatter as well as the level of stability of a cut.
- Spindle speed selection based on observed chatter frequencies suppress chatter and achieve stable cutting conditions.

Based on the results and findings of this study, the following recommendations are made for future work and expanded implementation:

- Integration into CNC control systems: The closed loop algorithm could be integrated into open source machine controls to enable automatic identification of both the tooth passing and chatter frequencies in real-time using in-built once-per-revolution machine data.
- Extension to multi-axis and complex machining operations: While this study was conducted using a 3-axis CNC milling machine and down milling operations using a flexible-workpiece-rigid-tool experimental setup, future research should extend the method to 4- and 5-axis machining, as well as other types of milling (e.g., up milling and climb milling) and a rigid-workpiece-flexible-tool setup, to further evaluate its robustness under more complex dynamic conditions.

- Automated surface quality assessment: The current method includes post-process surface inspection using a digital microscope and profilometer. Future work could explore automated image processing and machine vision tools for real-time surface quality assessment.
- Exploration of other sensor modalities: While the study demonstrated successful use of displacement, acceleration, and sound pressure sensors, future research could explore additional sensor modalities such as Hall effect, acoustic emission, or force sensors to enhance robustness and accuracy.

In summary, this study validates the effectiveness of a novel method for in situ chatter detection and spindle speed selection in milling operations using periodic sampling of time domain signals. The method demonstrates reliable performance across a variety of tools, workpieces, and sensors. With further development and integration, the technique has strong potential for improving machining stability, enhancing surface quality, and advancing adaptive manufacturing systems.

REFERENCES

1. Honeycutt, A. and Schmitz, T.L., 2016. A new metric for automated stability identification in time domain milling simulation. Journal of Manufacturing Science and Engineering, 138(7), p.074501.
2. Honeycutt, A. and Schmitz, T.L., 2017. Milling stability interrogation by subharmonic sampling. Journal of Manufacturing Science and Engineering, 139(4), p.041009.
3. Schmitz, T.L., Medicus, K. and Dutterer, B., 2002. Exploring once-per-revolution audio signal variance as a chatter indicator. Machining Science and Technology, 6(2), pp.215-233.
4. Schmitz, T.L., 2003. Chatter recognition by a statistical evaluation of the synchronously sampled audio signal. Journal of Sound and Vibration, 262(3), pp.721-730.
5. Rubeo, M.A. and Schmitz, T.L., 2016. Global stability predictions for flexible workpiece milling using time domain simulation. Journal of Manufacturing Systems, 40, pp.8-14.
6. Rubeo, M.A. and Schmitz, T.L., 2017. Amplitude ratio: a new metric for milling stability identification. Procedia Manufacturing, 10, pp.351-362.
7. Landge, S., 2016. A comparison of two analytical milling stability analyses with time-domain simulation (Master's thesis, The University of North Carolina at Charlotte).

8. Shepard, J., 2017. Chatter Simulation and Detection in CNC milling (Master's thesis, University of New Hampshire).
9. Schmitz, T., Cornelius, A., Karandikar, J., Tyler, C. and Smith, S., 2022. Receptance coupling substructure analysis and chatter frequency-informed machine learning for milling stability. CIRP annals, 71(1), pp.321-324.
10. Xie, M., Yu, X., Ren, Z. and Li, Y., 2022. Milling chatter recognition based on dynamic and wavelet packet decomposition. Mechanical Sciences, 13(2), pp.803-815.
11. Zhan, D., Lu, D., Gao, W., Wei, H. and Sun, Y., 2024. Chatter Detection in Thin-Wall Milling Based on Multi-Sensor Fusion and Dual-Stream Residual Attention CNN. Machines, 12(8), p.559.
12. Schmitz, T., 2024. Milling Stability Modeling by Sample Partitioning with Chatter Frequency-Based Test Point Selection. Journal of Manufacturing and Materials Processing, 8(3), p.109.
13. Schmitz, T., Son, J. and Gomez, M., 2025. Chatter detection and spindle speed selection by scanned periodic sampling frequency. Journal of Manufacturing Processes, 142, pp.409-423.
14. Schmitz, T.L. and Smith, K.S., 2009. Machining dynamics. Springer, p.303.
15. Tlusty, J. and Andrews, G.C., 1983. A critical review of sensors for unmanned machining. CIRP annals, 32(2), pp.563-572.
16. Tlusty, J. and Ismail, F., 1983. Special aspects of chatter in milling.

17. Ryabov, O., Mori, K. and Kasashima, N., 1998. Laser displacement meter application for milling diagnostics. Optics and lasers in engineering, 30(3-4), pp.251-263.
18. Hashimoto, M., Marui, E. and Kato, S., 1996. Experimental research on cutting force variation during regenerative chatter vibration in a plain milling operation. International Journal of Machine Tools and Manufacture, 36(10), pp.1073-1092.
19. Mann, B.P., Insperger, T., Bayly, P.V. and Stépán, G., 2003. Stability of up-milling and down-milling, part 2: experimental verification. International Journal of Machine Tools and Manufacture, 43(1), pp.35-40.
20. Gradišek, J., Kalveram, M., Insperger, T., Weinert, K., Stépán, G., Govekar, E. and Grabec, I., 2005. On stability prediction for milling. International Journal of Machine Tools and Manufacture, 45(7-8), pp.769-781.
21. Albrecht, A., Park, S.S., Altintas, Y. and Pritschow, G., 2005. High frequency bandwidth cutting force measurement in milling using capacitance displacement sensors. International Journal of Machine Tools and Manufacture, 45(9), pp.993-1008.
22. Delio, T., Tlusty, J. and Smith, S., 1992. Use of audio signals for chatter detection and control.
23. Tran, M.Q., Liu, M.K. and Elsisi, M., 2022. Effective multi-sensor data fusion for chatter detection in milling process. ISA transactions, 125, pp.514-527.

24. Schuster, A., Otto, A., Rentzsch, H. and Ihlenfeldt, S., 2024. Multi-Sensory Tool Holder for Process Force Monitoring and Chatter Detection in Milling. Sensors (Basel, Switzerland), 24(17), p.5542.
25. Arriaza, O.V., Tumurkhuyagc, Z. and Kim, D.W., 2018. Chatter identification using multiple sensors and multi-layer neural networks. Procedia Manufacturing, 17, pp.150-157.
26. Wang, W.K., Wan, M., Zhang, W.H. and Yang, Y., 2022. Chatter detection methods in the machining processes: A review. Journal of Manufacturing Processes, 77, pp.240-259.
27. Smith, S. and Delio, T., 1989, December. Sensor-based control for chatter-free milling by spindle speed selection. In Symposium on Control Issues in Manufacturing (Vol. 18, pp. 107-114).
28. Toh, C.K., 2004. Vibration analysis in high speed rough and finish milling hardened steel. Journal of Sound and Vibration, 278(1-2), pp.101-115.
29. Aslan, D. and Altintas, Y., 2018. On-line chatter detection in milling using drive motor current commands extracted from CNC. International Journal of Machine Tools and Manufacture, 132, pp.64-80.
30. Chang, L., Weiwei, X. and Lei, G., 2020. Identification of milling chatter based on a novel frequency-domain search algorithm. The International Journal of Advanced Manufacturing Technology, 109(9), pp.2393-2407.

31. Schmitz, T.L., Davies, M.A., Medicus, K. and Snyder, J., 2001. Improving high-speed machining material removal rates by rapid dynamic analysis. CIRP Annals, 50(1), pp.263-268.
32. Schmitz, T.L., Medicus, K. and Dutterer, B., 2002. Exploring once-per-revolution audio signal variance as a chatter indicator. Machining Science and Technology, 6(2), pp.215-233.
33. Zhao, Y., Adjallah, K.H., Sava, A. and Wang, Z., 2021. MaxEnt feature-based reliability model method for real-time detection of early chatter in high-speed milling. ISA transactions, 113, pp.39-51.
34. Yang, K., Wang, G., Dong, Y., Zhang, Q. and Sang, L., 2019. Early chatter identification based on an optimized variational mode decomposition. Mechanical Systems and Signal Processing, 115, pp.238-254.
35. Xie, M., Yu, X., Ren, Z. and Li, Y., 2022. Milling chatter recognition based on dynamic and wavelet packet decomposition. Mechanical Sciences, 13(2), pp.803-815.
36. Cao, H., Yue, Y., Chen, X. and Zhang, X., 2017. Chatter detection in milling process based on synchrosqueezing transform of sound signals. The International Journal of Advanced Manufacturing Technology, 89, pp.2747-2755.
37. Fu, Y., Zhang, Y., Zhou, H., Li, D., Liu, H., Qiao, H. and Wang, X., 2016. Timely online chatter detection in end milling process. Mechanical Systems and Signal Processing, 75, pp.668-688.

38. Wang, L. and Liang, M., 2009. Chatter detection based on probability distribution of wavelet modulus maxima. Robotics and Computer-Integrated Manufacturing, 25(6), pp.989-998.
39. Jo, H.N., Park, B.E., Ji, Y., Kim, D.K., Yang, J.E. and Lee, I.B., 2020. Chatter detection and diagnosis in hot strip mill process with a frequency-based chatter index and modified independent component analysis. IEEE Transactions on Industrial Informatics, 16(12), pp.7812-7820.
40. Jauhari, K., Rahman, A.Z., Al Huda, M., Widodo, A. and Prahasto, T., 2025. A hybrid deep learning-based approach for on-line chatter detection in milling using deep stem-inception networks and residual channel-spatial attention mechanisms. Mechanical Systems and Signal Processing, 226, p.112357.
41. Kounta, C.A.K.A., Arnaud, L., Kamsu-Foguem, B. and Tangara, F., 2023. Deep learning for the detection of machining vibration chatter. Advances in Engineering Software, 180, p.103445.
42. Alberts, M., St. John, S., Jared, B., Karandikar, J., Khojandi, A., Schmitz, T. and Coble, J., 2024. Chatter detection in simulated machining data: a simple refined approach to vibration data. The International Journal of Advanced Manufacturing Technology, 132(9), pp.4541-4557.
43. Lamraoui, M., Barakat, M., Thomas, M. and Badaoui, M.E., 2015. Chatter detection in milling machines by neural network classification and feature selection. Journal of Vibration and Control, 21(7), pp.1251-1266.

44. Kuljanic, E., Totis, G. and Sortino, M., 2009. Development of an intelligent multisensor chatter detection system in milling. Mechanical Systems and Signal Processing, 23(5), pp.1704-1718.
45. Wang, Y., Bo, Q., Liu, H., Hu, L. and Zhang, H., 2018. Mirror milling chatter identification using Q-factor and SVM. The International Journal of Advanced Manufacturing Technology, 98, pp.1163-1177.
46. Gao, H., Wang, H., Shen, H., Xing, S., Yang, Y., Wang, Y., Liu, W., Yu, L., Ali, M. and Khan, I.A., 2025. Multi-modal denoised data-driven milling chatter detection using an optimized hybrid neural network architecture. Scientific Reports, 15(1), p.3953.
47. Xu, D., 2003. A fuzzy logic approach for chatter detection and suppression in end milling (pp. 1509-1509). Université d'Ottawa/University of Ottawa.
48. Liang, M., Yeap, T. and Hermansyah, A., 2004. A fuzzy system for chatter suppression in end milling. Proceedings of the Institution of Mechanical Engineers, Part B: Journal of Engineering Manufacture, 218(4), pp.403-417.
49. Gomez, M.F. and Schmitz, T.L., 2019. Displacement-based dynamometer for milling force measurement. Procedia Manufacturing, 34, pp.867-875.
50. Gomez, M. and Schmitz, T., 2020. Low-cost, constrained-motion dynamometer for milling force measurement. Manufacturing Letters, 25, pp.34-39.
51. Gomez, M. and Schmitz, T., 2021. Tool wear evaluation using a constrained-motion dynamometer.

52. Nazario, J., Pollard, D. and Schmitz, T., 2025. Milling force measurement using a constrained motion dynamometer with compensation. Manufacturing Letters, 44, pp.694-703.
53. Pollard, Dylan Michael, "Mechanistic force model calibration for milling in multiple materials. " Master's Thesis, University of Tennessee, 2025. https://trace.tennessee.edu/utk_gradthes/14551

APPENDIX

A. MATLAB code.

```
%% Tobechukwu Nwabueze 07/18/25
clc;
clear;
close all;

% Ask for the new spindle speed range before starting data collection
min_spindle_speed = input('Enter the minimum spindle speed (RPM): ');
max_spindle_speed = input('Enter the maximum spindle speed (RPM): ');

addpath(genpath('Data INSITU\'))

% Set variables for fs and sensor sensitivity
fs = 25000;                % Hz samplin frequency for data aquisition
ScaleA1 = 5.24*1e-3;   % V/G sensitivity for Accelerometer

% Set up daq with proper inputs
devices = daqlist;    % search for daq
s = daq("ni");         % using National Instruments daq
s.Rate = fs;           % set sample frequency

% Set hardware channel (FX)
Axc = addinput(s, 'cDAQ1Mod1','ai0','Accelerometer'); % Setting accelerometer
channel to A0 input
   Axc.Name = 'Ax';                    % Change name
   Axc.Sensitivity = ScaleA1;          % Set sensitivity


s.Channels  % List Channels
s.start        % Intialize daq
pause(1)     % Wait

% Start data collection once ICP has settled
close all;
input('Press enter (did you change file name, rpm & no. of teeth?)') % Wait for input to
start data collection

FILENAME = 'stable_5027_8a_3r_5fl_1018st_.mat'; % Set file name
t1 = 10;                           % Time to collect data
s.start("duration",t1)          % Start collection
data=read(s,seconds(t1));
```

```
% Store data vectors from the time and data and scale accelerometer signal
C_time=seconds(data.Time);
C_accel=(data.Ax);

% Plot total time interval of the signal
figure(1)
plot(C_time,C_accel, 'b', LineWidth=2, MarkerSize=15)
set(gca, 'FontSize', 15)
xlabel('Time (s)')
ylabel('Acceleration (m/s^2)')
grid on

% Plot the magnified time interval of the signal
figure(2)
plot(C_time,C_accel, 'b', LineWidth=2)
set(gca, 'FontSize', 15)
xlabel('Time (s)')
ylabel('Acceleration (m/s^2)')
xlim([2.0 2.03])
grid on

% Define frequency range for metric sampling
fsample_vector = 100:0.5:1500;
metric_sample = zeros(1, length(fsample_vector));
dt = 1 / s.Rate; % Time step based on sample rate

% Loop through each sample frequency to compute M values
for loop = 1:length(fsample_vector)
   fsample = fsample_vector(loop);          % Current sampling frequency
   dtsample = 1/fsample;                    % Time step for this sample rate
   steps_sample = round(dtsample/dt);    % Steps per sample

   % Process the data to remove transients and resample
   xtpos = C_accel;
   xtpos = xtpos(round(0.5*length(xtpos)):length(xtpos));
   xtpos_s = xtpos(1:steps_sample:length(xtpos)); % Resample the signal

   % Step 18: Calculate the metric M for each fsample
   metric_sample(loop) = sum(abs(diff(xtpos_s)))/length(xtpos_s);
end

% Plot the M values vs sampling frequency
figure(3);
```

```
plot(fsample_vector, metric_sample, 'b.', LineWidth=2, MarkerSize=15);
set(gca, 'FontSize', 15)
title('Metric vs Sampling Frequency');
xlabel('Sampling Frequency (Hz)');
ylabel('Metric M (m/s^2)');
grid on;

% Define spindle speed and tooth passing frequency
omega = 5027;                % Spindle speed (RPM)
Nt = 5;                      % Number of teeth
ftooth = omega * Nt / 60    % Tooth passing frequency (Hz)

hold on;
plot(ftooth, 0, 'bo', MarkerSize=15, LineWidth=3);  % Mark tooth passing frequency
xlim([min(fsample_vector) 1000]);

% Find local minima in the M values
[min_vals, min_locs] = findpeaks(-metric_sample);
min_freqs = fsample_vector(min_locs);

% Step 11: Check stability ONLY if local minimum is exactly at tooth passing frequency
tolerance = 10; % very small tolerance for floating-point equality
if any(abs(min_freqs - ftooth) < tolerance)
   disp('Local minimum occurs at ftooth, the cut is stable.')
   stable_cut = true;
   chatter_freq = [];
else
   disp('Local minimum does not occur at ftooth, the cut is unstable.')
   stable_cut = false;

   % Step 12: Use FFT to identify exact chatter frequency
   N = length(C_accel);
   Y = fft(C_accel);
   f = (0:N-1)*(1/dt)/N;  % Frequency vector
   P2 = abs(Y/N);
   P1 = P2(1:floor(N/2));
   f1 = f(1:floor(N/2));

   % Find the highest peak in the spectrum (ignoring DC)
   [~, max_idx] = max(P1(2:end));
   chatter_freq = f1(max_idx+1);

   disp(['Estimated chatter frequency (Hz): ', num2str(chatter_freq)]);
```

```
    % Step 13: Recommend new spindle speeds
    j_values = 1:7;
    new_spindle_speeds = (60 * chatter_freq) ./ (j_values * Nt);

    valid_speeds = new_spindle_speeds(new_spindle_speeds >= min_spindle_speed & ...
                                      new_spindle_speeds <= max_spindle_speed);

    if isempty(valid_speeds)
        disp('No valid spindle speed within machine range.')
    else
        disp('Recommended new spindle speeds (RPM):')
        disp(valid_speeds)
    end
end


% Save the file, if there is a duplicate file name it will save as a temp file and you have
to rename Temp.mat file
save('Temp.mat','C_time','C_accel','fs','ScaleA1')
if exist(FILENAME, 'file') == 2
    choice = input('File exists. Overwrite? (y/n): ', 's');
    if strcmpi(choice, 'n')
        disp('File not saved. Manually save if needed');
        return; % Exit without saving
    end
end
save(FILENAME,'C_time','C_accel','fs','ScaleA1')
        disp('Data save sucessful!')

%% Function for collecting data as it becomes available in real-time
function collectData(src, event, h)
    % Update the global variables with the new data
    global collected_data collected_time;

    % Append new data to the collected arrays
    collected_data = [collected_data; event.Data];
    collected_time = [collected_time; event.TimeStamps];

    % Update progress bar during data collection
    waitbar(event.TimeStamps(end) / src.DurationInSeconds, h);
end
```

B. **Supplementary list of figures.**

Figure 4.49: Tool tip and workpiece, *x* (blue lines) and *y* (red lines) directions, frequency response function. 94

Figure 4.50: Stability lobe diagram with the selected unstable point (black dot) corresponding to a spindle speed of 7000 rpm and axial depth of cut of 5 mm. 94

Figure 4.51: The total time interval of the signal from the CMD (displacement signal) showing when the tool interacts with the workpiece. 95

Figure 4.52: The magnified time interval of the signal from the CMD (displacement signal). 95

Figure 4.53: Magnitude plot of *x* frequency content for 150 rotations, with f_c (red dot) identified at 593 Hz and f_{tooth} (black circle) at 467 Hz. 96

Figure 4.54: Variation in *M* value with periodic f_s. A local minimum occurs at f_c of 593 Hz (red dot) where M = 1.97 µm, not at f_{tooth} (black circle). 96

Figure 4.55: The total time interval of the signal from the accelerometer (acceleration signal) showing when the tool interacts with the workpiece. 97

Figure 4.56: The magnified time interval of the signal from the accelerometer (acceleration signal). 97

Figure 4.57: Magnitude plot of *a* frequency content for 150 rotations, with f_c (red dot) identified at 593 Hz and f_{tooth} (black circle) at 467 Hz. 98

Figure 4.58: Variation in *M* value with periodic f_s. A local minimum occurs at f_c of 593 Hz (red dot) where M = 27 m/s^2, not at f_{tooth} (black circle). 98

Figure 4.59: The total time interval of the signal from the microphone (sound pressure signal) showing when the tool interacts with the workpiece. 99

Figure 4.60: The magnified time interval of the signal from the microphone (sound pressure signal). 99

Figure 4.61: Magnitude plot of p frequency content for 150 rotations, with f_c (red dot) identified at 593 Hz and f_{tooth} (black circle) at 467 Hz. 100

Figure 4.62: Variation in M value with periodic f_s. A local minimum occurs at f_c of 593 Hz (red dot) where M = 1.27 Pa, not at f_{tooth} (black circle). 100

Figure 4.63: Surface of the AISI 4140 steel workpiece with visible chatter marks after the unstable cut. 101

Figure 4.64: Tool tip and workpiece, x (blue lines) and y (red lines) directions, frequency response function. 104

Figure 4.65: Stability lobe diagram with the selected marginally stable point (black dot) corresponding to a spindle speed of 5770 rpm and axial depth of cut of 5 mm. 104

Figure 4.66: The total time interval of the signal from the CMD (displacement signal) showing when the tool interacts with the workpiece. 105

Figure 4.67: The magnified time interval of the signal from the CMD (displacement signal). 105

Figure 4.68: Magnitude plot of x frequency content for 150 rotations, with f_{tooth} (black circle) identified at 385 Hz and runout frequencies (magenta dots) also identified. 106

Figure 4.69: Variation in M value with periodic f_s. A local minimum occurs at f_{tooth} of 385 Hz (black circle) where M = 1.33 µm. 106

Figure 4.70: The total time interval of the signal from the accelerometer (acceleration signal) showing when the tool interacts with the workpiece. 107

Figure 4.71: The magnified time interval of the signal from the accelerometer (acceleration signal). 107

Figure 4.72: Magnitude plot of a frequency content for 150 rotations, with f_{tooth} (black circle) identified at 385 Hz and runout frequencies (magenta dots) also identified. 108

Figure 4.73: Variation in M value with periodic f_s. Local minima occur at f_{tooth} of 385 Hz (black circle) where M = 9.46 m/s^2 and near the runout frequencies (magenta dots). 108

Figure 4.74: The total time interval of the signal from the microphone (sound pressure signal) showing when the tool interacts with the workpiece. 109

Figure 4.75: The magnified time interval of the signal from the microphone (sound pressure signal). 109

Figure 4.76: Magnitude plot of p frequency content for 150 rotations, with f_{tooth} (black circle) identified at 385 Hz. 110

Figure 4.77: Variation in M value with periodic f_s. A local minimum occurs at f_{tooth} of 385 Hz (black circle) where M = 0.79 Pa. 110

Figure 4.78: Surface of the AISI 4140 steel workpiece with periodic feed marks after the marginally stable cut. 111

Figure 4.79: Tool tip and workpiece, *x* (blue lines) and *y* (red lines) directions, frequency response function. 114

Figure 4.80: Stability lobe diagram with the selected stable point (black dot) corresponding to a spindle speed of 5100 rpm and axial depth of cut of 5 mm. 114

Figure 4.81: The total time interval of the signal from the CMD (displacement signal) showing when the tool interacts with the workpiece. 115

Figure 4.82: The magnified time interval of the signal from the CMD (displacement signal). 115

Figure 4.83: Magnitude plot of *x* frequency content for 150 rotations, with f_{tooth} at 340 Hz and its 1st harmonic identified (black circles). 116

Figure 4.84: Variation in *M* value with periodic f_s. A local minimum occurs at f_{tooth} of 340 Hz (black circle), where M = 0.85 µm. 116

Figure 4.85: The total time interval of the signal from the accelerometer (acceleration signal) showing when the tool interacts with the workpiece. 117

Figure 4.86: The magnified time interval of the signal from the accelerometer (acceleration signal). 117

Figure 4.87: Magnitude plot of *a* frequency content for 150 rotations, with f_{tooth} at 340 Hz and its 1st harmonic identified (black circles). 118

Figure 4.88: Variation in *M* value with periodic f_s. Local minima occur at f_{tooth} of 340 Hz, where M = 6.05 m/s^2, and at its 1st harmonic (black circles). 118

Figure 4.89: The total time interval of the signal from the microphone (sound pressure signal) showing when the tool interacts with the workpiece. 119

Figure 4.90: The magnified time interval of the signal from the microphone (sound pressure signal). 119

Figure 4.91: Magnitude plot of p frequency content for 150 rotations, with f_{tooth} at 340 Hz and its 1st harmonic identified (black circles). 120

Figure 4.92: Variation in M value with periodic f_s. Local minima occur at f_{tooth} of 340 Hz, where M = 0.34 Pa, and at its 1st harmonic (black circles). 120

Figure 4.93: Surface of the AISI 4140 steel workpiece with periodic feed marks after the stable cut. 121

Figure 4.94: Spindle power consumption peaked at 2.37 kW during the unstable cut at a spindle speed of 7000 rpm, axial and radial depths of cut of 5 mm and 2 mm respectively. 122

Figure 4.95: Spindle power consumption peaked at 1.81 kW during the marginal cut at a spindle speed of 5770 rpm, axial and radial depths of cut of 5 mm and 2 mm respectively. 123

Figure 4.96: Spindle power consumption peaked at 1.27 kW during the stable cut at a spindle speed of 5100 rpm, axial and radial depths of cut of 5 mm and 1 mm respectively. 123

Figure 4.97: Frequency response function of the tool tip and workpiece, x (blue lines) and y (red lines) directions. 127

Figure 4.98: Stability lobe diagram with the selected unstable point (black dot) corresponding to a spindle speed of 6000 rpm and axial depth of cut of 8 mm. 127

Figure 4.99: The total time interval of the signal from the CMD (displacement signal) showing when the tool interacts with the workpiece. 128

Figure 4.100: The magnified time interval of the signal from the CMD (displacement signal). 128

Figure 4.101: Magnitude plot of *x* frequency content for 100 rotations, with f_c (red dot) identified at 599 Hz and f_{tooth} (black circle) at 500 Hz. 129

Figure 4.102: Variation in *M* value with periodic f_s. A local minimum occurs at f_c of 599 Hz (red dot) where M = 0.91 µm, not at f_{tooth} (black circle). 129

Figure 4.103: The total time interval of the signal from the accelerometer (acceleration signal) showing when the tool interacts with the workpiece. 130

Figure 4.104: The magnified time interval of the signal from the accelerometer (acceleration signal). 130

Figure 4.105: Magnitude plot of *a* frequency content for 100 rotations, with f_c (red dot) identified at 599 Hz and f_{tooth} (black circle) at 500 Hz. 131

Figure 4.106: Variation in *M* value with periodic f_s. A local minimum occurs at f_c of 599 Hz (red dot) where M = 4.57 m/s^2, not at f_{tooth} (black circle). 131

Figure 4.107: The total time interval of the signal from the microphone (sound pressure signal) showing when the tool interacts with the workpiece. 132

Figure 4.108: The magnified time interval of the signal from the microphone (sound pressure signal). 132

Figure 4.109: Magnitude plot of *p* frequency content for 100 rotations, with f_c (red dot) identified at 599 Hz and f_{tooth} (black circle) at 500 Hz. 133

Figure 4.110: Variation in M value with periodic f_s. A local minimum occurs at f_c of 599 Hz (red dot) where 0.35 Pa, not at f_{tooth} (black circle). 133

Figure 4.111: Surface of the AISI 4140 steel workpiece with chatter marks after the unstable cut. 134

Figure 4.112: Frequency response function of the tool tip and workpiece, x (blue lines) and y (red lines) directions. 137

Figure 4.113: Stability lobe diagram with the selected marginal point (black dot) corresponding to a spindle speed of 6000 rpm and axial depth of cut of 4 mm. 137

Figure 4.114: The total time interval of the signal from the CMD (displacement signal) showing when the tool interacts with the workpiece. 138

Figure 4.115: The magnified time interval of the signal from the CMD (displacement signal). 138

Figure 4.116: Magnitude plot of x frequency content for 100 rotations, with f_c (red dot) identified at 595 Hz and f_{tooth} (black circle) at 500 Hz. 139

Figure 4.117: Variation in M value with periodic f_s. A local minimum occurs at f_c of 595 Hz (red dot) where M = 1.09 µm, not at f_{tooth} (black circle). 139

Figure 4.118: The total time interval of the signal from the accelerometer (acceleration signal) showing when the tool interacts with the workpiece. 140

Figure 4.119: The magnified time interval of the signal from the accelerometer (acceleration signal). 140

Figure 4.120: Magnitude plot of a frequency content for 100 rotations, with f_c (red dot) identified at 595 Hz and f_{tooth} (black circle) at 500 Hz. 141

Figure 4.121: Variation in M value with periodic f_s. A local minimum occurs at f_c of 595 Hz (red dot) where M = 8.65 m/s^2, not at f_{tooth} (black circle). 141

Figure 4.122: The total time interval of the signal from the microphone (sound pressure signal) showing when the tool interacts with the workpiece. 142

Figure 4.123: The magnified time interval of the signal from the microphone (sound pressure signal). 142

Figure 4.124: Magnitude plot of p frequency content for 100 rotations, with f_c (red dot) identified at 595 Hz and f_{tooth} (black circle) at 500 Hz. 143

Figure 4.125: Variation in M value with periodic f_s. A local minimum occurs at f_c of 595 Hz (red dot) where M = 0.39 Pa, not at f_{tooth} (black circle). 143

Figure 4.126: Surface of the AISI 4140 steel workpiece with chatter marks after the marginally unstable cut. 144

Figure 4.127: Frequency response function of the tool tip and workpiece, x (blue lines) and y (red lines) directions. 147

Figure 4.128: Stability lobe diagram with the selected stable point (black dot) corresponding to a spindle speed of 4000 rpm and axial depth of cut of 4 mm. 147

Figure 4.129: The total time interval of the signal from the CMD (displacement signal) showing when the tool interacts with the workpiece. 148

Figure 4.130: The magnified time interval of the signal from the CMD (displacement signal). 148

Figure 4.131: Magnitude plot of x frequency content for 100 rotations, with f_{tooth} identified at 333 Hz (black circles). 149

Figure 4.132: Variation in M value with periodic f_s. A local minimum occurs at f_{tooth} of 333 Hz (black circle), where M = 0.91 µm. 149

Figure 4.133: The total time interval of the signal from the accelerometer (acceleration signal) showing when the tool interacts with the workpiece. 150

Figure 4.134: The magnified time interval of the signal from the accelerometer (acceleration signal). 150

Figure 4.135: Magnitude plot of a frequency content for 100 rotations, with f_{tooth} (black circle) identified at 333 Hz and a runout frequency (magenta dot) also identified. 151

Figure 4.136: Variation in M value with periodic f_s. A local minimum occurs at f_{tooth} of 333 Hz (black circle), where M = 3.79 m/s^2. 151

Figure 4.137: The total time interval of the signal from the microphone (sound pressure signal) showing when the tool interacts with the workpiece. 152

Figure 4.138: The magnified time interval of the signal from the microphone (sound pressure signal). 152

Figure 4.139: Magnitude plot of p frequency content for 100 rotations, with f_{tooth} (black circle) identified at 333 Hz. 153

Figure 4.140: Variation in M value with periodic f_s. A local minimum occurs at f_{tooth} of 333 Hz (black circle), where M = 0.24 Pa. 153

Figure 4.141: Surface of the AISI 4140 steel workpiece with periodic feed marks after the stable cut. 154

Figure 4.142: Spindle power consumption peaked at 1.84 kW during the unstable cut at a spindle speed of 6000 rpm, axial and radial depths of cut of 8 mm and 1 mm respectively. 156

Figure 4.143: Spindle power consumption peaked at 1.41 kW during the unstable cut at a spindle speed of 6000 rpm, axial and radial depths of cut of 4 mm and 1 mm respectively. 157

Figure 4.144: Spindle power consumption peaked at 1.19 kW during the unstable cut at a spindle speed of 4000 rpm, axial and radial depths of cut of 4 mm and 1 mm respectively. 157

Figure 4.145: Frequency response function of the tool tip and workpiece, *x* (blue lines) and *y* (red lines) directions. 160

Figure 4.146: Stability lobe diagram with the selected unstable point (black dot) corresponding to a spindle speed of 6800 rpm and axial depth of cut of 5 mm. 161

Figure 4.147: The total time interval of the signal from the CMD (displacement signal) showing when the tool interacts with the workpiece. 161

Figure 4.148: The magnified time interval of the signal from the CMD (displacement signal). 162

Figure 4.149: Magnitude plot of *x* frequency content for 150 rotations, with f_c (red dot) identified at 551 Hz and f_{tooth} (black circle) at 453 Hz. 162

Figure 4.150: Variation in *M* value with periodic f_s. A local minimum occurs at f_c of 551 Hz (red dot) where M = 2.17 μm, not at f_{tooth} (black circle). 163

Figure 4.151: The total time interval of the signal from the accelerometer (acceleration signal) showing when the tool interacts with the workpiece. 163

Figure 4.152: The magnified time interval of the signal from the accelerometer (acceleration signal). 164

Figure 4.153: Magnitude plot of *a* frequency content for 150 rotations, with f_c (red dot) identified at 551 Hz and f_{tooth} (black circle) at 453 Hz. 164

Figure 4.154: Variation in *M* value with periodic f_s. A local minimum occurs at f_c of 551 Hz (red dot) where M = 26.34 m/s^2, not at f_{tooth} (black circle). 165

Figure 4.155: The total time interval of the signal from the microphone (sound pressure signal) showing when the tool interacts with the workpiece. 165

Figure 4.156: The magnified time interval of the signal from the microphone (sound pressure signal). 166

Figure 4.157: Magnitude plot of *p* frequency content for 150 rotations, with f_c (red dot) identified at 551 Hz and f_{tooth} (black circle) at 453 Hz. 166

Figure 4.158: Variation in *M* value with periodic f_s. A local minimum occurs at f_c of 551 Hz (red dot) where M = 0.95 Pa, not at f_{tooth} (black circle). 167

Figure 4.159: Surface of the AISI 4140 steel workpiece with chatter marks after the unstable cut. 167

Figure 4.160: Frequency response function of the tool tip and workpiece, *x* (blue lines) and *y* (red lines) directions. 170

Figure 4.161: Stability lobe diagram with the selected stable point (black dot) corresponding to a spindle speed of 4133 rpm and axial depth of cut of 5 mm. 171

Figure 4.162: The total time interval of the signal from the CMD (displacement signal) showing when the tool interacts with the workpiece. 171

Figure 4.163: The magnified time interval of the signal from the CMD (displacement signal). 172

Figure 4.164: Magnitude plot of *x* frequency content for 150 rotations, with f_{tooth} at 276 Hz and its 1st harmonic (black circles) identified. 172

Figure 4.165: Variation in *M* value with periodic f_s. A local minimum occurs at f_{tooth} of 276 Hz (black circle), where M = 1.64 µm. 173

Figure 4.166: The total time interval of the signal from the accelerometer (acceleration signal) showing when the tool interacts with the workpiece. 173

Figure 4.167: The magnified time interval of the signal from the accelerometer (acceleration signal). 174

Figure 4.168: Magnitude plot of *a* frequency content for 150 rotations, with f_{tooth} at 276 Hz and its 1st harmonic (black circles) identified. 174

Figure 4.169: Variation in *M* value with periodic f_s. Local minima occur at f_{tooth} of 276 Hz and its first harmonic (black circles), where M = 5 m/s^2..... 175

Figure 4.170: The total time interval of the signal from the microphone (sound pressure signal) showing when the tool interacts with the workpiece. 175

Figure 4.171: The magnified time interval of the signal from the microphone (sound pressure signal). 176

Figure 4.172: Magnitude plot of *p* frequency content for 150 rotations, with f_{tooth} at 276 Hz and its 1st harmonic (black circles) identified. 176

Figure 4.173: Variation in M value with periodic f_s. A local minimum occurs at f_{tooth} of 276 Hz (black circle), where M = 0.33 Pa. 177

Figure 4.174: Surface of the AISI 4140 steel workpiece with periodic feed marks after the stable cut. 177

Figure 4.175: Frequency response function of the tool tip and workpiece, x (blue lines) and y (red lines) directions. 181

Figure 4.176: Stability lobe diagram with the selected marginal point (black dot) corresponding to a spindle speed of 4650 rpm and axial depth of cut of 8 mm. 182

Figure 4.177: The total time interval of the signal from the accelerometer (acceleration signal) showing when the tool interacts with the workpiece. 182

Figure 4.178: The magnified time interval of the signal from the accelerometer (acceleration signal). 183

Figure 4.179: Magnitude plot of a frequency content for 150 rotations, identifying f_c (red dot) at 824 Hz, and f_{tooth} (black circle) at 388 Hz with its 1st harmonic (black circle). 183

Figure 4.180: Variation in M value with periodic f_s. A local minimum occurs at f_c of 824 Hz (red dot) where M = 0.18 m/s^2, not at f_{tooth} (black circle). 184

Figure 4.181: Surface of the AISI 1018 steel workpiece after the marginal cut..... 184

Figure 4.182: Frequency response function of the tool tip and workpiece, x (blue lines) and y (red lines) directions. 187

Figure 4.183: Stability lobe diagram with the recommended stable point (black dot) corresponding to a spindle speed of 4942 rpm and axial depth of cut of 8 mm. 187

Figure 4.184: The total time interval of the signal from the accelerometer (acceleration signal) showing when the tool interacts with the workpiece. 188

Figure 4.185: The magnified time interval of the signal from the accelerometer (acceleration signal). 188

Figure 4.186: Magnitude plot of *a* frequency content for 150 rotations, with f_{tooth} at 412 Hz and its 1st harmonic at 824 Hz (black circles) identified. 189

Figure 4.187: Variation in *M* with periodic f_s. Local minima occur at f_{tooth} of 412 Hz (black circle) where $M = 0.18$ m/s^2 and its first harmonic (black circle) at $M = 0.15$ m/s^2. 189

Figure 4.188: Surface of the AISI 1018 steel workpiece with periodic feed marks after the stable cut. 190

Figure 4.189: Frequency response function of the tool tip and workpiece, *x* (blue lines) and *y* (red lines) directions. 193

Figure 4.190: Stability lobe diagram with the selected unstable point (black dot) corresponding to a spindle speed of 4700 rpm and axial depth of cut of 8 mm. 193

Figure 4.191: The total time interval of the signal from the microphone (sound pressure signal) showing when the tool interacts with the workpiece. 194

Figure 4.192: The magnified time interval of the signal from the microphone (sound pressure signal). 194

Figure 4.193: Magnitude plot of *p* frequency content for 150 rotations, identifying f_c (red dot) at 833 Hz, and f_{tooth} (black circle) at 392 Hz. 195

Figure 4.194: Variation in M value with periodic f_s. A local minimum occurs at f_c of 833 Hz (red dot) where M = 0.40 Pa, not at f_{tooth} (black circle). 195

Figure 4.195: Surface of the AISI 1018 steel workpiece with visible chatter marks after the unstable cut. 196

Figure 4.196: Frequency response function of the tool tip and workpiece, x (blue lines) and y (red lines) directions. 198

Figure 4.197: Stability lobe diagram with the recommended stable point (black dot) corresponding to a spindle speed of 4998 rpm and axial depth of cut of 8 mm. 199

Figure 4.198: The total time interval of the signal from the microphone (sound pressure signal) showing when the tool interacts with the workpiece. 199

Figure 4.199: The magnified time interval of the signal from the microphone (sound pressure signal). 200

Figure 4.200: Magnitude plot of p frequency content for 150 rotations, with f_{tooth} at 417 Hz and its 1st harmonic at 834 Hz (black circles) identified. 200

Figure 4.201: Variation in M with periodic f_s. Local minima occur at f_{tooth} of 417 Hz (black circle) where M = 0.31 Pa and its first harmonic (black circle). 201

Figure 4.202: Surface of the AISI 1018 steel workpiece with periodic feed marks after the stable cut. 201

Figure 4.203: Frequency response function of the tool tip and workpiece, x (blue lines) and y (red lines) directions. 204

Figure 4.204: Stability lobe diagram with the selected unstable point (black dot) corresponding to a spindle speed of 4780 rpm and axial depth of cut of 8 mm. 205

Figure 4.205: The total time interval of the signal from the accelerometer (acceleration signal) showing when the tool interacts with the workpiece. 205

Figure 4.206: The magnified time interval of the signal from the accelerometer (acceleration signal). 206

Figure 4.207: Magnitude plot of *a* frequency content for 150 rotations, identifying f_c (red dot) at 838 Hz, and f_{tooth} (black circle) at 398 Hz with its 1st harmonic (black circle). 206

Figure 4.208: Variation in *M* value with periodic f_s. A local minimum occurs at f_c of 838 Hz (red dot) where $M = 0.57$ m/s^2, not at f_{tooth} (black circle). 207

Figure 4.209: Surface of the AISI 1018 steel workpiece with visible chatter marks after the unstable cut. 207

Figure 4.210: Frequency response function of the tool tip and workpiece, *x* (blue lines) and *y* (red lines) directions. 210

Figure 4.211: Stability lobe diagram with the selected stable point (black dot) corresponding to a spindle speed of 5027 rpm and axial depth of cut of 8 mm. 211

Figure 4.212: The total time interval of the signal from the accelerometer (acceleration signal) showing when the tool interacts with the workpiece. 211

Figure 4.213: The magnified time interval of the signal from the accelerometer (acceleration signal). 212

Figure 4.214: Magnitude plot of *a* frequency content for 150 rotations, with f_{tooth} at 419 Hz and its 1st harmonic at 838 Hz (black circles) identified. 212

Figure 4.215: Variation in M with periodic f_s. Local minima occur at f_{tooth} of 419 Hz (black circle) where M = 0.17 m/s^2 and its first harmonic. 213

Figure 4.216: Surface of the AISI 1018 steel workpiece with periodic feed marks after the stable cut. 213

Figure 4.217: Minimum and maximum M values for the stable, marginally unstable, and unstable cuts from the 2-flute endmill on 6061 aluminum displacement signals... 214

Figure 4.218: Minimum and maximum M values for the stable, marginally stable, and unstable cuts from the 4-flute endmill on 4140 steel acceleration signals..... 215

Figure 4.219: Minimum and maximum M values for the stable, marginally unstable, and unstable cuts from the 5-flute endmill on 4140 steel sound pressure signals. 215

VITA

Tobechukwu Nwabueze was born in Enugu, Nigeria. He received his Bachelor of Engineering (B.Eng.) degree in Electrical and Electronics Engineering from the University of Port Harcourt, Rivers State, Nigeria, in 2015. His undergraduate final-year project focused on the design and construction of a light-following robot for hole detection in surface pipes, which sparked his enduring interest in sensor technologies and automation.

He completed an internship with the Nigerian National Petroleum Corporation (NNPC), where he gained practical experience in process instrumentation, control systems, and industrial maintenance. Following graduation, he completed a Graduate Trainee program at Frontier Oil Limited in Eket, Akwa Ibom State, Nigeria, supporting instrument and electrical operations at the Uquo marginal oil field. From 2018 to 2021, he served as a Senior Instrumentation Engineer at DON-B Chemical Engineering Services Ltd., Enugu, Nigeria, where he led calibration, maintenance, and procurement of industrial instrumentation systems to ensure reliable process control and measurement accuracy.

In 2022, Mr. Nwabueze joined the University of Tennessee, Knoxville, as a Graduate Research Assistant with the Machine Tool Research Center (MTRC) at the Tennessee Manufacturing and Design Enterprise (TN-MADE). His research has focused on machine data monitoring, collection, and analysis, the development and application of Hall effect sensors for displacement measurements, and the use of in situ signal-based methods for chatter detection and stability evaluation in milling operations. His doctoral work presents an experimentally validated, in situ chatter detection method based on scanned

periodic sampling frequency of time-domain milling signals, enabling intelligent process monitoring and spindle speed selection for chatter suppression.

Mr. Nwabueze has presented his research at national and international conferences, including NAMRC and ASPE, and has contributed to manufacturing workforce development through the America's Cutting Edge (ACE) initiative. His work has resulted in peer-reviewed publications, collaborative projects with Oak Ridge National Laboratory, National Center for Defense Manufacturing and Machining (NCDMM), and America Makes, with a pending patent for a force dynamometer for in-situ spindle load measurement in additive friction stir deposition. His professional interests include precision machining, smart sensor development, real-time process monitoring, and data-driven manufacturing systems.

Upon completion of his Ph.D. in Mechanical Engineering in Fall 2025, Tobechukwu Nwabueze intends to continue advancing manufacturing science through research and innovation in intelligent machining and cyber-physical production systems.